ANALYSIS OF γ^2 VELORUM PHOTOMETRY FROM THE SOUTH POLE

BY

MARYJANE TAYLOR

A DISSERTATION PRESENTED TO THE GRADUATE SCHOOL
OF THE UNIVERSITY OF FLORIDA IN PARTIAL FULFILLMENT
OF THE REQUIREMENTS FOR THE DEGREE OF
DOCTOR OF PHILOSOPHY

UNIVERSITY OF FLORIDA

1988

ACKNOWLEDGEMENTS

At this time, I would like to express my gratitude to those people without whose contributions this work would have been far more frustrating.

First, I would like to thank the chairman of my Ph.D. committee, Dr. John P. Oliver, for his dedication and expertise in the construction of the South Pole Optical Telescope (SPOT), and for his knowledge in the development of the software necessary to automate the SPOT system. I thank him for the many hours that he has dedicated to this project and for the endless headaches incurred, especially near the beginning of each observing season.

I would also like to express my sincere appreciation to Dr. Kwan-Yu Chen, principal investigator of the SPOT project, for his contributions to this research. He has provided valuable advice in various aspects of this research, and has read this dissertation with a very keen eye. Dr. Chen has also supplied me with references to current papers in the literature on Wolf-Rayet stars, and on γ^2 Velorum.

Thanks also go to Dr. Frank Bradshaw Wood, principal investigator of the project in its infancy, for suggesting

the topic of this dissertation. Dr. Wood has also made me aware of current topics in the literature, and has carefully read this dissertation.

In addition, I extend my thanks to the two other members of my Ph.D. committee, Dr. Jerry L. Weinberg and Dr. Bruce T. Edwards, for reading this work and making constructive criticisms which have improved its quality.

Thanks also go to Dr. Stephen T. Gottesman, chairman of the Astronomy Department at the University of Florida, for taking the time to share his knowledge of the interpretation of power spectra with me, despite not being a formal member of my Ph.D. committee.

I would like to express my sincere appreciation to Dr. John E. Merrill for his devotion to the South Pole project, and for always keeping the members of the team on track. His experience and insight into many of the problems has been extremely useful.

I would like to extend my sincere thanks and appreciation to Dr. Lance Erickson for the long discussions on the application of the methods of Fourier Transform and least-squares analysis as they pertain to this work. I would also like to thank him for the weekends that never were and for helping me to maintain my sanity these last few months.

Finally, warmest thanks go to my father whose never-ending patience, encouragement, and support for the last

twenty-one years have made me always strive for the best. I owe my love of astronomy to him. In addition, he is to be thanked for the long hours devoted to the tedious process of formatting this dissertation in accordance with Graduate School regulations, and for the use of his Hewlett-Packard printer.

The Steller Photometry Program was supported by grants from the Division of Polar Programs of the National Science Foundation.

TABLE OF CONTENTS

Abstract of Dissertation Presented to the Graduate School of the University of Florida in Partial Fulfillment of the Requirements for the Degree of Doctor of Philosophy

ANALYSIS OF γ^2 VELORUM PHOTOMETRY FROM THE SOUTH POLE

BY

MARYJANE TAYLOR

DECEMBER, 1988

Chairman: John Parker Oliver
Major Department: Astronomy

Several hundred photometric observations of the Wolf-Rayet star, γ^2 Vel, have been obtained with the South Pole Optical Telescope using filters centered on the HeII and CIII emission lines at 4686Å and 5696Å, respectively. The observations are reduced to intensities using a region of the continuum centered at 4768Å as the comparison source.

Two independent techniques are used to determine periodic behavior of variations in the strengths of these emission lines. The first of these methods uses power spectrum analysis based on Deeming's method of Fast Fourier Transforms. The second process involves fitting a first-order sine wave to the data using least-squares analysis.

The results of the analysis of the HeII feature indicate a "fundamental period" of 1.20 hours with an amplitude of fluctuation of a few percent. Several harmonics and subharmonics of this period are also detected. The presence of a 1.20 hour period of variability has certain theoretical implications which are discussed in the context of recent theoretical developments. It is suggested that these spectral changes are due to radial pulsations of γ^2 Vel.

An attempt is made to arrive at satisfactory models to describe intensity variations of the CIII emission line. Despite the weakness of this feature, periods are determined which indicate slightly more rapid fluctuations than those found to describe variations in the corresponding helium data. It is suggested that this result may provide clues indicating the relative locations of line formation in the extended wind.

In addition to the analysis of narrowband photometry, observations in the visual and blue filters are reduced to photometric magnitudes using comparison star HR3452. The analyses of these data do not reveal any evidence of an optical eclipse in the γ^2 Vel system, at least within the limitations of these data.

CHAPTER 1
BACKGROUND

In 1867, C. Wolf and G. Rayet discovered several stars which exhibited very unusual spectral characteristics; namely, numerous broad emission features superimposed on a faint continuum. At that time, the only star known to have an emission line in its spectrum was γ Cassiopeia. Normal stellar spectra consisted of a continuum marked by absorption rather than emission lines. In fact, the only astronomical objects which were known to have spectra dominated by emission features were gaseous nebulae. Wolf and Rayet both realized that the spectral characteristics of the stars they had discovered were considerably different from either those of γ Cas or gaseous nebulae. Although originally classified in the Henry-Draper Catalogue as spectral type O, these peculiar objects have now been assigned the separate spectral classification of W and are called Wolf-Rayet stars.

In general, the spectrum of a star is used as an indication of the evolutionary state of that star. However, even today, over a century after their discovery, neither the evolutionary status, nor many of the physical, geometrical and chemical properties of Wolf-Rayet objects

are well understood. It follows then, that in the case of Wolf-Rayet stars, an understanding of the nature of the emission line mechanisms producing such a peculiar spectrum is needed before establishing an appropriate evolutionary scenario. It is this unusual emission line spectrum which is commonly referred to as the "Wolf-Rayet phenomenon." The most currently accepted interpretations of observations of such an intriguing class of stellar objects are presented in the following few paragraphs.

Analysis of spectroscopic observations of Wolf-Rayet stars allows us to state with considerable confidence, the characteristics of the spectra. Very succinctly, the spectra are dominated by emission lines superimposed on a continuum which is characteristic of an O or an early B type star. Only in a few cases are intrinsic absorption features observed. Generally, the only absorption features in a Wolf-Rayet stellar spectrum are the P Cygni absorption components of certain emission lines in some stars. Such P Cyg absorptions indicate expansion of material surrounding the Wolf-Rayet star. The width of the emission lines can be used to infer the velocities of expansion. Although the breadth of the emission lines varies for each ion, probably because different ions are formed at different depths of the atmosphere, these widths correspond to velocities ranging between hundreds and thousands of kilometers per second.

Spectral observations have led astronomers to realize that there are two main sequences of Wolf-Rayet stars. The WN type Wolf-Rayet star has an optical spectrum dominated by nitrogen and helium ions. Several of the WN subtypes exhibit traces of carbon: in particular, the CIV lines at 5801Å and 5812Å in the optical region of the spectrum and at 1550Å in the ultraviolet region. The enhanced abundances of helium and nitrogen, as well as the lower than "normal" abundances of carbon and oxygen, may be explained by the fact that these stars expose material which has been processed in the CNO cycle. The second sequence of Wolf-Rayet stars are the WC types. As their nomenclature indicates, these stars have spectra which are almost entirely dominated by carbon ions, but which may also display helium and oxygen lines as well. Unlike the WN types, the presence of nitrogen in WC stars is very weak. The possible blends of NIII ions with strong carbon features have been identified (Underhill 1959, Bappu 1973) at optical wavelengths and blends of NIV and NV ions with other carbon emissions may be present also at ultraviolet wavelengths (Willis 1980). The (WC) class of Wolf-Rayet stars exposes material which has probably been processed by a helium-burning convective core. In this case, however, the presence of carbon and oxygen is enhanced at the expense of nitrogen and helium. Recently, Barlow and Hummer (1982) have identified a third class of Wolf-Rayet stars, WO. The

WO types represent stars which exhibit strong amounts of oxygen rather than carbon and are probably a result of extreme helium burning.

The ratio of hydrogen to helium in Wolf-Rayet stars remains a controversial topic. Based on analyses of optical spectra, the H/He ratios are quite low; generally significantly less than unity. It is not yet known if this is a reflection of the true chemical composition of these stars. The ratio of abundances of these elements is often determined by using measurements of the HeII Pickering series. Since even quantum number HeII lines occur at nearly the same wavelength as the hydrogen Balmer lines, significant amounts of hydrogen could be inferred from an increase in the strength of the HeII line intensities which produces a non-smooth Pickering decrement. According to Smith (1973), an analysis carried out in this manner resulted in $N(H)/N(He) \approx 1\text{-}2$ for late WN Wolf-Rayet stars (WNL): namely, WN7 and WN8. She found considerably lower ratios, $N(H)/N(He) \approx 0$ for earlier WN types (WNE). These results indicate that stars which exhibit the Wolf-Rayet phenomenon may indeed be chemically evolved stars with WNE types more evolved than WNL types. A similar study was carried out for WC stars by Rublev (1972) who concluded, $N(H)/N(He) < 0.08$. This result must be regarded with a little more caution than those results for WN types, because of the severe blending effects of the HeII Pickering lines

with several carbon and oxygen transitions. However, it is the apparent position of this class of stars on the Hertzsprung-Russell diagram which contradicts the observational evidence for low hydrogen abundances. In fact, this is the primary reason that Underhill (1982) is still of the opinion that the low H/He ratios do not necessarily indicate a true absence of hydrogen: it is still her assertion that Wolf-Rayet stars are chemically similar to our Sun with $3 < H/He < 10$. The temperatures and luminosities which have been derived for these stars place them in the hydrogen-burning band of the Hertzsprung-Russell diagram. More specifically, the late type WN stars are expected to lie near the B0 supergiants while the early WN types and the WC stars seem to reside near the B0 giants. In addition, current stellar models, which have been calculated for He-rich stars with masses and luminosities similar to those for Wolf-Rayet stars, indicate considerably higher effective temperatures than are observed for Wolf-Rayet stars. One could agree with Underhill, who states that perhaps certain physical processes occur in the atmospheres of these complicated stars which may explain the low amounts of detected hydrogen relative to helium. It is true that if the temperatures or densities of the atmosphere are not appropriate, hydrogen emission may not be observed in the assumed amounts. Hydrogen emission occurs in the Balmer lines as a result of a recombination event. Such a

deionization can occur only if the electron temperatures are low enough and the density of material is adequate to allow a sufficient number of recombinations to occur in a small enough period so that the transitions involved appear in the Balmer series. Underhill contends that the densities and temperatures may not be appropriate to allow hydrogen to emit readily. Additional observational evidence indicates that this is not the case. Since the x-ray flux is relatively low, one would infer that the temperatures of Wolf-Rayet stellar atmospheres are not high enough to allow hydrogen emissions to occur. Given current theories of the evolution of hot, massive stars, it is not difficult to imagine that these objects eject much of the material from their atmospheres during their long-term evolutionary development. The spectral observations can be easily misinterpreted since many of the emission features in the spectra of Wolf-Rayet objects are either very broad or the result of blending of several different species.

One representative of the Wolf-Rayet class of stars, γ^2 Velorum, is located in the southern sky at right ascension $8^h09^m12^s$, and declination $-47^\circ18'$ (1988.5). The γ^2 Vel system is the brightest Wolf-Rayet star in the sky with a visual magnitude of $1\overset{m}{.}76$. The star is an intriguing system for both observational and theoretical astronomers. It has been the object of many investigations in the last twenty years or so and is the subject of this dissertation.

The γ^2 Vel system was discovered to be a spectroscopic binary by Sahade in 1955. The system consists of a Wolf-Rayet star of spectral classification WC8 and a hot supergiant component of spectral type O9 (Conti and Smith 1972). Ganesh and Bappu (1967) carried out the first spectroscopic study in order to determine the orbital parameters of the γ^2 Vel system. Using the CIII-IV blend at 4650Å which is assumed to be formed in the envelope of the Wolf-Rayet component, and the hydrogen absorption line of the O star at 4340Å, they found an orbital period of $78\overset{d}{.}5$. A more accurate estimate of the period was accomplished by Niemela and Sahade (1980). They determined a radial velocity curve using the strong violet-shifted absorption line, HeI at 3888Å. The position of this feature was measured relative to the H8 absorption line of the O9 supergiant. They determined a period of revolution of $78\overset{d}{.}5002$ with an eccentricity of 0.40. Moffat et al. (1986) carried out another radial velocity analysis of the γ^2 Vel system in an attempt to define the orbital elements of the system more precisely. They used radial velocity curves obtained for several emission features but were unable to improve upon the $78\overset{d}{.}5002$ period or the 0.40 eccentricity. However, their refined ephemeris coupled with the period of Niemela and Sahade, is given by the following equation:

$$E_o = JD2445768.96 + 78\overset{d}{.}5002. \qquad (1\text{-}1)$$

With the aid of equation (1-1), the O9 star is found to be in front of the WC8 star at phase 0.0 and behind the Wolf-Rayet component near phase 0.5. According to the study by Moffat et al. (1986) the epoch of periastron passage is determined to be JD2445802.6. Although an eclipse has been detected in the ultraviolet region of the spectrum (Willis and Wilson 1976) at phase 0.65, no definite eclipse effects have been recorded at optical wavelengths. Gaposchkin (1959) reported a $16\overset{d}{.}2334$ period with an amplitude of variation ranging between $0\overset{m}{.}19$ and $0\overset{m}{.}13$ using visual and photographic measurements, but to date no other work has been able to confirm these results.

The masses of the individual components can be determined from the simple relation

$$\frac{K_{abs}}{K_{em}} = \frac{M_{WR}}{M_{O9}} , \qquad (1\text{-}2)$$

where K_{abs} and K_{em} are the amplitudes of the absorption and emission radial velocity curves and M_{WR}/M_{O9} represents the ratio of the mass of the WC8 star to the O9 supergiant. According to the study by Moffat et al., the best values for K_{abs} and K_{em} are given by

$K_{abs} = 70 \pm 2$ km/sec, and

$K_{em} = 130 \pm 6$ km/sec.

These values are in good agreement with independently determined results by Niemela and Sahade but have smaller uncertainties. They indicate that the mass of the Wolf-Rayet companion is approximately 0.54 times that of the O9 star, with minimum masses of $17M_{\odot}$ for the WC8 component and $32M_{\odot}$ for the supergiant.

In an attempt to measure the radius of the individual components of γ^2 Vel as well as the separation distance of this binary system, Brown et al. (1970) obtained interferometry measurements with the stellar intensity interferometer at the Narrabri Observatory. Their measurements in the continuum at 4430Å included the effects of both γ^2 Vel and γ^1 Vel, which is located 41" away from γ^2. However, the analysis is simplified by the fact that the assumed contribution from γ^1 Vel is negligible. These data indicate an angular diameter of the Wolf-Rayet component of $0\overset{''}{.}44 \pm 0\overset{''}{.}05 \times 10^{-3}$, and an angular semi-major axis of the orbit of $4\overset{''}{.}3 \pm 0\overset{''}{.}5 \times 10^{-3}$. Using spectroscopic observations of Ganesh and Bappu (1967), together with these angular measurements, the distance modulus for the γ Vel system is 7.7 ± 0.3 or about 350pc. A simple trigonometric computation yields a radius for the WC8 component of $17R_{\odot}$. A more conventional method of measuring Hß indices of several stars in the vicinity of γ Vel results in a distance of 457pc, and hence, a radius for the Wolf-Rayet star of $22R_{\odot}$.

Since an eclipse in the optical region of the spectrum has not been detected, the inclination of the system can be assumed to be approximately 70°. Using the angular semi-major axis of the orbit obtained by Brown et al., the projected semi-major axis is 2.09 ± 0.05 x 10^{13}cm, or assuming i=70°, 2.22 + 0.13 x 10^{13}cm. These measurements imply a separation distance of approximately $319R_{\odot}$.

Brown et al. also obtained measurements of the CIII-IV emission line of γ^2 Vel at 4650Å. These data include effects of both components of γ^2 Vel in addition to the effects from the material surrounding the Wolf-Rayet component. The interferometry measurements give an angular diameter of the region emitting at the CIII-IV frequency of 2".05 ± 0".19 x 10^{-3}. If one assumes the 350pc distance established by Brown et al., these data indicate that the CIII-IV blend is formed in a region around the WC8 component, and at a distance of 76 ± $10R_{\odot}$ from that star. Wood (1941) derived a relationship between the dimensions of Roche equipotential surfaces, relative to the semi-major axis, as a function of the mass ratio. Given the described dimensions for γ^2 Vel, the radius of the Roche lobe is $83R_{\odot}$. Hence, evidence indicates that this emission feature at 4650Å is formed in the outer regions of the circumstellar material, and in fact, in material which nearly fills the Roche lobe of the γ^2 Vel binary system. These and other properties of this intriguing system are summarized in Table 1-1. In light of

the discussion presented earlier, it is interesting to note that H/He < 0.02 for γ^2 Vel; certainly much different from the chemical composition of the Sun.

The γ^2 Vel system is a very peculiar binary which has attracted much attention in the last two decades. One of the most intriguing features of this system is the indication of possible variability in some of the emission lines which are present in the spectrum of the Wolf-Rayet component. It is this primary characteristic which has made γ^2 Vel the subject of so many photometric and spectroscopic studies. As early as 1918, variation in the shapes of certain emission lines were reported (Perrine 1918). West (1972) was the first author to assert that variation in line intensities might also exist. The results of 24 hours of observation with the Orbiting Astronomical Observatory, OAO-2, indicated no short term variations in the CIII emission line at 1909Å. Since then however, several authors have presented evidence of variations in both line profile and line strength.

Jeffers et al. (1973a), first reported a 6 minute periodicity in both line intensity and line shape using photometric measurements of the HeII (4686Å) and CIII-IV (4650Å) features. A later re-analysis of their data (1973b) revealed even more rapid fluctuations on the order of 154 ± 3 seconds with an amplitude of only about 2%.

Table 1-1
Properties of the γ Velorum System

Spectroscopic binary	WC8 + O9I
a) $P = 78^{d}.5002$	
b) $V = 1^{m}.76$	
c) $M_{WR} * \sin^3 i > 17M_{\odot}$	
d) $M_{O9} * \sin^3 i > 32M_{\odot}$	
e) $q = 0.54$	
f) $R_{WR} = 17 \pm 3R_{\odot}$	
g) $R_{O9} = 76 \pm 10R_{\odot}$	
h) $a * \sin(i) > 319R_{\odot}$	
i) H/He = 0.02	

Austin, Schneider, and Wood (1973) carried out a very extensive photometric study of γ^2 Vel at the Mt. John Observatory in New Zealand. They used six narrowband filters with $\Delta\lambda$ = 10Å. Three of these filters isolated the emission lines identified as HeII at 4686Å, CIII at 5696Å, and CIV at 5812Å; the other three filters were centered on the continuum at 4804Å, 5302Å, and 6106Å. These authors found that the continuum remained essentially constant as did the triply-ionized carbon feature, at least in the time interval spanned by their observations. Austin et al. detected definite night-to-night variations in the strengths of the CIII and HeII features. The amplitude of variation for the doubly-ionized carbon line amounted to about $0\overset{m}{.}12$. Fluctuations of $0\overset{m}{.}03$ also occurred in a time period of less than 2 hours. The singly ionized helium feature exhibited an increase in brightness of $0\overset{m}{.}06$ in less than 90 minutes, but, Austin et al. also note that this line appears to remain quite stable (i.e., within $0\overset{m}{.}02$) for relatively long time intervals. Austin et al. carried out a more intensive γ^2 Vel observing program, concentrating only on variations in the HeII line. Their results were inconclusive; γ^2 Vel exhibited no detectable variations in a 20 minute time period on the first night of observation. On the second night, however, the ionized HeII line increased in brightness by as much as $0\overset{m}{.}10$ in 20 minutes, and again later that night, brightened by the same amount in only 2 minutes. In summary, Austin

et al. confirmed previous results that rapid variations can occur, although not with the rapidity of the degree reported by Jeffers et al. They found these variations to be temporal and not periodic.

Another photometric study carried out by Lindgren et al. (1975) did not provide evidence for stable variations between 1 and 10 minutes in length, in either the CIII-IV line at 4650Å or the HeII line at 4686Å. However, Lindgren et al. did confirm nightly variations in emission line strength, in particular, a $0^{m}.03$ to $0^{m}.05$ change in the 4650Å feature. The observations that were utilized for this investigation covered an interesting phase of γ Vel: that is, when the O star was in front of the Wolf-Rayet component. These results may indicate an eclipse of some part of the supergiant by a portion of the circumstellar material associated with the WC8 star.

Bahng presented results of several spectrophotometric studies of the γ^{2} Vel system, studying the short term variations in emission line strengths using a photoelectric spectrum scanner in the spectral range 4600Å to 4720Å. In 1973, Bahng reported on results of spectrum scans which were acquired on four different nights. The emission lines of particular interest were CIII-IV (4650Å) and HeII (4686Å). Although a power spectrum analysis did not yield evidence of a periodic phenomenon, Bahng did find variations in the equivalent widths of these lines. These changes amounted to

a 2% variation for CIII-CIV, and a 4% variation for HeII and occurred on time scales of 4 to 20 minutes. Later, Bahng (1974) recorded a 6 hour spectrophotometry observation in which variations were detected between 10 and 20 minutes. Again, however, no predominant periodicity was found. In his 1975 paper, Bahng analyzed spectroscopic scans which were obtained in 1973 and 1974. He compares the theoretical rms deviations computed from photon counting statistics with the rms deviations of the measured equivalent widths of the emission lines of interest. Since the rms deviations of the data exceed the theoretical rms deviations by more than a factor of three, Bahng considers these variations to be statistically significant, indicating that real short term variations in the emission lines of the γ^2 Vel system do exist. Although there is no predominant periodicity, a power spectrum analysis indicates considerable power near a frequency corresponding to a period of about 1 minute. Using integrated magnitudes, Bahng finds evidence of variation with a semi-amplitude of $0^m.01$ with a periodicity of 339.5 seconds. In addition, a significant peak at 16.2 minutes was also present in the data.

We have presented only a brief summary of some of the more notable observational studies of γ^2 Vel which have appeared in the literature over the last few years. As pointed out by Haefner et al. (1977), ultra-short period variations (i.e., those on the order of minutes) seem to be

detected only in observations which do not exceed much more than 30 minutes in length. Fluctuations of this nature are not generally detected in longer runs of continuous data, but variations in both emission line strength and profile are almost always detected on a nightly basis.

CHAPTER 2
INSTRUMENTATION AND DATA ACQUISITION SYSTEM

Instrumentation

The data used for this research were obtained with the automated optical telescope located at the Amundsen-Scott South Pole Station on Antarctica. This instrument is a two-mirror siderostat zenith telescope with an f/6, 7.8cm achromatic lens (Figure 2-1). As one would expect, certain special design considerations are necessary to ensure normal operation in the extremely low-temperature, harsh environment which prevails at the South Pole. A specially insulated building measuring 12' x 8' x 8' was constructed on site by carpenters of ITT Antarctic Services during the 1985 austral summer. The telescope occupies an 8' x 8' section of the building, while the computer system and control electronics are housed in an adjacent room measuring 4' x 8'. This smaller room can be completely isolated from the telescope room and heated when necessary. Under normal circumstances, the telescope room temperature is maintained at approximately -20°C.

The optical head of the telescope contains two optically-flat front-surfaced mirrors which act to redirect

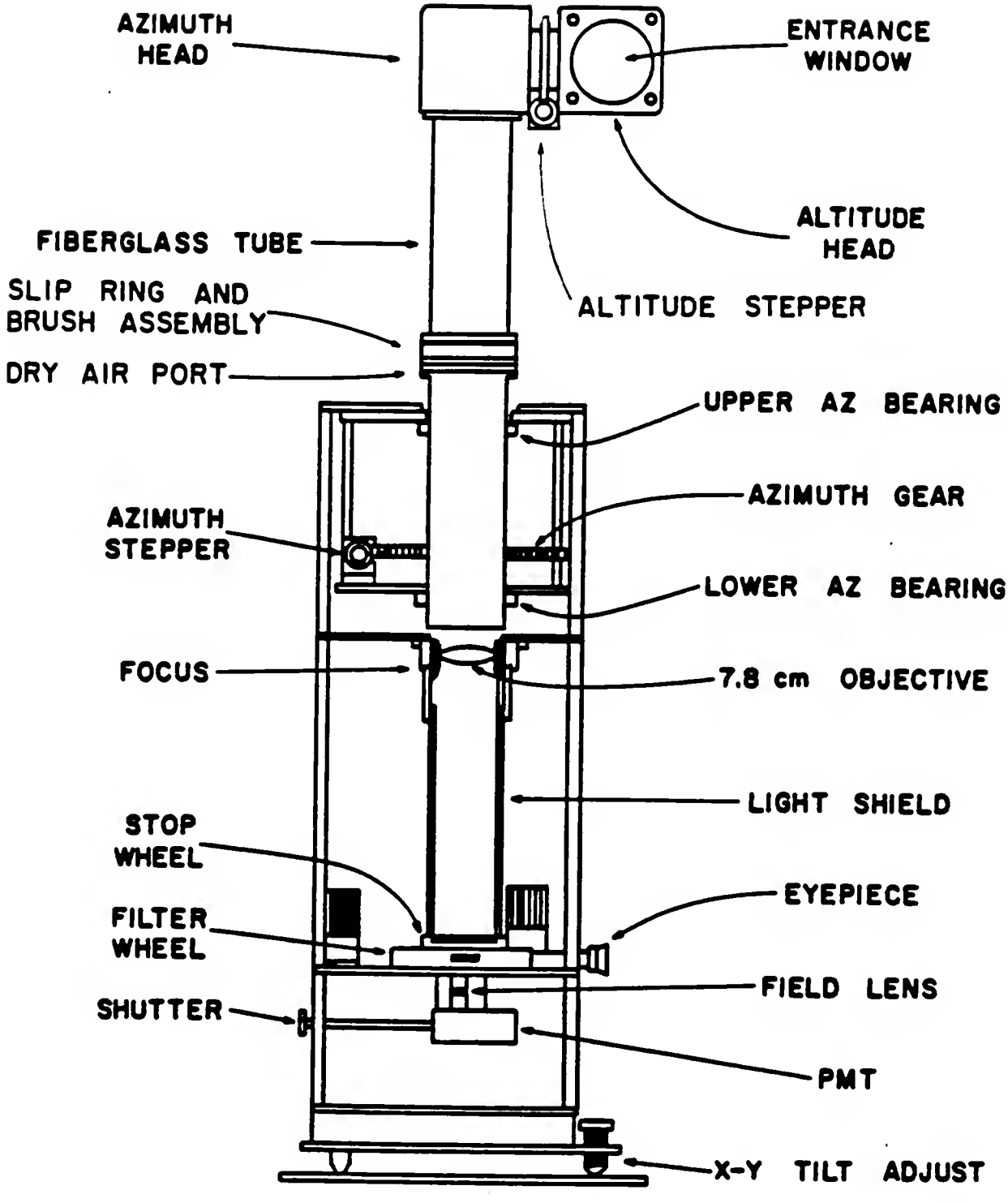

Figure 2.1 South Pole Optical Telescope.

incoming light onto the objective lens and eventually to the photometer. It is this section of the telescope which protrudes from the roof of the building and is therefore exposed to ambient conditions. In order to prevent blowing snow and other sources of moisture from entering the optical head, a transparent window is used to completely seal the interior of the telescope. During the 1986 observing season, the formation of frost on this window and on the mirrors in the optical head interfered with some of the observations. Since this time, however, upgrades to the system have been installed and all of the optics are maintained frost-free. This was accomplished by pumping existing dry polar air (the absolute humidity is equivalent to about 0.15mm of precipitable water vapor) through a cylindrical tube containing a desiccant, and into the optical head of the telescope. Here, the air is heated so that a temperature gradient of about 5°C is maintained between the air in the optical head and the air immediately outside of the entrance window, with the inside air being the warmer.

Of the entire design of the telescope, the only moving part which is directly exposed to ambient conditions is the elevation axle. The gear system which moves the telescope in the east to west direction, also moves the entire telescope tube in both azimuthal directions. The azimuth-motion resides well within the telescope room, and a worm gear

drive is controlled by a stepper motor assembly. This same technique provides motion to the field stop and filter wheels. With the siderostat design, the elevation motor must move only the optical head in the north to south direction, and it is therefore necessarily mounted outside on the optical head assembly. The elevation axis joint is located between the two portions of the optical head which house the two optically-flat mirrors. This "up and down" motion of the telescope is provided with an assembly of teflon ball bearings.

The optical design of the telescope (Figure 2-1) is straight forward. Incoming light rays strike the objective after being deflected by the two front-surfaced mirrors in the optical head; each is positioned at about 45° with respect to the normal. As the photons emerge from the lens, they pass through a diaphragm, a filter, and a fabry lens which images the objective of the telescope onto the photomultiplier. It is the photometer which measures the signal and converts it into an equivalent number of photons.

The South Pole Optical Telescope (SPOT) is equipped with several diaphragms and filters allowing the selection of any one of a number of combinations depending upon the brightness of the source, the tracking rate of the telescope, and the type of observation desired. The current system has diaphragms which restrict the field of view to 1°, 5′, 2′, or 1′ regions of the sky. The 1° field of view

is used only in the initial star pointing procedure while the 5′, 2′, and 1′ diaphragms are used in the star centering procedure and for the actual measurement of the object's brightness; the smaller the diaphragm, the smaller the contribution from sky background, and the fainter the limiting magnitude of the telescope. The filters which are currently mounted in the filter wheel include the Johnson standard B and V filters, a neutral density filter, and four narrowband filters. The neutral density filter is a ND5 and is used in the star find procedure. This filter's sole purpose is to prevent the telescope from observing a source which is too bright: that is, one which could saturate, and subsequently damage the photomultiplier. Of the narrowband filters, one is used to monitor auroral and/or sky variations. This filter is centered on the very strong OI emission line at 5577Å. The remaining three narrowband filters were chosen specifically for our research on the Wolf-Rayet star, γ^2 Vel. Two of these filters isolate emission features in the spectrum of γ^2 Vel; the HeII emission line at 4686Å and the CIII emission line at 5696Å. The third filter isolates the continuum region at 4768Å. More specific details of each of these filters are presented in Table 2-1. Also, the response curves for six of the filters are presented in Figures 2-2 through 2-6. In addition to the filters, one position on the filter wheel contains a mirror which directs the light beam perpendicular

Table 2-1
Filter Specifications

Peak Wavelength (Å)	Half-Power band-width (Å)	Integration time (secs)	Purpose
4400	900	2	B
5500	900	2	V
4686	32	4	HeII
5696	32	8	CIII
4768	92	2	Continuum
5577	100	8	OI

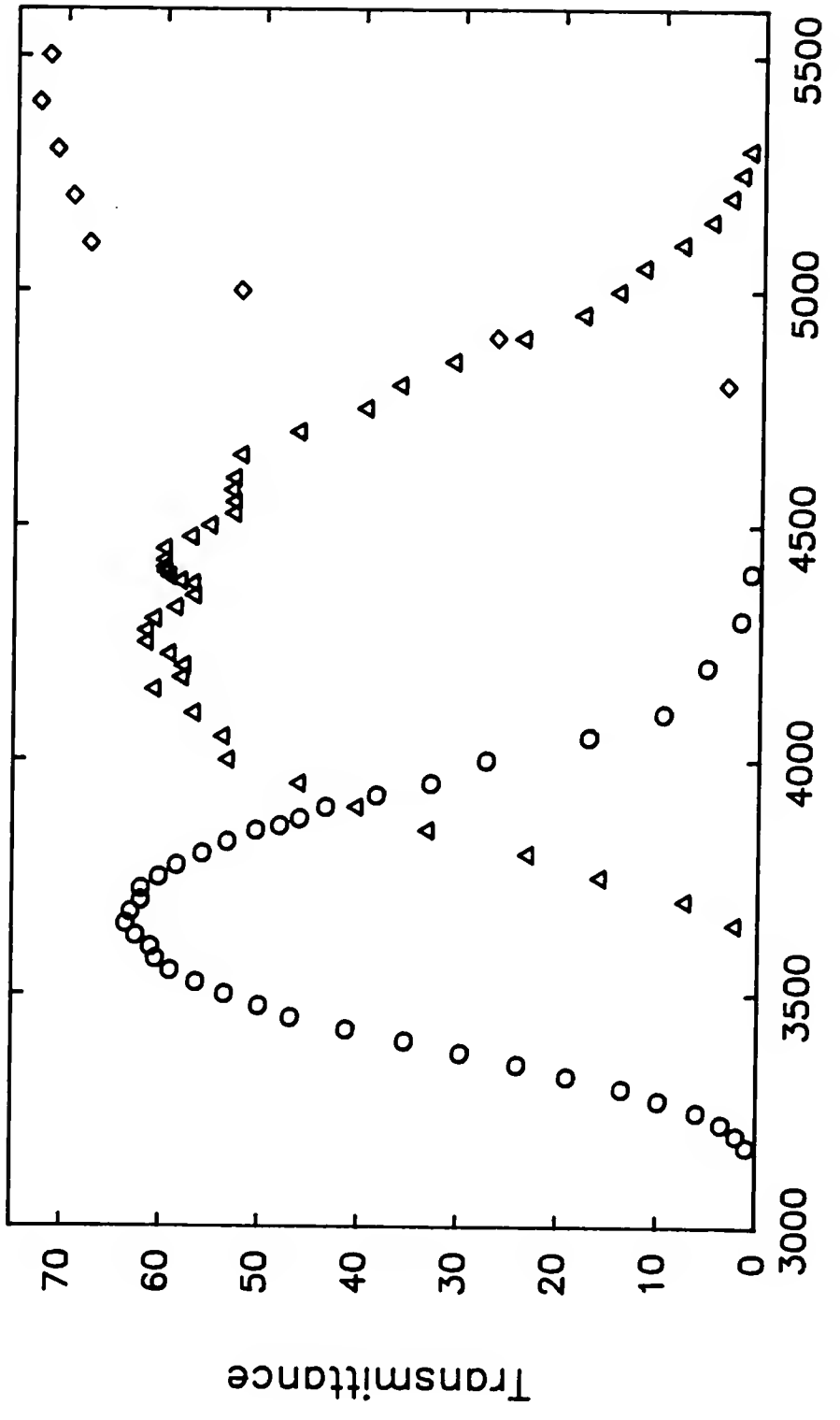

Figure 2-2 Response curves for the U (O), B (Δ), and V (◊) filters.

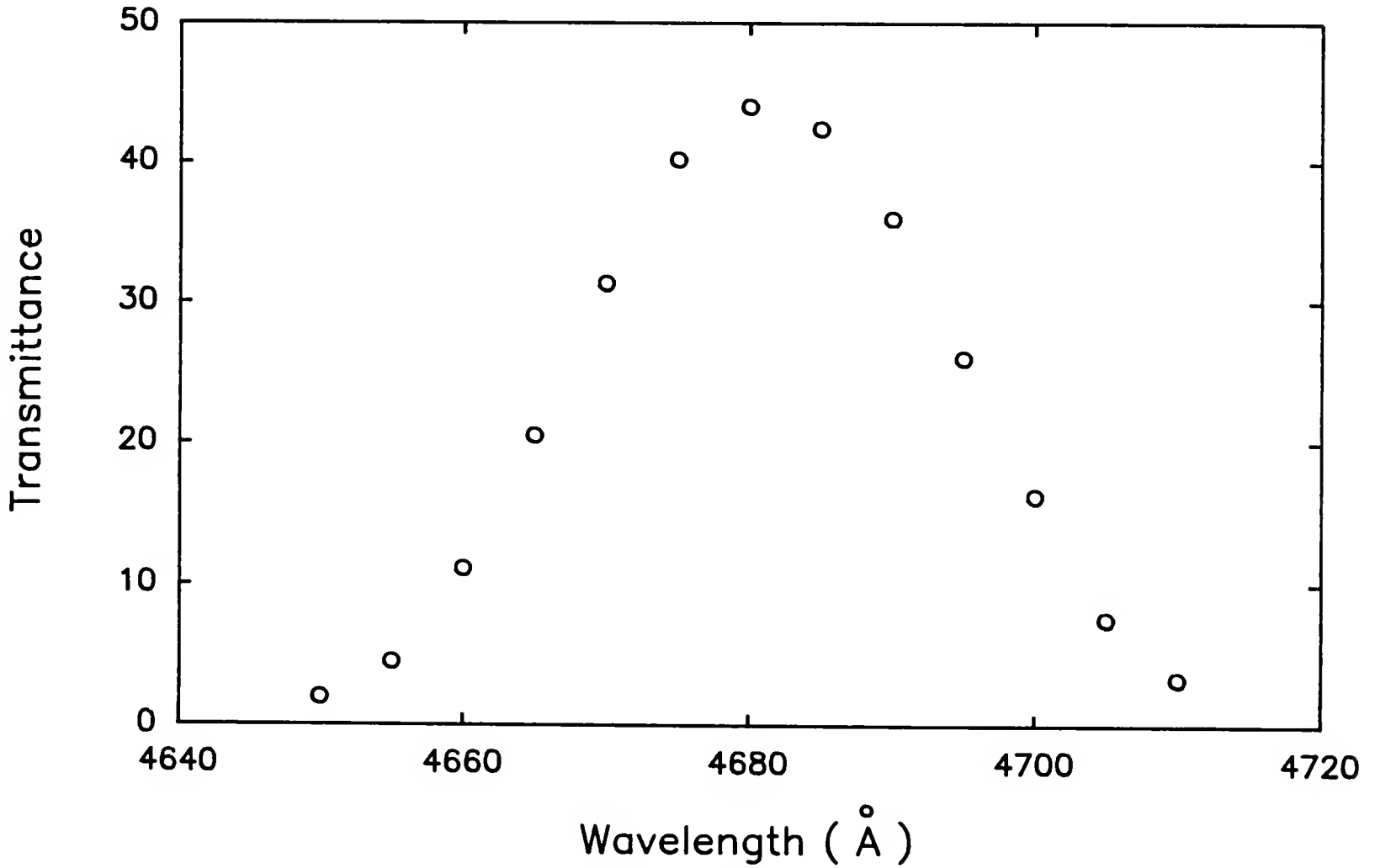

Figure 2-3 Response curve for the helium emission filter.

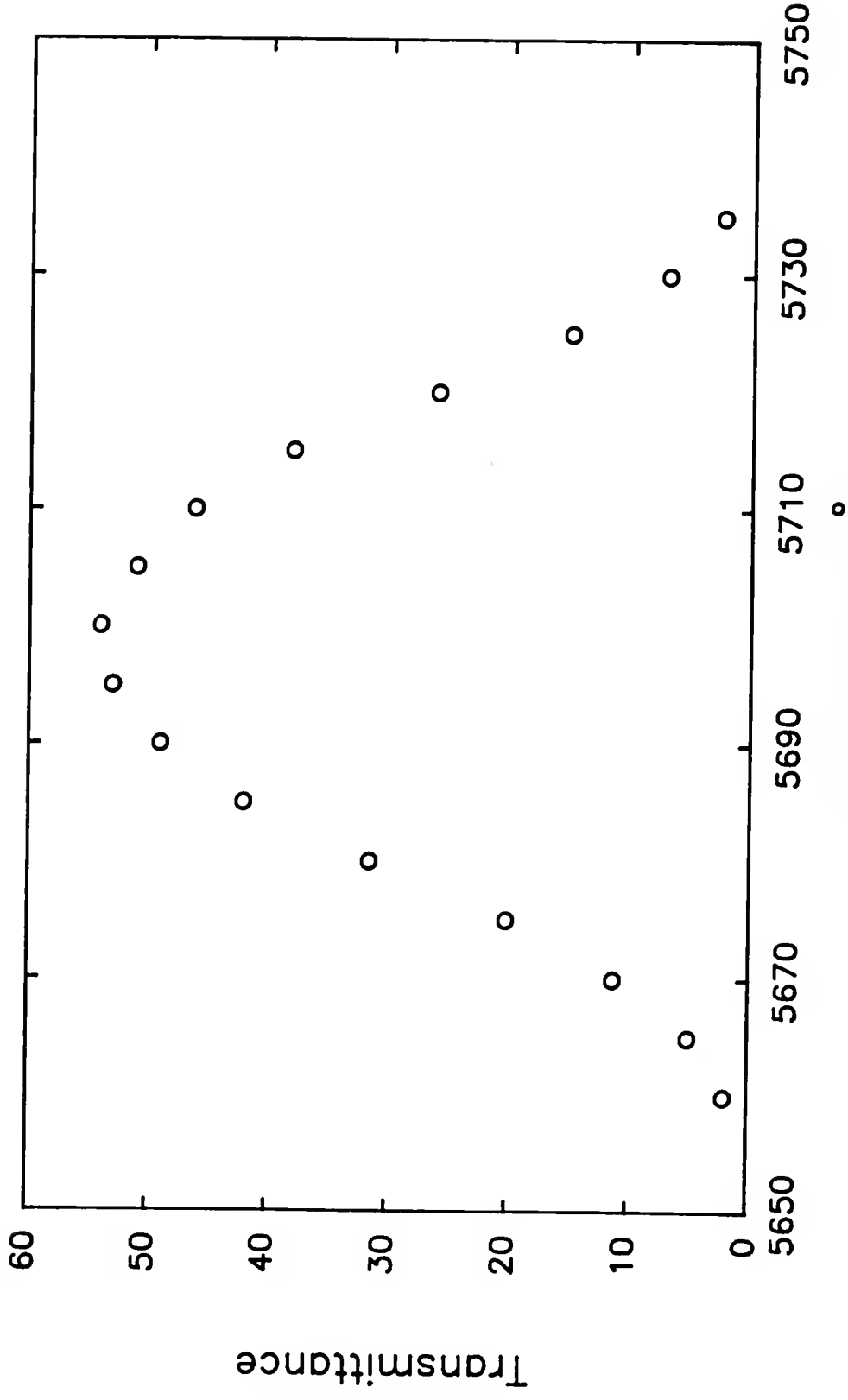

Figure 2-4 Response curve for the carbon emission filter.

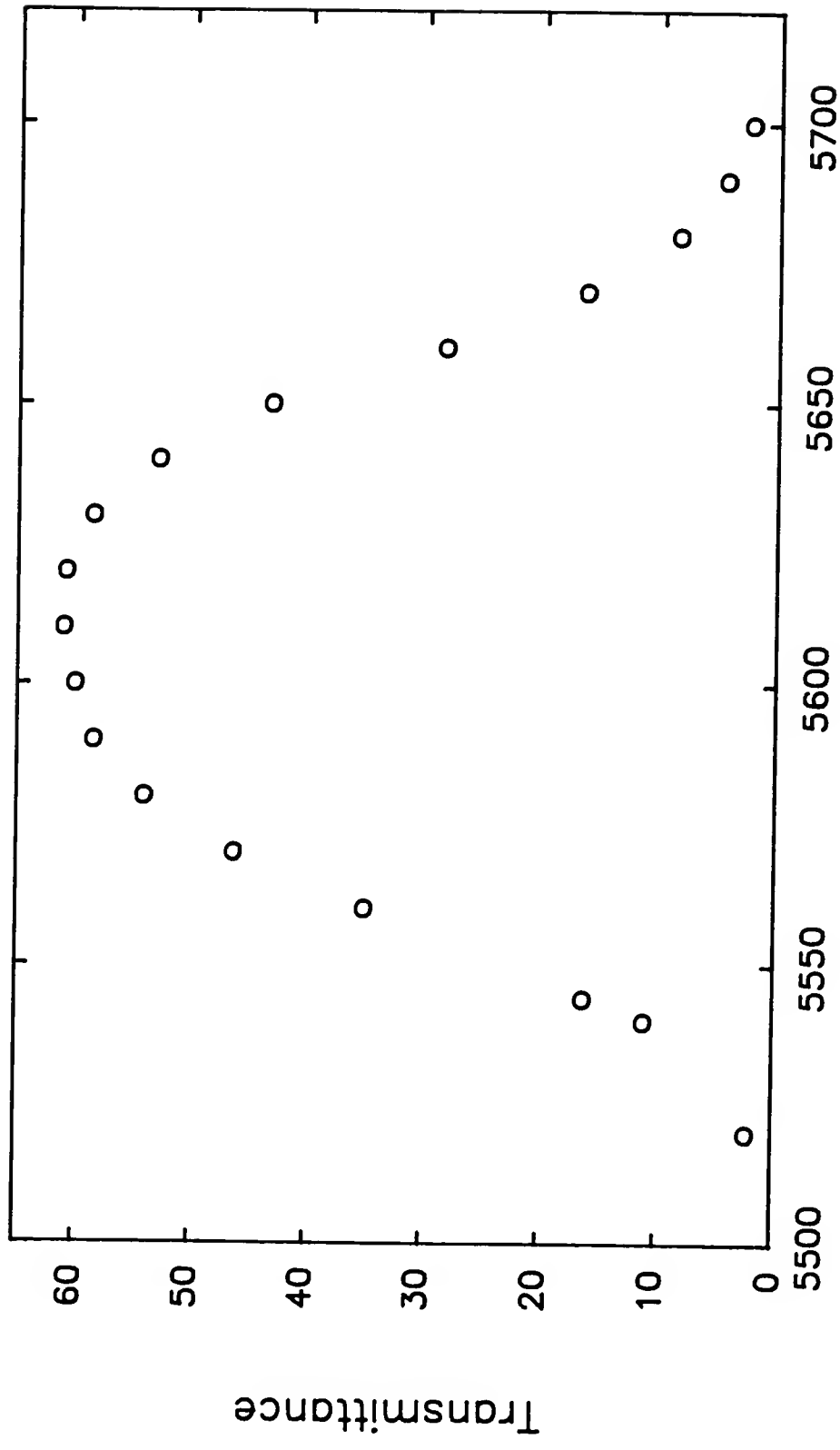

Figure 2-5 Response curve for the oxygen emission filter.

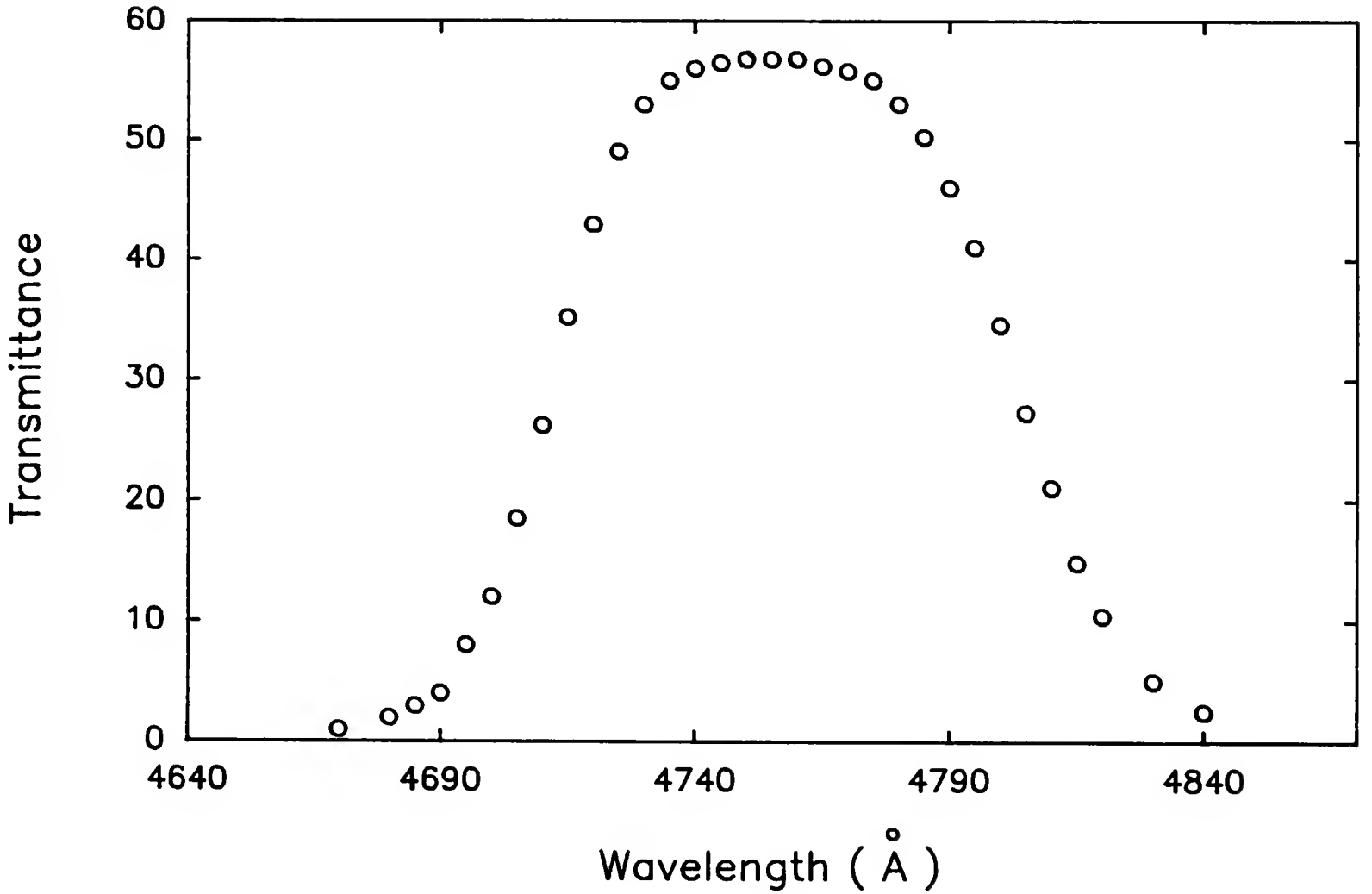

Figure 2-6 Response curve for the continuum filter.

to the optical axis where it can be viewed through an eyepiece. This section of the telescope is maintained at a temperature below -20°C in an effort to reduce the dark current in the system. During the three years in which the telescope has been operating, this level has remained nearly constant at 3.7 counts/sec. Other regions of the telescope are also maintained at optimum temperatures according to a thermal design analysis carried out by Esper (1986). These temperatures are achieved with thermal insulation, heaters, and residual heat generated by stepping motors and other electronic components. The entire thermal design of the telescope works in concert with ambient temperatures ranging from -40°C to -80°C.

Data Acquisition

The SPOT system is controlled with a modified Dynatem RM-65 computer system with an 8-bit 6502 microprocessor. The computer system controls the motions of the telescope in azimuth and elevation, as well as the motions of the component parts including the field stop and filter wheels. The necessary special functions and interfacing of the telescope are provided by custom built circuits supplied by the electronics shop at the University of Florida. The software is written in 6502 assembler language and FORTH. FORTH is a computer language designed specifically for instrument control processes. As mentioned previously, the

computer system is located in the SPOT building. However, in some cases, the telescope can be commanded from a remote terminal. The data storage media which are currently employed are 8-inch floppy disks.

During an observing session, photometric and engineering data are accumulated until a one kilobyte region of memory is filled. At that time, the buffered data are written onto a disk file. At the beginning of each hour, the telescope suspends the acquisition of photometric data and records the status of various aspects of the telescope. Such things as the azimuth and elevation positions of the telescope, the Julian Date and Sidereal Time, and the temperatures of various sections of the telescope are stored as engineering records. After these data are obtained, the telescope resumes its observing program. Observing programs instruct the telescope with respect to pointing, diaphragm, appropriate filtering, and number of seconds to integrate for each filter. In addition, in the case of stellar photometry, the telescope is given the number of steps and directional information for sky readings. Observing programs can be modified, deleted, and added from the remote terminal. Depending upon the observing program and sky conditions, a given floppy disk may fill in a week to ten days. At this time, the winter-over scientist changes the disks, copies the contents of the filled disk to tape for archival purposes, and transmits the data to a mainframe

computer in Malabar, Florida, via the ATS-3 satellite communication link. These data are retrieved from the VAX system in Malabar, and stored on the ATS-VAX at the University of Florida where the reduction of the data proceeds.

CHAPTER 3
DATA REDUCTION TECHNIQUES

During the 1986, 1987, and 1988 observing seasons, SPOT obtained data for several different research projects. In order to optimize telescope time and to make the best use of clear skies, the data for more than one research project were usually acquired within the same observing program. The research project that is the subject of this dissertation has two major objectives: 1) the search for variations in emission line strengths using the HeII, CIII, and continuum filters; and, 2) the search for eclipse effects requiring observations in the B and V filters, as well as integrations on the comparison star, HR3452. In some observing programs, both γ^2 Vel and HR3452 were observed using all available filters. In other cases, an increase in the time-resolution of the data was accomplished by removing HR3452 from the observing program and omitting the B and V filter observations. Therefore, several different observing sequences were required to obtain the data necessary for this investigation. Specific details of these programs will be presented in Chapter 4 where individual data sets are discussed. In general however, the data acquired for this project were obtained with the use of the 5′ diaphragm in

conjunction with the B, V, HeII, CIII, OI, and continuum filters.

As one would expect, the photometric integration times necessary to obtain adequate signals for a given star and filter varies from star to star, and from filter to filter. The required integration length depends on a particular star's color and its distance from the zenith. For example, to obtain comparable deflections in B and V filters for a red star, it is necessary to integrate for a longer time period in the blue region than in the yellow. In addition, the increased scattering of blue light at large zenith distances requires the use of longer integration times for the blue filter than for the visual filter. The optimum integration times for the stars and filters used in this study are based on this knowledge, as well as experience that was acquired during the early portions of the 1986 observing season. Integration times are presented in Table 3-1.

Since a star does not wholly fill the observing diaphragm, each stellar deflection is actually the sum of the star and surrounding sky emissions. In order to obtain a net star-reading, it is necessary to remove an appropriate value for the sky intensity from each of the stellar measurements. In the case of a single channel photometer, this is easily accomplished by integrating on a region of sky which is devoid of stars within the limitations of the

Table 3-1
Optimum Integration Times for γ^2 Vel and HR3452

Star	Filter	Integration time (secs)
γ^2 Vel	B	2
	V	2
	HeII	4
	CIII	8
	Continuum	2
	OI	8
HR3452	B	10
	V	10

telescope but which is reasonably close to the star under observation. In an automated telescope system, it is necessary to make certain that both of these criteria are satisfied. A search of the Palomar Sky Survey (1954) prints indicates that a displacement of 15′ in the positive azimuth direction from the star is an appropriate displacement for a typical sky reading. In very general terms, each stellar deflection is accompanied by a corresponding sky deflection which is used in the data reduction procedures.

During the observing season, data are periodically transmitted from the South Pole to the VAX 11/750 computer at the University of Florida. Each of the programs used in the reduction and analysis of the γ^2 Vel photometry was written in Fortran-77. In order to optimize computer run-time, the data were initially passed through a program which unpacked the data from hexadecimal to decimal format and divided the data into two files: an engineering file containing information relating to the design and operation of the telescope, and a separate photometric file containing the data relating to the stellar deflections. The raw stellar deflections were then reduced to photometric magnitudes using standard reduction techniques (Henden and Kaitchuck 1982). Since each deflection is recorded as a counts-per-time quantity, and since an integration time varies from filter to filter, it is necessary to convert all measurements to the same unit; a counts per second quantity.

Once this is done, the next step is to remove the sky background from each stellar measurement. This is accomplished through a simple linear interpolation of the sky readings to the time of the star reading. The number of counts (per second) due to the background are then subtracted from the total counts (per second) due to the star. In the case of the B and V data, HR3452 was chosen as the comparison star. HR3452 is very close in color to γ^2 Vel with a spectral classification of B1V and is located only 24' from the variable. For these reasons, and the fact that HR3452 has not been reported to be variable, it meets the criteria for a reasonably good comparison star. A second linear interpolation scheme is then used to determine the intensity of the comparison star, HR3452, at the time of the variable star reading. Finally, equation (3-1) is used to give the differential photometric magnitude

$$\Delta m = -2.5 * \log \left(\frac{D_V}{D_C} \right), \qquad (3\text{-}1)$$

where Δm is the differential magnitude between γ^2 Vel and HR3452, and D_V and D_C are the deflections (in counts per second) of γ^2 Vel and of HR3452, respectively.

A major portion of this research is the search for periodic intensity variations in the HeII and CIII emission lines of γ^2 Vel. One technique which is commonly employed in

period determination analyses uses the method of Fourier transformation of time and intensity measurements. In particular, Deeming's method (1975) of Fast Fourier transforms is well suited for data which are unequally spaced in time. In general, Fourier transform analysis is used to transform data from the time domain into the frequency domain, or vice-versa. For instance, a continuous function of time, f(t), can be transferred into frequency space according to the formula

$$F(\nu) = FT[f] = \int_{-\infty}^{+\infty} f(t) * \exp(-2\pi i \nu t)\, dt. \qquad (3\text{-}2)$$

The inverse Fourier transform is given by

$$f(t) = FT[F] = \int_{-\infty}^{+\infty} F(\nu) * \exp(2\pi i \nu t)\, d\nu. \qquad (3\text{-}3)$$

In equation (3-2), $F(\nu)$ represents a spectrum of frequencies. Each peak in $F(\nu)$ corresponds to the relative strength of each frequency in the data, f(t). In most cases, and in this data, f(t) is not a continuous function, but rather a sampled-set determined at discrete times, t_i. Hence, equation (3-2) can be re-written as a discrete transform

$$F(\nu) = 2 \sum_{1}^{N} [f(t) * \exp(-2\pi i \nu t)], \qquad (3\text{-}4)$$

with N equal to the number of data points in f(t). The periodic exponential function in equation (3-4) indicates that the Fourier transform of f(t) has both real and imaginary components. Since it is the power as a function of frequency, rather than the Fourier transform that is of interest, the derivation must be carried one step further. If f(t) is assumed to be real, then $F(\nu)$ must satisfy the relation

$$F(-\nu) = F^*(\nu), \tag{3-5}$$

where $F^*(\nu)$ is the complex conjugate of $F(\nu)$. Then, according to Rayleigh's theorem which states:

$$\int_{-\infty}^{+\infty} |f(t)|^2 \, dt = \int_{-\infty}^{+\infty} |F(\nu)|^2 \, d\nu, \tag{3-6}$$

we can define the power, $P(\nu)$, as the product of $F(\nu)$ and its complex conjugate, which leaves only the real quantity

$$P(\nu) = |F(\nu)|^2 = C^2(\nu) + S^2(\nu). \tag{3-7}$$

$C(\nu)$ and $S(\nu)$ in equation (3-7) are the cosine and sine components, respectively, and are defined as

$$C(\nu) = \frac{2}{N} \Sigma [f(t) * \cos(2\pi\nu t)], \text{ and} \tag{3-8}$$

$$S(\nu) = \frac{2}{N} \Sigma [f(t) * \sin (2\pi\nu t)]. \qquad (3\text{-}9)$$

Since the data used in this investigation are acquired over a finite span of time and are not sampled at equal time intervals, the Fourier transform is contaminated with the sampling function. This spectral window or "beam", as it is frequently referred to, is given by the relation,

$$W(\nu) = G^2(\nu) + H^2(\nu). \qquad (3\text{-}10)$$

In (3-10), $G(\nu)$ and $H(\nu)$ are defined in the following manner:

$$G(\nu) = \frac{1}{N} \Sigma [\cos (2\pi\nu t)], \text{ and} \qquad (3\text{-}11)$$

$$H(\nu) = \frac{1}{N} \Sigma [\sin (2\pi\nu t)]. \qquad (3\text{-}12)$$

According to equations (3-10) to (3-12), the spectral window function is normalized so that $W(0) = 1$. The Fourier convolution theorem states that the Fourier transform of the signal, FT[f], is the convolution of the data with the sampling function (i.e., beam). The fact that the data are unequally spaced over a finite time interval has several consequences. The sampling period of the data puts a constraint on the lowest frequency which is resolvable in the data. The frequency resolution in a discrete data set corresponds to the width of the beam (W) at $\nu = 0$ and is

related to the sampling period by equation (3-13)

$$\delta\nu \approx 1/T, \tag{3-13}$$

where T is the length of the data set. Therefore, the minimum frequency which is retrievable from a given data set is given by the Nyquist frequency

$$\nu_{min} = 1/(2\Delta T). \tag{3-14}$$

It is the data spacing which puts an upper limit on the frequency that can be recovered from a given data set. In the case of a function consisting of points spaced at equal time intervals Δt, the maximum frequency is given by the Nyquist frequency. Since the data used in this study are unequally spaced in time, Δt is not a constant. For purposes of this investigation, it was deemed appropriate to calculate the average time interval for a given data set and use that value for Δt, according to equation (3-15):

$$\nu_{max} = 1/(2\Delta t). \tag{3-15}$$

In addition to upper and lower limits being placed on the frequencies which can be recovered from the data, the data are also not represented by a continuous function of time. The discrete nature of the data contributes several

features to the spectral window (beam) which adds considerable complexity to the nature of the spectrum. Since the Fourier transform of the data is a convolution of the spectrum with the window, the resulting "dirty" spectrum may be subsequently contaminated with spurious sampling features. This aliasing can be masked as either a damping of real features or an enhancement of "false" features, making interpretation difficult. For this reason, a one-dimensional deconvolution (CLEAN) algorithm (Högbom 1974) has been adopted for use in this study. The CLEAN algorithm is that used by Roberts, Lehàr, and Drehar (1987) which deconvolves the sampling function from the dirty spectrum to give a better representation of the true spectrum. This deconvolution is accomplished in the following manner: First, the largest peak in the dirty spectrum is located and stored. The spectral window (beam), is then superimposed onto the dirty spectrum so that the main peak in the beam coincides with the largest peak in the dirty spectrum. A given percentage of the spectral window is subtracted from the corresponding dirty spectrum. The peak of the spectrum which is removed from the data spectrum is stored as a CLEAN component. The spectrum which results after subtracting the spectral window is also stored in a residual file. This procedure is repeated for a given number of deconvolutions (peaks). A gaussian representation of the spectral window is then convolved with each CLEAN spectra. Finally, in

order to preserve the noise which existed in the original spectrum, the residual values are added back to the convolved CLEAN components giving the CLEAN spectrum. The input parameters for the CLEAN algorithm include the number of CLEANs to be performed (peaks) and the gain. It is the gain which governs the percentage of the spectral window which is removed from the dirty spectrum during each CLEAN iteration.

The CLEAN procedure is used to improve the strongest features of a spectrum and is of limited use in data which may have a small signal-to-noise ratio. In fact, experience has shown that over-CLEANing data can actually introduce spurious features in the clean spectrum. Figures 3-1 to 3-6 are used to demonstrate the hazards that can result from the improper use of this algorithm. Figures 3-1 and 3-2 represent the spectral window, and the dirty spectrum, respectively, for a sample data set. Figures 3-3 to 3-6 represent the clean spectra after 10, 100, 500, and 1000 iterations of CLEAN. It is quite clear from these graphs that the peak at $\nu = 40$ (cycles per day) in Figure 3-3 decreases in strength as the number of CLEANs increases, while the peak at $\nu = 235 d^{-1}$ gets progressively stronger. In fact, in Figure 3-6 this is the only peak which remains in the spectrum with considerable amplitude. It is likely that a misinterpretation of the data would result in this type of over-application. In this study, care has been

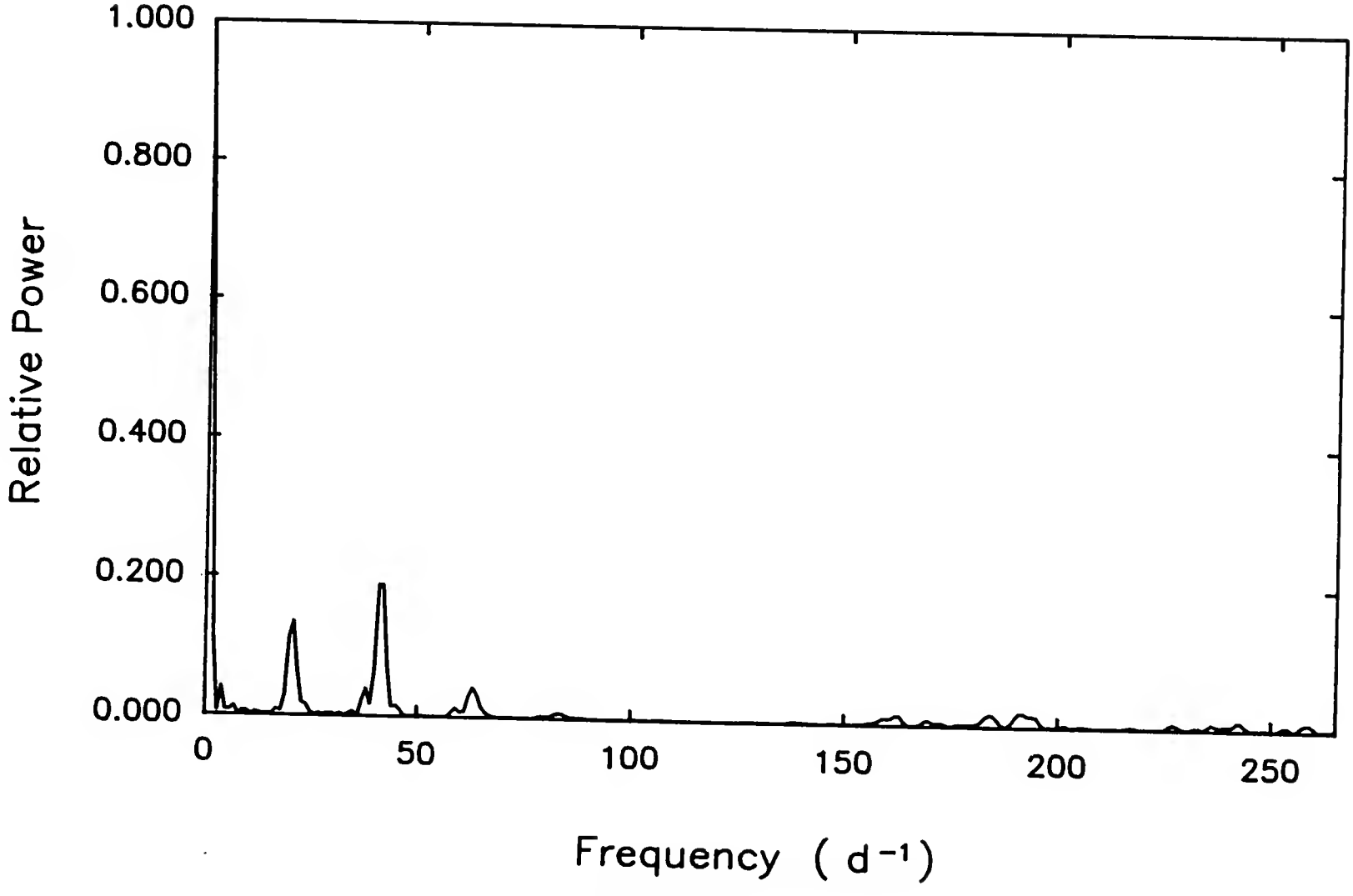

Figure 3-1 Spectral window function for the test data set.

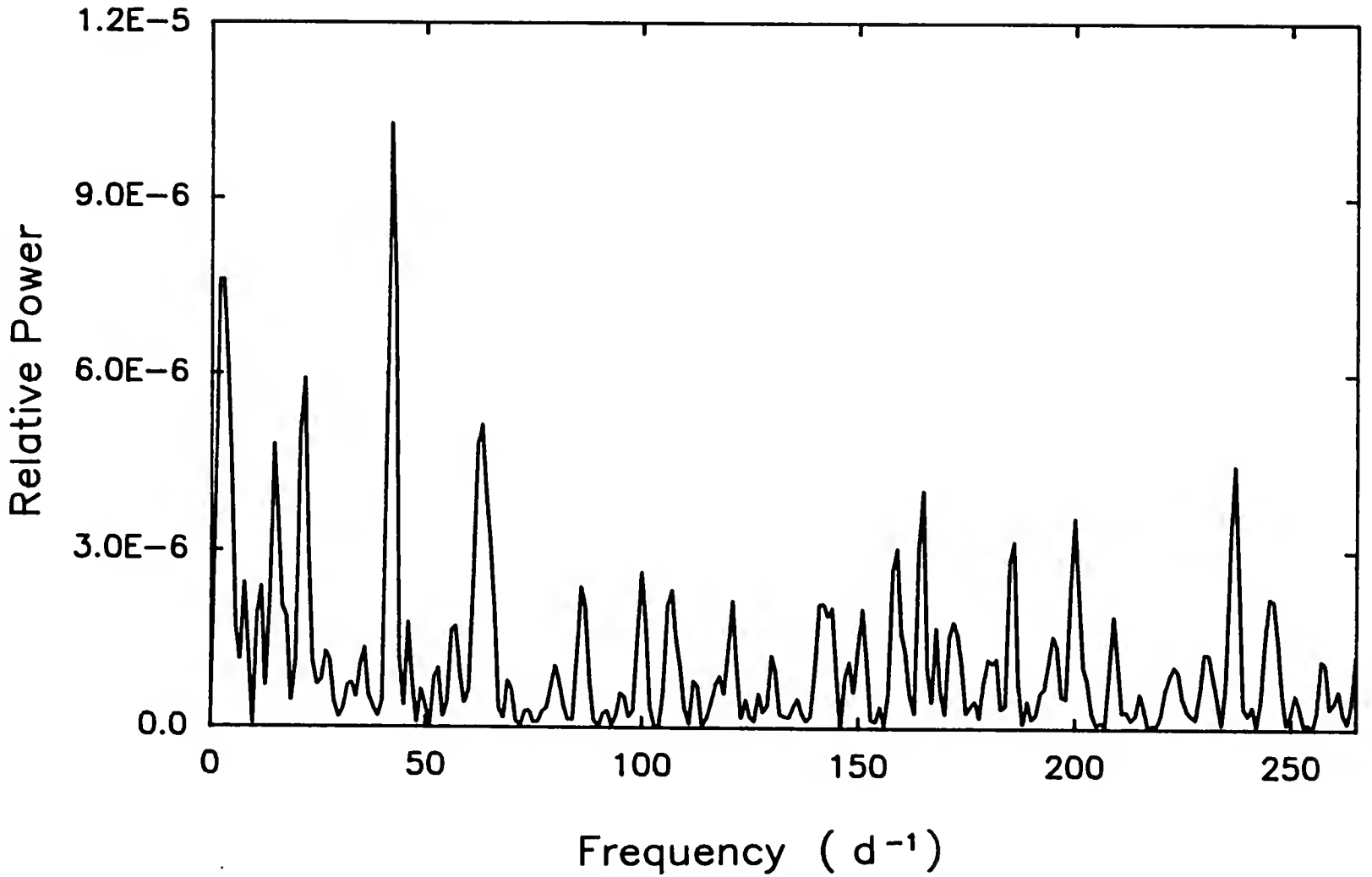

Figure 3-2 Power spectrum for the test data set before execution of the clean algorithm.

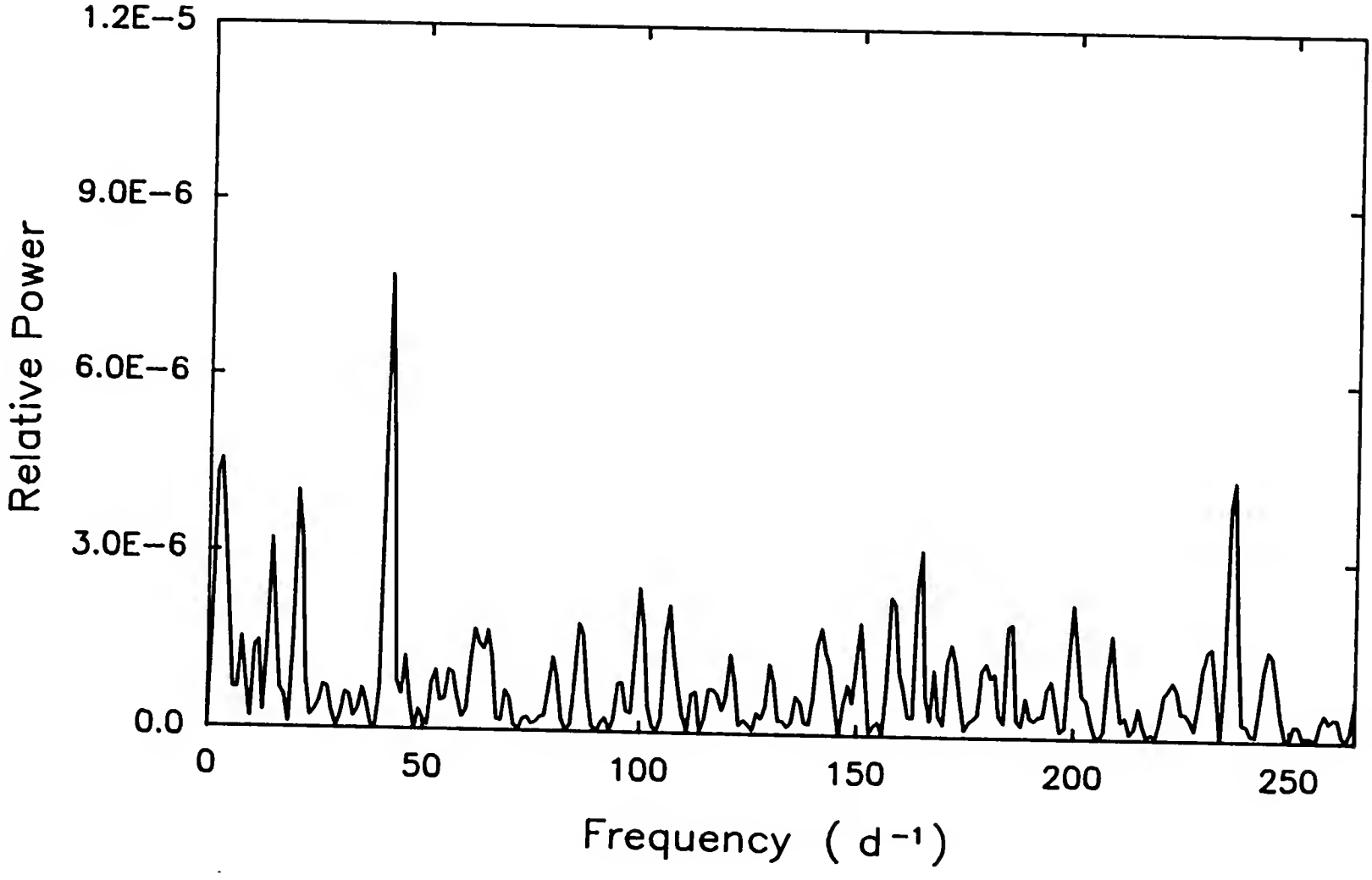

Figure 3-3 Power spectrum for the test data set after 10 iterations of the clean algorithm.

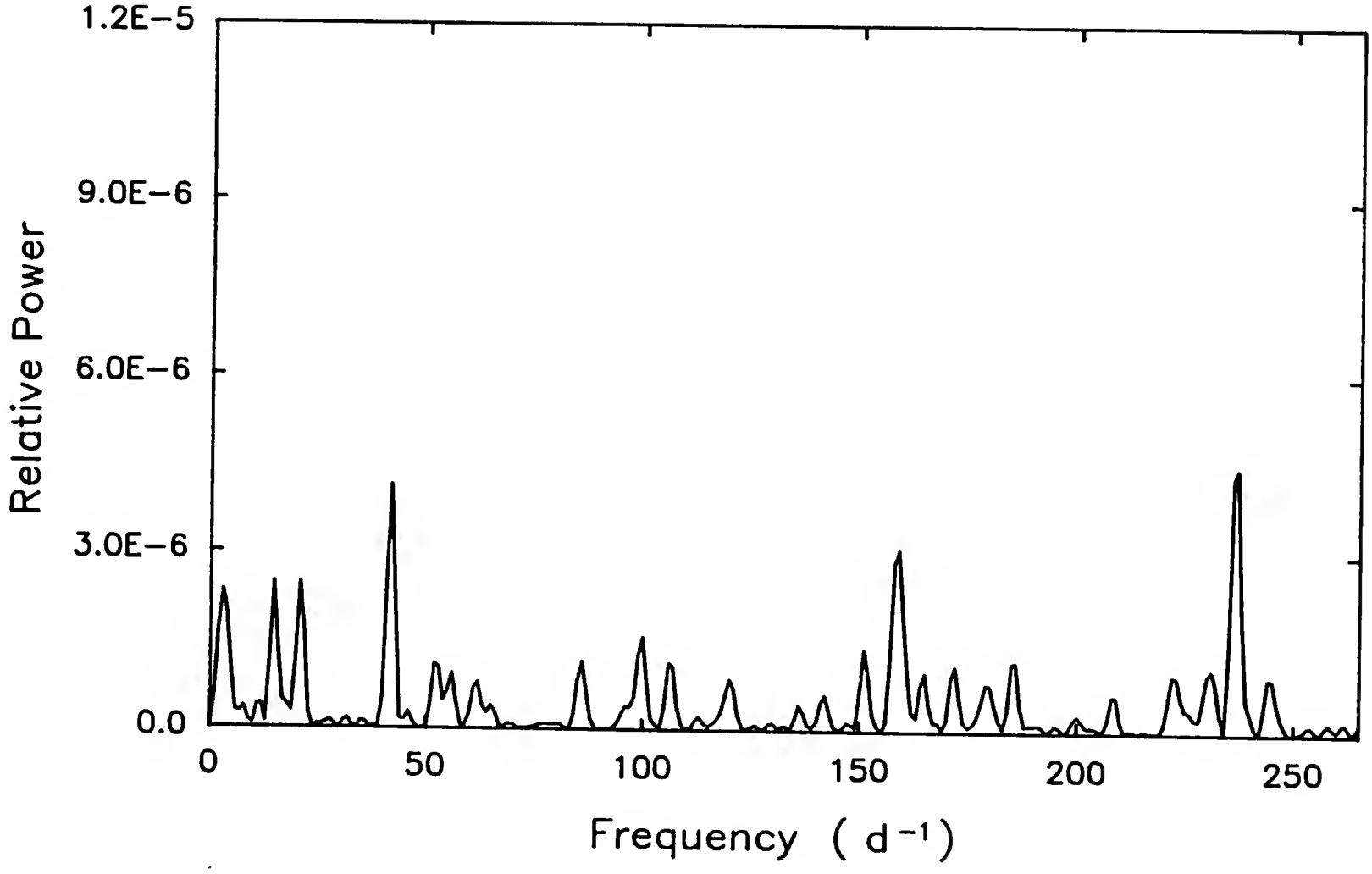

Figure 3-4 Power spectrum for the test data set after 100 iterations of the clean algorithm.

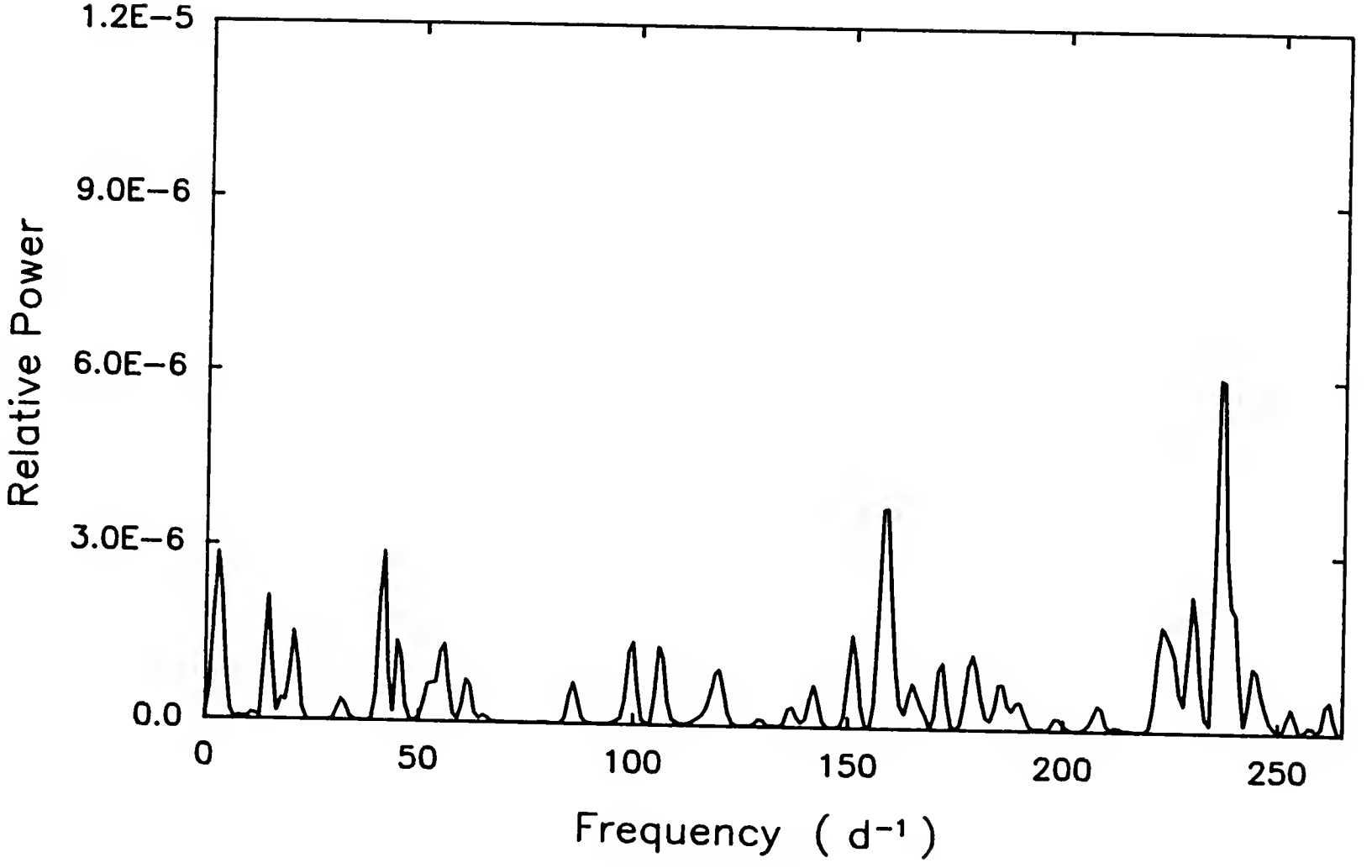

Figure 3-5 Power spectrum for the test data set after 500 iterations of the clean algorithm.

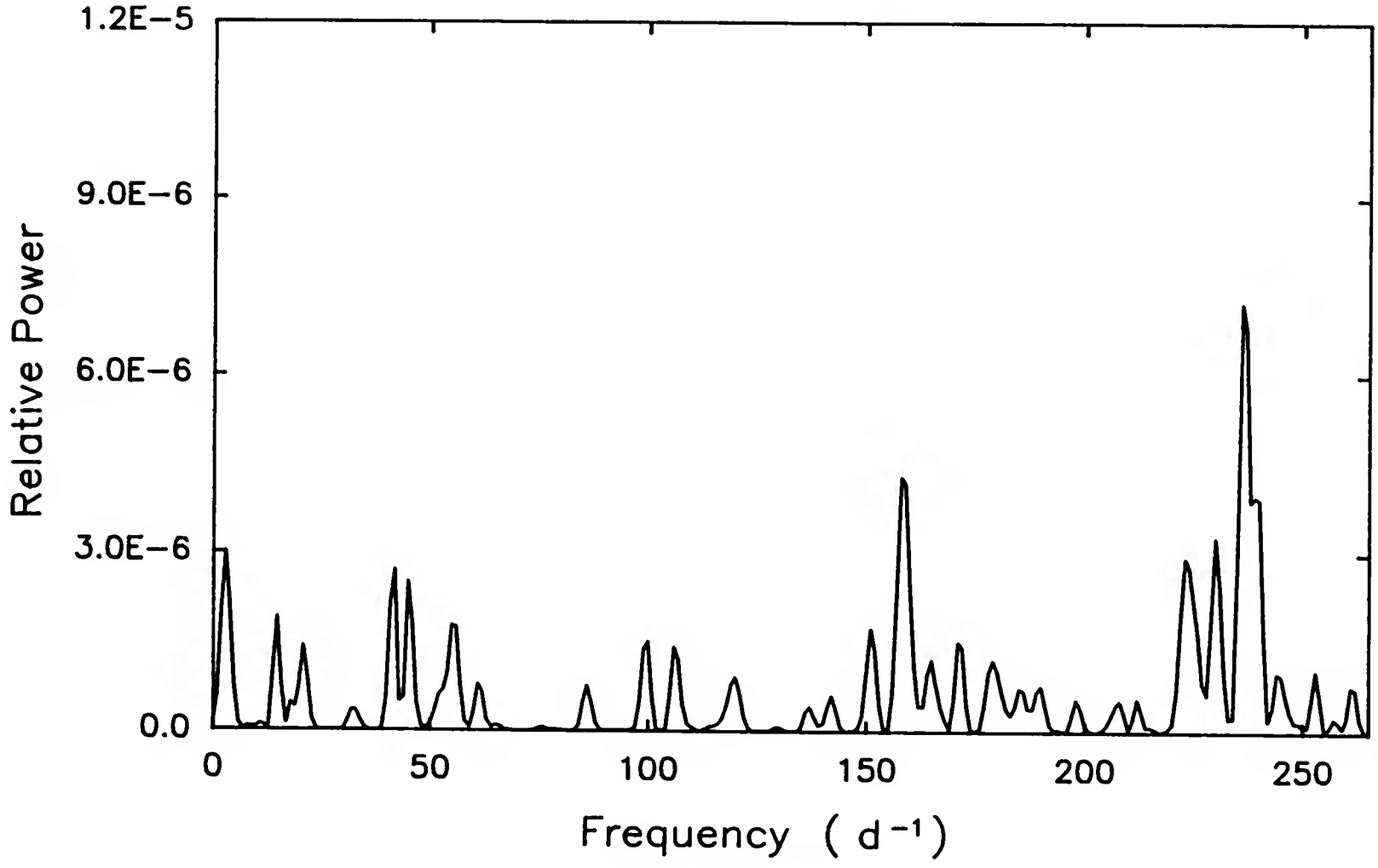

Figure 3-6 Power spectrum for the test data set after 1000 iterations of the clean algorithm.

taken to minimize the introduction of such spurious features into the power spectrum. This has been accomplished by restricting the CLEAN procedure to data above the $3\sigma_N$ level. In addition, more stability is provided in the CLEAN algorithm through use of a smaller gain size and more iterations. In our case, a gain parameter of 0.25 was adopted.

Because of the possible uncertainties of the power spectrum analysis, an independent method of period determination was also used. This method is based on fitting models to the data with the aid of the method of least-squares. The intensity variations which may exist in the γ^2 Vel system are probably much more complex than that which can be described as a simple cosine or sine function. However, the main purpose of this research is to use the long, continuous observational runs of γ^2 Vel to establish whether variations in the strengths of the HeII and CIII emission lines do, in fact, occur. It is not necessarily our purpose to mathematically describe such variability precisely. A shift in phase could certainly cause a poor fit to the data. In any event, the variations which would exist in such a complicated system are probably aperiodic at best. So, for purposes of this investigation, a first-order sine function of the following form is assumed:

$$D(t_i) = A_0 + A_1 * \sin\left(\frac{t_i - t_0}{P}\right). \qquad (3\text{-}16)$$

In equation (3-16), $D(t_i)$ represents the calculated deflection at time t_i, A_0 is the baseline in intensity units, A_1 is the amplitude of the sine wave expressed in intensity units, t_0 is the "phase" or time of maximum, and P is the period. It should be noted at this point that P is expressed in days divided by 2π radians, a representation that was chosen so that when one complete cycle had elapsed, that is, $t_i - t_0 = P$, then $\cos (t_i - t_0)/P = 1$. In the least-squares procedure, four parameters are adjusted. They are: A_0, A_1, t_0, and P. A first-order Taylor expansion is computed using the partial derivatives of equation (3-16) with respect to each of these variables. The routine used in this context is that of Banachiewicz (1942) and uses Cracovian calculus. If the errors which were calculated in the least-squares routine exceed the convergence criteria, corrections are computed and added to A_0, A_1, t_0, and P to give the new quantities:

$A_0 + \Delta A_0$,

$A_1 + \Delta A_1$,

$t_0 + \Delta t_0$, and

$P + \Delta P$.

The convergence criteria are the following:

$E(A_0) < 1 \times 10^{-3}$,

$E(A_1) < 1 \times 10^{-3}$,

$E(t_0) < 5 \times 10^{-3}$, and

$E(P) < 5 \times 10^{-4}$.

In these relations, E represents the difference between the new and old values for each quantity considered.

If all of the parameters do not converge within 30 iterations, it is assumed that a satisfactory model could not be found within the given input parameters. In the case of the HeII photometry, an initial intensity-amplitude of 0.01 and a baseline of 0.35 were used. For the CIII data, an amplitude of 0.01 and a baseline of 0.10 were used as initial inputs. These two parameters were not as sensitive to small variations as were the period and phase. To account for the increased sensitivity in P, an initial and final period were entered along with a desired incremental step value. Upper and lower limits on the period assumed two samples per cycle in accordance with the Fourier transform analysis. To account for increased sensitivity (to small perturbations) in the phase parameter, a similar approach is adopted. That is, a desired increment in the phase is entered as an input parameter. In every case, the time of the first observation was used as an initial "guess" of the value for t_0. The parameter was incremented from this initial value to the initial value plus 2π.

Weather reports are recorded at the South Pole every six hours. Photometric data recorded between two consecutive periods of reported clear skies were used in this investigation of γ^2 Vel. In addition, since the telescope does not have the capability to monitor the star and nearby sky simultaneously, data recorded during times of auroral activity were omitted from the study. These omission criteria resulted in the selection of seven individual data sets obtained during the 1986 austral winter. Individual observations in each data set were omitted if the observation in the continuum filter and the observation in one or more of the emission line filters deviated by more than 10%. The analysis of the data sets that resulted is presented in the following chapter.

CHAPTER 4
DATA ANALYSIS

Spectral Photometry of the HeII and CIII Emission Lines

Data Set I.

This data set includes observations of γ^2 Vel that extend from JD2446577.6847 through JD2446577.7792. These (81) data-points were obtained for each of the helium, carbon, and continuum filters with an average spacing between successive readings with a given filter of $0^d.0012$. Both γ^2 Vel and HR3452, the comparison star used to reduce the blue and visual photometry, were observed. The exact sequence of observations is presented in Table 4-1. In the table, an "X" is used to indicate that an integration was accomplished with the corresponding filter listed at the top of the table.

These data were reduced to a ratio of intensities using methods described in Chapter 3. The data were first transformed into frequency space using Deeming's method of Fast Fourier Transforms and assuming a minimum of two samples per cycle. Given the data spacing of $0^d.0012$ and the 2.3 hour time interval spanned by this data, the minimum and maximum frequencies which can be retrieved from the data set with a reasonable amount of confidence, are $\nu_{min} = 11d^{-1}$ and $\nu_{max} = 417d^{-1}$. Figure 4-1 represents the sampling

Table 4-1
Observing Program 1

Star	B	V	He	C	O	Continuum
C*[1]	X	X				
CS[2]	X					
C*	X	X				
V*[3]	X	X	X	X	X	X
V*[4]	X	X	X	X	X	X
V*	X	X	X	X	X	X
V*	X	X	X	X	X	X
VS	X	X	X	X	X	X
V*			X	X	X	X
V*			X	X	X	X
V*			X	X	X	X
V*			X	X	X	X
C*	X	X				
CS	X	X				
C*	X	X				
V*			X	X	X	X
V*			X	X	X	X
V*			X	X	X	X
V*			X	X	X	X
V*	X	X	X	X	X	X
V*	X	X	X	X	X	X
V*	X	X	X	X	X	X
V*	X	X	X	X	X	X
V*			X	X	X	X
V*			X	X	X	X
V*			X	X	X	X
V*			X	X	X	X

[1] C* = comparison star
[2] CS = comparison sky
[3] V* = variable star
[4] VS = variable sky

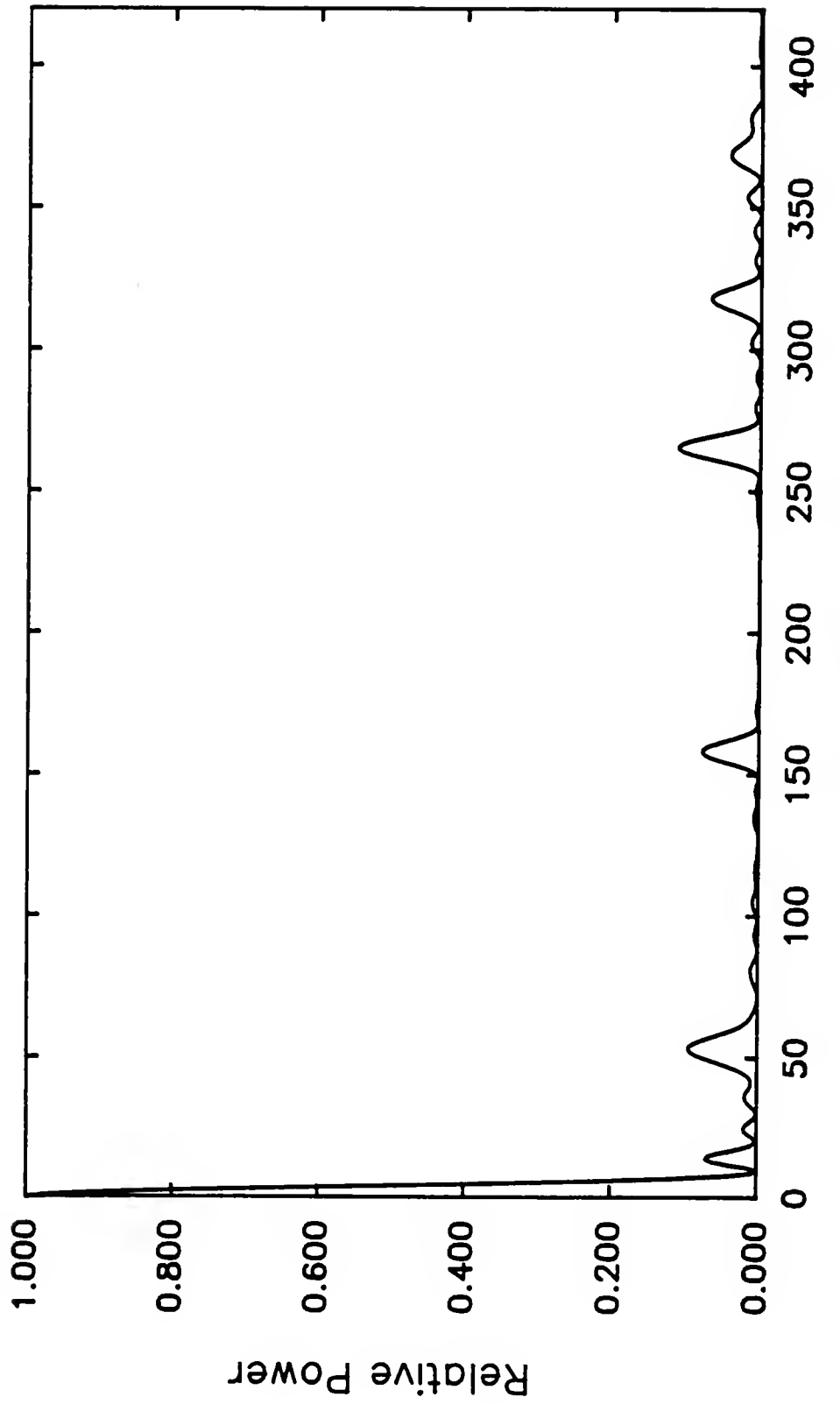

Figure 4-1 Spectral window function for data set I.

function for both the helium and the carbon observations. The peaks at ν = 52, 158, 364, and 470d^{-1} are the odd harmonics ν_1, ν_3, ν_5, and ν_7, and the peak at ν = 318d^{-1} is the even harmonic, ν_6. The convolution of the helium data with the spectral window function gives the spectrum in Figure 4-2. The noise level is denoted in the lower left-hand portion of the plot at 5.16 x 10^{-6}. All features to the right of the arrow satisfy the Nyquist criterion of a minimum of two samples per cycle. The peaks at ν = 170, 323, and 377d^{-1} represent statistically significant features at the $4\sigma_N$ level. A closer look at the spectrum reveals that the peak at ν = 377d^{-1} is part alias with that at ν = 323d^{-1} and the peak at ν = 170d^{-1} is part alias with a peak at ν = 8d^{-1}. This last feature is shown in Figure 4-2 but since it does not satisfy the Nyquist criterion, it is discarded in this study. Spurious features at or above the $3\sigma_N$ level are removed from this spectrum with a deconvolution process; the resulting power spectrum is depicted in Figure 4-3. Here, we see that the peak at ν = 323d^{-1} is the only feature which remains above the $4\sigma_N$ level, at $4.25\sigma_N$. This frequency corresponds to a period of 4.5 minutes. According to the least-squares routine, the best fit to the data, within the limitations of the Nyquist criterion, occurs for P = 4.4 minutes, and is described by:

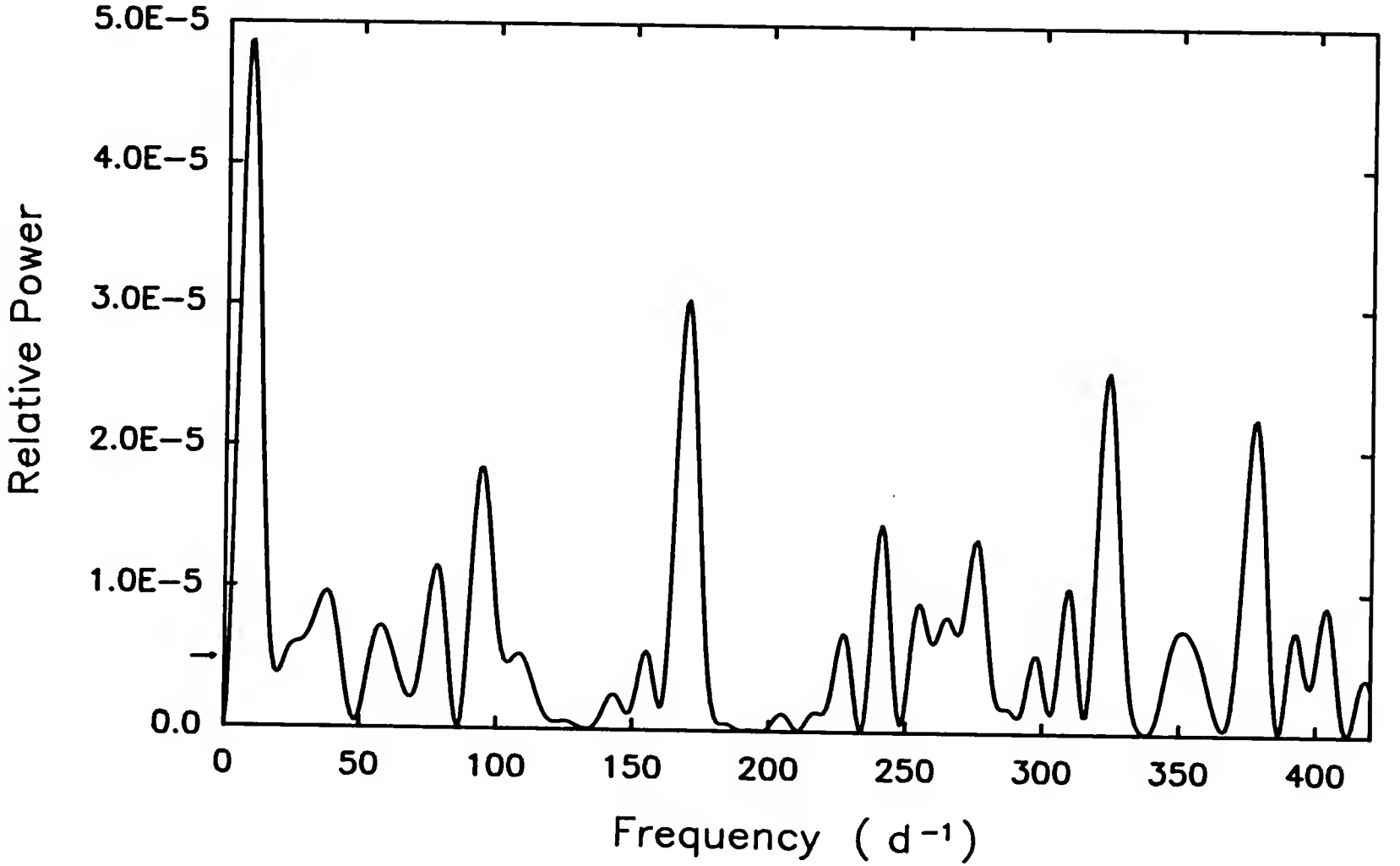

Figure 4-2 Power spectrum for the helium observations of data set I before execution of the clean algorithm.

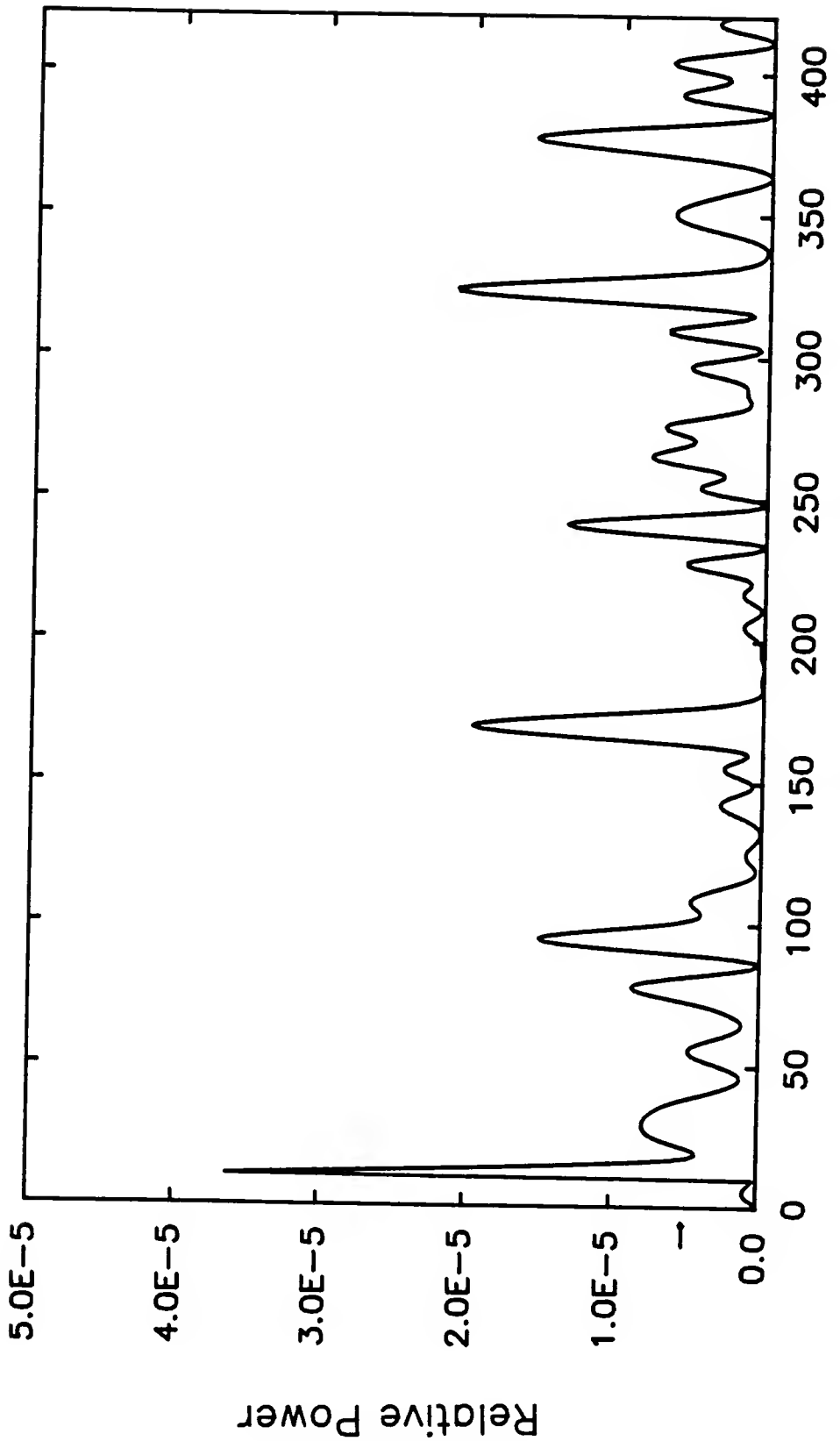

Figure 4-3 Power spectrum for the helium observations of data set I after execution of the clean algorithm.

$$D(t_i) = 0.35099 + 0.00813 * \sin\left(\frac{t_i - 0.18518}{0.00049}\right). \qquad (4\text{-}1)$$

The model computed from this equation is presented in Figure 4-4 and seems to fit the observations quite well. However, because there are only an average of 2.5 points per cycle, one should regard this result with some skepticism. A visual inspection of a plot of intensity as a function of time indicates that perhaps the data are changing at a more gradual rate. The least-squares routine was executed for periods on the order of the time interval spanned by the data set; convergence occurred for a period of 2.40 hours. The model, given by

$$D(t_i) = 0.34986 + 0.00724 * \sin\left(\frac{t_i - 0.10507}{0.01592}\right), \qquad (4\text{-}2)$$

is graphically presented in Figure 4-5. The amplitude of the variation of this model is only slightly lower than that for the more rapid fluctuations depicted in Figure 4-4.

The power spectrum for the carbon data obtained in this time interval is shown in Figure 4-6. Again, the arrow in the lower left of the plot represents the noise level at 1.287×10^{-6}. It should be noted that the peak at $\nu = 70d^{-1}$ is part alias with that at $\nu = 20d^{-1}$ and should, in principle, be removed with the CLEAN algorithm (Figure 4-7).

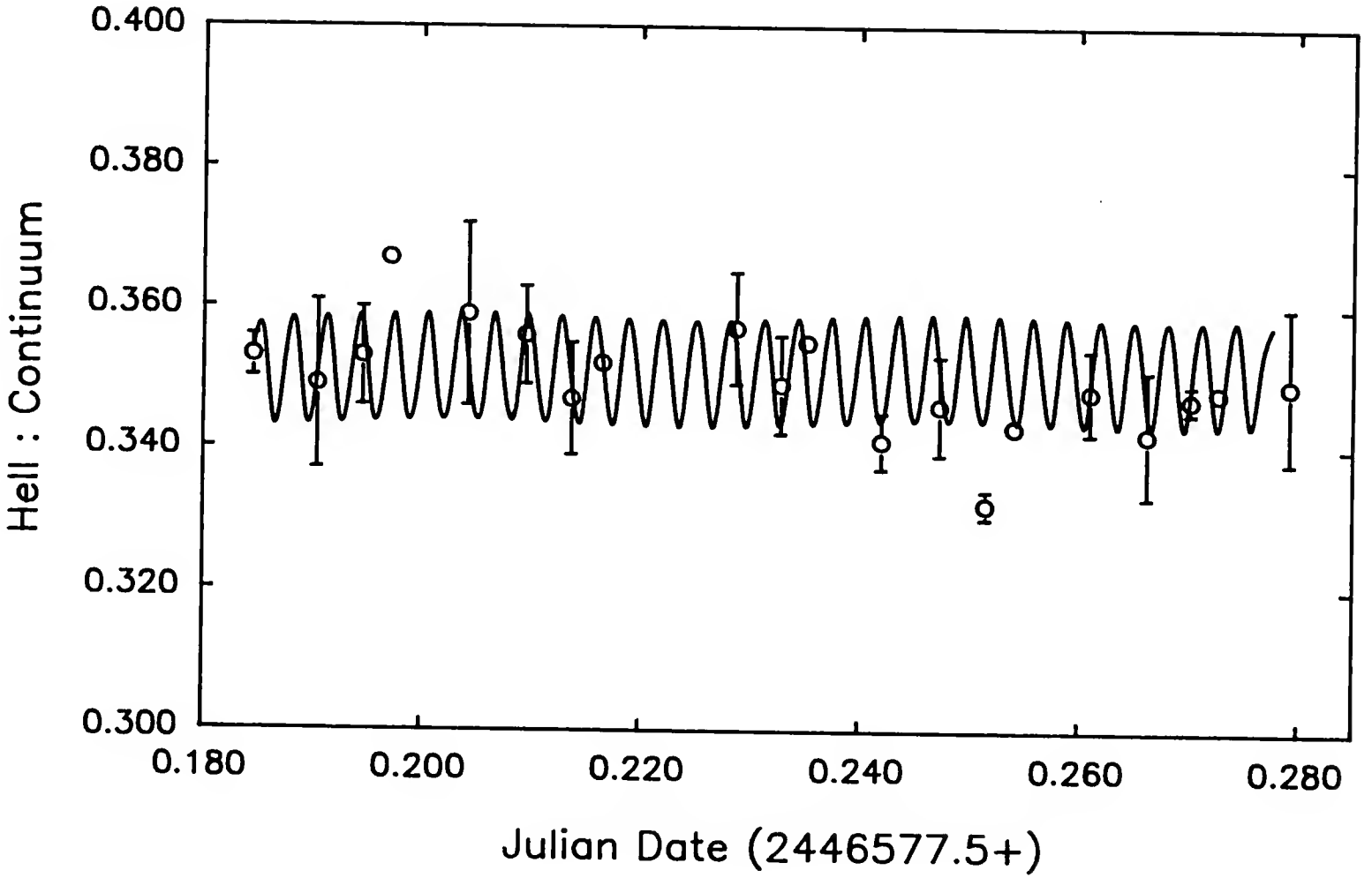

Figure 4-4 Model of the variations of the helium data for data set I with P = 4.43 minutes. Each plotted point represents the average intensity within a $0^d.0040$ interval.

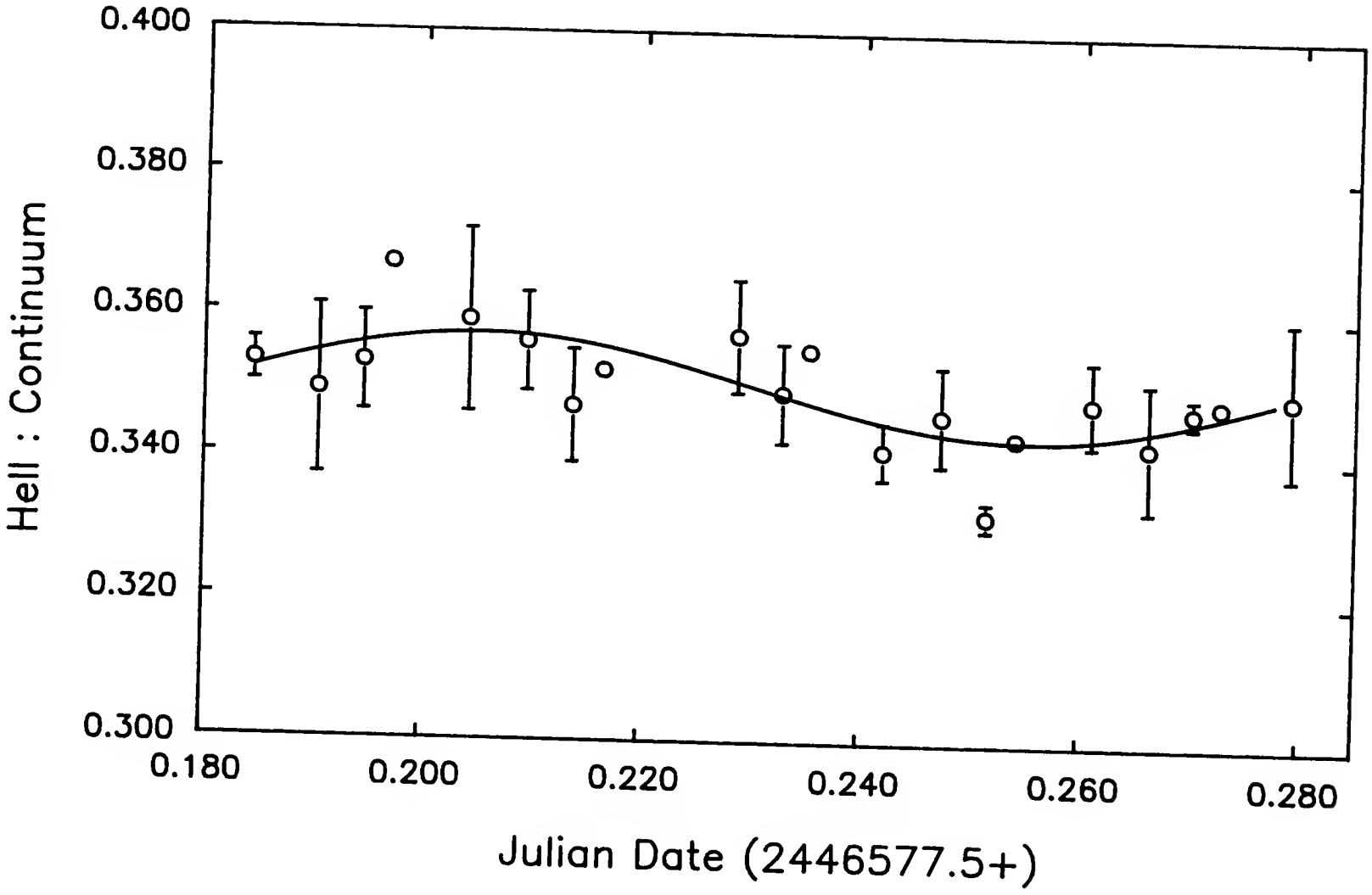

Figure 4-5 Model of the variations of the helium data for data set I with P = 2.40 hours. Each plotted point represents the average intensity within a $0^{d}.0040$ interval.

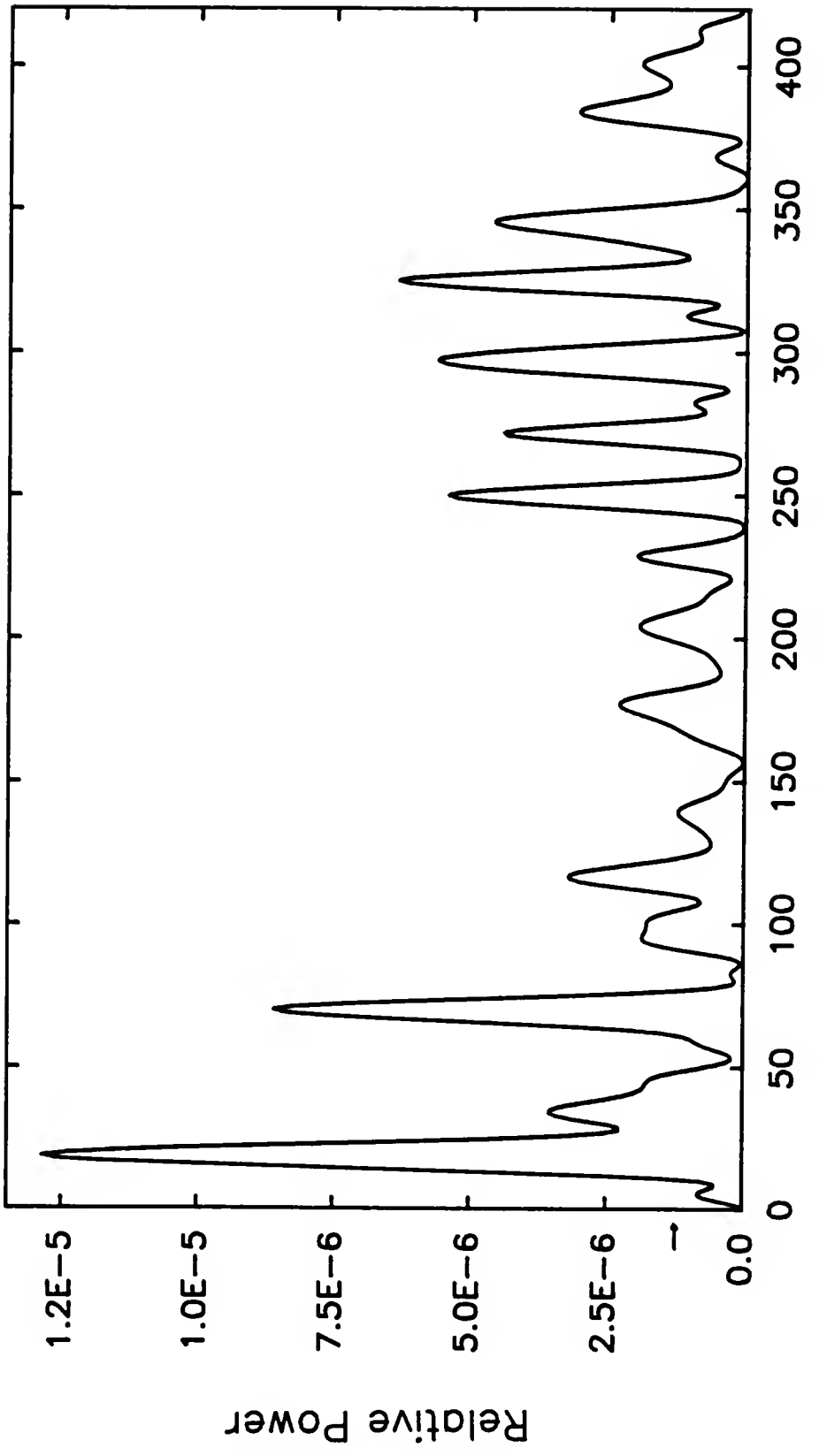

Figure 4-6 Power spectrum for the carbon observations of data set I before execution of the clean algorithm.

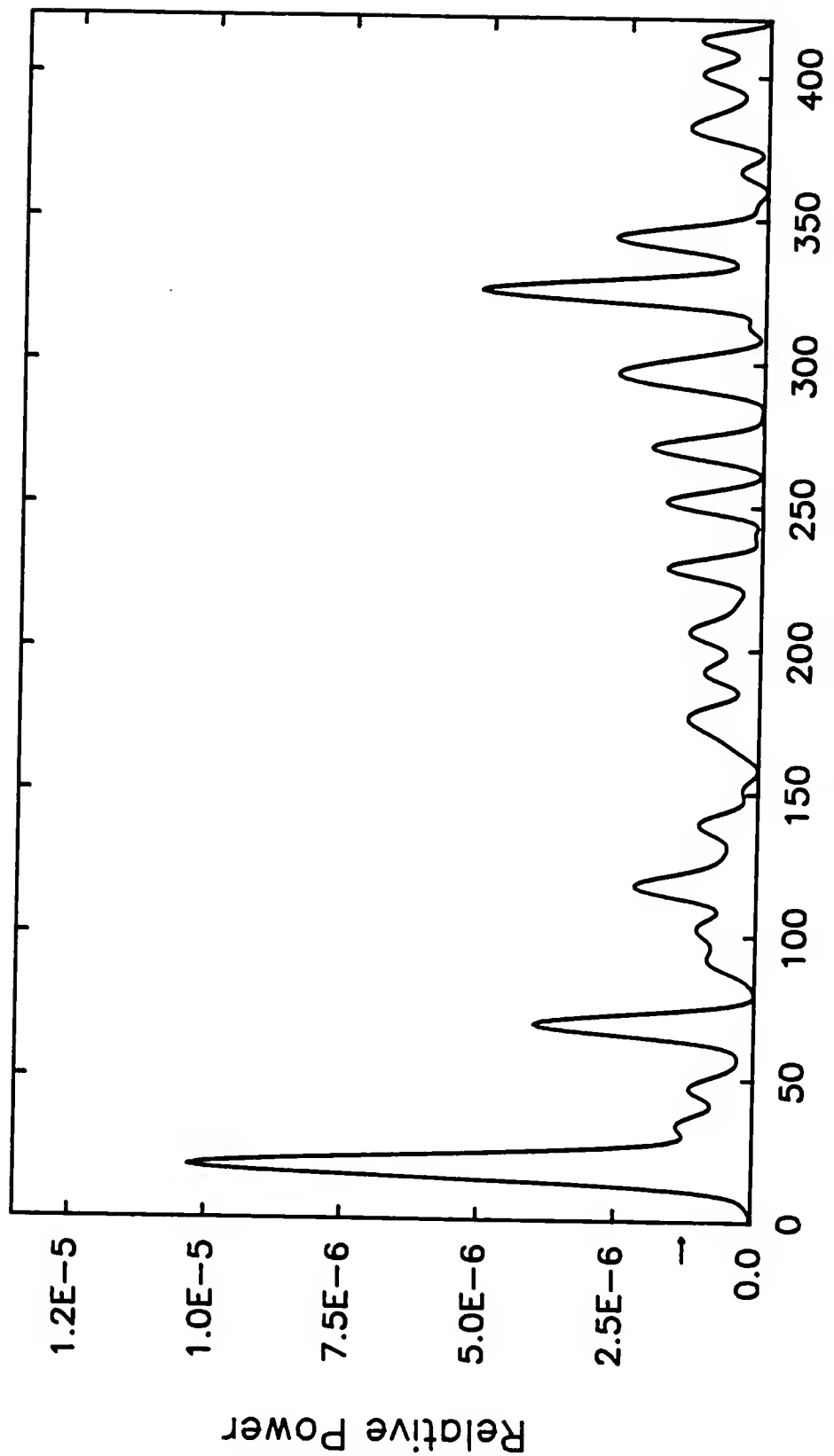

Figure 4-7 Power spectrum for the carbon observations of data set I after execution of the clean algorithm.

This is indeed the case, and the only peak which survives the CLEANing process is that at $\nu = 20d^{-1}$ corresponding to $0^d.050$ (1.20 hours). The signal-to-noise ratio for this peak is quite large at $8.04\sigma_N$. The least-squares routine converges to a set of quantites with a similar period, $P = 0^d.0459$ (1.10 hours), according to the following relation:

$$D(t_i) = 0.11117 + 0.00231 * \sin\left(\frac{t_i - 0.45362}{0.00731}\right). \qquad (4\text{-}3)$$

The fit to the data using equation (4-3) is presented in Figure 4-8. Although the amplitude is quite low, this period may be considered as a satisfactory representation to the fluctuations since both the power spectrum analysis and the least-squares routine give similar results.

In summary, the helium data seem to follow two different periods. The shortest period of about 4.4 minutes represents very rapid fluctuations and was arrived at by both the power spectrum analysis and the least-squares solution. In addition, models were computed for periods corresponding to the length of the data set with the best fit solution having a period of P = 2.40 hours. Both fits seem to be quite satisfactory. The intensity variations of the CIII emission line, although low in amplitude, can be modeled with a period of 1.10 hours.

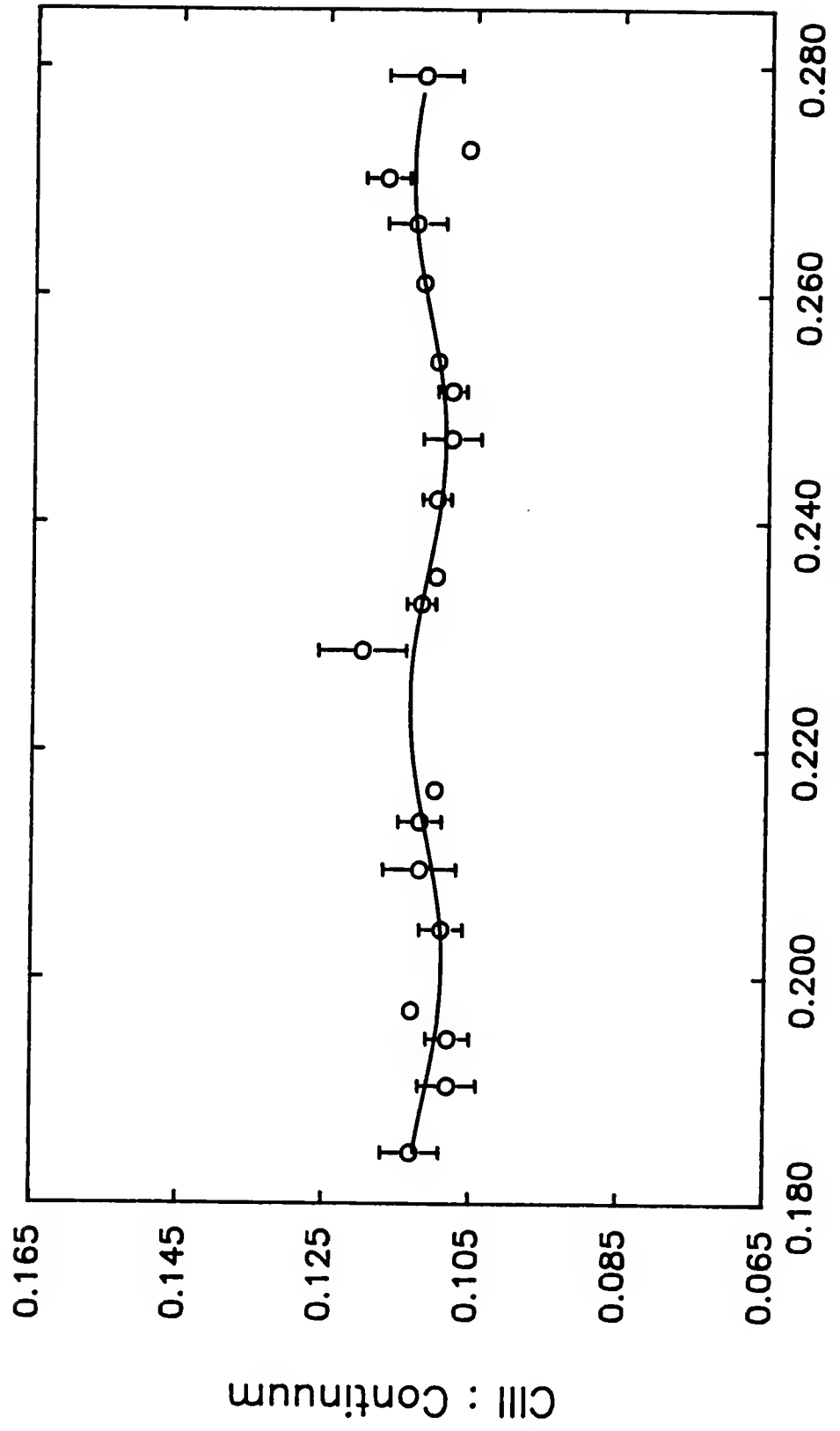

Figure 4-8 Model for the variations of the carbon data for data set I with P = 1.10 hours. Each plotted point represents the average intensity within a $0^d.0040$ interval.

Data Set II.

One-hundred and eighty-nine observations of γ^2 Vel were obtained in the helium and carbon filters using the observing sequence presented in Table 4-2. The time interval spanned by these data extends from JD2446606.6048 through JD2446606.9553. The average spacing between successive observations for a given filter is $0^d.0019$. The decrease in time-resolution of these data relative to the time-resolution of the data discussed in the previous section, is an artifact of the new observing program. As can be seen from Table 4-2, several new objects have been added to the original observing program (Table 4-1). This ultimately limits the high frequency components which are recoverable in the data analysis.

The spectral window for these data is given in Figure 4-9, and includes first, second, third, and fourth harmonics at ν = 23, 43, 64, and $84d^{-1}$, respectively. In general, as in this case, spectral windows for unequally sampled data tend to be more complex at high frequencies. The power spectrum of the helium data is computed for frequencies between $\nu_{min} = 6d^{-1}$ and $\nu_{max} = 265d^{-1}$ (Figure 4-10). The noise level in this figure is denoted in the lower left-hand portion of this plot at 9.976×10^{-7}. Given this level of noise, the peaks at ν = 16, 22, 42, and $218d^{-1}$ might be classified as statistically significant. However, when one superimposes the spectral window on the power spectrum, it

Table 4-2
Observing Program 2

Star	B	V	He	C	O	Continuum
V*[1]	X	X	X	X	X	X
V*	X	X	X	X	X	X
V*	X	X	X	X	X	X
V*	X	X	X	X	X	X
V*			X	X	X	X
V*			X	X	X	X
V*			X	X	X	X
V*			X	X	X	X
VS[2]	X	X	X	X	X	X
V*			X	X	X	X
V*			X	X	X	X
V*			X	X	X	X
V*			X	X	X	X
V*	X	X	X	X	X	X
V*	X	X	X	X	X	X
V*	X	X	X	X	X	X
V*	X	X	X	X	X	X
C*[3]	X	X				
CS[4]	X	X				
C*	X	X				
V*	X	X	X	X	X	X
C*	X	X				
CS	X	X				
C*	X	X				
V*	X	X	X	X	X	X
V*	X	X	X	X	X	X
V*	X	X	X	X	X	X
V*	X	X	X	X	X	X
V*			X	X	X	X
V*			X	X	X	X
V*			X	X	X	X
V*			X	X	X	X
VS	X	X	X	X	X	X
V*			X	X	X	X
V*			X	X	X	X
V*			X	X	X	X
V*			X	X	X	X

Table 4-2--continued

Star	B	V	He	C	O	Continuum
V*	X	X	X	X	X	X
V*	X	X	X	X	X	X
V*	X	X	X	X	X	X
V*	X	X	X	X	X	X
C*	X	X				
CS	X	X				
C*	X	X				
Sky B[5]	X	X				
α Gru	X	X	X	X	X	X
α Gru S[6]	X	X	X	X	X	X
α Gru	X	X	X	X	X	X
ß Gru	X	X				
ß Gru S[7]	X	X				
ß Gru	X	X				
Sky A[8]	X	X				

[1] V* = variable star
[2] VS = variable sky
[3] C* = comparison star
[4] CS = comparison sky
[5] Sky B = 1° region of sky 180° from variable star
[6] α Gru S = α Gru sky
[7] ß Gru S = ß Gru sky
[8] Sky A = 1° region of sky 180° from Sky B

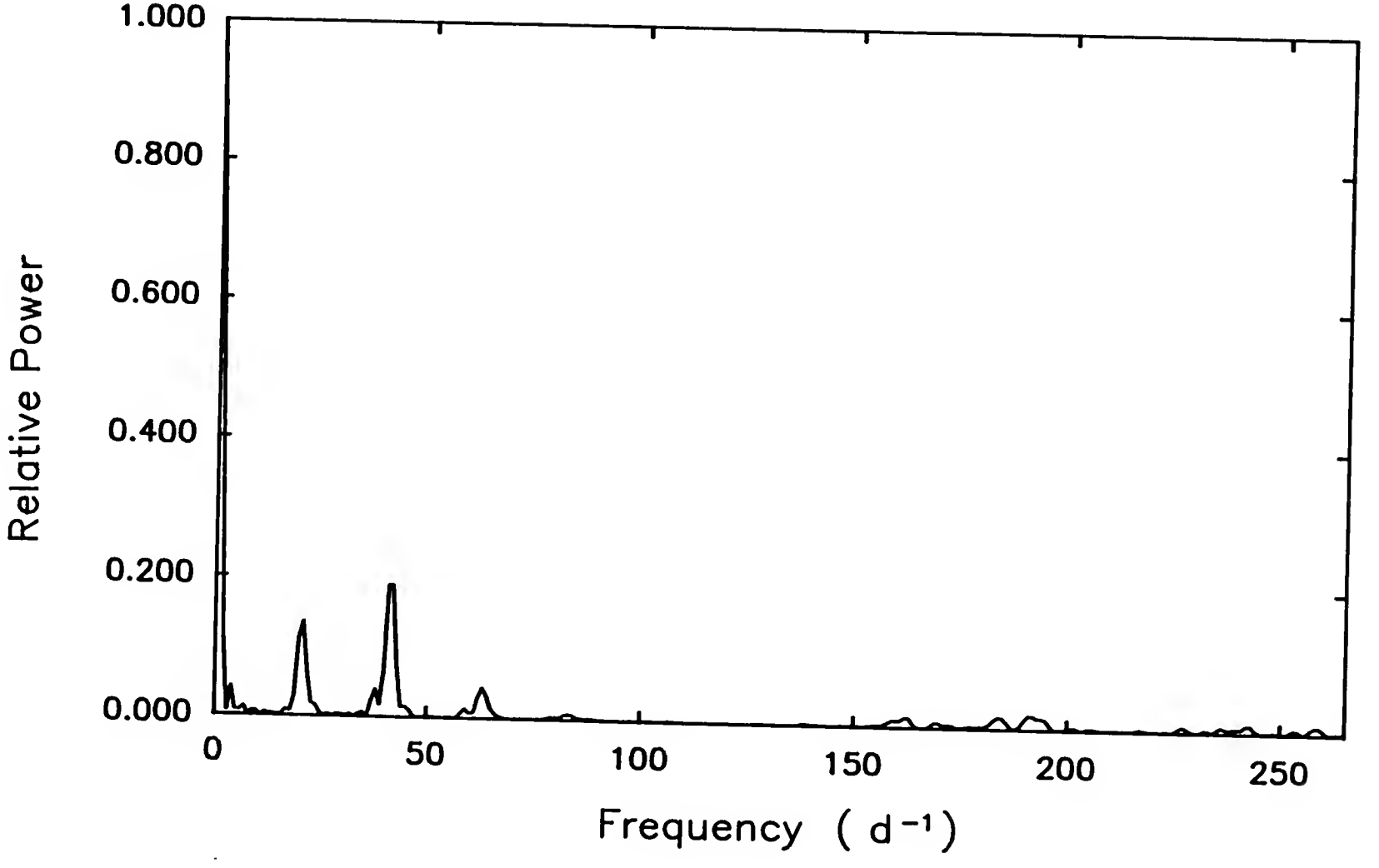

Figure 4-9 Spectral window function for data set II.

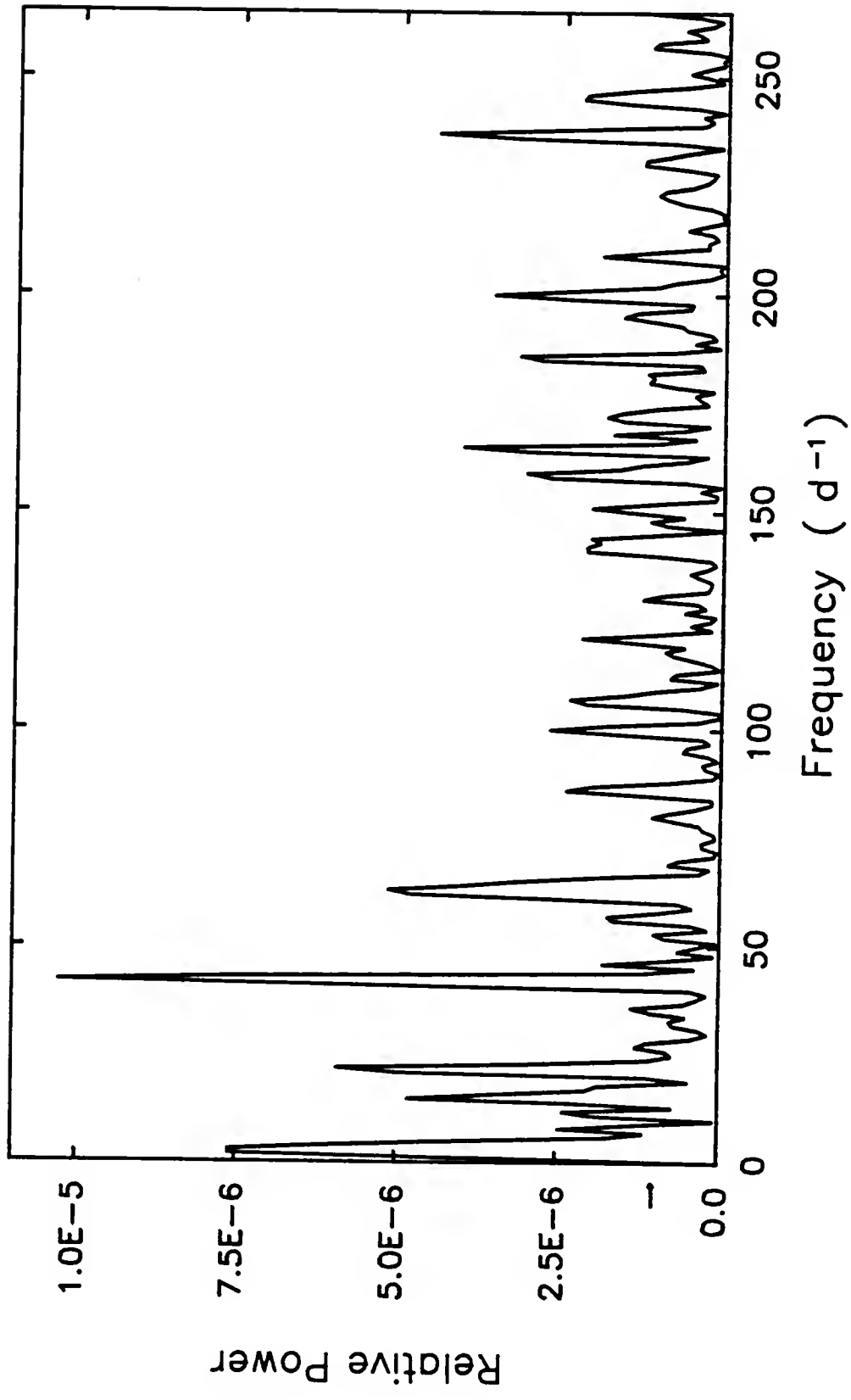

Figure 4-10 Power spectrum for the helium observations of data set II before execution of the clean algorithm.

is apparent that the peaks at $\nu = 22d^{-1}$ and $\nu = 62d^{-1}$ are part aliases of the considerably stronger peak at $\nu = 42d^{-1}$. The CLEAN algorithm has been used in an attempt to eliminate these spurious features, and the results are shown in Figure 4-11. Now, only two peaks have survived the CLEANing process while remaining statistically significant. They include the feature at $\nu = 42d^{-1}$ ($P = 0^d.0238$) with a signal-to-noise ratio of $7.7\sigma_N$ and the feature at $\nu = 238d^{-1}$ ($P = 0^d.0042$) which has a weaker signal of $4.5\sigma_N$.

Although the least-squares routine converges for periods corresponding to each of these frequencies, the largest amplitude of variation and the lowest observed minus calculated (O-C) residuals occurs for $P = 0^d.0476$ ($\nu = 21d^{-1}$). It is interesting to note that this period is exactly twice the period concluded from the power spectrum analysis and perhaps this is an indication of the presence of harmonics of a fundamental period. In order to determine whether or not one of these periods fits the data more satisfactorily than another, models are computed for each. Results indicate that these data are most adequately represented by $P = 0^d.0476$ (Figure 4-12) according to the equation

$$D(t_i) = 0.34430 + 0.00379 * \sin\left(\frac{t_i - 0.48459}{0.00757}\right). \qquad (4\text{-}4)$$

Perhaps this period reflects the fundamental mode of

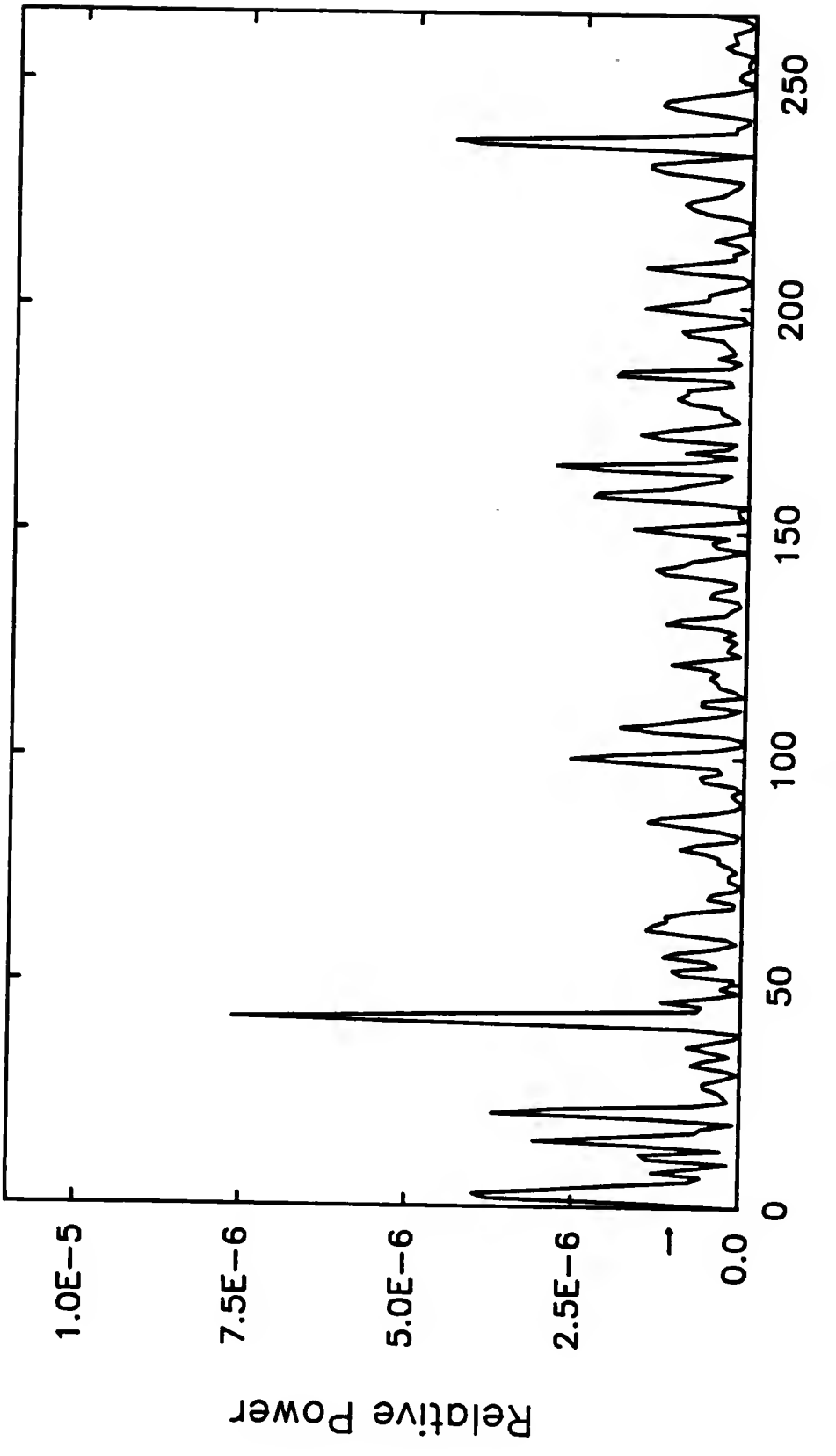

Figure 4-11 Power spectrum for the helium observations of data set II after execution of the clean algorithm.

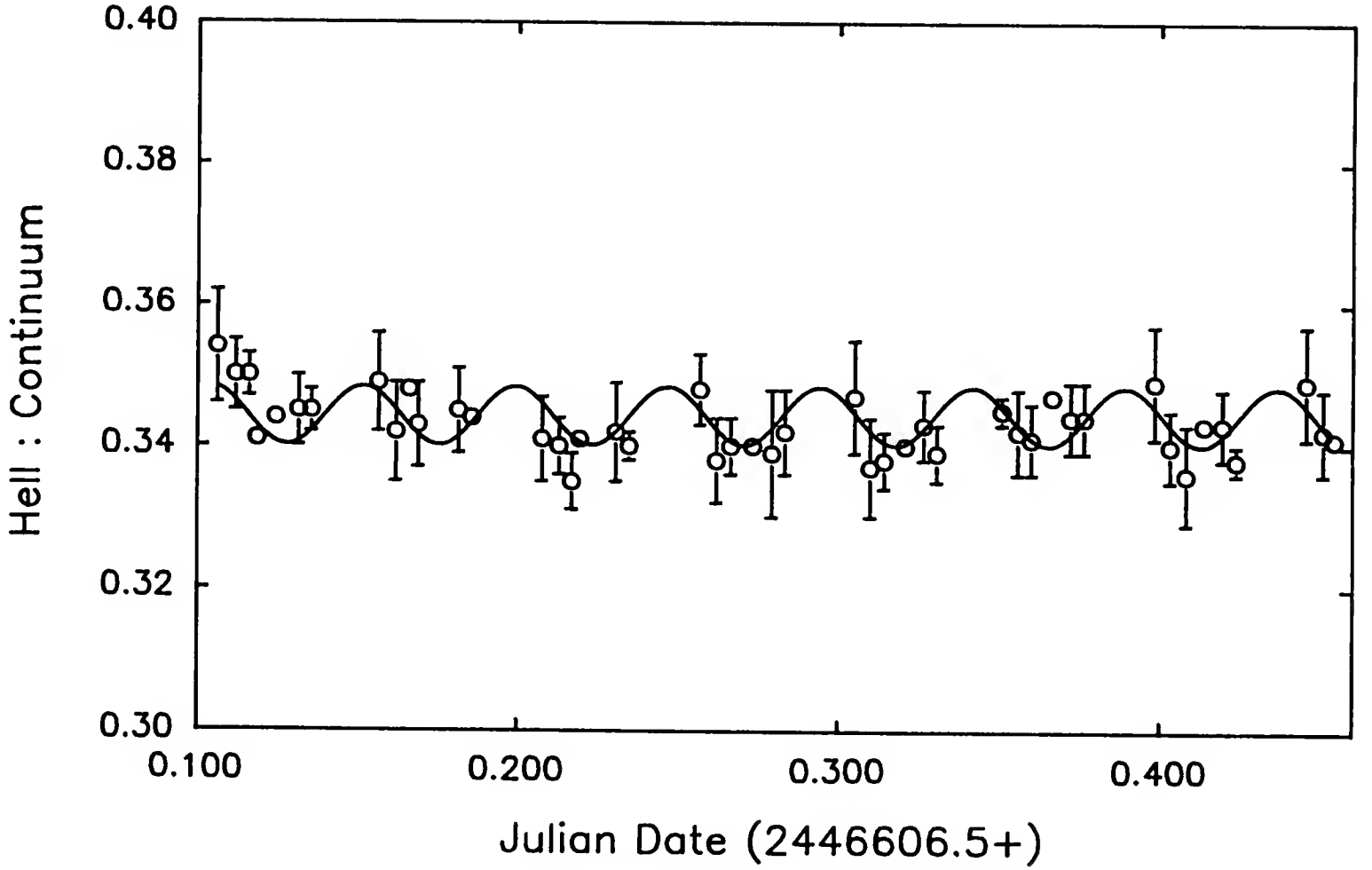

Figure 4-12 Model for the variations of the helium data for data set II with P = 1.14 hours. Each plotted point represents the average intensity within a $0^{d}.0040$ interval.

variation while the prominent feature in the power spectrum may represent the first harmonic. The carbon data have also been analyzed in a manner comparable to that used in the analysis of the helium data. The dirty and clean spectrums are presented in Figures 4-13 and 4-14, respectively. Although the feature at $\nu = 42d^{-1}$ is considerably weaker than the corresponding peak in the power spectrum for the helium data, it still remains the strongest feature in the plot at $5.8\sigma_N$ where $\sigma_N = 1.680 \times 10^{-7}$. Three other peaks rise just above the $4\sigma_N$ level; they occur at $\nu = 12$, 57, and $204d^{-1}$.

The least-squares routine is executed for periods ranging between $0^d.0038$ ($\nu = 263d^{-1}$) and $0^d.1759$ ($\nu = 6d^{-1}$). Solutions with periods corresponding to each of the frequencies, found from the power spectrum analysis, result. Once again, the strongest convergence occurs for a period of $0^d.0477$ ($\nu = 21d^{-1}$). One must realize that in all of these models, the amplitude of variation of the CIII emission line is so small that results cannot be considered to represent significant intensity changes. The largest variation in this case is only 1% of the average deflection. It is for this reason that no specific model is suggested for this data.

In summary, power spectrum analysis gives a period of $0^d.0238$ for both helium and carbon data. The least-squares routine, although still converging for periods on this

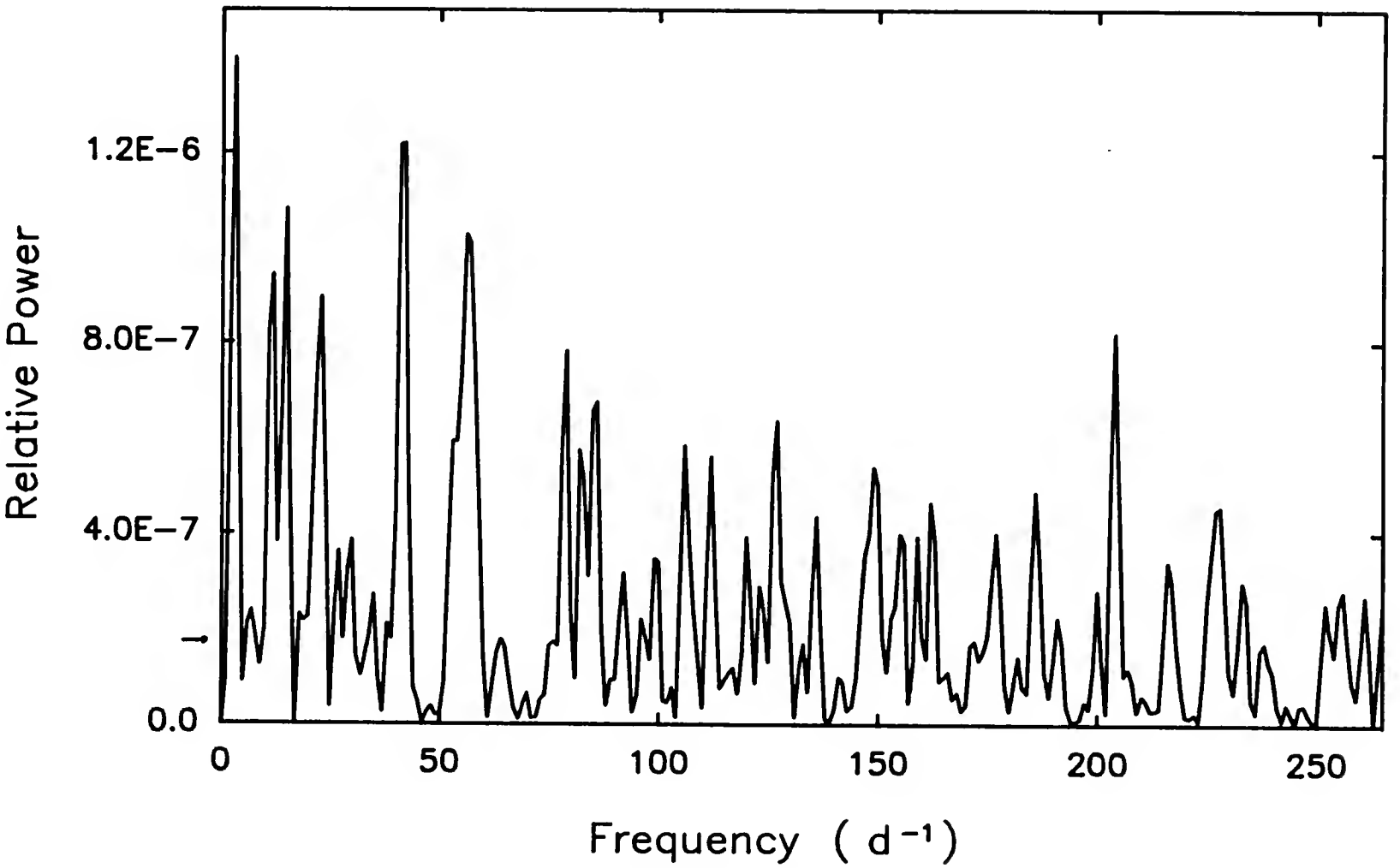

Figure 4-13 Power spectrum for the carbon observations of data set II before execution of the clean algorithm.

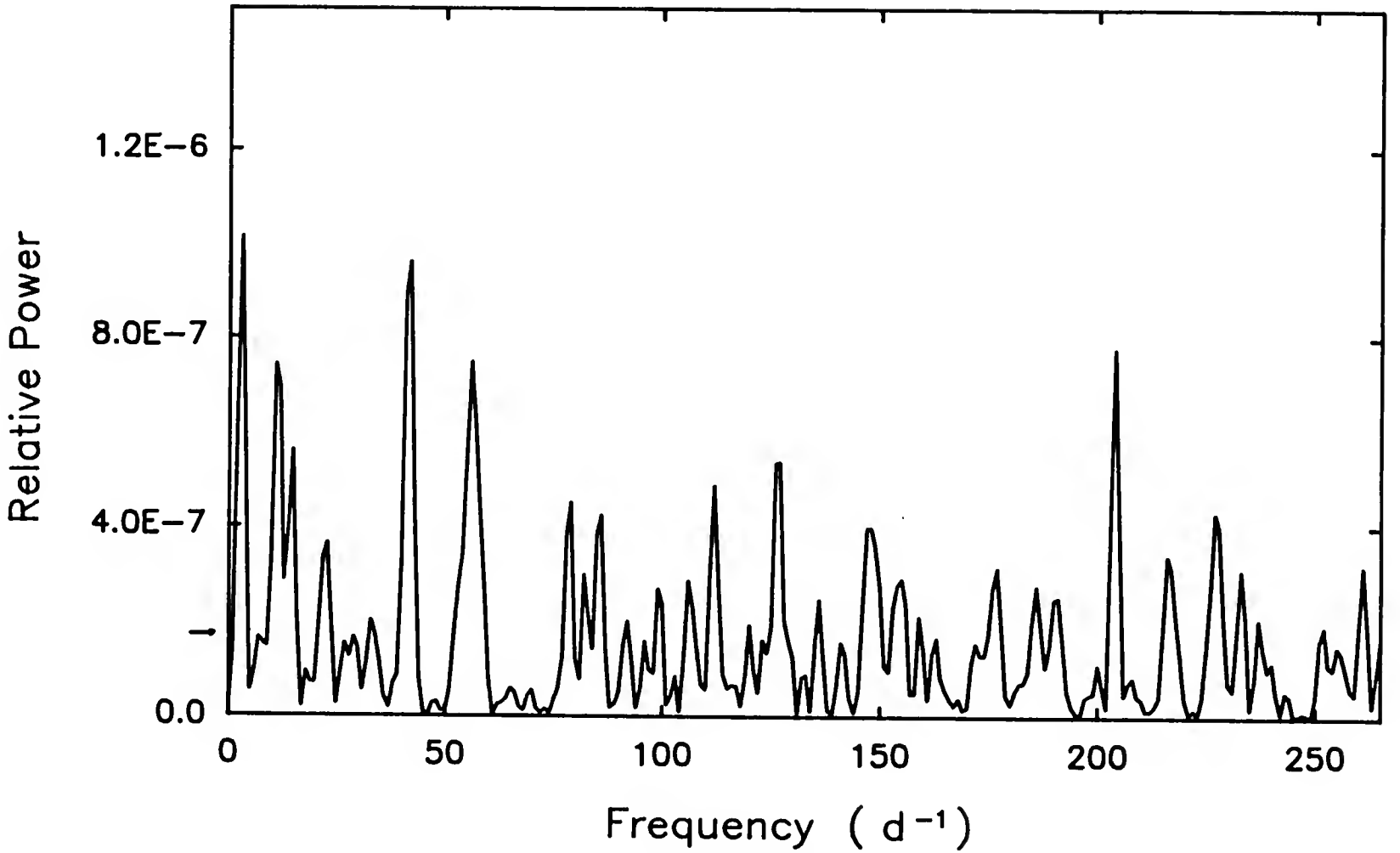

Figure 4-14 Power spectrum for the carbon observations of data set II after execution of the clean algorithm.

order, give a best-fit with a period equal to twice this period, or, P = $0^d.0476$.

Data Set III.

This data set spans the time interval that extends from JD2446607.9853 through JD2446608.1921. The set includes 90 observations of γ^2 Vel for the helium, carbon, and continuum filters.

The observing sequence used to obtain these data is that shown in Table 4-2, with $\Delta t = 0^d.0023$. Assuming a minimum of two samples per cycle and a minimum of two cycles per data set, frequencies from $\nu_{min} = 10d^{-1}$ to $\nu_{max} = 217d^{-1}$ can be tested. Figure 4-15 shows the sampling function which results from the acquisition of these data. The peak at $\nu = 20d^{-1}$ has considerable power amounting to about one-third that of the main peak at $\nu = 0d^{-1}$. The second harmonic at $\nu = 41d^{-1}$, and the third harmonic at $\nu = 62d^{-1}$ are also identified. In addition, a broad feature centered at $\nu = 33d^{-1}$ has a second harmonic at $\nu = 55d^{-1}$. The convolution of the helium data with the beam is determined and presented in Figure 4-16 in terms of relative power. The noise level of these data is indicated by an arrow at the bottom left of the plot at 2.719×10^{-6}. The features at $\nu = 11$, 73, and $215d^{-1}$ rise above the $4\sigma_N$ level, but the peak at $\nu = 73d^{-1}$ is part alias with the stronger feature at $\nu = 11d^{-1}$. The CLEANing process leaves two of the three peaks mentioned above as statistically significant (Figure 4-17). The

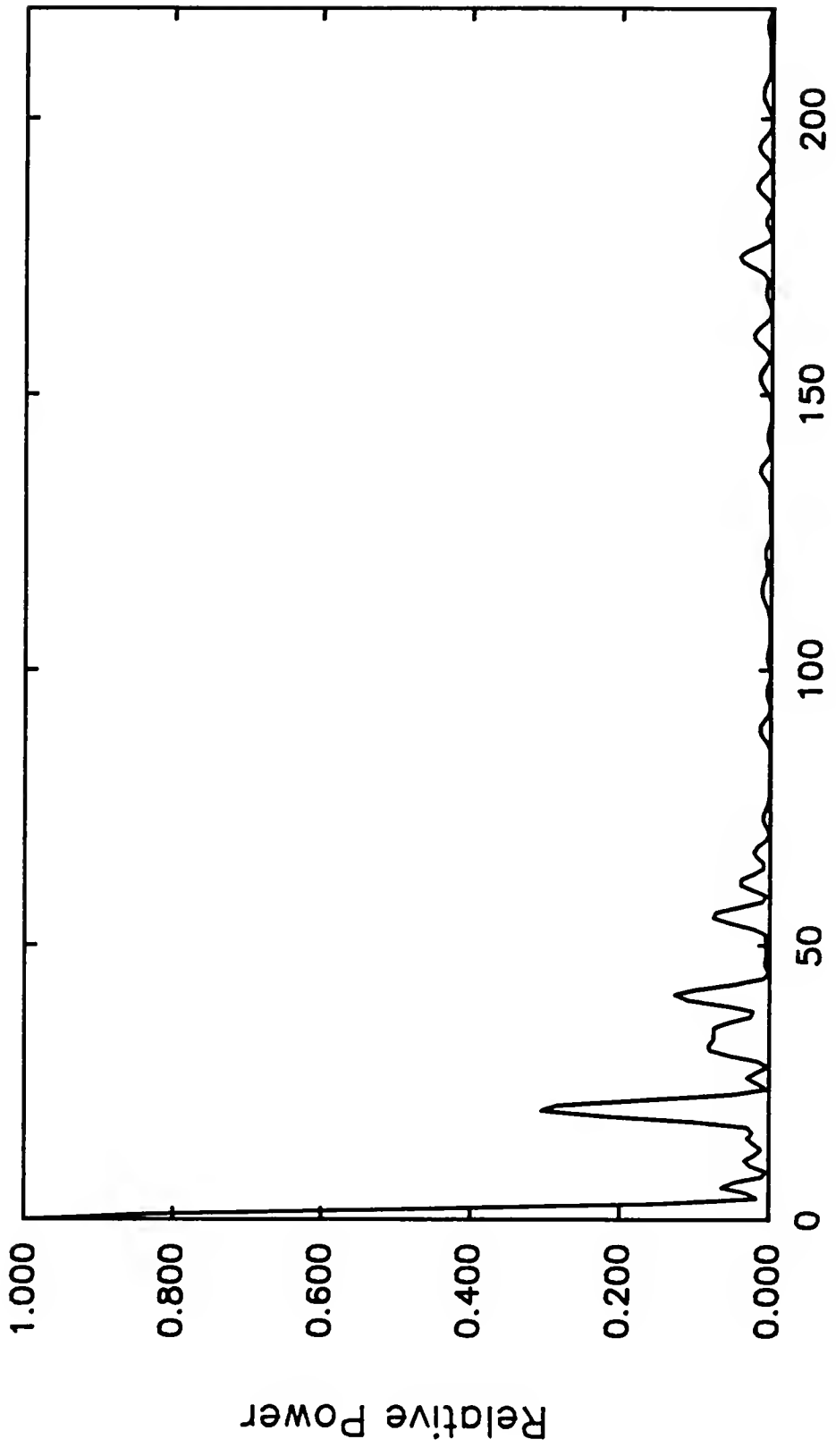

Figure 4-15 Spectral window function for data set III.

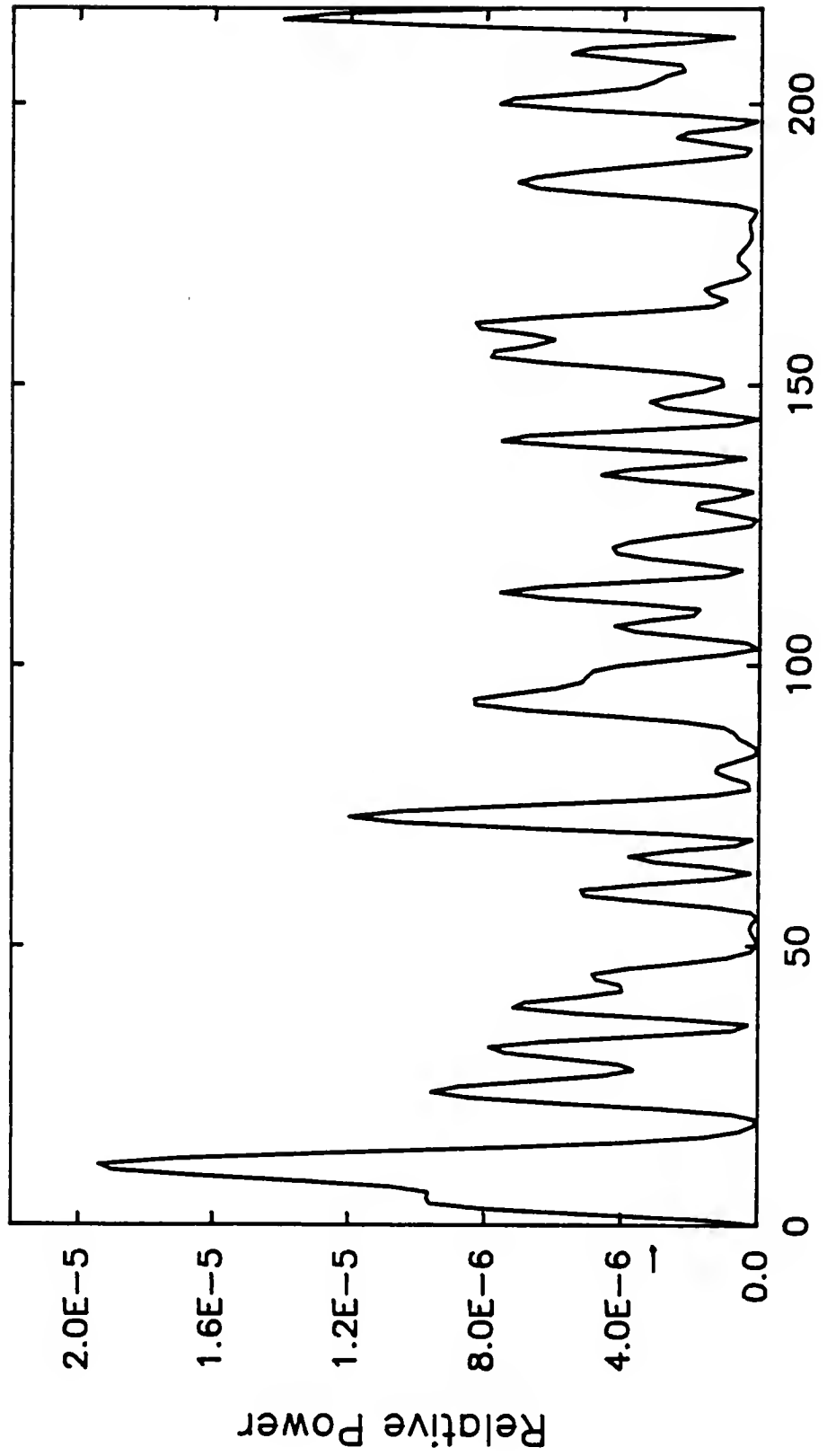

Figure 4-16 Power spectrum for the helium observations of data set III before execution of the clean algorithm.

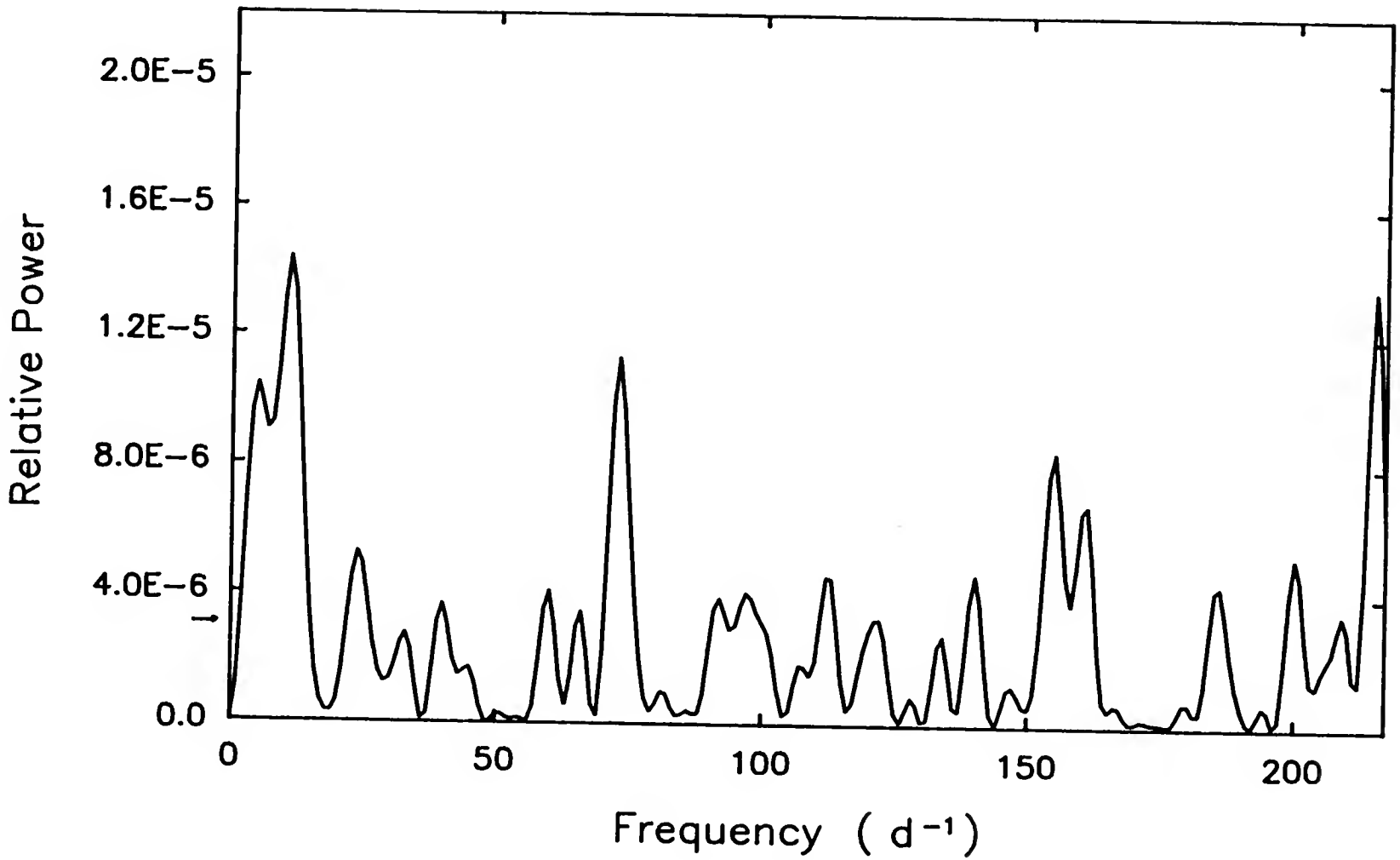

Figure 4-17 Power spectrum for the helium observations of data set III after execution of the clean algorithm.

feature at $\nu = 11d^{-1}$ has a relative power of $4.9\sigma_N$ while the peak at $\nu = 215d^{-1}$ has the slightly lower signal-to-noise ratio of $4.6\sigma_N$ and represents more-rapid fluctuations in intensity. The least-squares routine converges to two sets of parameters with almost the same amplitude in each case. The first of these models has a period of 2.00 hours and corresponds to the peak at $\nu = 11d^{-1}$ in Figure 4-17. The model for this period is shown in Figure 4.18, and has been computed with the relation

$$D(t_i) = 0.34410 + 0.00354 * \sin\left\{\frac{t_i - 0.50673}{0.01328}\right\}. \qquad (4\text{-}5)$$

The second set of parameters which results from the least-squares routine has a period of 2.75 hours and is described by equation (4-6):

$$D(t_i) = 0.34442 + 0.00329 * \sin\left\{\frac{t_i - 0.59261}{0.01820}\right\}. \qquad (4\text{-}6)$$

Even though this period does not correspond to any prominent feature in the power spectrum, the model, pictured in Figure 4-19, seems to fit the data as well as that described by equation (4-5). Even though the O-C residuals computed from equation (4-5) are slightly smaller than the residuals determined with equation (4-6), gaps in the data make it

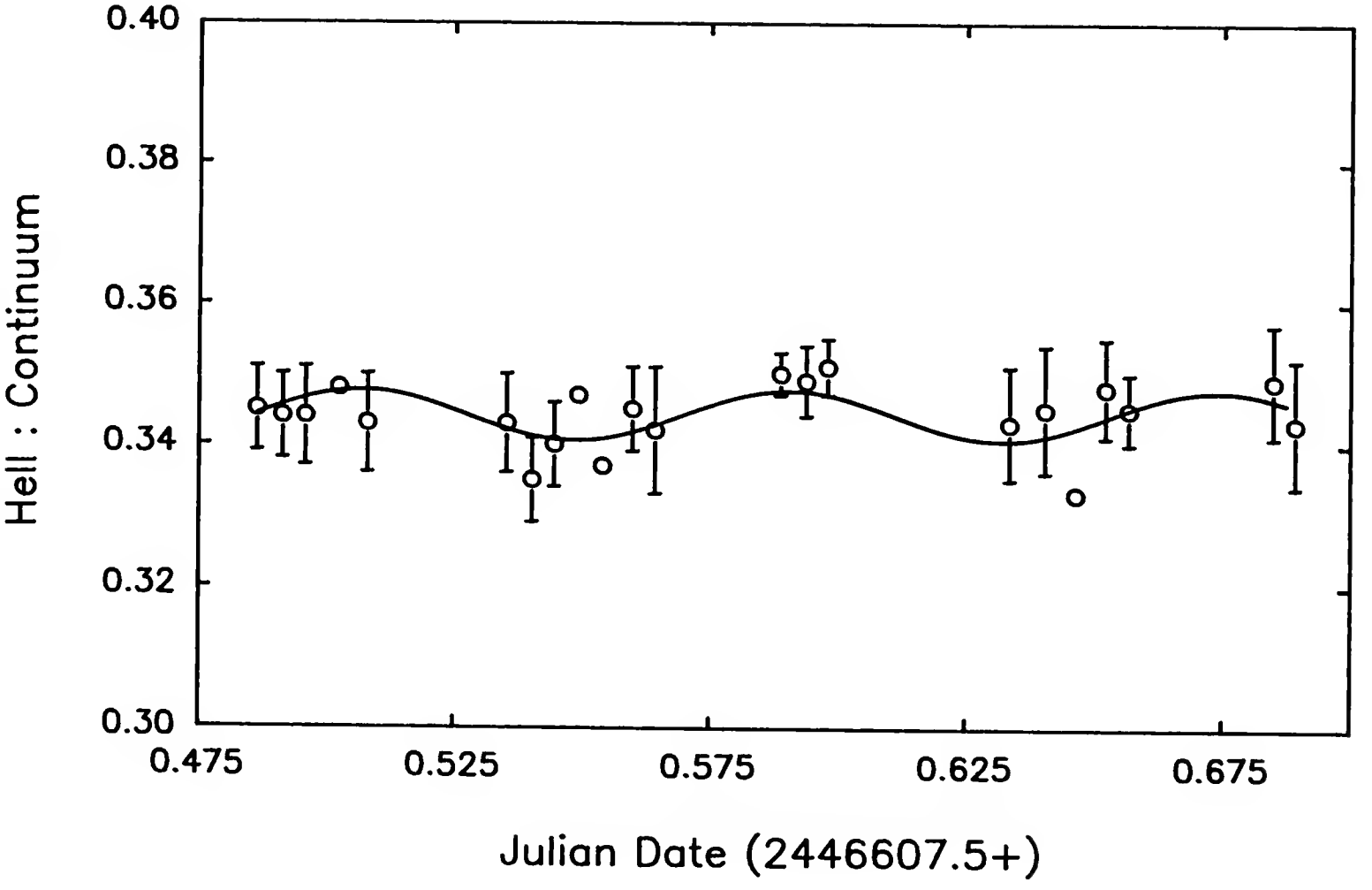

Figure 4-18 Model for the variations of the helium data for data set III with P = 2.00 hours. each plotted point represents the average intensity within a $0^{d}.0040$ interval.

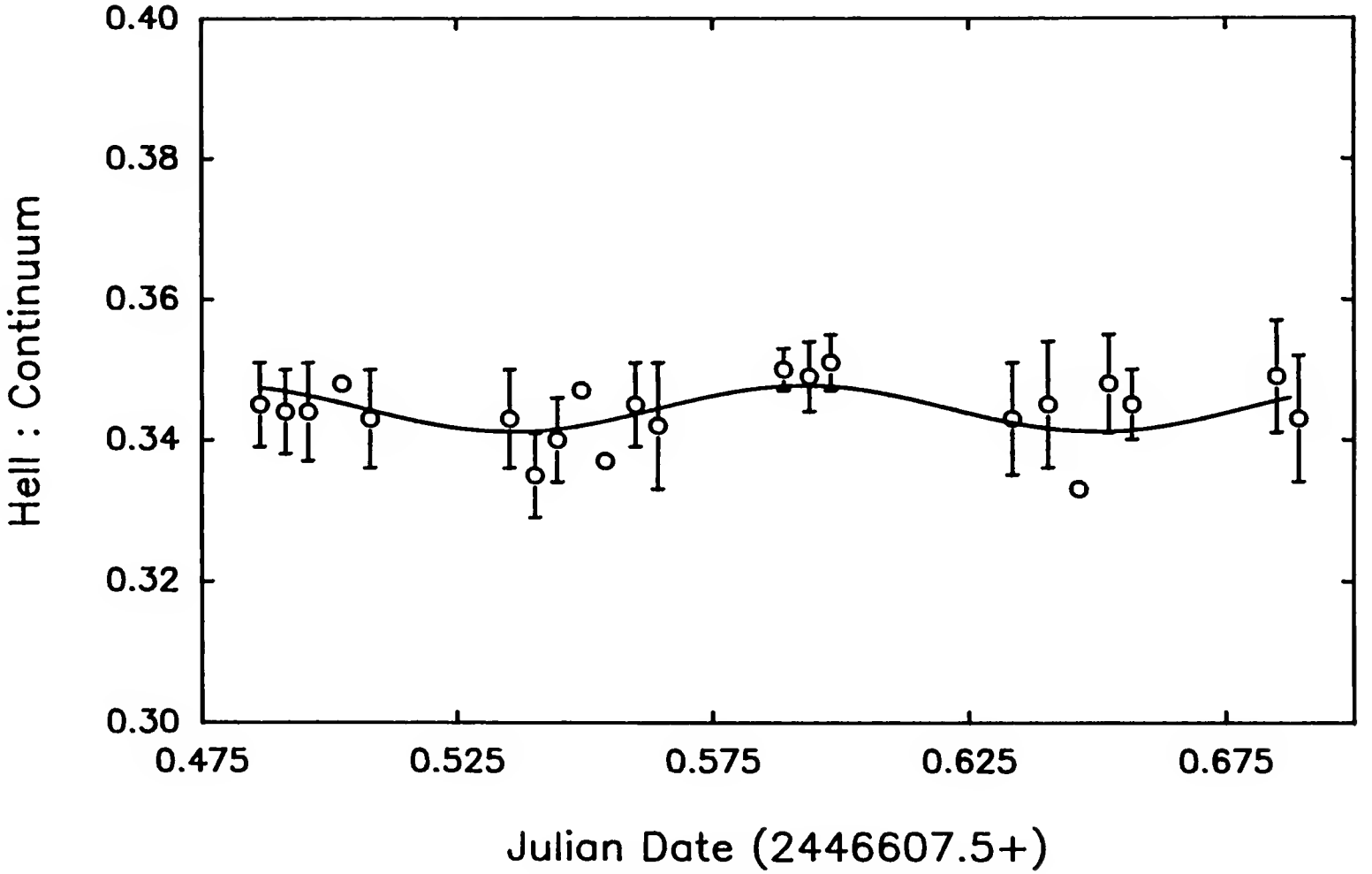

Figure 4-19 Model for the variations of the helium data for data set III with P = 2.74 hours. Each plotted point represents the average intensity within a $0^{d}.0040$ interval.

difficult to determine which fit is better. Since the first of the two periods is supported by both methods of analysis, P = 2.00 hours may be the more appropriate period.

The Fourier transform of the carbon data is converted to power, and Figures 4-20 and 4-21 show the results before and after the removal of spurious features. The 1σ noise level of these data is at 5.685×10^{-7}. Since the carbon emission feature is considerably weaker than the helium line, it is more difficult to discern intensity variations in the carbon feature from random noise. In this particular case, the CLEANing process reduces the strongest peaks in Figure 4-20 below the $4\sigma_N$ level. The least-squares routine has the strongest convergence for a period of 34.4 minutes. However, since the amplitude of variation is only a very small fraction of the total deflection in that filter, one cannot regard this result with much confidence.

In summary, the intensity variations of the helium emission line are probably best described with a period of 2.0 hours. This period was selected by both power spectrum and least-squares analytic techniques. In addition, the data have been modeled with a period of 2.75 hours, which was a solution of the least-squares method only. Relatively large gaps in the data make it difficult to determine which period, if either, is the more appropriate. The power spectrum of the carbon data indicates no strong periodicity. A least-squares solution with a period of 34.4 minutes is

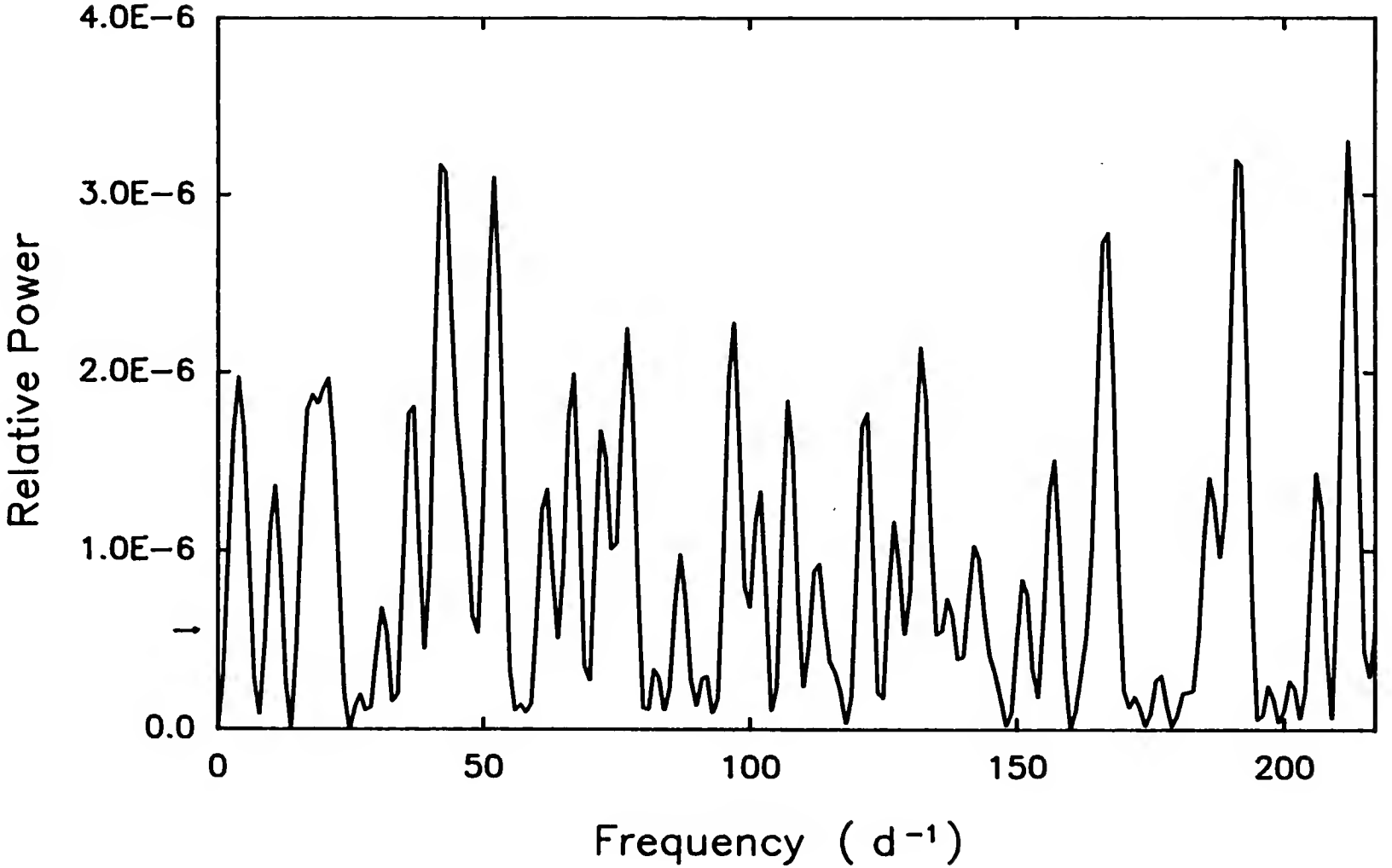

Figure 4-20 Power spectrum for the carbon observations of data set III before execution of the clean algorithm.

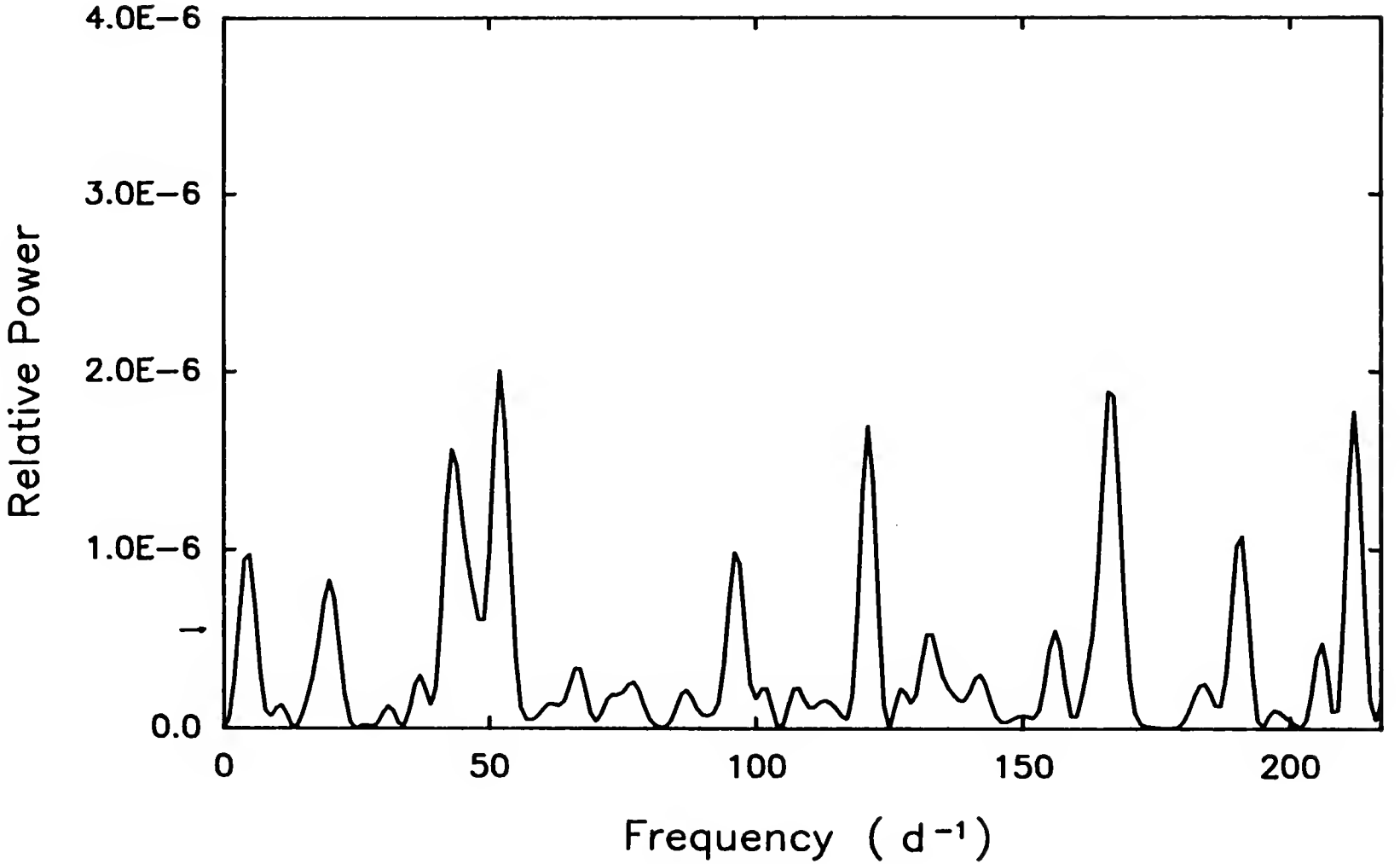

Figure 4-21 Power spectrum for the carbon observations of data set III after execution of the clean algorithm.

found, but because of the low amplitude of the variation, this period is not considered to be a true description of the variations within this weak feature.

Data Set IV.

This data set consists of 18.8 hours of photometry of γ^2 Vel extending from JD2446608.7789 through JD2446609.5624. The observing program displayed in Table 4-2 was used to obtain a total of 347 observations through each of the helium, carbon, and continuum filters. The average time interval between successive observations in any one of these filters is $0^d.0023$.

The spectral window is depicted in Figure 4-22 where peaks at $\nu = 17d^{-1}$ and $\nu = 35d^{-1}$ are separated by the same amount as the peaks at $\nu = 38d^{-1}$ and $\nu = 56d^{-1}$. The convolution of the intensity measurements of the helium emission line with this somewhat more complicated sampling function gives the power spectrum in Figure 4-23. The $1\sigma_N$ noise level at 8.850×10^{-7} indicates that peaks at $\nu = 11.5$, 35, and $166.5d^{-1}$ are statistically significant features. A strong feature also occurs at $\nu = 1.5d^{-1}$, but this frequency does not satisfy the Nyquist criterion of two samples per cycle. The peak at $\nu = 35d^{-1}$ is part alias with that at $\nu = 1.5d^{-1}$, and should, in principle, be reduced in strength by the CLEAN algorithm. Figure 4-24 shows the power spectrum that results after the spurious features are removed from the dirty spectrum. The only feature which

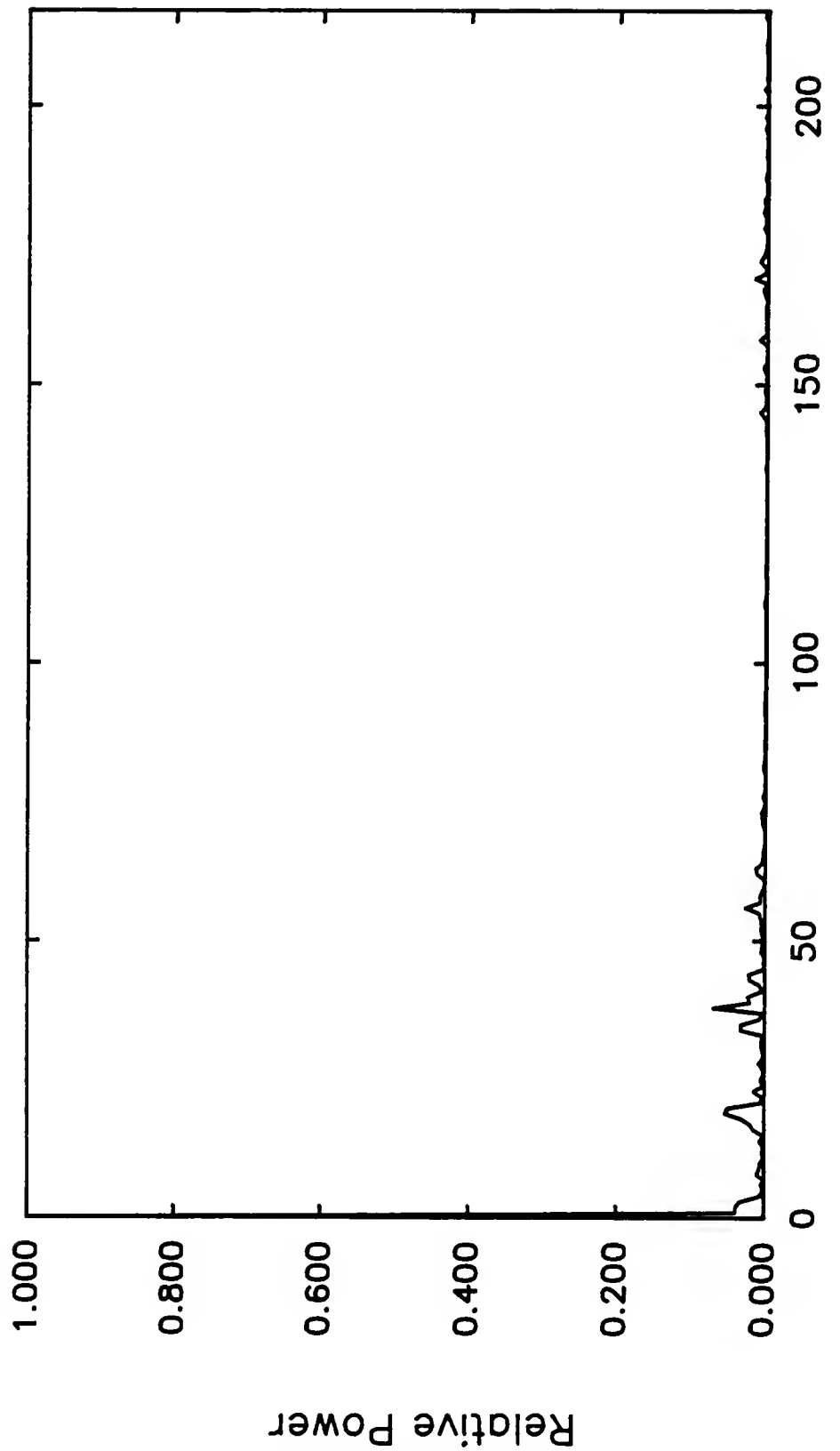

Figure 4-22 Spectral window function for data set IV.

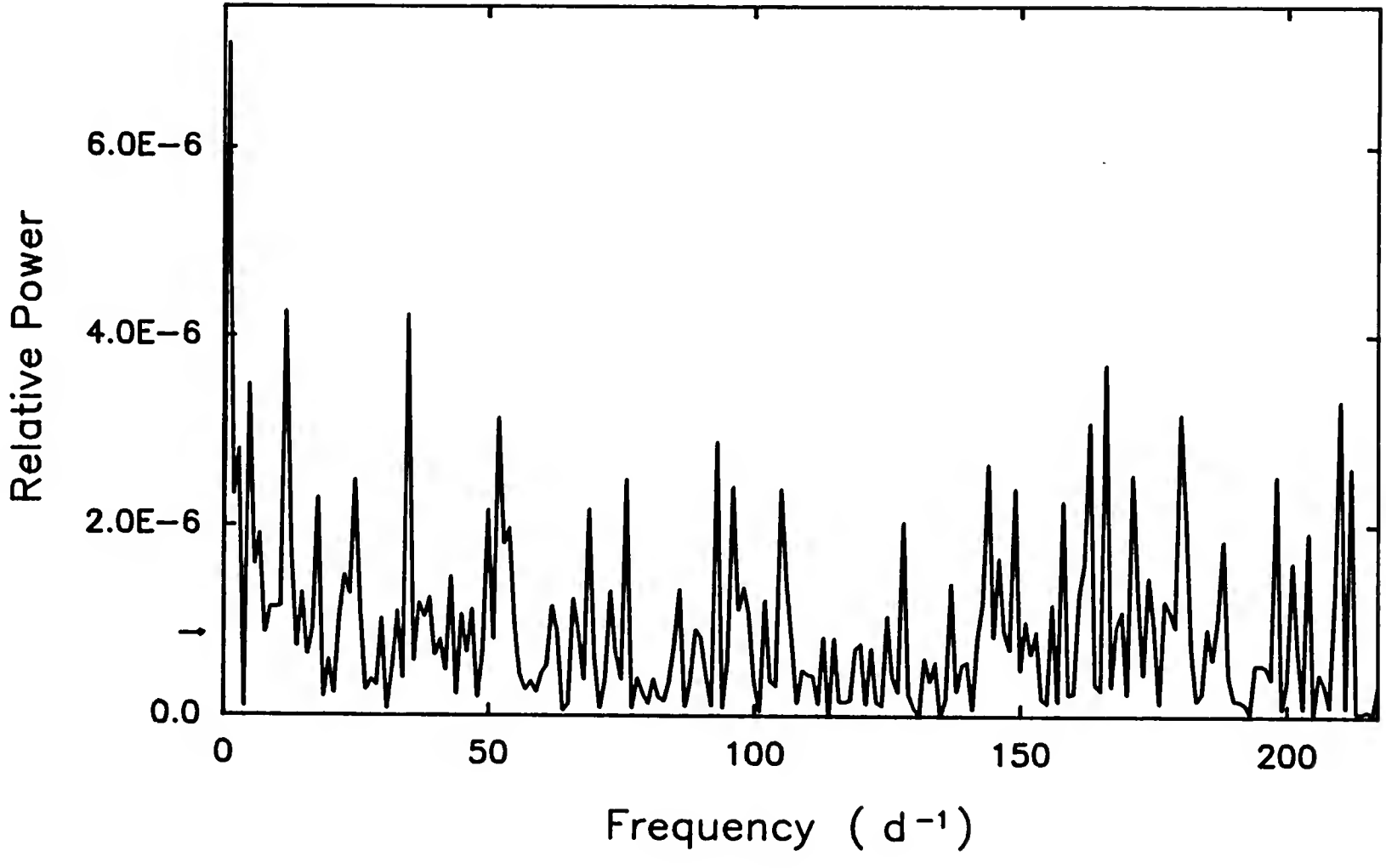

Figure 4-23 Power spectrum for the helium observations of data set IV before execution of the clean algorithm.

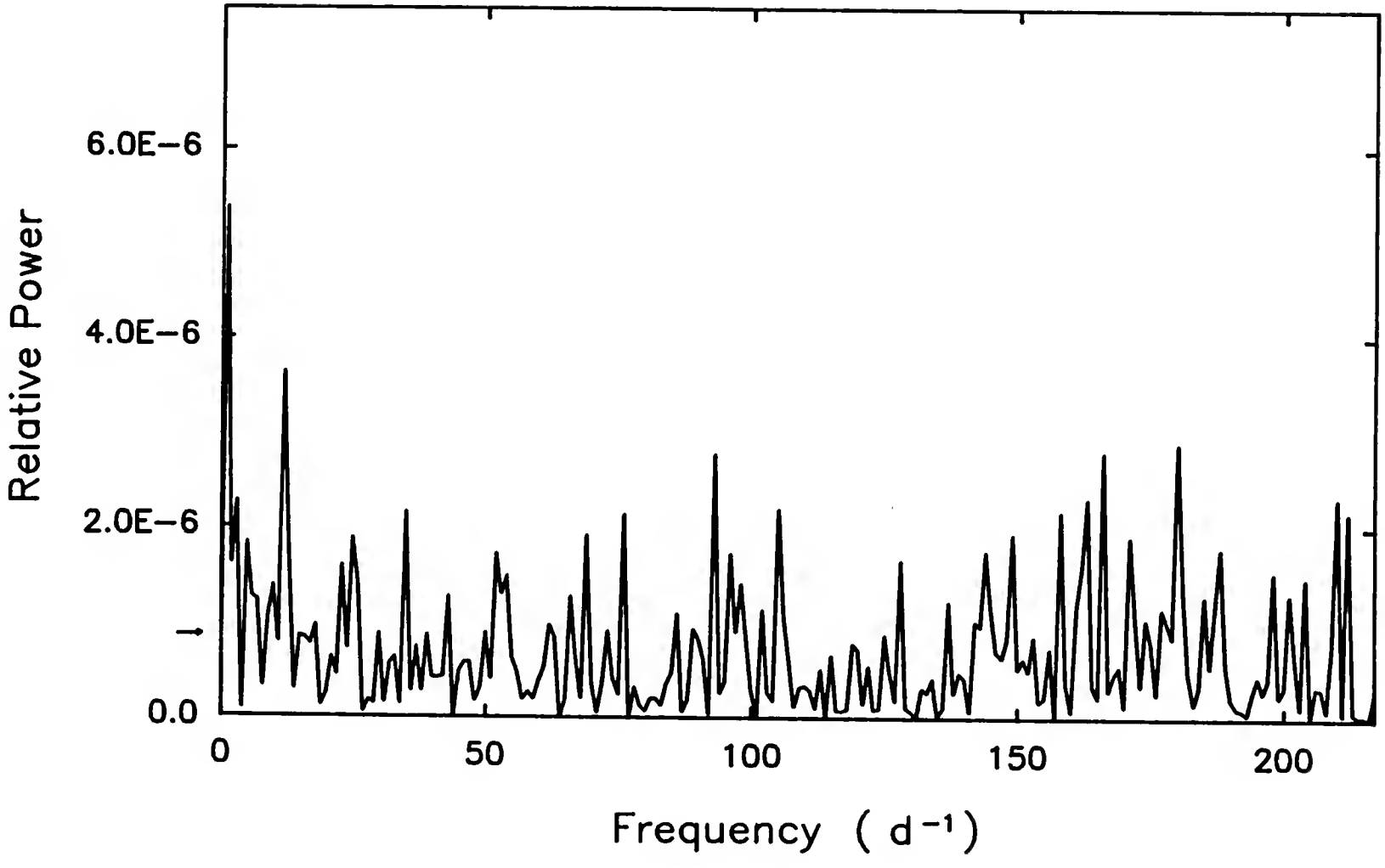

Figure 4-24 Power spectrum for the helium observations of data set IV after execution of the clean algorithm.

remains statistically significant is the peak at $\nu = 1.5d^{-1}$, but as mentioned previously, the period which corresponds to this frequency does not satisfy the Nyquist criterion, and thus cannot be considered in the context of this research. Although no peaks survive the CLEANing process, the least-squares routine is still executed. Convergence to a set of parameters with $P = 0^d.208$ (5.0 hours) is given by

$$D(t_i) = 0.34736 + 0.00250 * \sin\left\{\frac{t_i - 0.22157}{0.03316}\right\}. \qquad (4\text{-}7)$$

This fit, depicted in Figure 4-25, has a very low amplitude of variation and is certainly not a very good representation of the changes in intensity. This unsatisfactory fit is confirmed by the low power in the peaks of the CLEANed power spectrum (Figure 4-24). An attempt was made to improve the results obtained with these data by dividing the long data set into two subsets. The first subset contains observations made between JD2446608.7789 and JD2446609.1646, and has a time-resolution which is exactly the same as that for the whole data set. The shorter span of this subset allows for frequencies between $\nu_{min} = 5d^{-1}$ and $\nu_{max} = 217d^{-1}$ to be tested. The spectral window function for these data, depicted in Figure 4-26, shows similar, but slightly stronger, peaks as those from Figure 4-22. Dirty and clean spectra are shown in

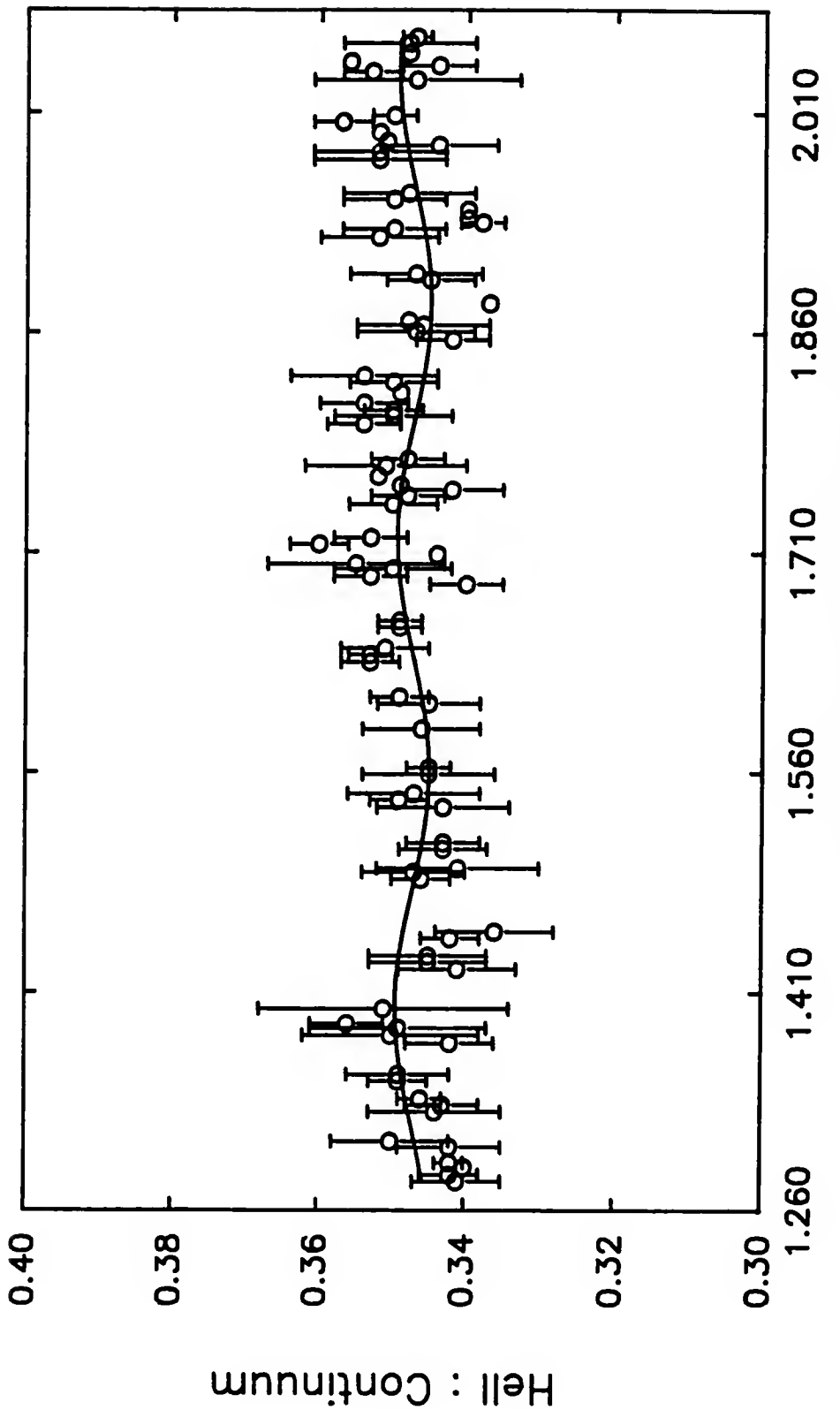

Figure 4-25 Model for the variations of the helium data of data set IV with P = 5.00 hours. Each plotted point represents the average intensity within a $0^d.0040$ interval.

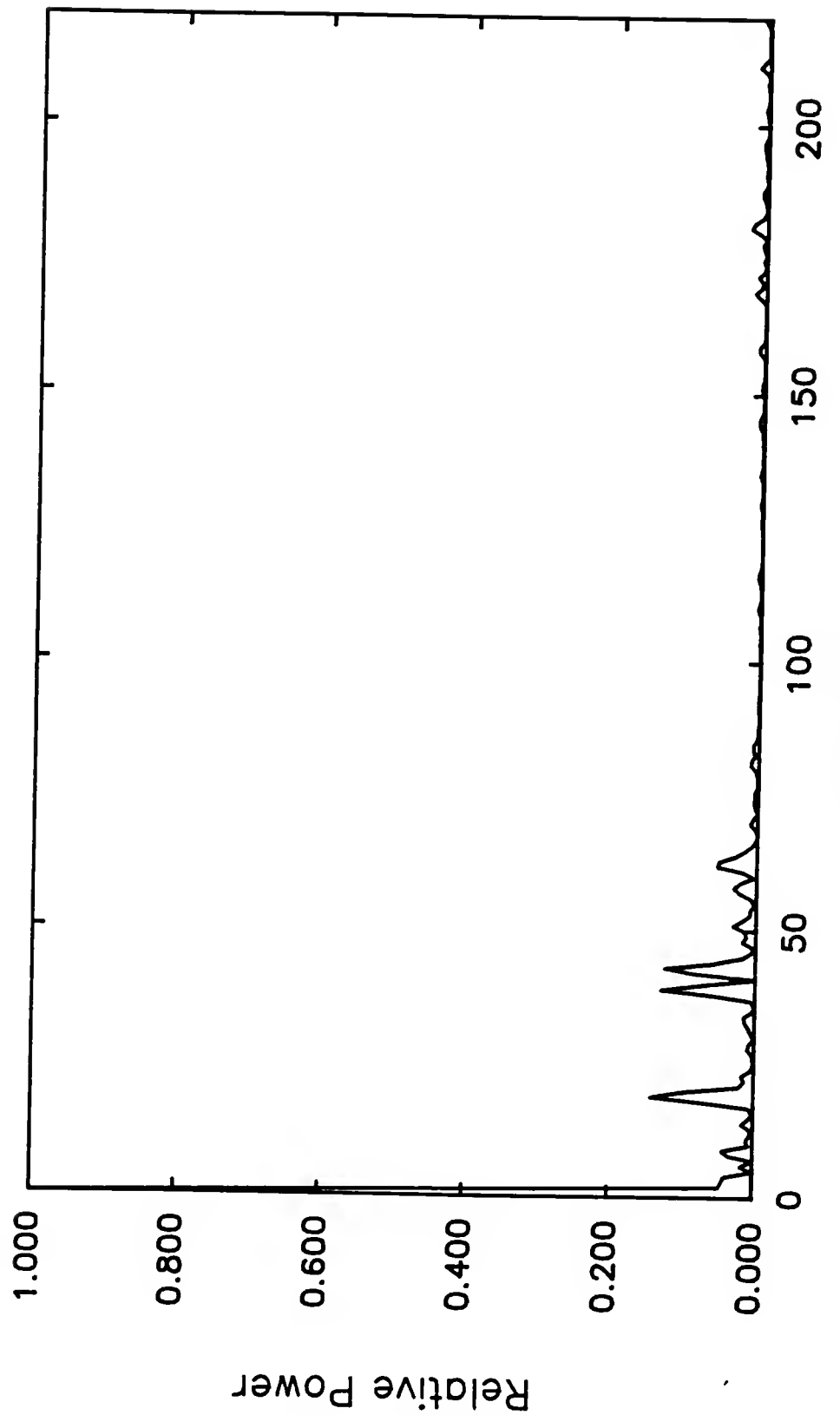

Figure 4-26 Spectral window function for subset I of data set IV.

Figures 4-27 and 4-28. The noise level in each of these plots is denoted in the lower left-hand portion of the figures at 1.737×10^{-6}. The CLEAN algorithm removes all spurious features at or below the $3\sigma_N$ level. As can be seen from Figure 4-28, this process again leaves no statistically significant features. The least-squares solution for this data set gives a period of 5.79 hours corresponding in frequency to the strongest peak in Figures 4-27 and 4-28, even though these peaks do not meet the statistical significance criterion. This model is described by

$$D(t_i) = 0.34527 + 0.00329 * \sin\left(\frac{t_i - 1.38569}{0.03842}\right), \qquad (4\text{-}8)$$

and is shown in Figure 4-29. The O-C residuals computed with this equation are marginally better than those determined with equation (4-7).

The second subset of data set IV covers the time range that extends from JD2446609.1870 through JD2446610.5624. The minimum and maximum frequencies retrievable from this subset are the same as for subset 1. Again, the spectral window (Figure 4-30) is qualitatively similar to the beam for the entire data set, but is quantitatively different. Figures 4-31 and 4-32 represent the power spectra before and after CLEANing the data. The only peaks which remain above the $4\sigma_N$ level after the CLEANing process are those at

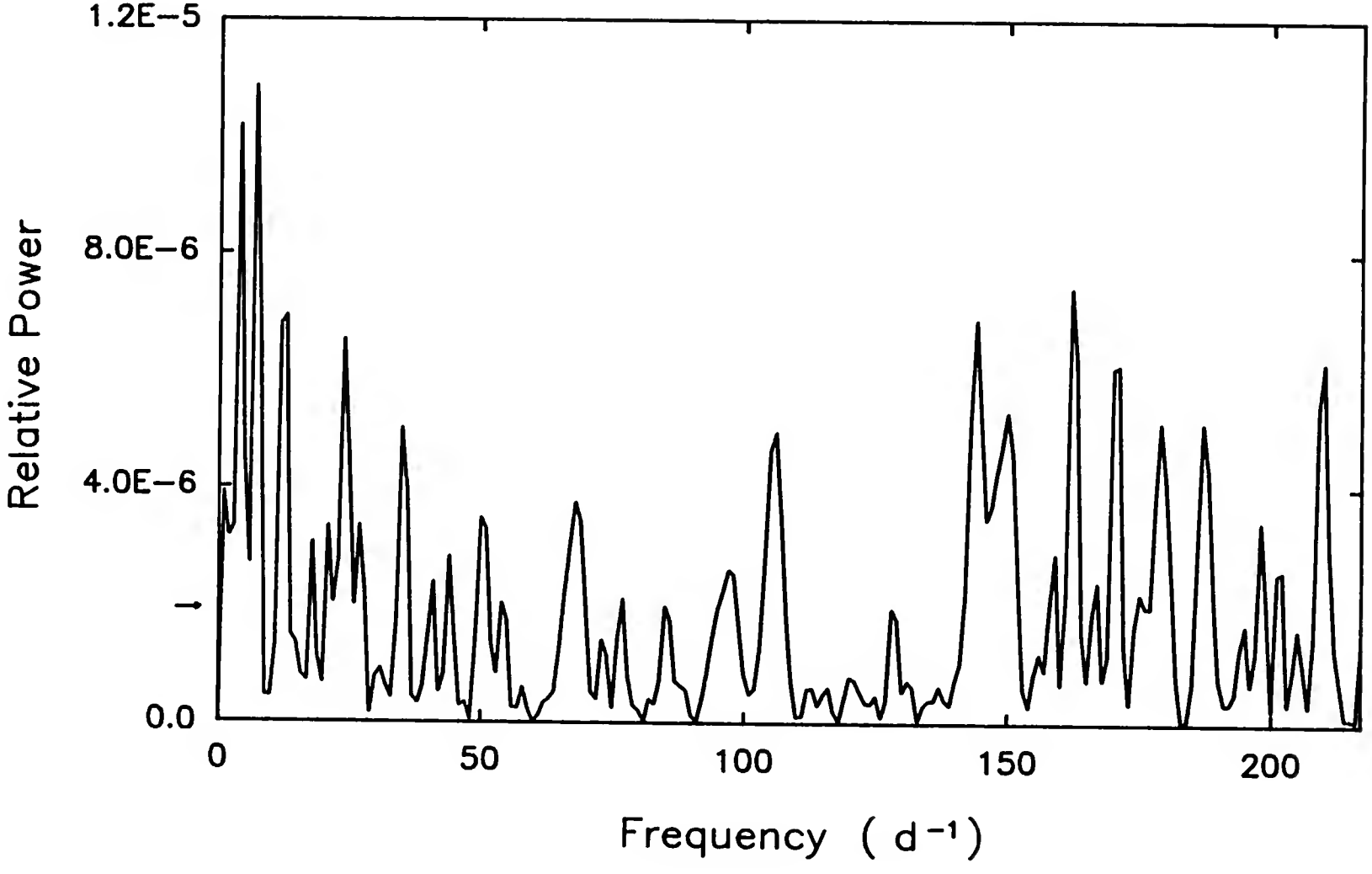

Figure 4-27 Power spectrum for the helium observations of subset I of data set IV before execution of the clean algorithm.

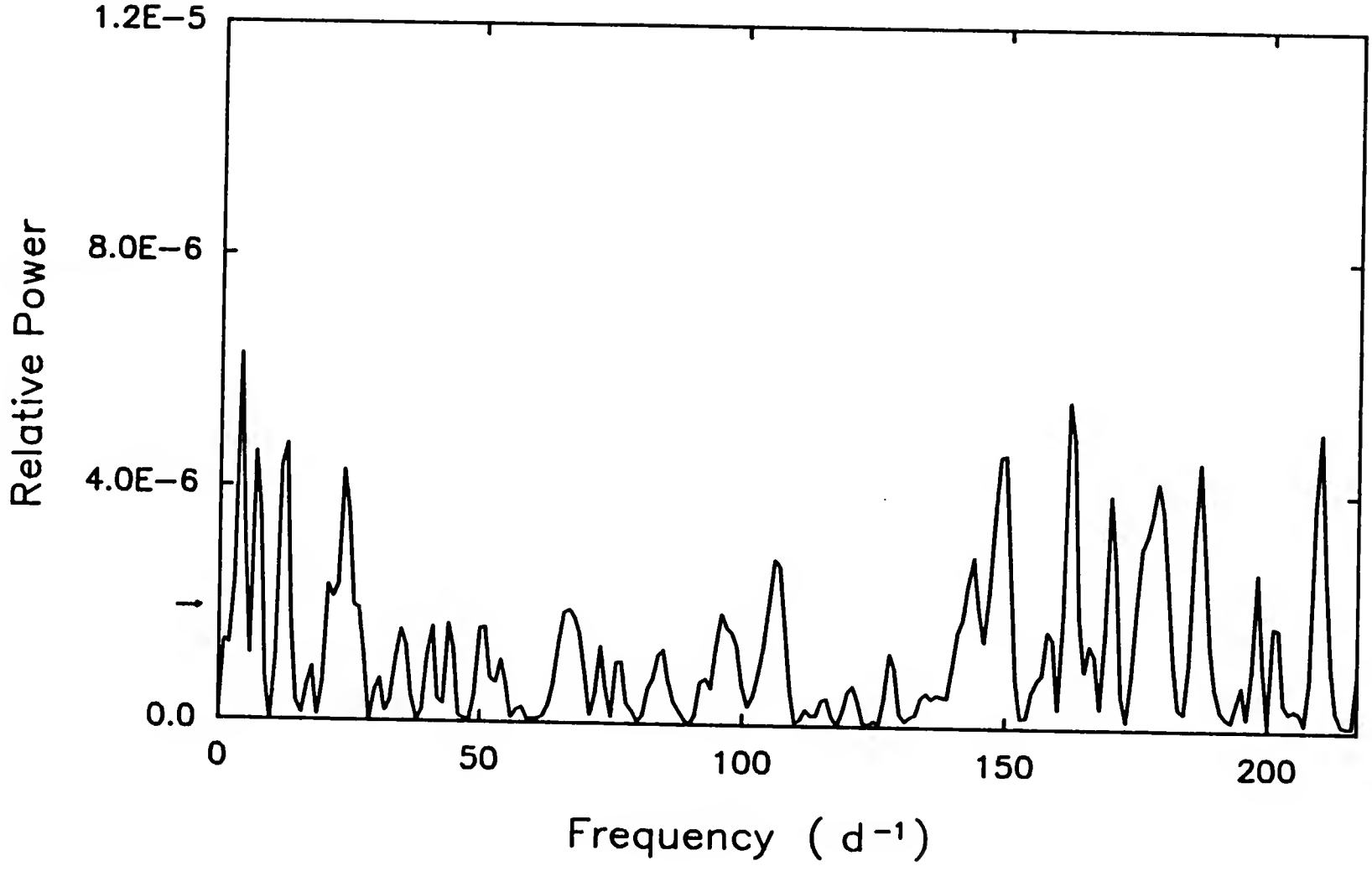

Figure 4-28 Power spectrum for the helium observations of subset I of data set IV after execution of the clean algorithm.

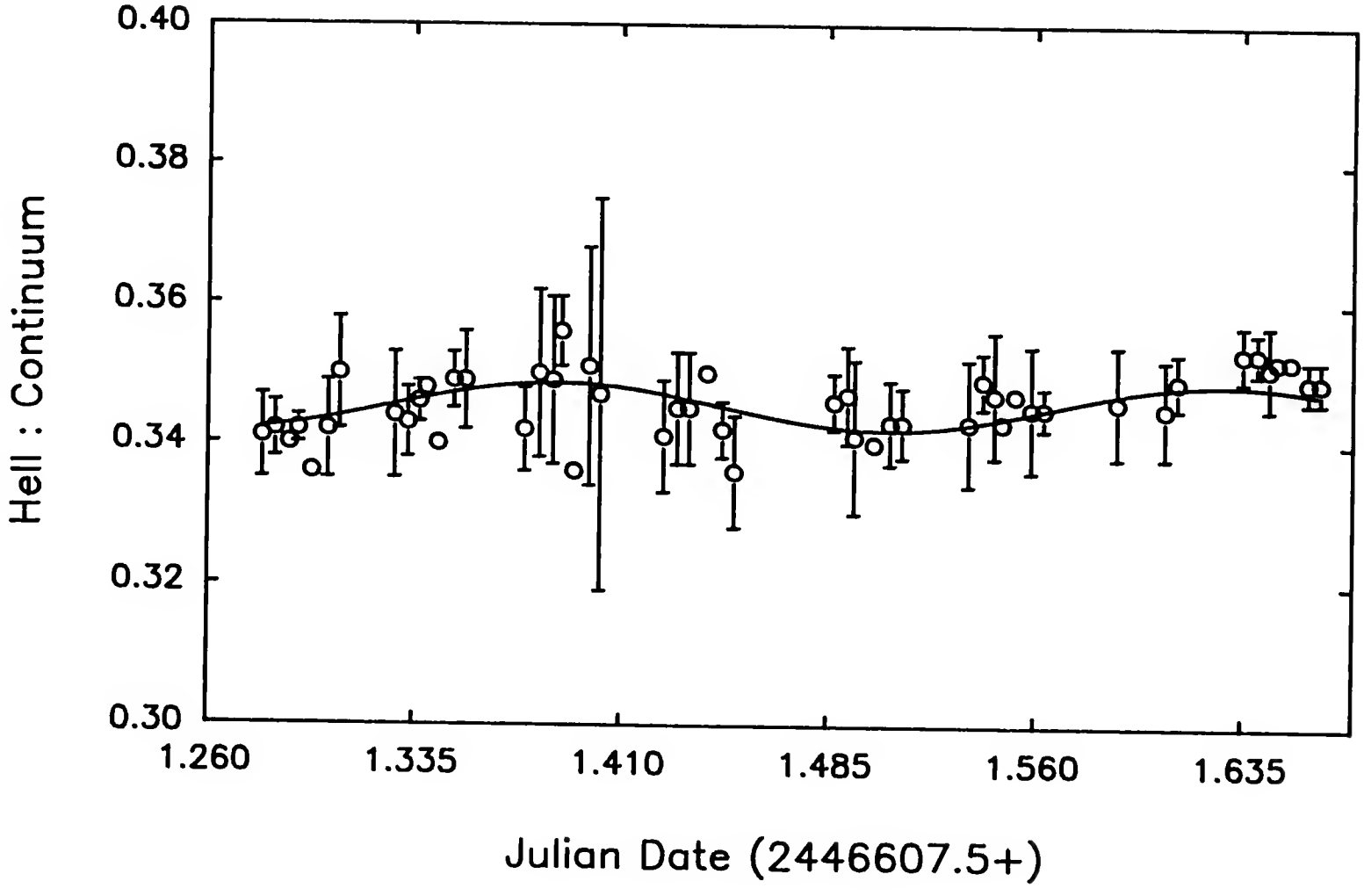

Figure 4-29 Model for the variations of the helium data of subset I of data set IV with P = 5.79 hours. Each plotted point represents the average intensity within a $0^{d}.0040$ interval.

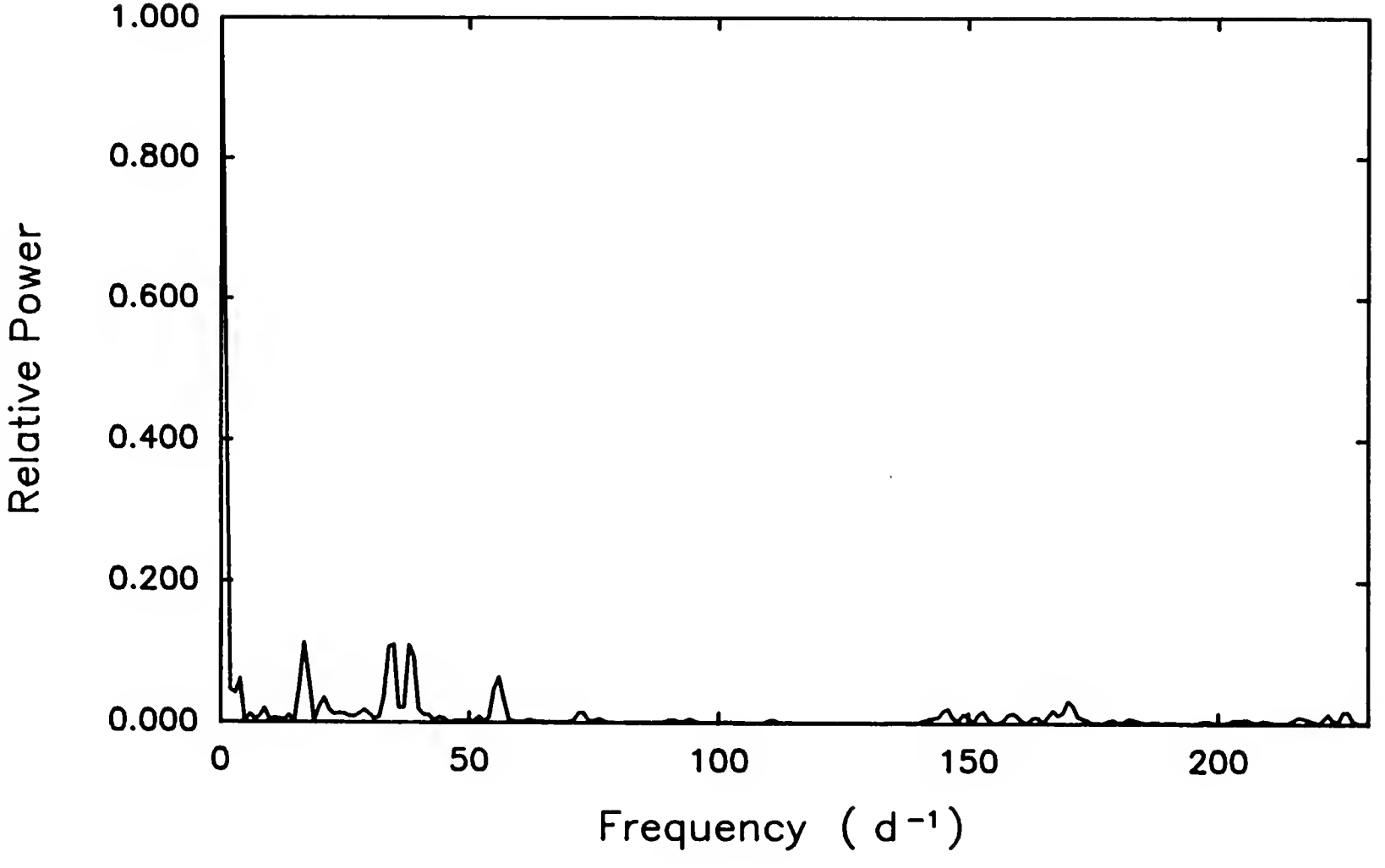

Figure 4-30 Spectral window function for subset II of data set IV.

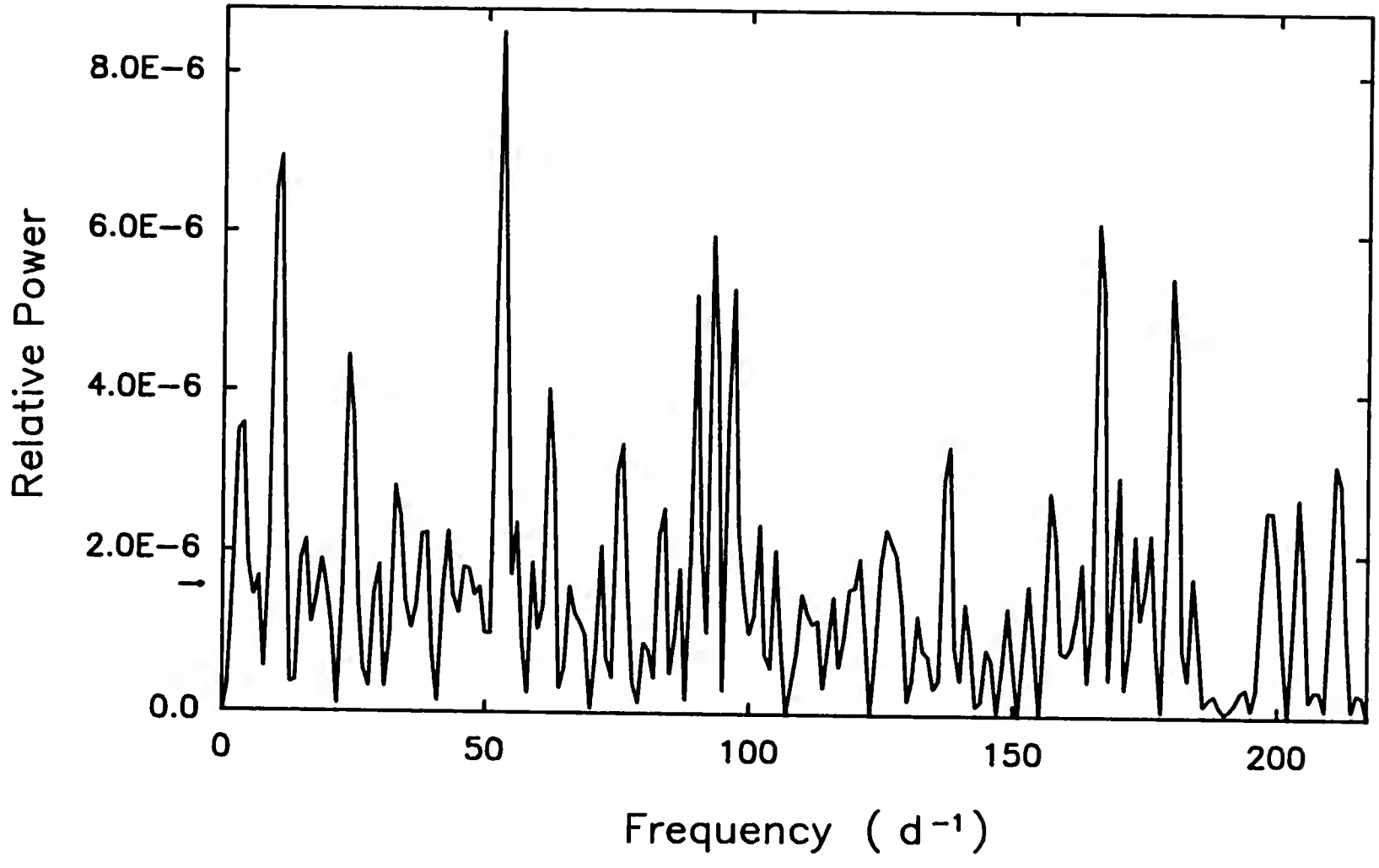

Figure 4-31 Power spectrum for the helium observations of subset II of data set IV before execution of the clean algorithm.

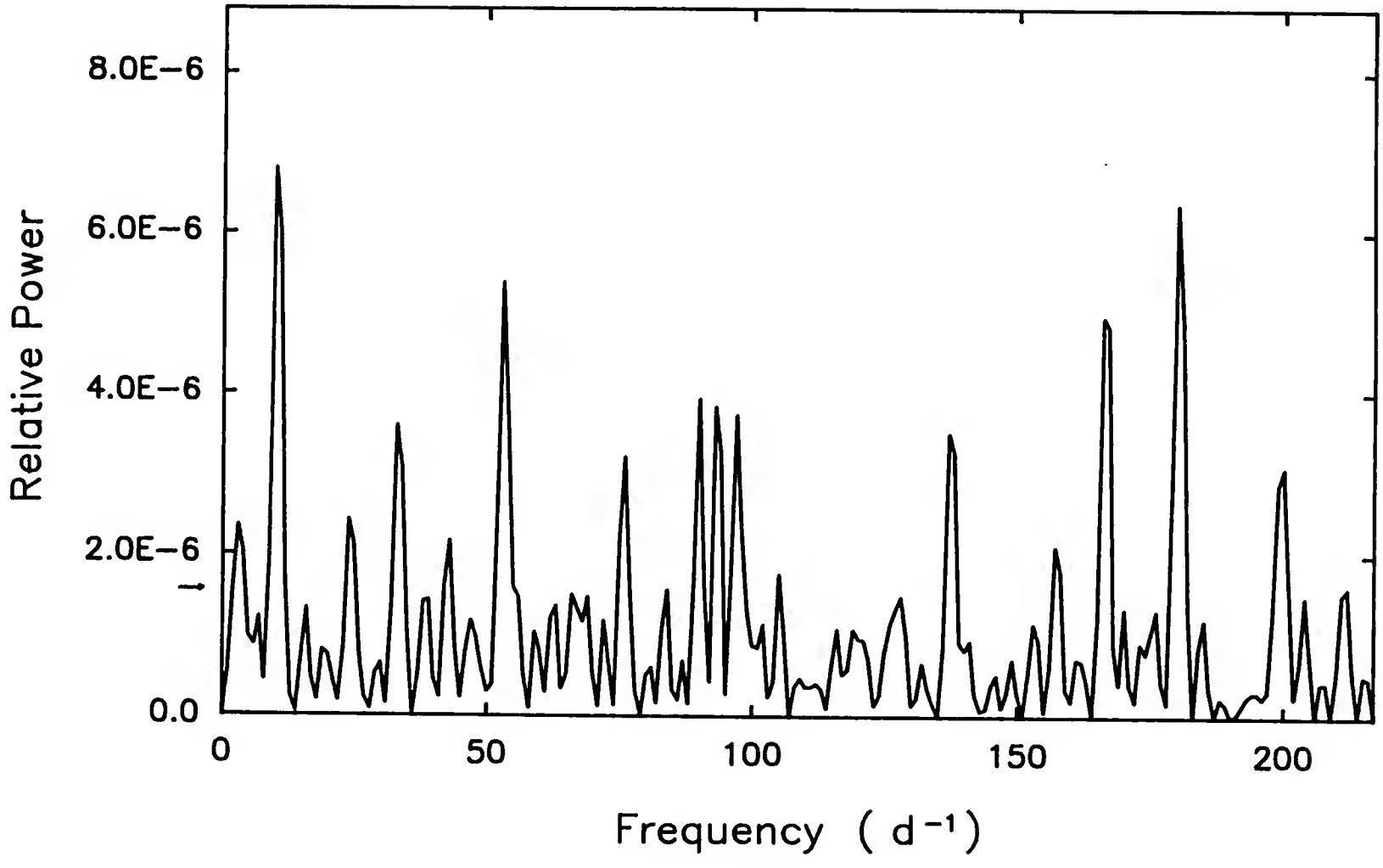

Figure 4-32 Power spectrum for the helium observations of subset II of data set IV after execution of the clean algorithm.

$\nu = 10d^{-1}$ and $\nu = 182d^{-1}$. The first of these features corresponds to P = $0^d.100$ (2.40 hours), and has a relative power of about $4.38\sigma_N$ where $\sigma_N = 1.553 \times 10^{-6}$. The second peak which rises above the $4\sigma_N$ level in Figure 4-32 represents rapid fluctuations with P = 7.91 minutes, and has a signal-to-noise ratio of 4.10. According to the least-squares analysis of subset 2, a period of $0^d.2631$ (6.31 hours) best satisfies the variations present in these data. This period does not agree with either of the periods found through power spectrum analysis. However, because it corresponds to a frequency which is less than ν_{min}, this is not a serious discrepancy. The model which is computed with the parameters chosen by the least-squares routine, namely

$$D(t_i) = 0.34796 + 0.00307 * \sin\left(\frac{t_i - 1.76215}{0.04187}\right), \qquad (4\text{-}9)$$

is shown with averaged points in Figure 4-33. In addition to this solution, a shorter period was also found through the least-squares method of analysis. This solution has a smaller amplitude of variation, but the period of 2.23 hours agrees well with the peak in Figure 4-32 at $\nu = 10d^{-1}$. The mathematical representation of this model is described by

$$D(t_i) = 0.34887 + 0.00238 * \sin\left(\frac{t_i - 1.72011}{0.01480}\right), \qquad (4\text{-}10)$$

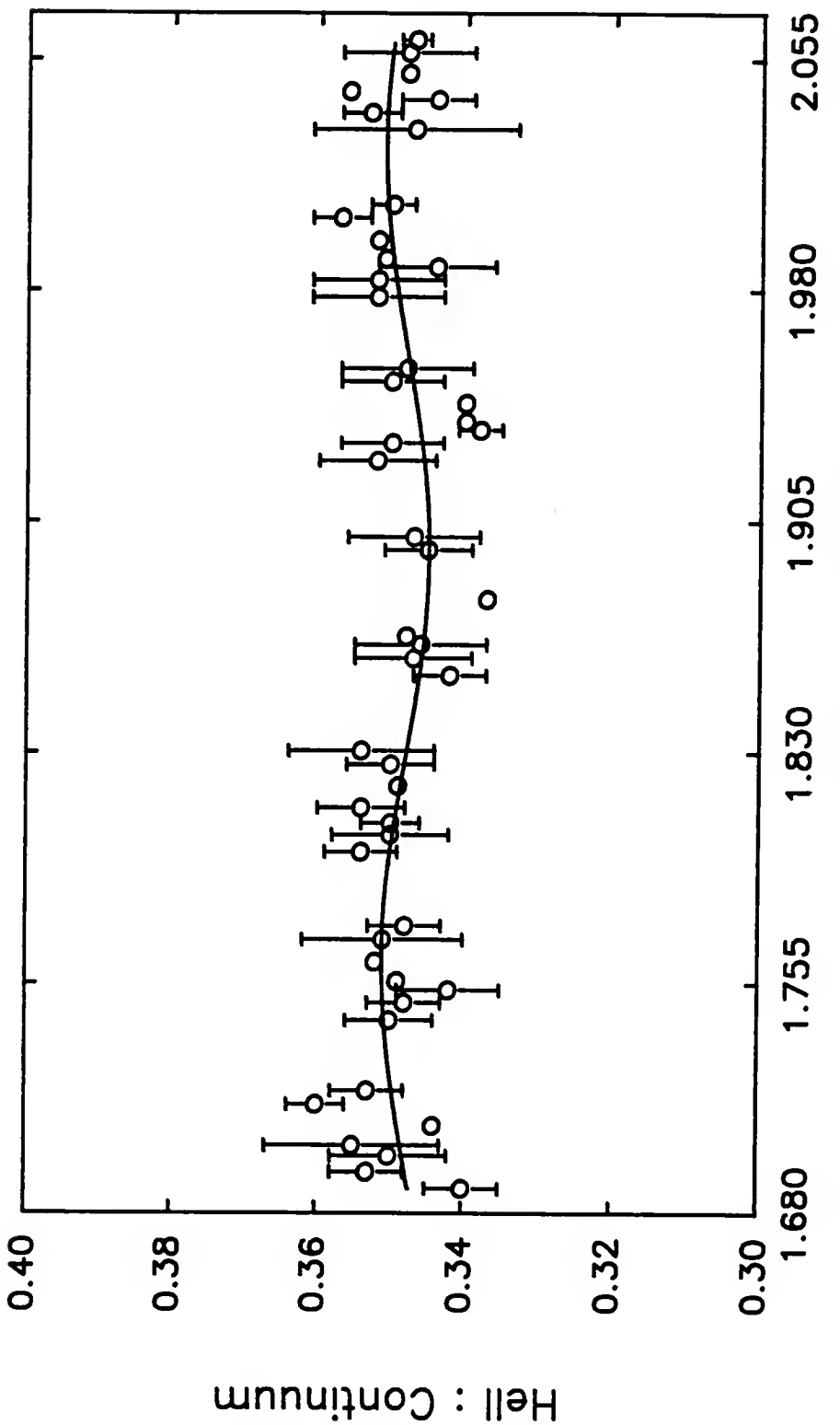

Figure 4-33 Model for the variations of the helium data of subset II of data set IV with P = 6.31 hours. Each plotted point represents the average intensity within a 0.0040 interval.

and is depicted in Figure 4-34. The the O-C residuals determined from this model are larger than those determined from equation (4-9). In addition, the amplitude of fluctuation in equation (4-10) represents a smaller percentage of the total intensity of the helium line than does equation (4-9). These considerations lead one to believe that equation (4-9) is a better representation of the changes in intensity of this subset.

Analysis of the carbon data are really quite inconclusive. The power spectra for the entire data set, before and after execution of the CLEAN algorithm, are shown in Figures 4-35 and 4-36, respectively. The noise level of these data, in terms of relative power, is denoted in the lower left-hand portion of the figures at 1.266×10^{-7}. None of the features in Figure 4-36 are statistically significant at the $4\sigma_N$ level. In an attempt to improve the interpretation of these data, the data set was again divided into two subsets which correspond in time to subsets I and II of the helium data. The dirty and clean power spectra which result after taking the Fourier transform of the first subset of these data, are shown in Figures 4-37 and 4-38. The noise level in each of these plots is at 2.316×10^{-7}.

As seen in these figures, three high-frequency components exceed the $4\sigma_N$ level by a small amount. Figures 4-39 and 4-40 are similar plots for the second subset. In this case, the peak at $\nu = 57 d^{-1}$ ($P = 0^d.0179$) has a larger

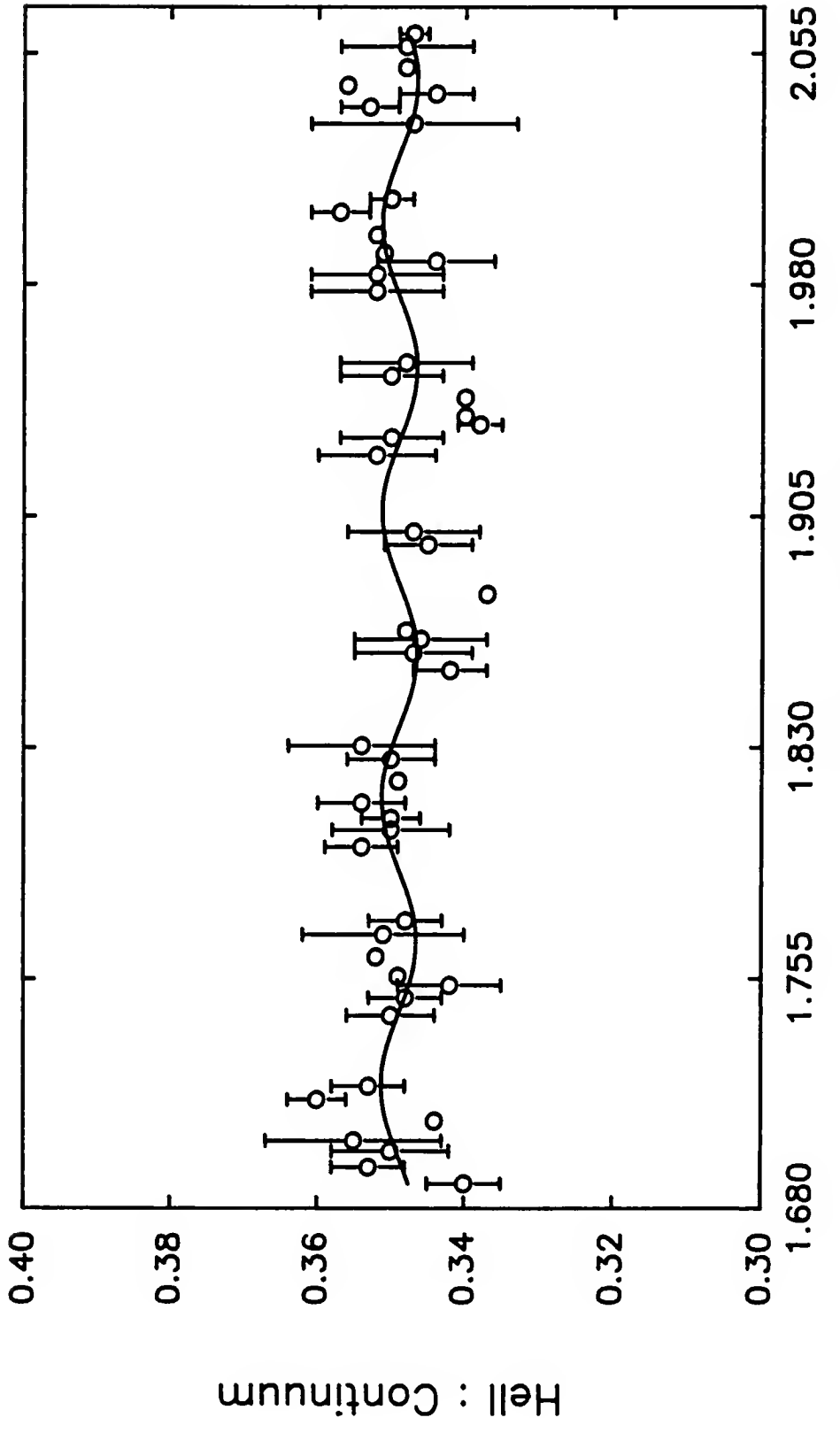

Figure 4-34 Model for the variations of the helium data of subset II of data set IV with P = 2.23 hours. Each plotted point represents the average intensity within a $0^d.0040$ interval.

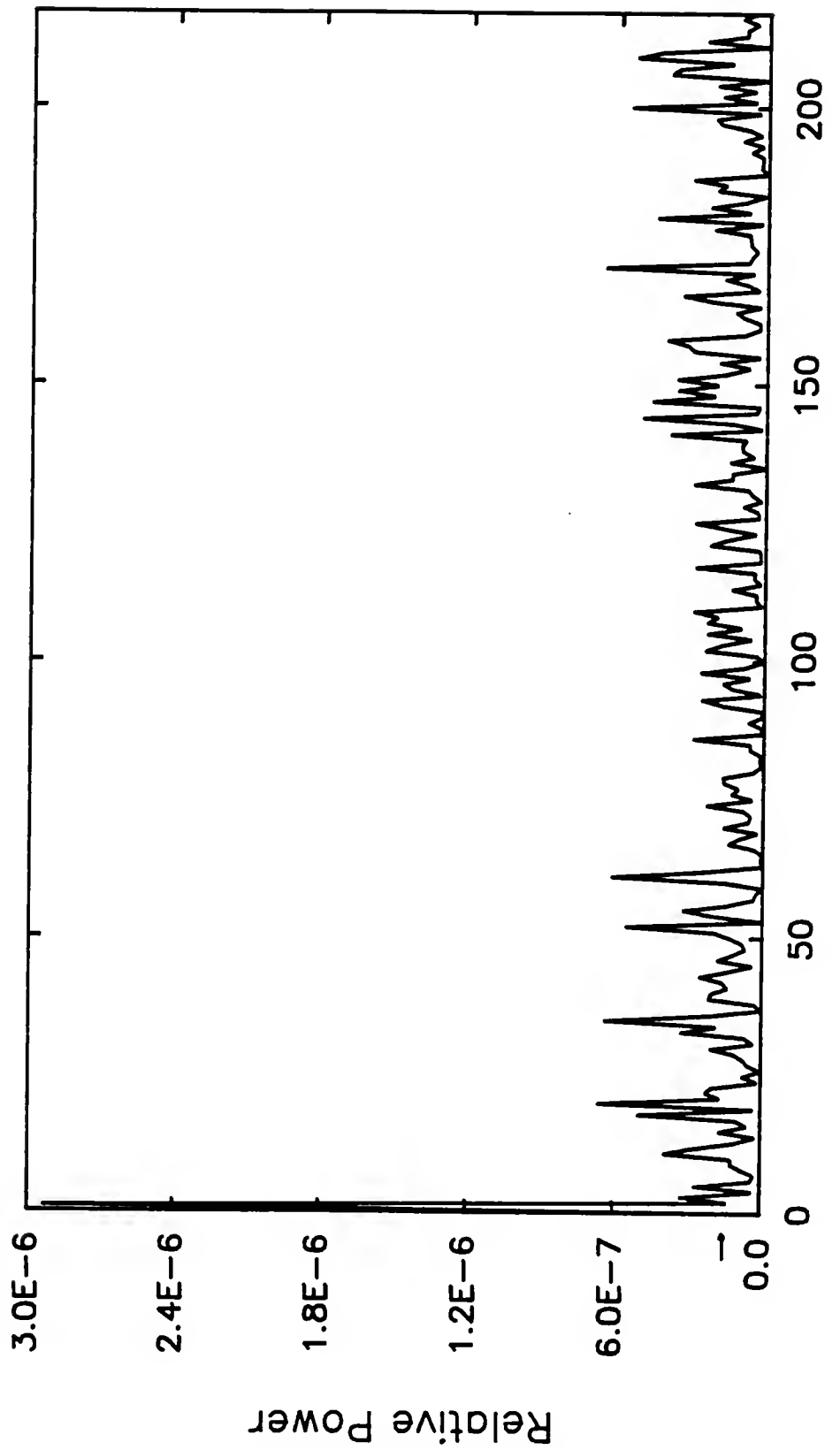

Figure 4-35 Power spectrum for the carbon observations of data set IV before execution of the clean algorithm.

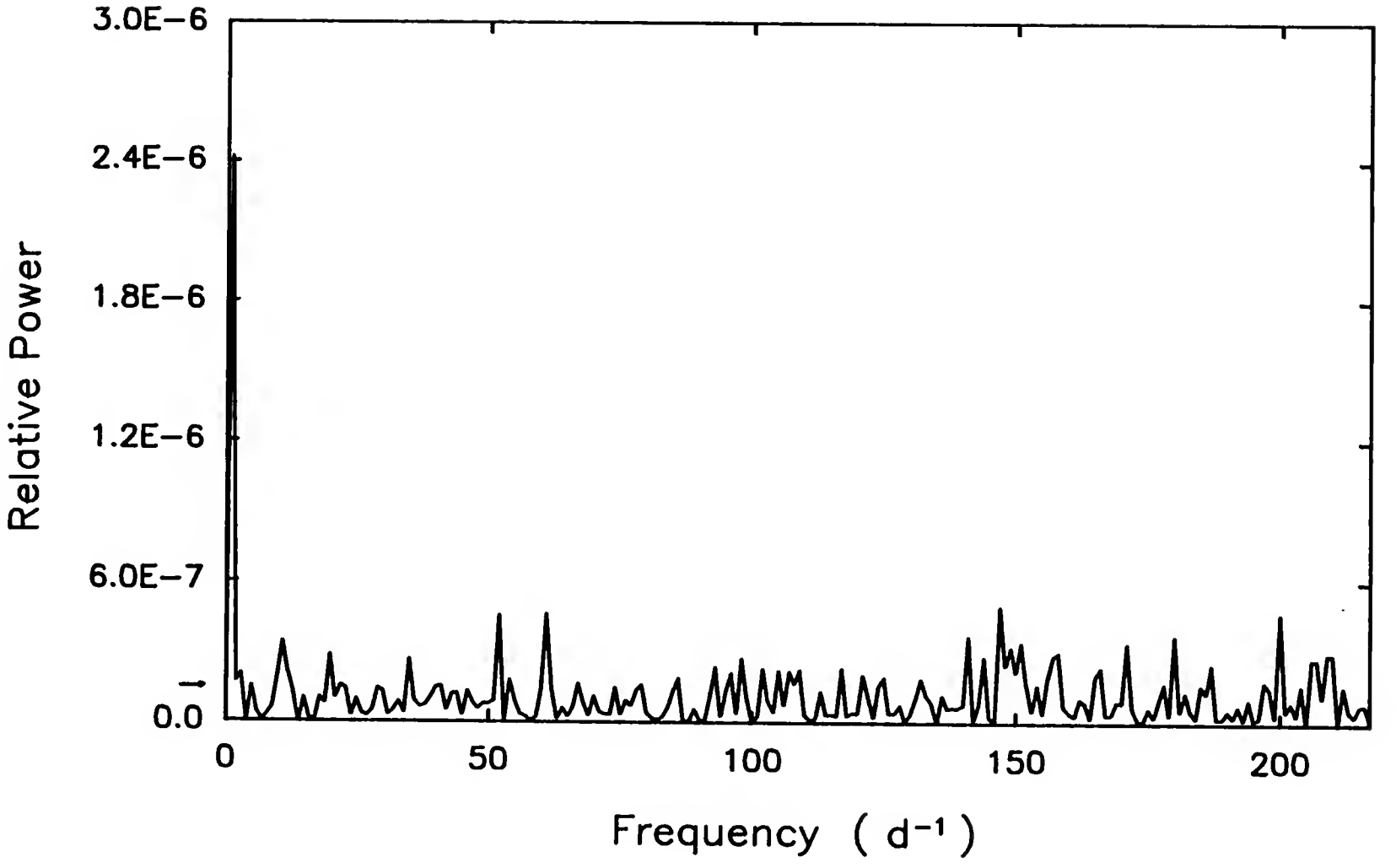

Figure 4-36 Power spectrum for the carbon observations of data set IV after execution of the clean algorithm.

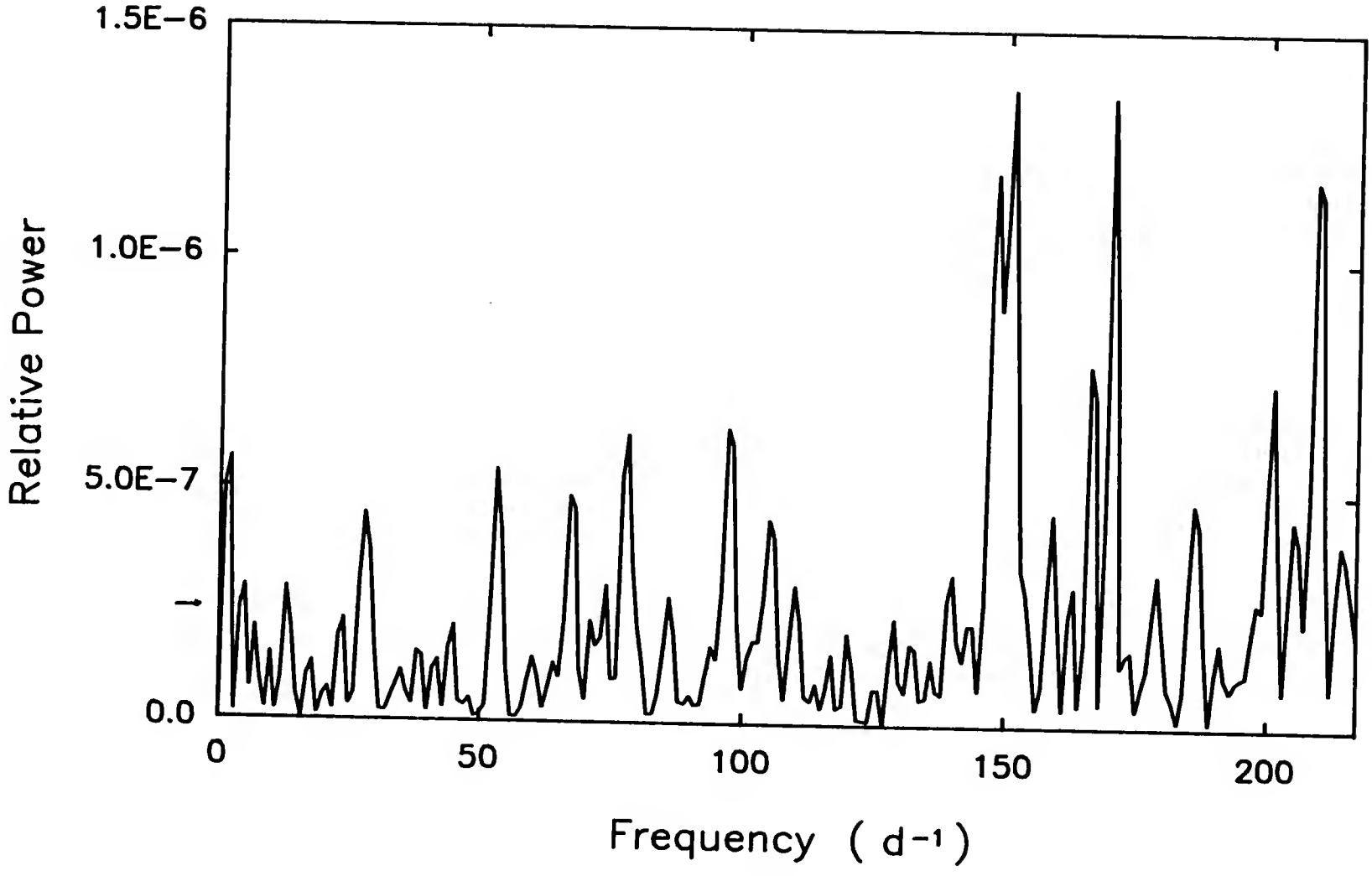

Figure 4-37 Power spectrum for the carbon observations of subset I of data set IV before execution of the clean algorithm.

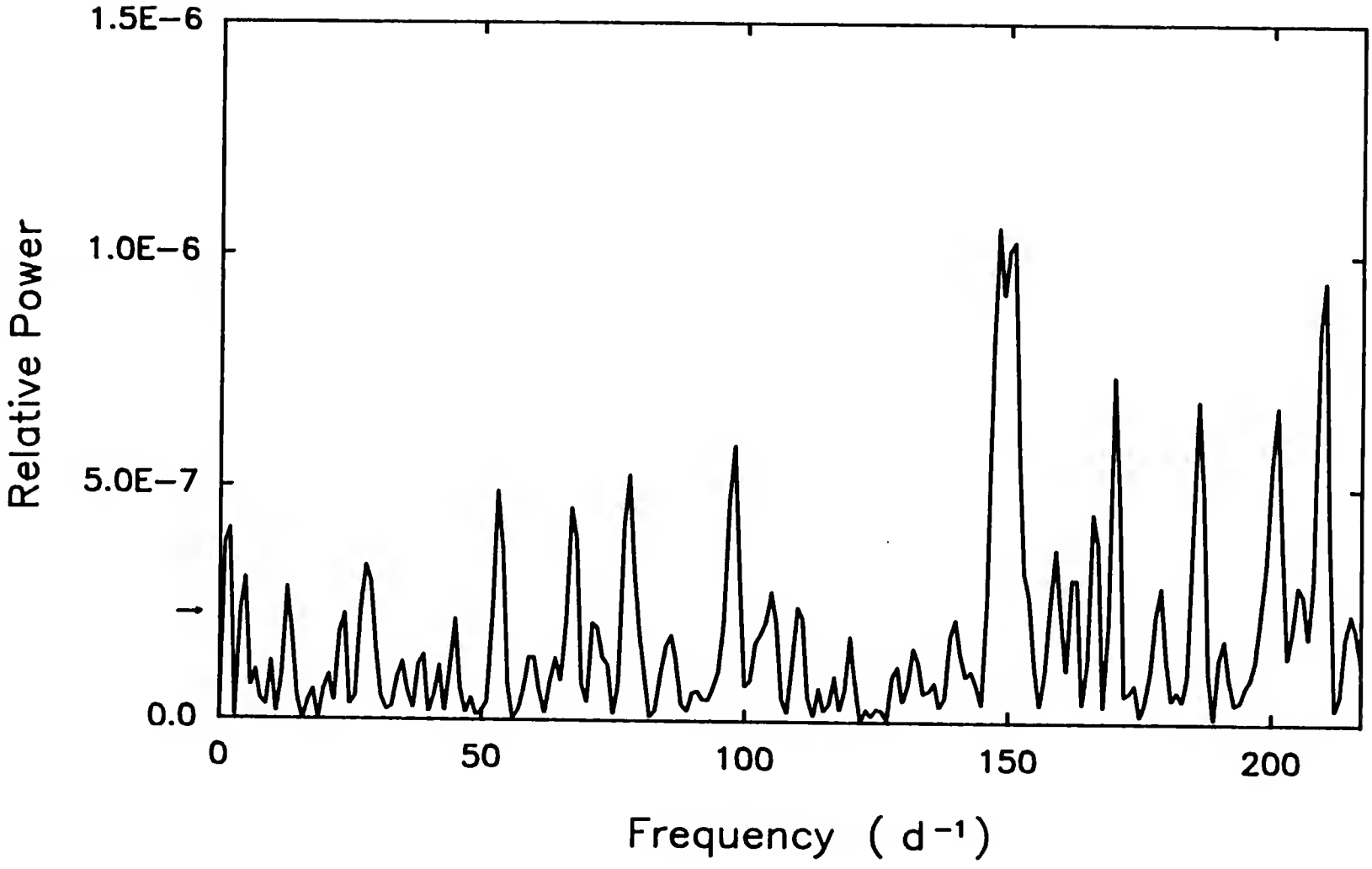

Figure 4-38 Power spectrum for the carbon observations of subset I of data set IV after execution of the clean algorithm.

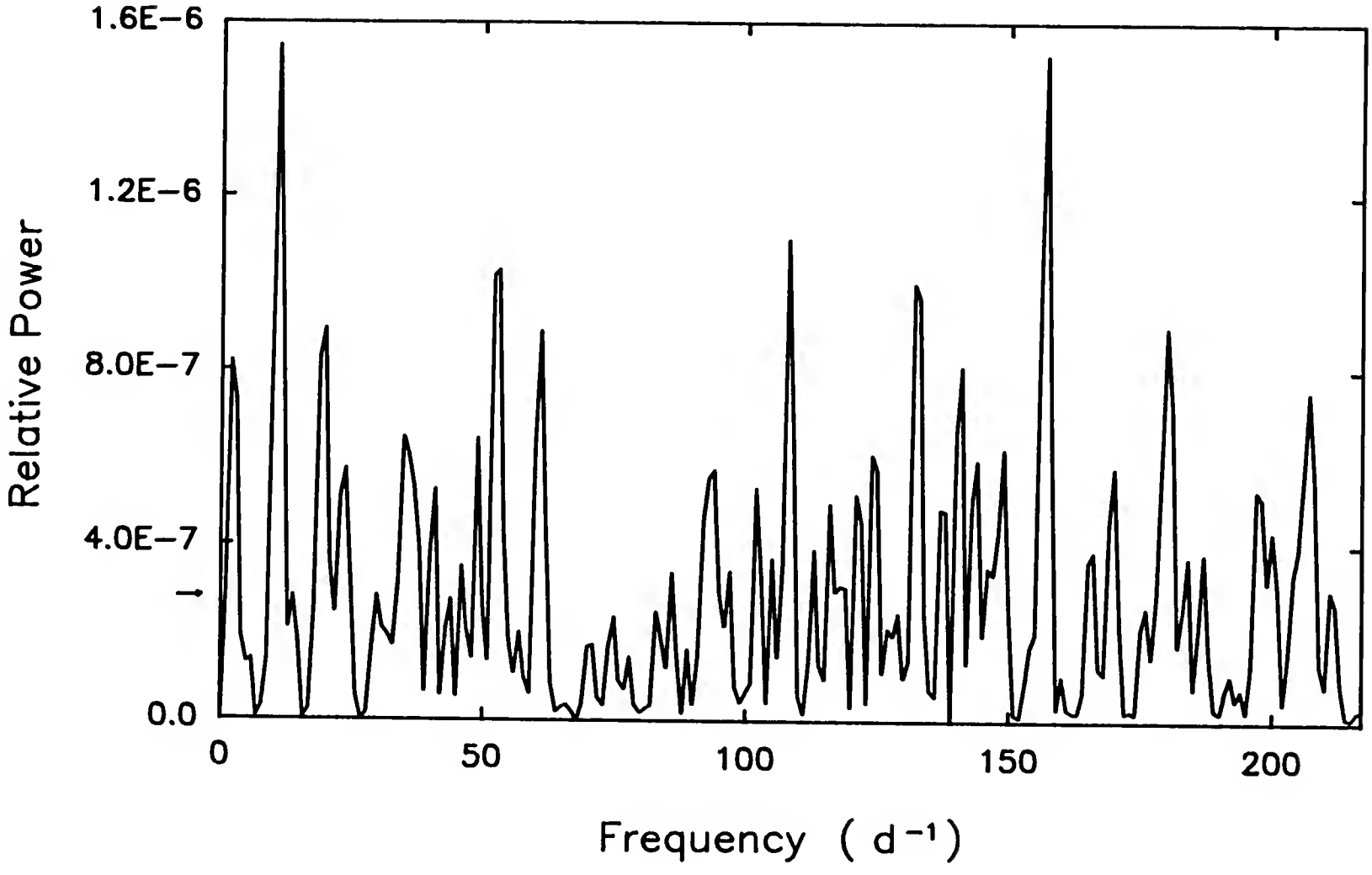

Figure 4-39 Power spectrum for the carbon observations of subset II of data set IV before execution of the clean algorithm.

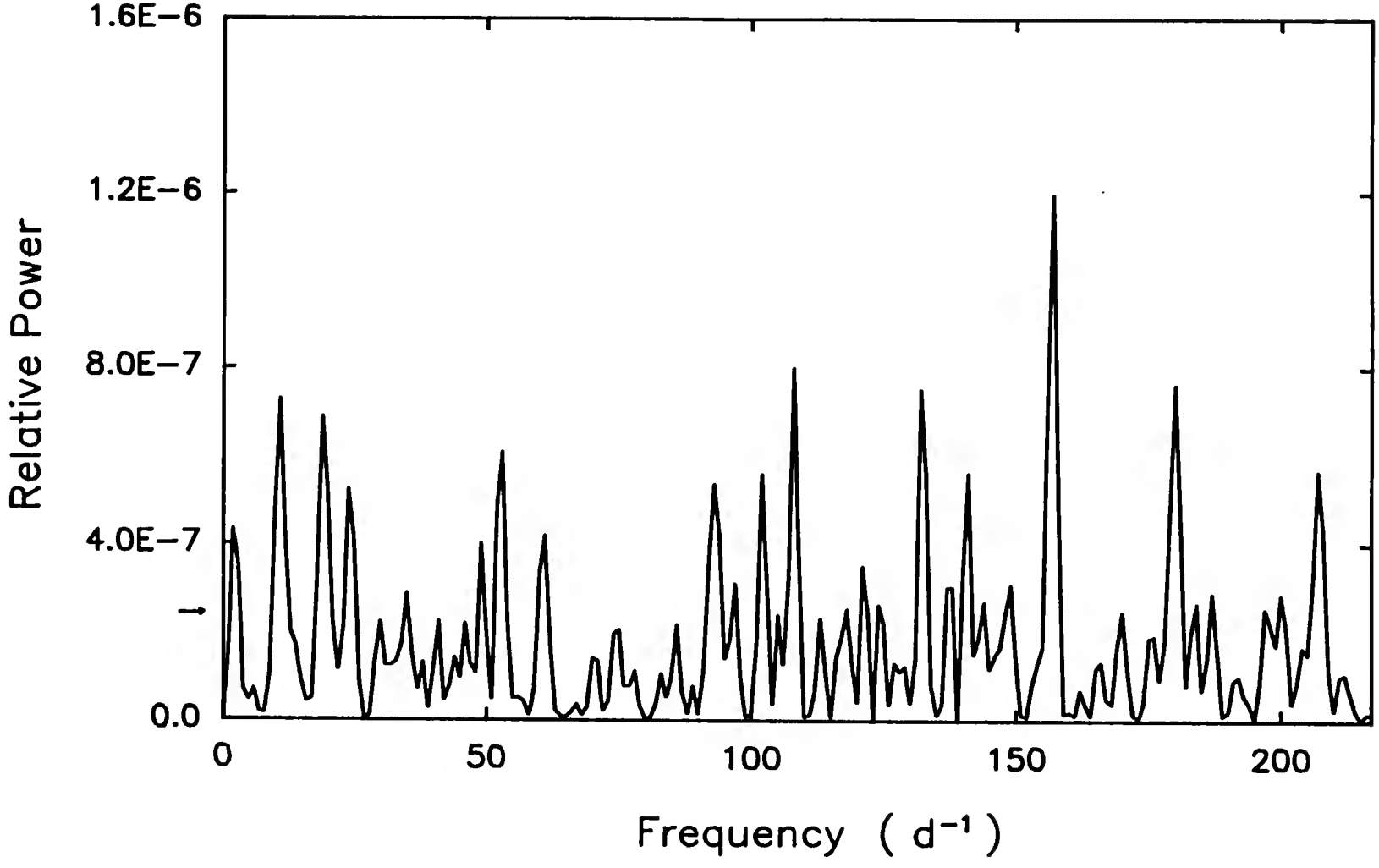

Figure 4-40 Power spectrum for the carbon observations of subset II of data set IV after execution of the clean algorithm.

signal-to-noise ratio of 6.9. The least-squares routine converges for a period very close to this frequency, but the amplitude of the resultant variation is again very small and therefore is not considered to be significant.

In summary, the variations in the helium intensity measurements are not well modeled when the entire data set is analyzed. Separating this data set into two subsets provides a better understanding of the fluctuations. The first of these subsets is best described with a period on the order of 5.79 hours. Although a period of 2.23 hours is determined from the least-squares method of analysis and corresponds in frequency to a peak in the power spectrum of these data, the second subset is best described with a longer period of 6.31 hours. If variations in the intensity of the carbon emission line exist, the amplitude of the fluctuations is too low to be modeled within the limitations of these data.

Data Set V.

The data set investigated in this section includes over 13 hours of continuous photometry of γ^2 Vel. The (421) data points cover the time interval extending from JD2446615.3343 to JD2446615.8918. The observing program used to secure these data is that described in Table 4-2. Successive observations in any single filter are separated by $0^d.0013$.

According to the Nyquist theorem, peaks in the power spectrum at frequencies between $\nu_{min} = 3.5d^{-1}$ and $\nu_{max} = 385d^{-1}$ can be regarded with confidence. The sampling function for this data set is computed for this range of frequencies and is shown in Figure 4-41. In the diagram we note that the complexity of the window increases toward high frequencies, but the first three odd harmonics at approximately, $\nu_1 = 50d^{-1}$, $\nu_3 = 100d^{-1}$, and $\nu_5 = 150d^{-1}$, are still identifiable. The convolution of the intensities of the helium emission line with the beam results in Figure 4-42. The noise level at 8.732×10^{-7} indicates that peaks at $\nu = 4.5$, 12, 19, 131, and $154d^{-1}$ are statistically significant. The peak at $\nu = 154d^{-1}$ corresponds to a peak in the spectral window, however the height of the peak in the beam is not sufficient to exclude the possibility that an additional component contributes to this feature. The corresponding peak in the beam is only about 5% as strong as the main component in that spectrum, while the peak at $\nu = 154d^{-1}$ shown in Figure 4-42 is nearly 75% of the main feature at $\nu = 4.5d^{-1}$. Deconvolving the power spectrum (Figure 4-42) from the spectral window function results in the CLEANed spectrum depicted in Figure 4-43 where the features at $\nu = 4.5$, 12, and $154d^{-1}$ remain statistically significant. The strongest of these features at $\nu = 4.5d^{-1}$, has a relative power of approximately $8.7\sigma_N$ and corresponds to a period of 5.3 hours. The feature at $\nu = 12d^{-1}$ also

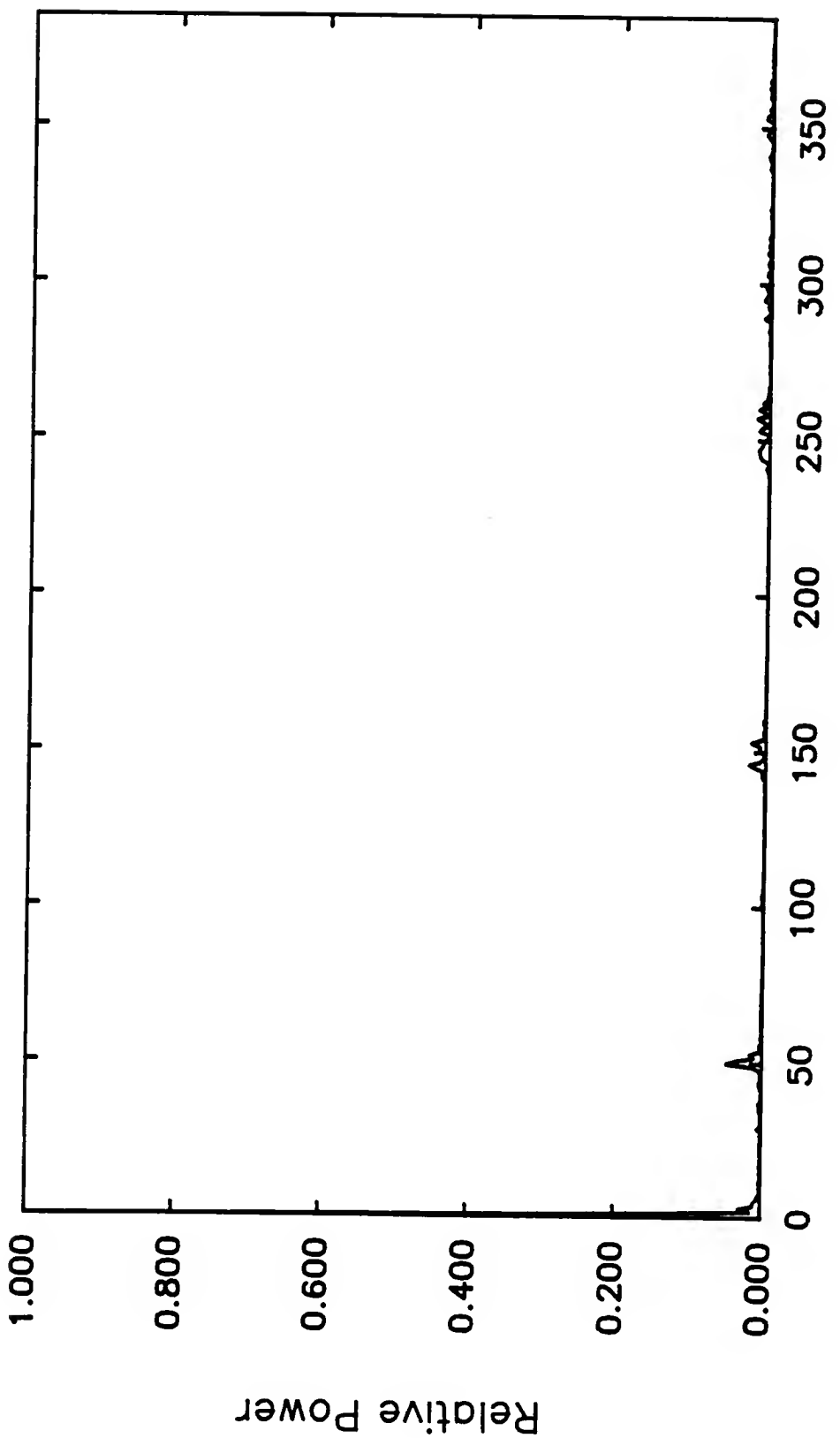

Figure 4-41 Spectral window function for data set V.

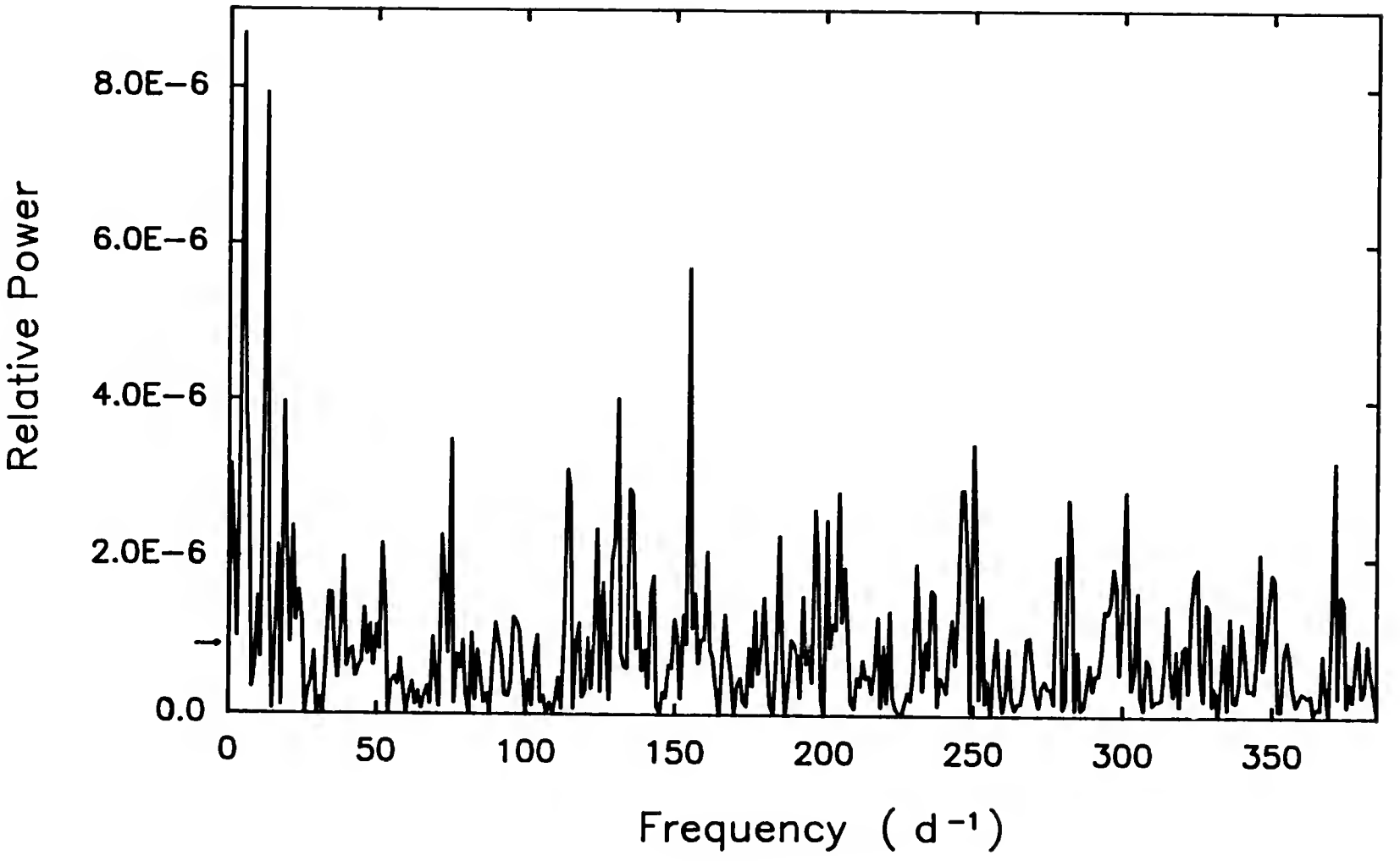

Figure 4-42 Power spectrum for the helium observations of data set V before execution of the clean algorithm.

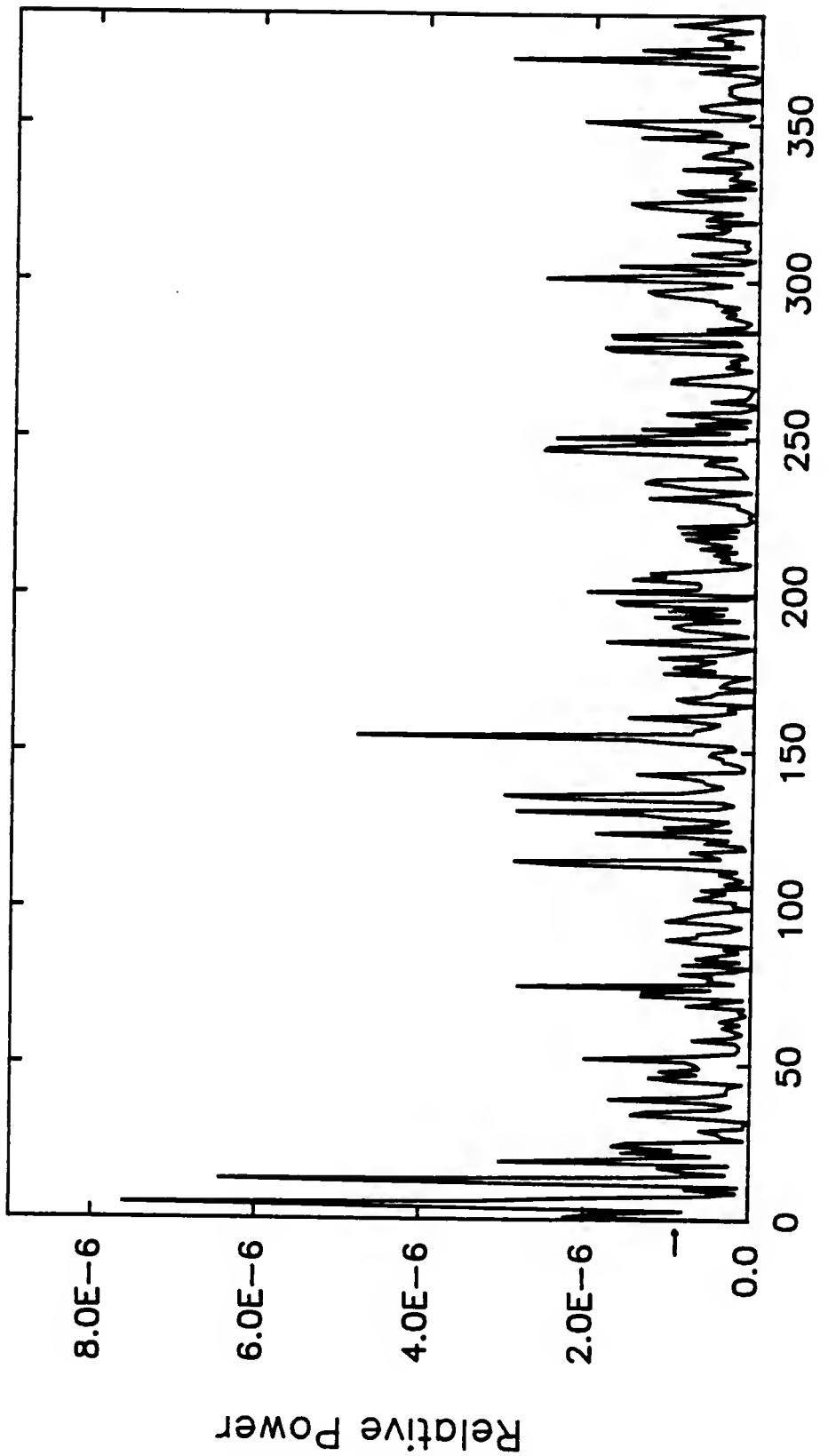

Figure 4-43 Power spectrum for the helium observations of data set V after execution of the clean algorithm.

rises substantially above the $4\sigma_N$ level at $7.7\sigma_N$ and corresponds to P = 2.0 hours. Finally, the peak at $\nu = 154d^{-1}$ has a relative power equal to 5.5 times that of the $1\sigma_N$ level and represents more rapid fluctuations on the order of 9.35 minutes. The least-squares routine converges to a period which corresponds most closely to the feature at $\nu = 4.5d^{-1}$ in Figure 4-43. The resulting model, described mathematically as

$$D(t_i) = 0.34509 + 0.00325 * \sin\left(\frac{t_i - 0.86470}{0.03217}\right), \qquad (4\text{-}11)$$

is depicted in Figure 4-44. This fit seems to represent the changes in the observations for the earlier points much more satisfactorily than for data points near the end of the data set. The change in the quality of the fit may indicate that the variations exhibited in these data might better be understood if the data are divided into two subsets. The separation point was chosen to coincide with a 32 minute gap in the data. Using the method of least-squares, the best-fit sine wave for the data obtained between JD2446615.3315 and JD2446615.4851 was accomplished with the equation

$$D(t_i) = 0.34441 + 0.00318 * \sin\left(\frac{t_i - 0.31000}{0.00786}\right), \qquad (4\text{-}12)$$

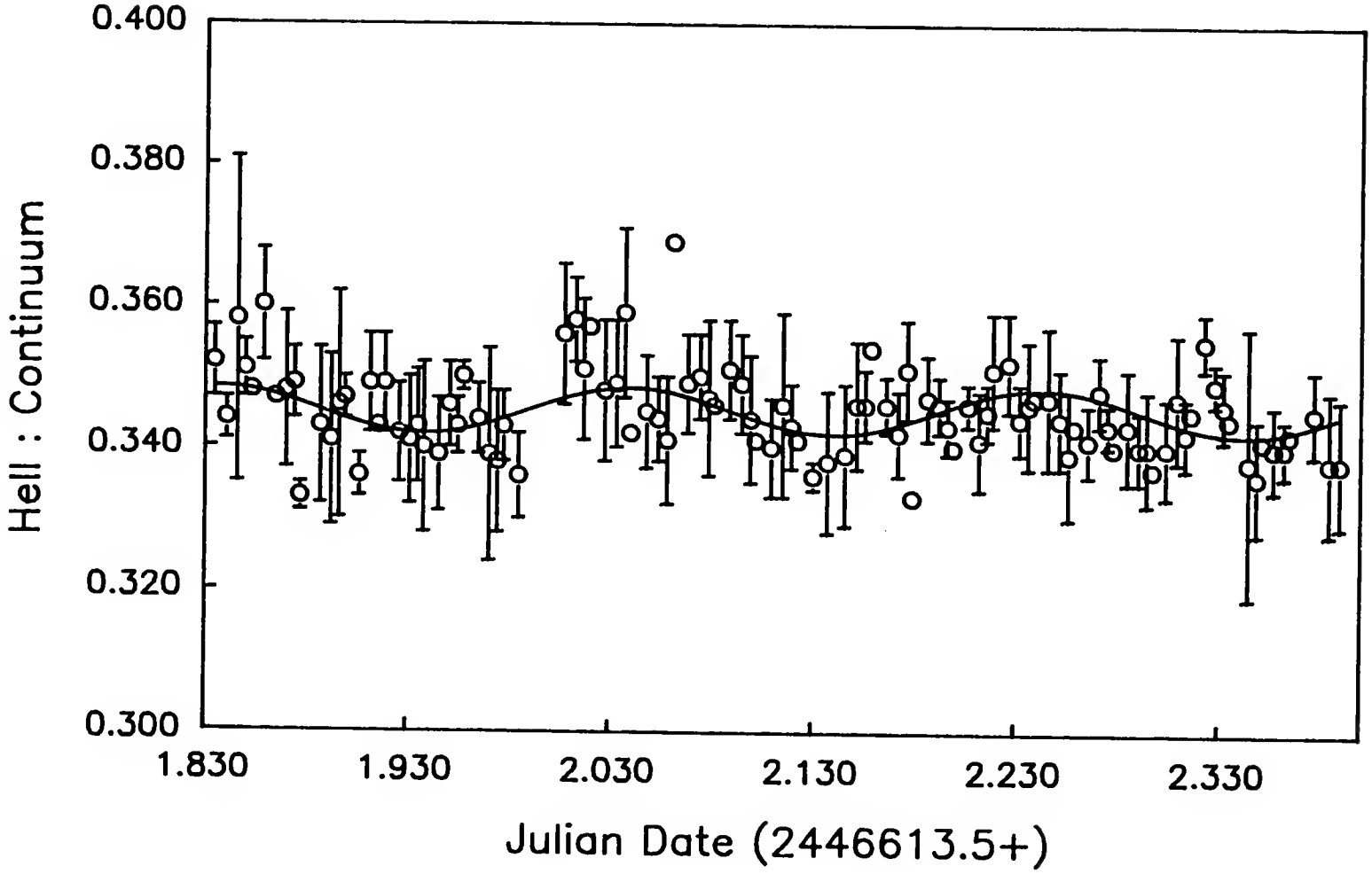

Figure 4-44 Model for the variations of the helium data for data set V with P = 4.85 hours. Each plotted point represents the average intensity within a $0^{d}.0040$ interval.

where P = 1.19 hours. The data spanning the remainder of the data set, JD2446615.5075 through JD2446615.8918, results in a variation which is slightly larger than that for the first subset, with P = 1.83 hours. The appropriate parameters selected by the least-squares routine results in equation (4-13):

$$D(t_i) = 0.34472 + 0.00340 * \sin\left[\frac{t_i - 0.59330}{0.01211}\right]. \qquad (4\text{-}13)$$

Models for each of these portions of the data are shown in Figures 4-45 and 4-46, where each plotted point is a $0^d.0040$ average. The accompanying error-bars represent the standard deviation associated with the individual points within each average.

Figures 4-47 and 4-48 show dirty and clean power spectra for the carbon data. Several peaks in each of these plots have a relative power in excess of $4\sigma_N = 5.940 \times 10^{-1}$. Although it is interesting to note that the three strongest peaks occur at frequencies around $\nu = 12d^{-1}$, it is not possible to single out the dominance of any one period. The least-squares routine also has difficulty in converging to a best overall period which satisfies the variations. In fact, the routine converges for several periods with the largest amplitude of variation amounting to only 1% of the intensity of the carbon emission feature. It is certainly

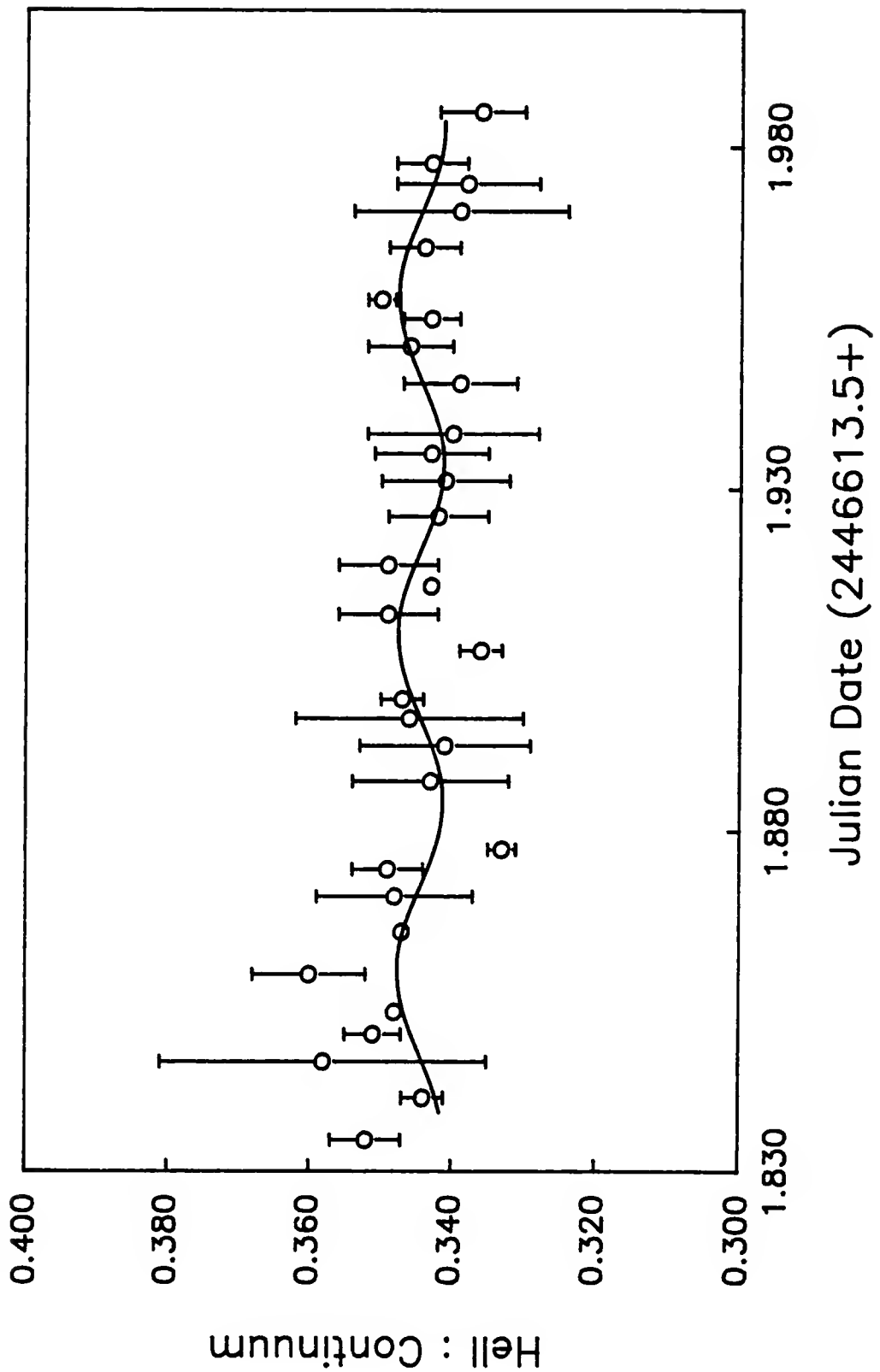

Figure 4-45 Model for the variations of the helium data for subset I of data set V with P = 1.19 hours. Each plotted point represents the average intensity within a $0^d.0040$ interval.

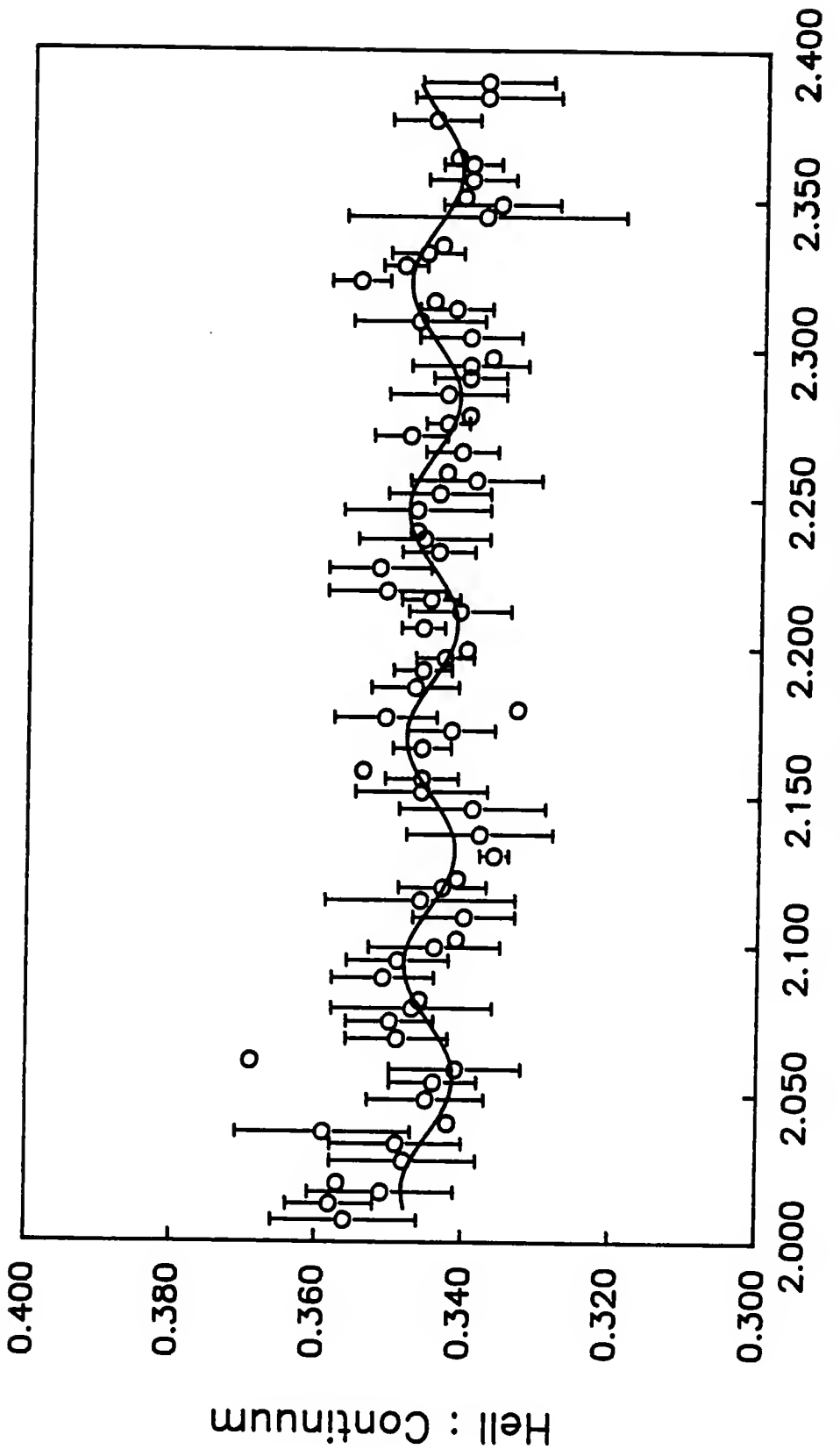

Figure 4-46 Model for the variations of the helium data for subset II of data set V with P = 1.83 hours. Each plotted point represents the average intensity within a 0.0040 interval.

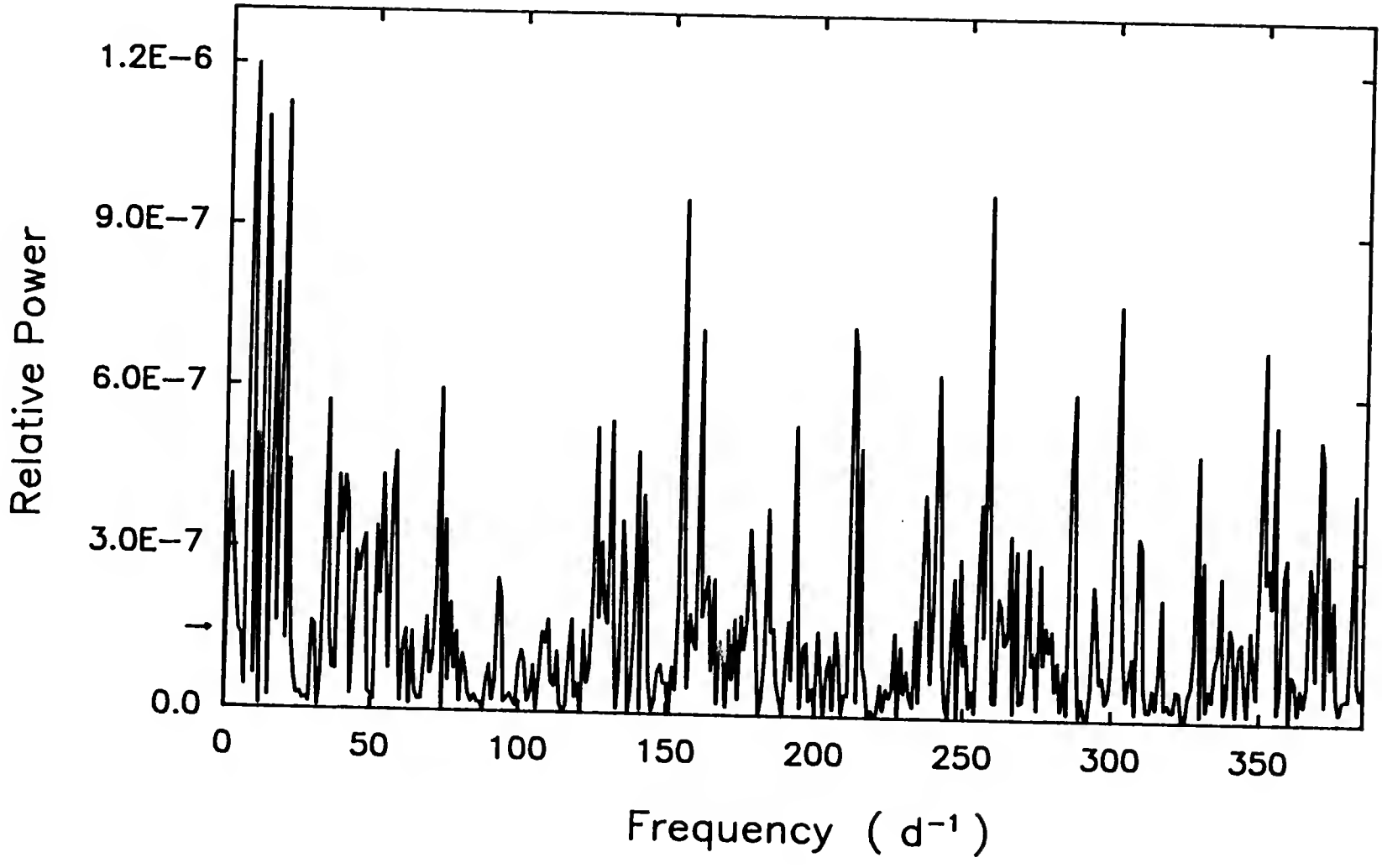

Figure 4-47 Power spectrum for the carbon observations of data set V before execution of the clean algorithm.

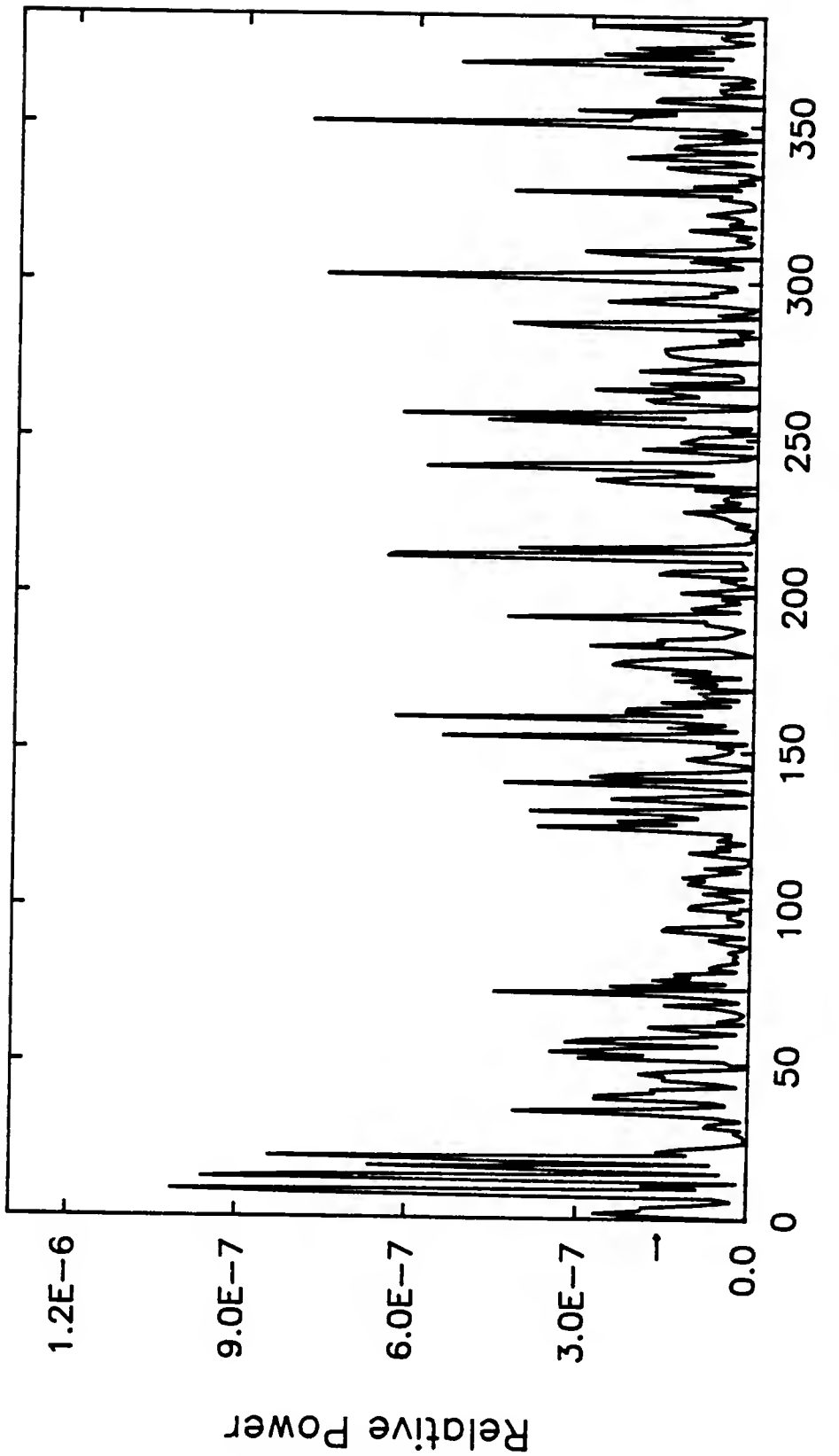

Figure 4-48 Power spectrum for the carbon observations of data set V after execution of the clean algorithm.

not possible to discern these small variations from the intrinsic noise which is present in the data.

This data set is certainly one of the most difficult to interpret. Neither the power spectrum analysis nor the least-squares method provide conclusive results. Probably no single period can be used to describe the fluctuations present during the time interval covered here. Figures 4-49 and 4-50 are plots of the last six hours of the data set. Figure 4-49 depicts the intensity of the helium emission line as a function of time, while Figure 4-50 is a similar plot of the changes in the carbon emission feature. These diagrams certainly seem to indicate a progressive change in the intensities of the emission lines, especially at JD2446615.82, but the phenomenon does not seem to repeat on a regular basis.

Data Set VI.

Five-hundred and ninety-eight observations of γ^2 Vel were obtained in the helium and carbon filters from JD2446621.7110 through JD2446622.3862. In order to eliminate gaps in the data set due to observations of objects other than γ^2 Vel and comparison star HR3452, a new observing program was written. This program (Table 4-3) consists only of deflections of γ^2 Vel and HR3452. The average spacing between reduced observations in each of the helium and carbon filters is $0^d.0011$. The time-resolution of these data taken together with the 16.2 hours spanned by the

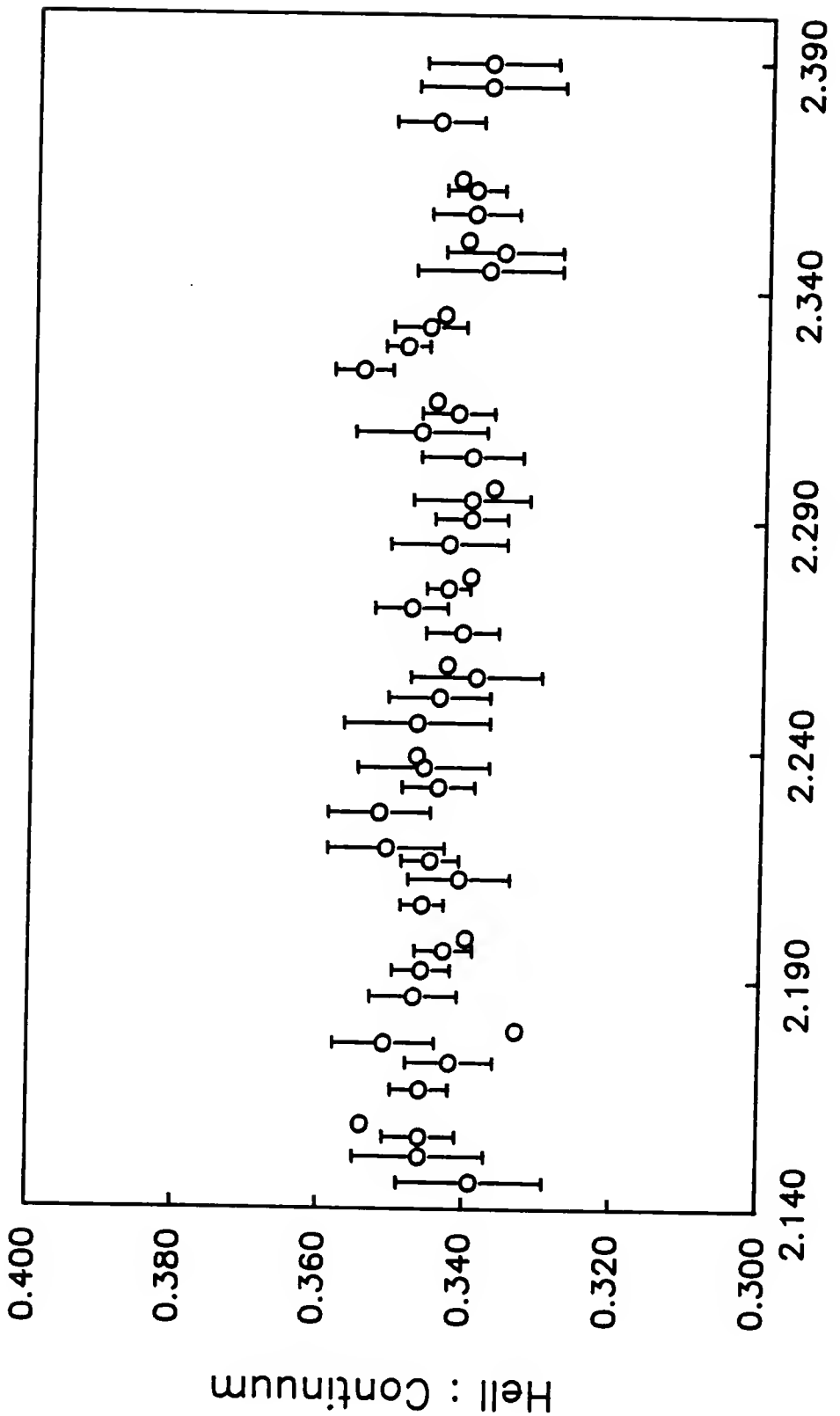

Figure 4-49 Plot of the intensity of the helium emission line for the last six hours of data set V.

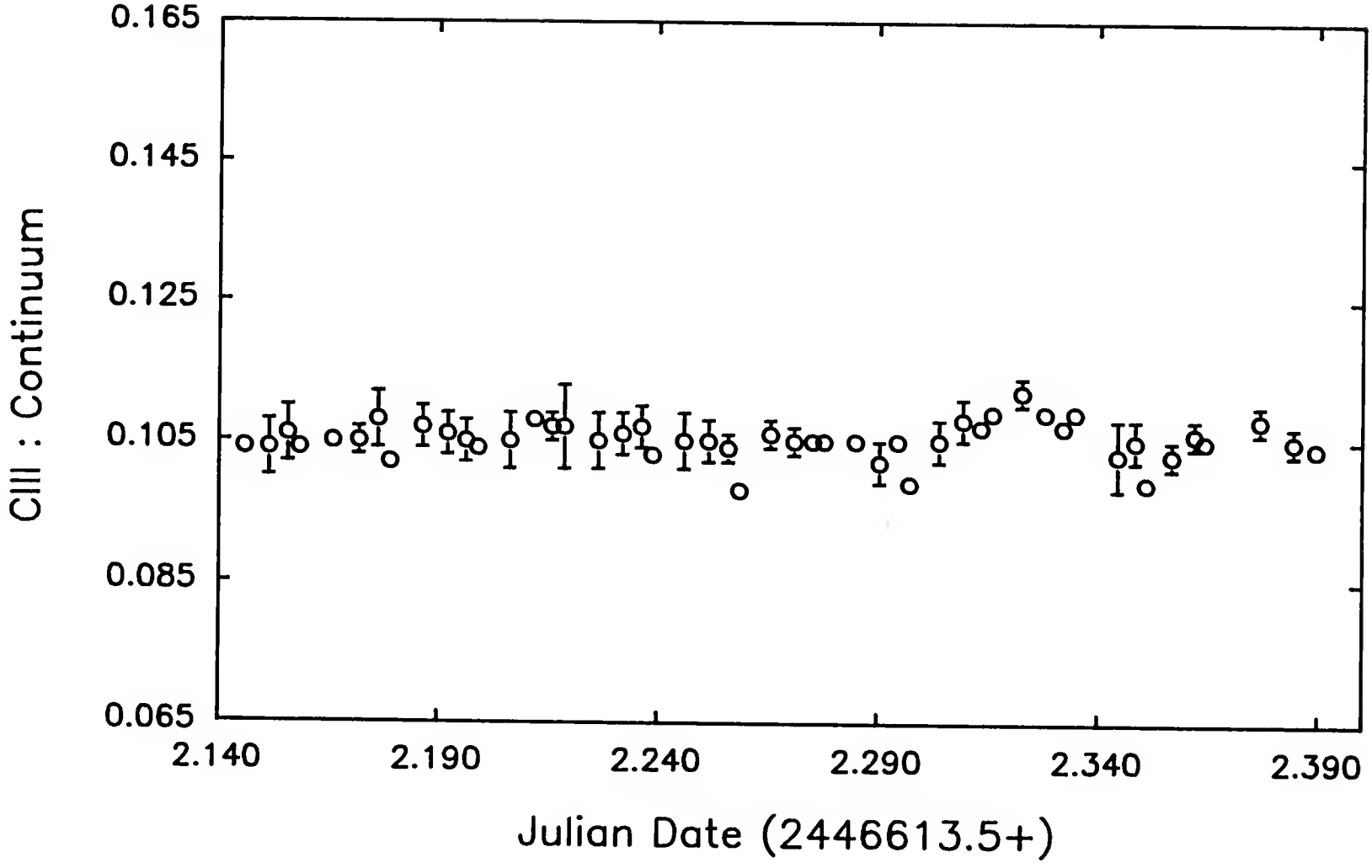

Figure 4-50 Plot of the intensity of the carbon emission line for the last six hours of data set V.

data set, allows for a wide range of frequencies to be analyzed: $\nu_{min} = 3d^{-1}$ and $\nu_{max} = 455d^{-1}$. Figure 4-51 shows the resulting spectral window function for this group of data. Although the relative power of the peaks is quite low, one can still identify first and second harmonics. After that, the beam becomes contaminated with extremely low amplitude noise. The strongest harmonic, other than that at $\nu = 0d^{-1}$, is located at about $\nu = 60d^{-1}$ and is only about 3.5% as strong as the main component. Hence, one would expect that the sampling function may introduce only small amplitude spurious features into the power spectrum of these data. Figures 4-52 and 4-53 show the Fourier transform of the helium intensity measurements in terms of relative power and the spectrum which results after cleaning at the $3\sigma_N$ level. The noise level for each of these plots is at 1.192×10^{-6}, and a number of peaks are statistically significant. In Figure 4-53, the strongest feature at $\nu = 3d^{-1}$ (P = 8.0 hours) occurs at the beginning of the plot and corresponds almost exactly to ν_{min}. This feature has a signal-to-noise ratio of approximately 12.4. The next strongest feature is at $\nu = 20d^{-1}$ (P = 1.20 hours) and has a relative power equivalent to $8.39\sigma_N$. Another reasonably strong peak is located at $\nu = 328d^{-1}$, suggesting rapid variations on the order of 263 seconds. This peak has a strength which exceeds the noise level by a factor of 5.5, and must be considered within the context of this analysis.

Table 4-3
Observing Program 3

Star	B	V	He	C	O	Continuum
C*[1]	X	X				
CS[2]	X	X				
C*	X	X				
V*[3]	X	X	X	X	X	X
V*	X	X	X	X	X	X
V*	X	X	X	X	X	X
V*	X	X	X	X	X	X
V*			X	X	X	
V*			X	X	X	
V*			X	X	X	
V*			X	X	X	
VS[4]	X	X	X	X	X	X
V*			X	X	X	
V*			X	X	X	
V*			X	X	X	
V*			X	X	X	
V*	X	X	X	X	X	X
V*	X	X	X	X	X	X
V*	X	X	X	X	X	X
V*	X	X	X	X	X	X
C*	X	X				
CS	X	X				
C*	X	X				

[1] C* = comparison star
[2] CS = comparison sky
[3] V* = variable star
[4] VS = variable sky

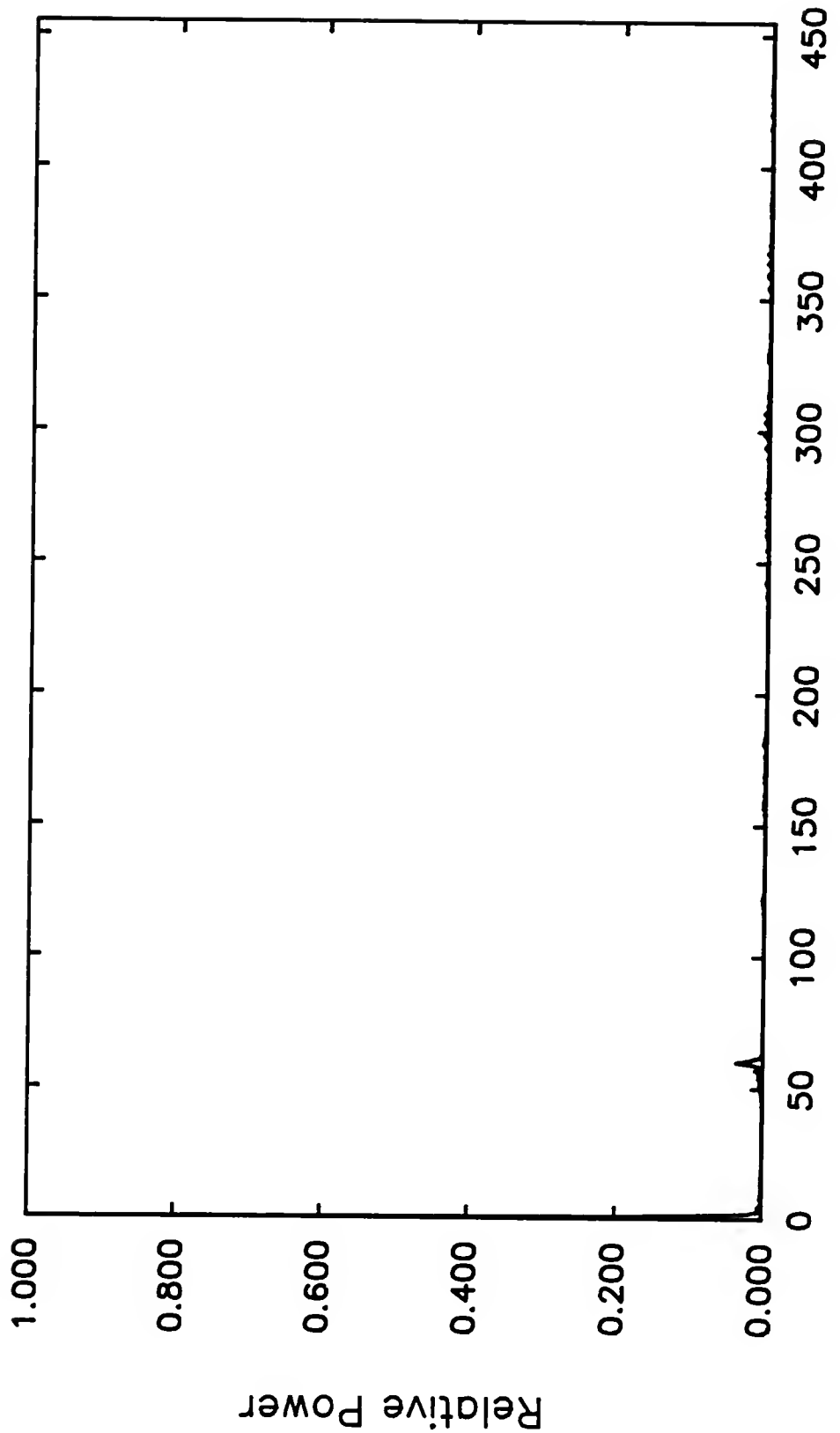

Figure 4-51 Spectral window function for data set VI.

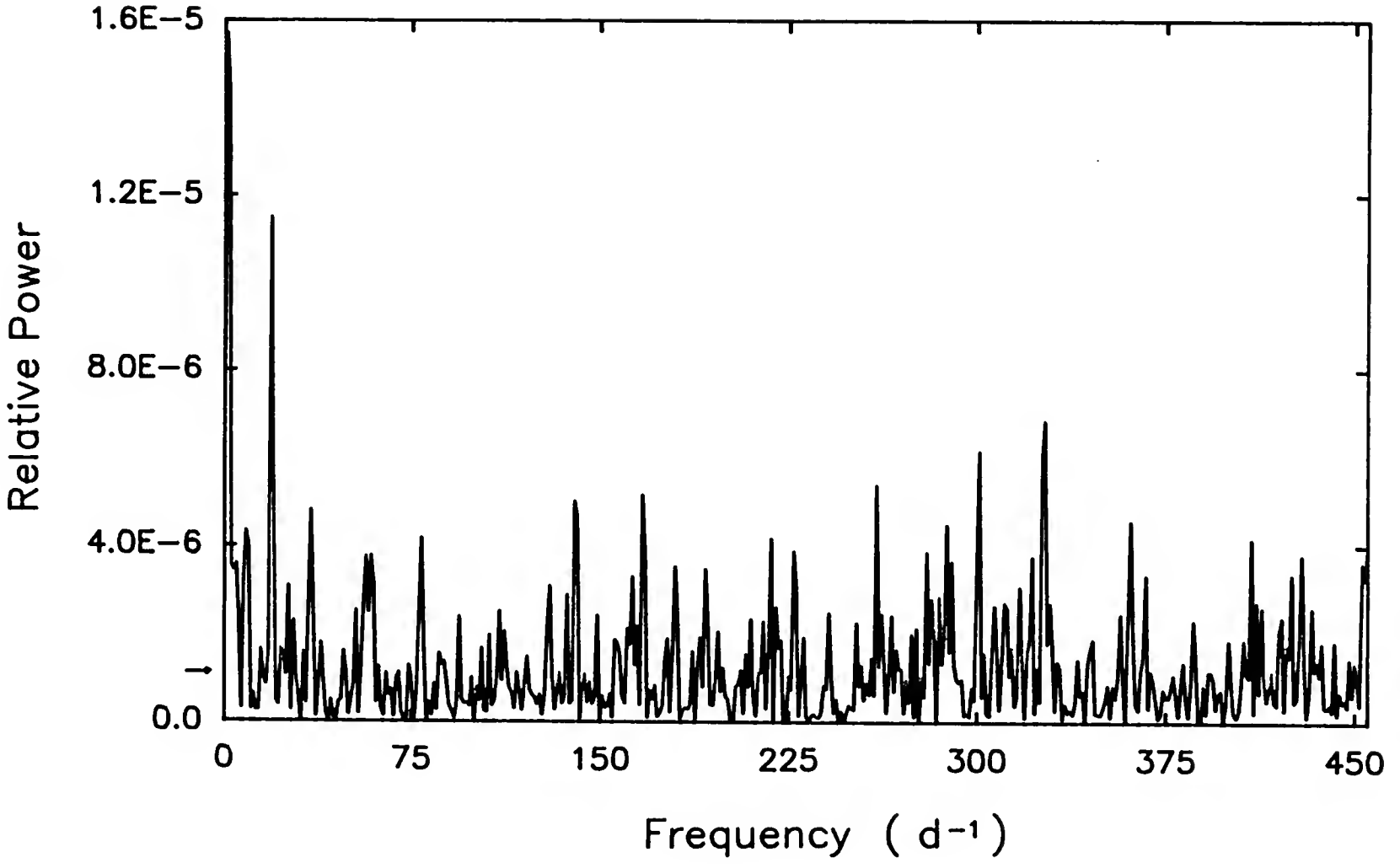

Figure 4-52 Power spectrum for the helium observations of data set VI before execution of the clean algorithm.

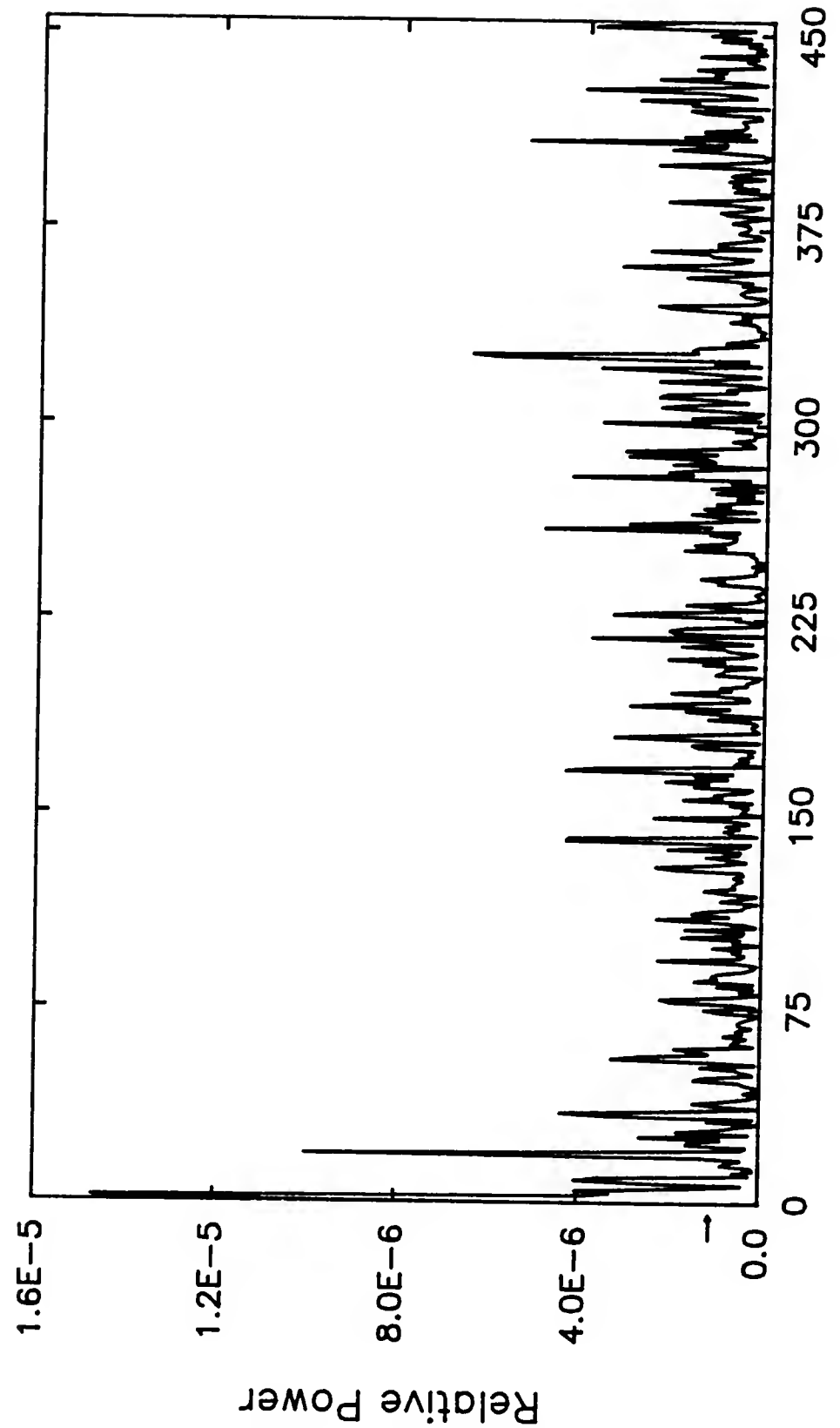

Figure 4-53 Power spectrum for the helium observations of data set VI after execution of the clean algorithm.

One last feature which should be mentioned is that at $\nu = 409 d^{-1}$ (P = 211 seconds). Although this peak is certainly not as strong as the three previous features which have been mentioned, it still remains statistically significant. The least-squares routine does not converge for a period this short, but the possible significance of the presence of this feature must not be overlooked. Very rapid fluctuations, between 150 and 200 seconds, have been previously reported (Jeffers et al. 1973a, 1973b) and the variation found in these data with P = 211 seconds may support the existence of intermittent rapid fluctuations of the intensity of the HeII emission line.

The least-squares routine converges for two primary sets of parameters: one has a period of 1.24 hours which corresponds quite well with the peak at $\nu = 20 d^{-1}$, from Figure 4-53. The other period which is identified has a length of 2.44 hours, almost exactly twice the 1.24 hour period. This is a good indication of a first harmonic. The model for the shorter of these periods is shown in Figure 4-54 and is described by equation (4-14):

$$D(t_i) = 0.34712 + 0.00403 * \sin\left(\frac{t_i - 0.22991}{0.00825}\right). \qquad (4\text{-}14)$$

Neither this model nor the model for the 2.44 hour period seems to be an adequate representation of these data.

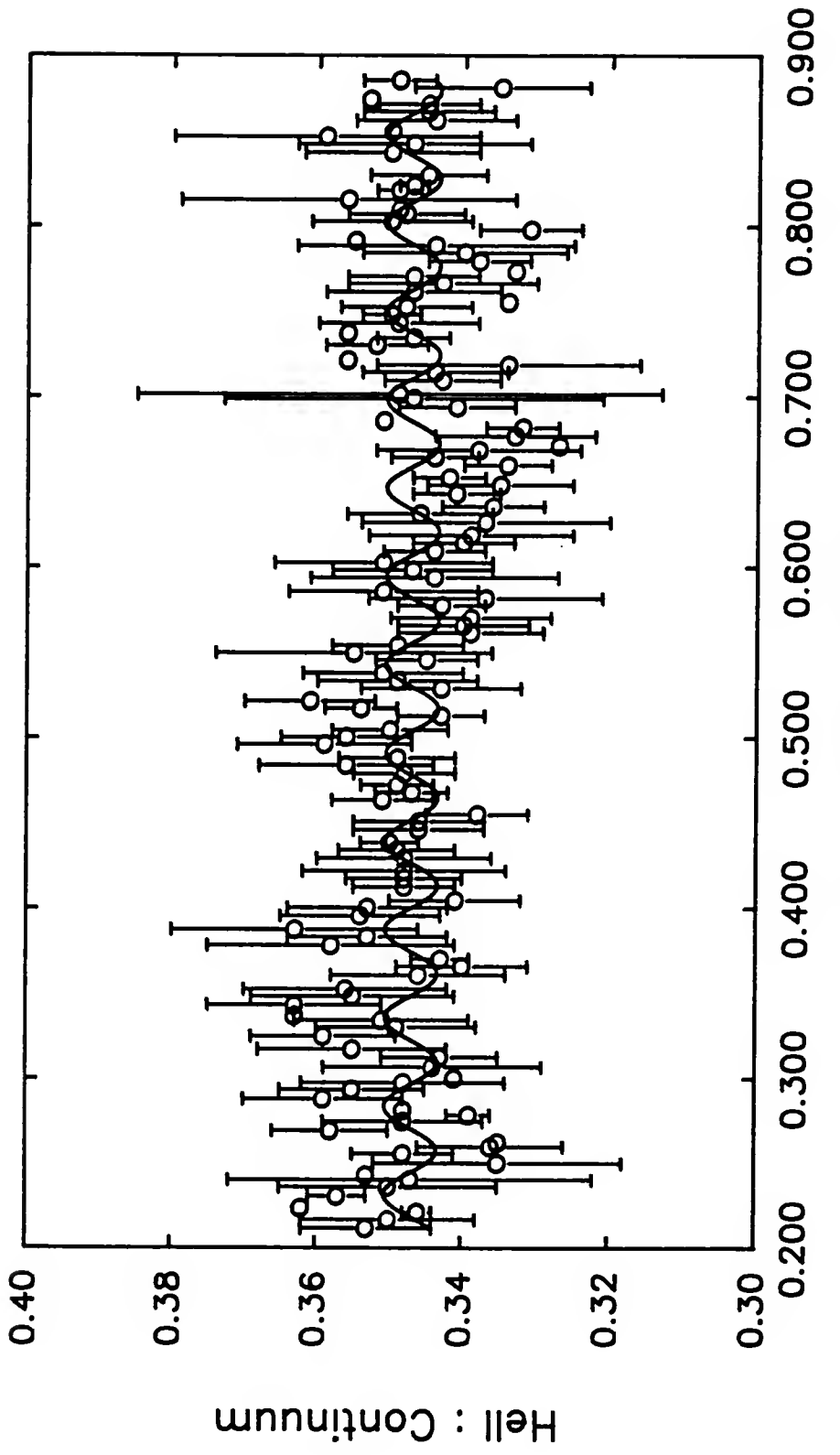

Figure 4-54 Model for the variations of the helium data of data set VI with P = 1.24 hours. Each plotted point represents the average intensity within a $0^d.0040$ interval.

However, a look at the deflections in the helium filter plotted as a function of time, indicates that perhaps a change in period or phase may have occurred at approximately JD2446621.9118. The fluctuations seem to be quite regular to this point, when a new period seems to become more dominant.

To investigate this possibility, the original data set was again divided into two subsets. The first subset covered the interval between JD2446621.7110 and JD2446621.9118, while the second subset covered the remainder of the data extending from JD2446621.9126 through JD2446622.3862.

The sampling function for the first data set is exactly the same as that pictured in Figure 4-51. According to the power spectrum analysis procedure, the most dominant period in this data, 1.26 hours, is the most prominent feature in both the dirty (Figure 4-55) and the clean (Figure 4-56) spectra. Although three peaks rise above the statistically significant level at $4\sigma_N$, only one feature remains significant after eliminating spurious features due to the sampling function. This peak, located at $\nu = 20d^{-1}$, has a relative power of 6.6 times the noise level. The least-squares routine converges to a period of 1.30 hours, and has one of the largest amplitudes of variation found in the data so far. The model which corresponds to these

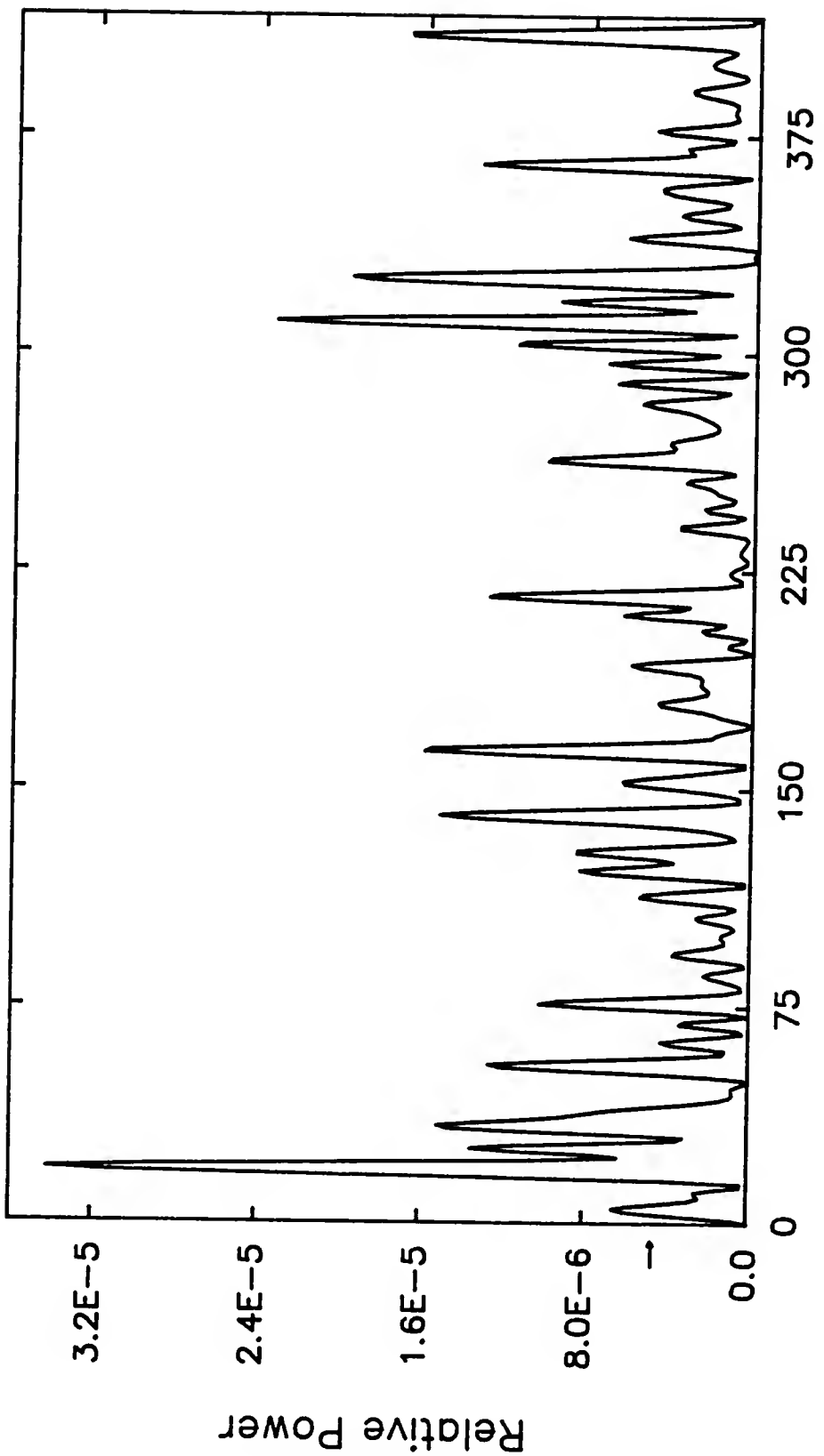

Figure 4-55 Power spectrum for the helium observations of subset I of data set VI before execution of the clean algorithm.

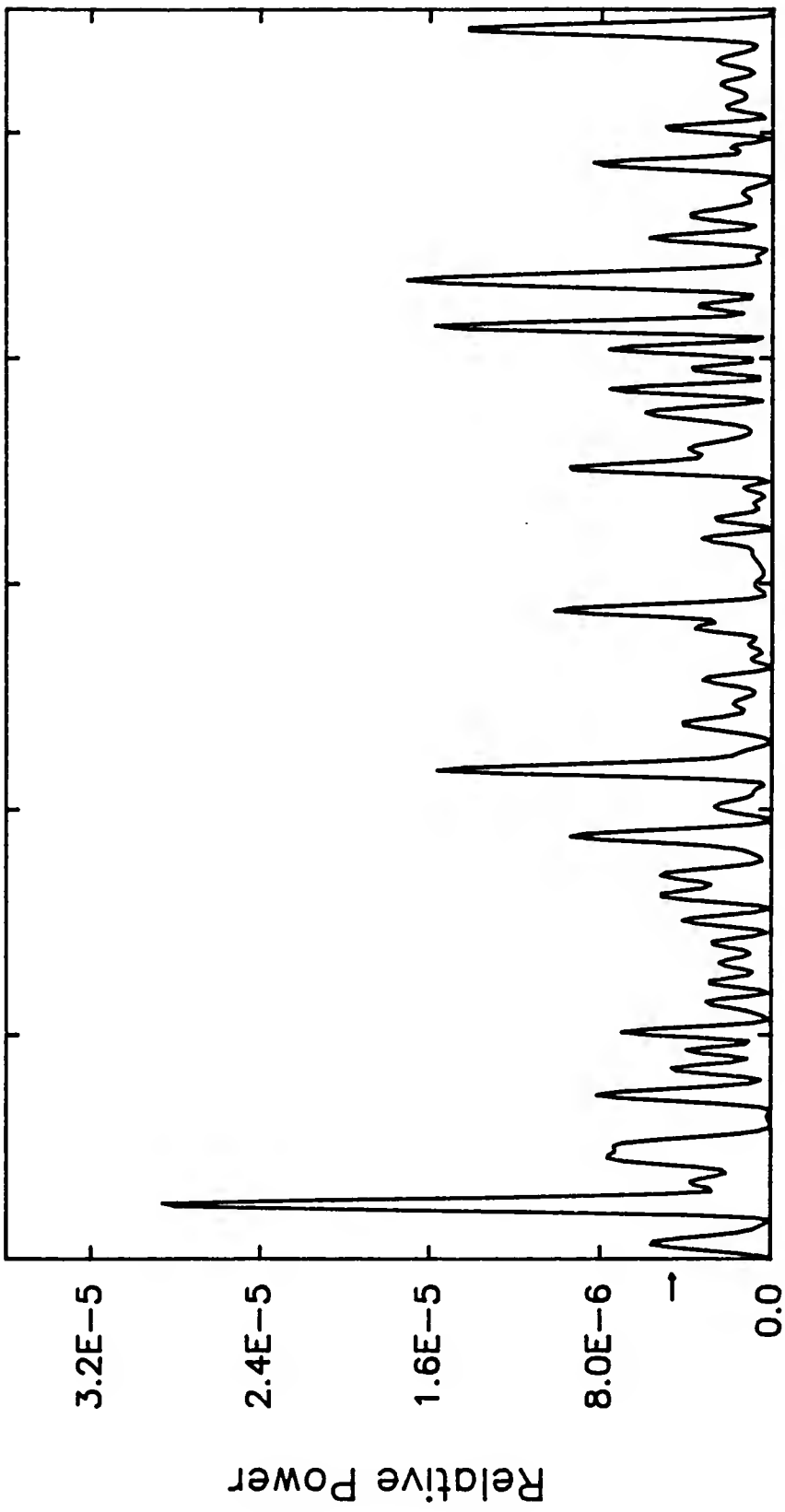

Figure 4-56 Power spectrum for the helium observations of subset I of data set VI after execution of the clean algorithm.

values is shown in Figure 4-57, and is computed with equation (4-15):

$$D(t_i) = 0.35033 + 0.00642 * \sin\left(\frac{t_i - 0.22766}{0.00861}\right). \qquad (4\text{-}15)$$

Although the error-bars from the plot are rather large, the model seems to represent a periodic variation on the order of 1.30 hours.

Again, as one might expect, the beam for the second subset is very similar to that computed for the whole data set (Figure 4-51). The noise level for these data is in fact quite low at 1.585×10^{-6}, and several peaks in the power spectrum (Figure 4-58) might be considered as statistically significant. The CLEAN procedure reduces the spurious peaks, leaving one dominant feature at $\nu = 3d^{-1}$, and two lower amplitude features at $\nu = 9d^{-1}$ and $\nu = 166d^{-1}$ (Figure 4-59). The feature at $\nu = 3d^{-1}$ is actually not within the Nyquist frequency limit for this subset, but the good agreement with the least-squares routine implies that this may represent a possible periodicity in these data. The equation used to describe these variations is

$$D(t_i) = 0.34457 + 0.00472 * \sin\left(\frac{t_i - 0.51460}{0.05324}\right), \qquad (4\text{-}16)$$

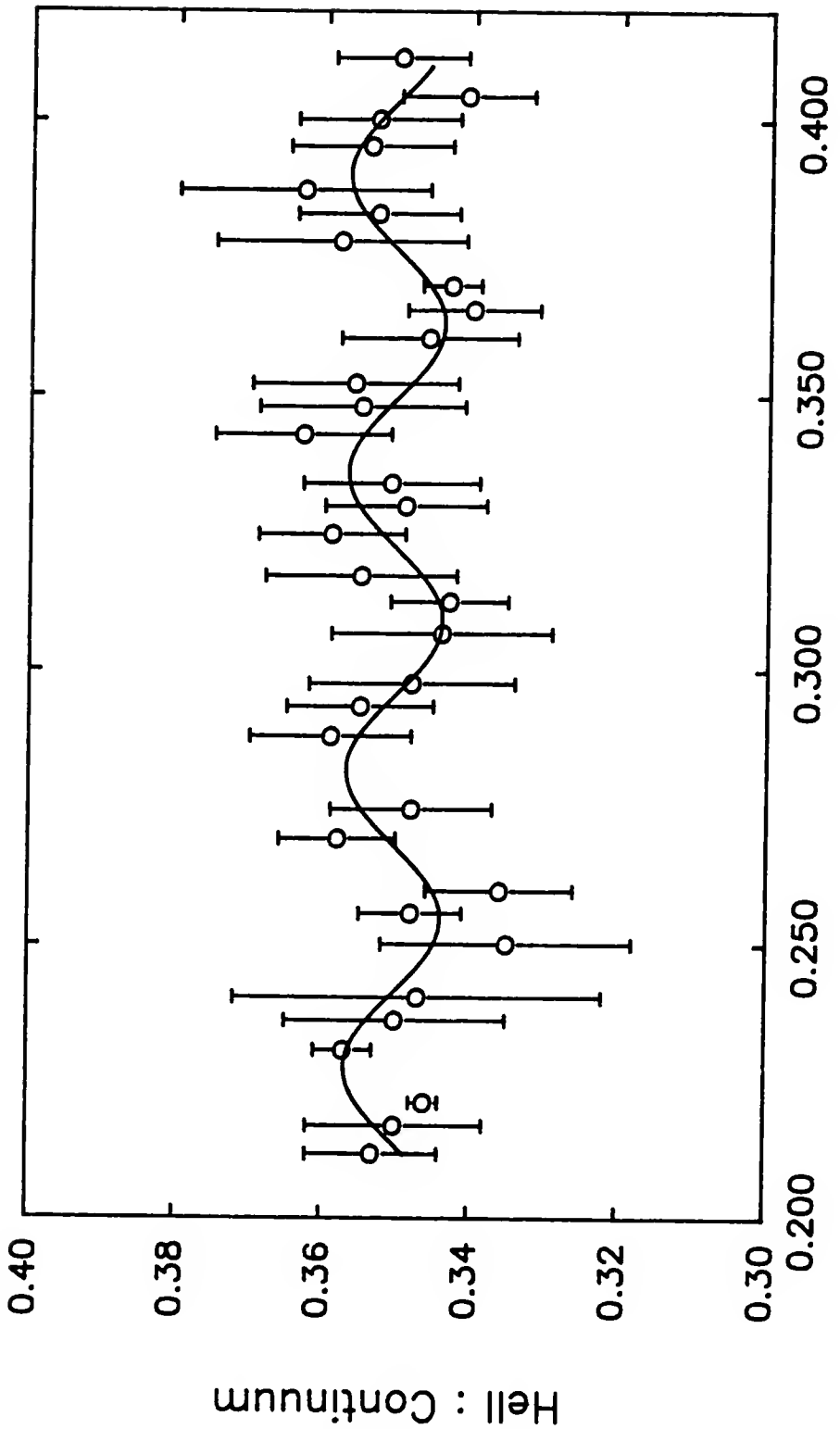

Figure 4-57 Model for the variations of the helium data for subset I of data set VI with P = 1.30 hours. Each plotted point represents the average intensity within a $0^d.0040$ interval.

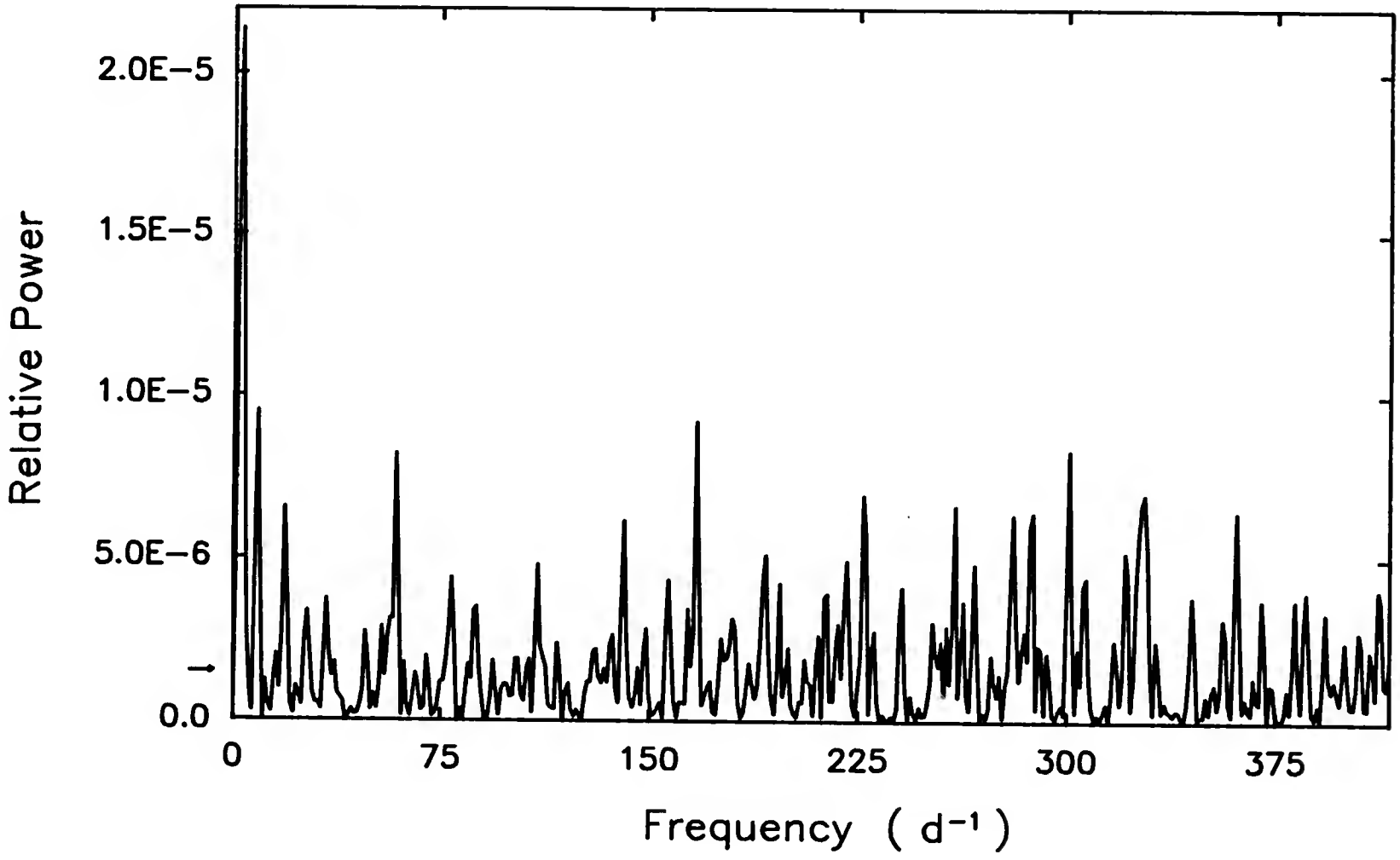

Figure 4-58 Power spectrum for the helium observations of subset II of data set VI before execution of the clean algorithm.

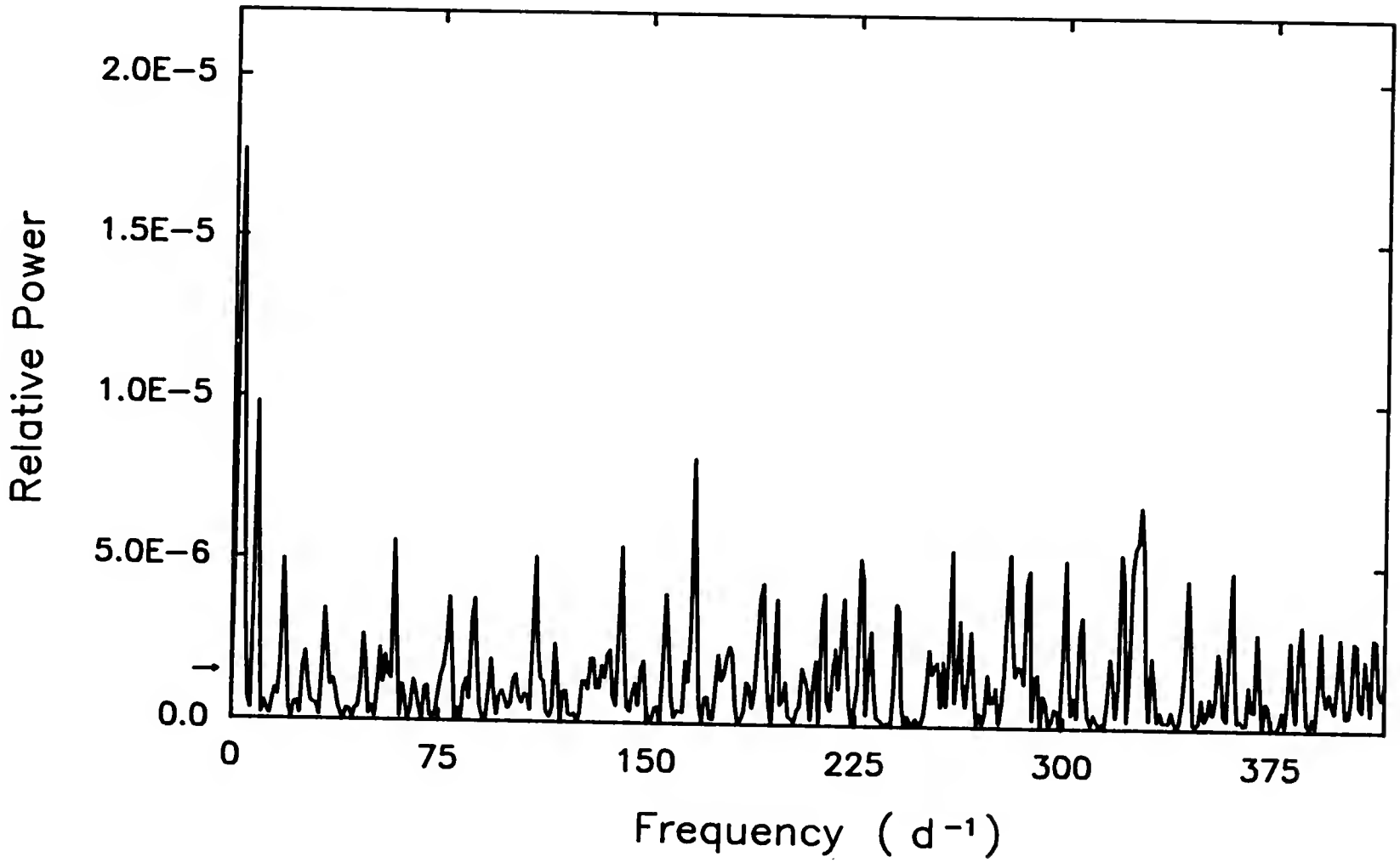

Figure 4-59 Power spectrum for the helium observations of subset II of data set VI after execution of the clean algorithm.

and the resulting model is shown in Figure 4-60 along with $0^{d}.0040$ average intensity measurements. A second solution for the quantities A_0, A_1, t_0, and P is also produced through the least-squares method of analysis. The period, 2.64 hours, corresponds to a frequency of $\nu = 9d^{-1}$ and is also a prominent feature in the power spectrum. The model for this solution is depicted in Figure 4-61, and is computed with the relation

$$D(t_i) = 0.34565 + 0.00314 * \sin\left(\frac{t_i - 0.50998}{0.01751}\right). \qquad (4\text{-}17)$$

The two models for this subset of the data indicate periodic variations in the intensity measurements of the helium emission feature. In one case a model with a period of about 8 hours is fit to the data, and in the other case, a model with a period of 2.64 hours is used.

The power spectra for the carbon data are shown in Figures 4-62 to 4-65. Figures 4-62 and 4-63 are the dirty and clean spectra for the first subset, and Figures 4-64 and 4-65 are the corresponding spectral plots for the second subset. As has been frequently the case in the analysis of the carbon data, the fluctuations have a very low amplitude and one cannot be certain of the reality of the results. As an example, a fit has been computed with the least-squares routine. The strongest variation is described by

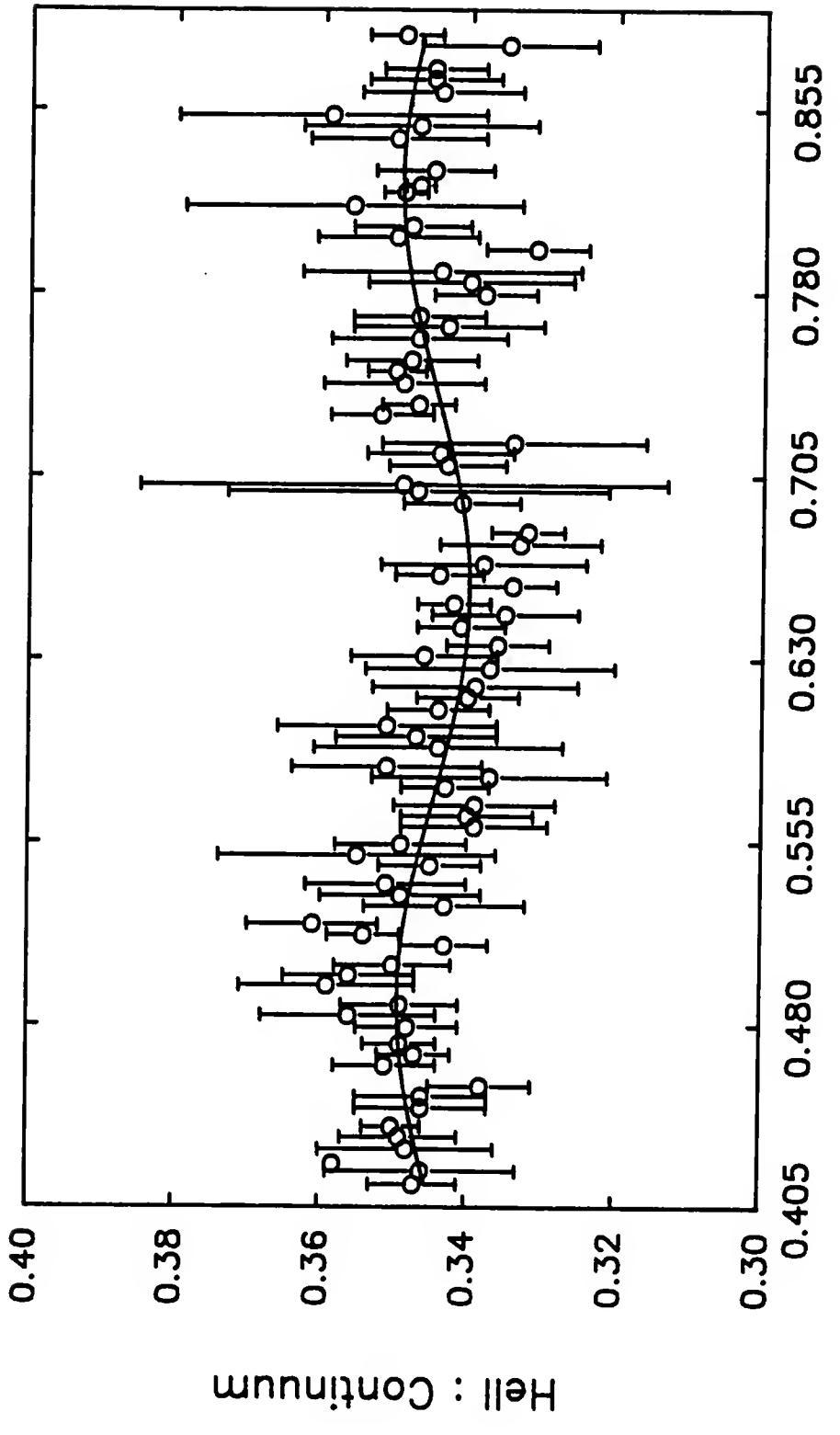

Figure 4-60 Model for the variations of the helium data for subset II of data set VI with P = 8.03 hours. Each plotted point represents the average intensity within a $0^d.0040$ interval.

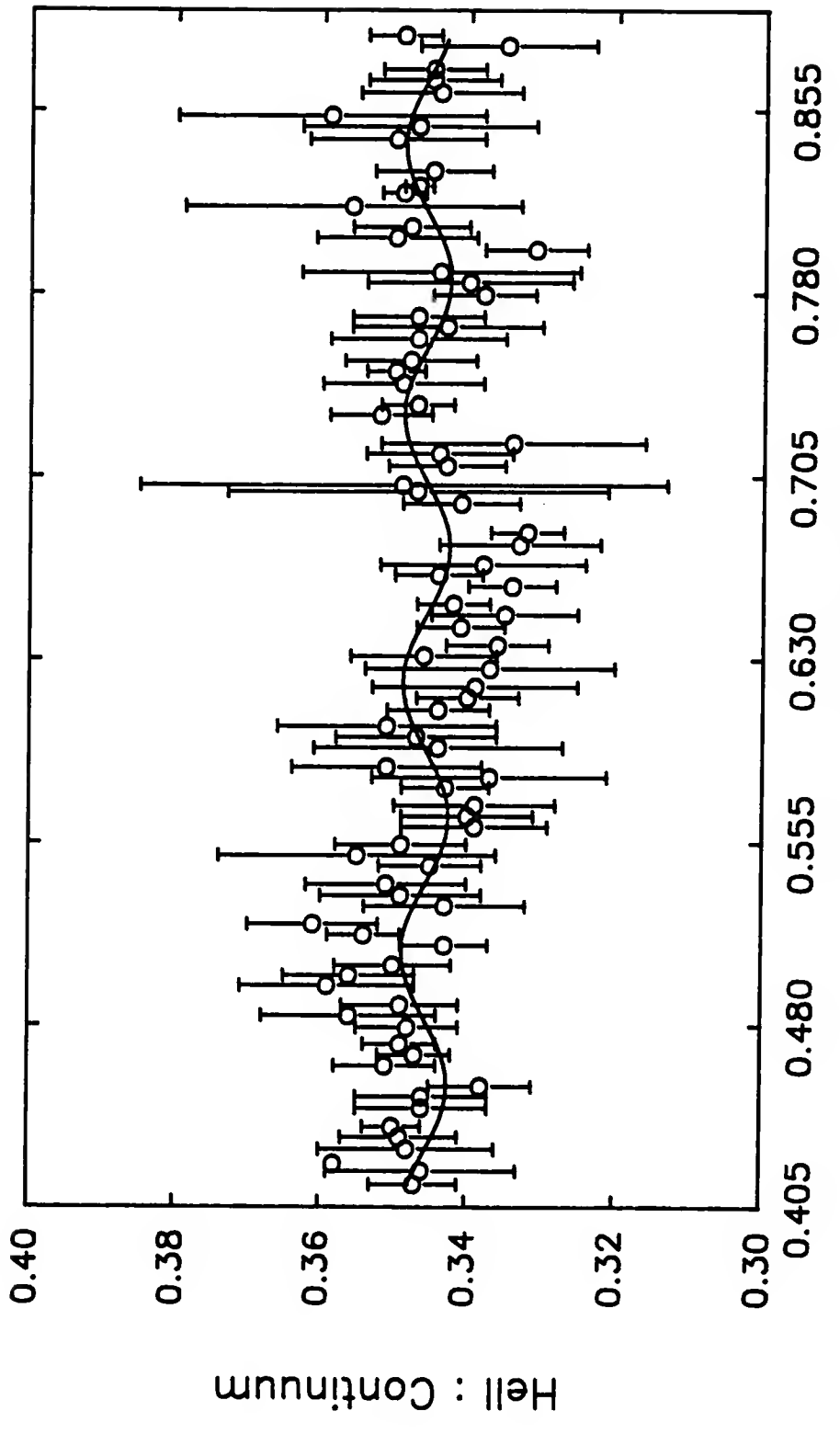

Figure 4-61 Model for the variations of the helium data for subset II of data set VI with P = 2.64 hours. Each plotted point represents the average intensity within a $0^d.0040$ interval.

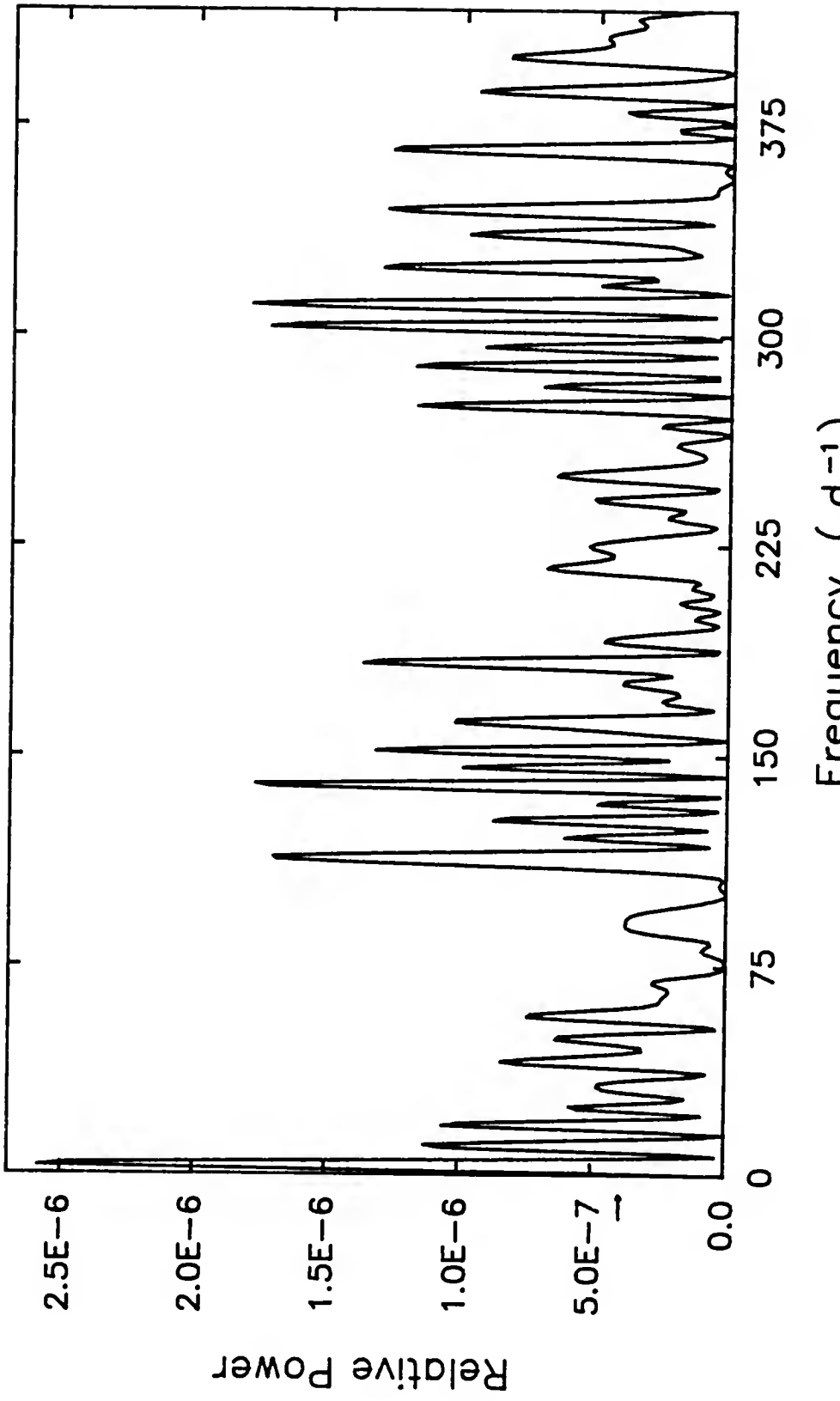

Figure 4-62 Power spectrum for the carbon observations of subset I of data set VI before execution of the clean algorithm.

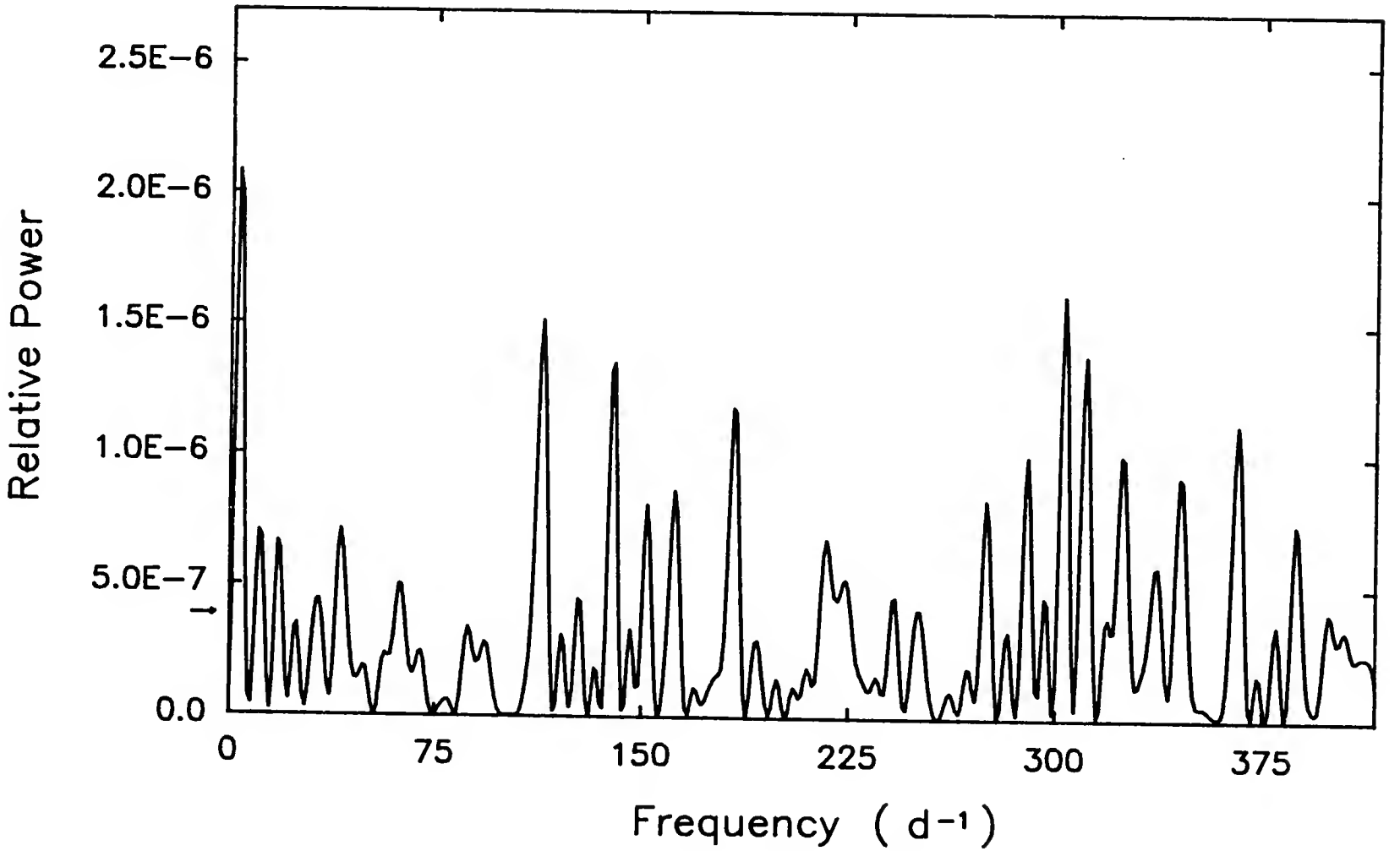

Figure 4-63 Power spectrum for the carbon observations of subset I of data set VI after execution of the clean algorithm.

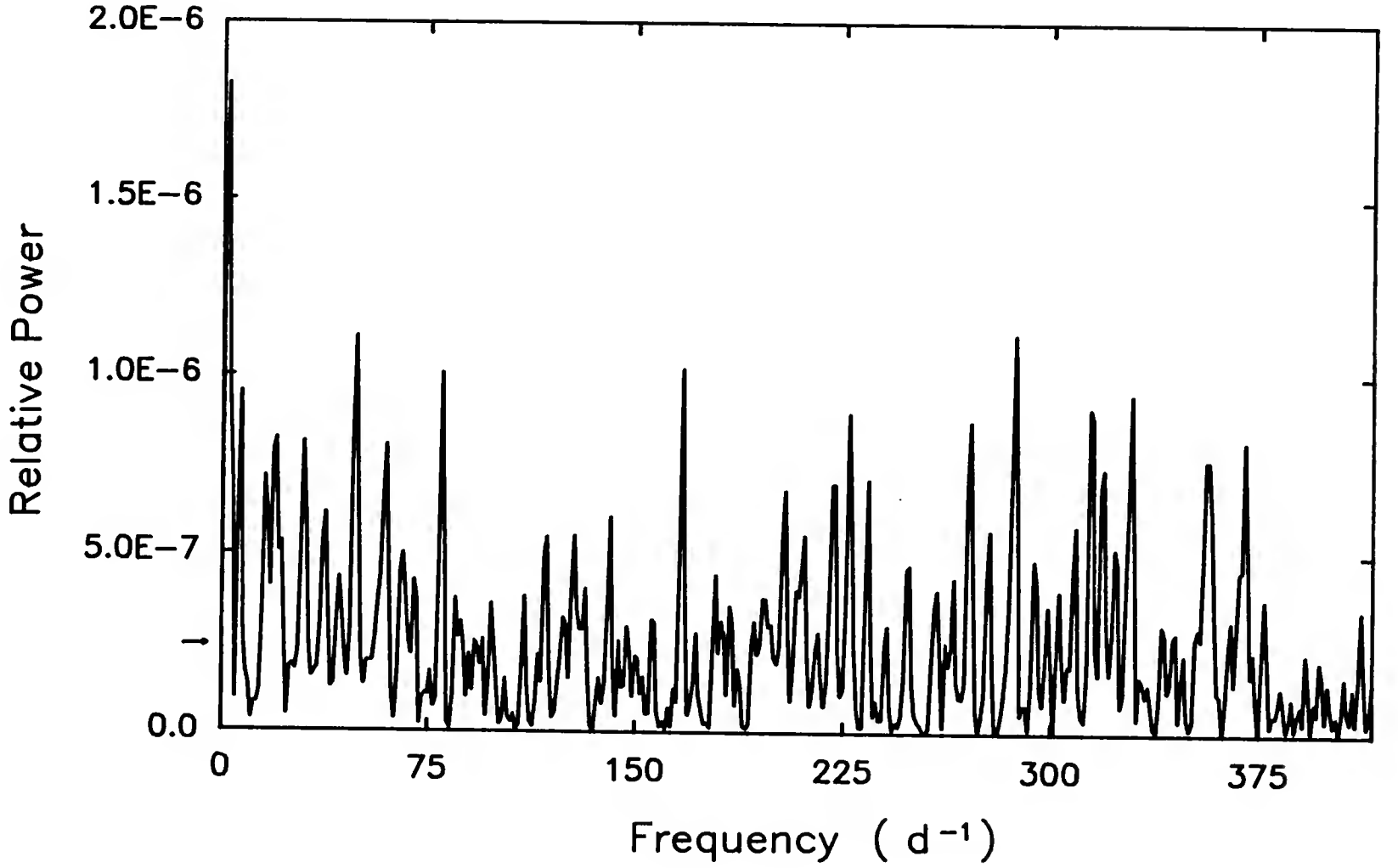

Figure 4-64 Power spectrum for the carbon observations of subset II of data set VI before execution of the clean algorithm.

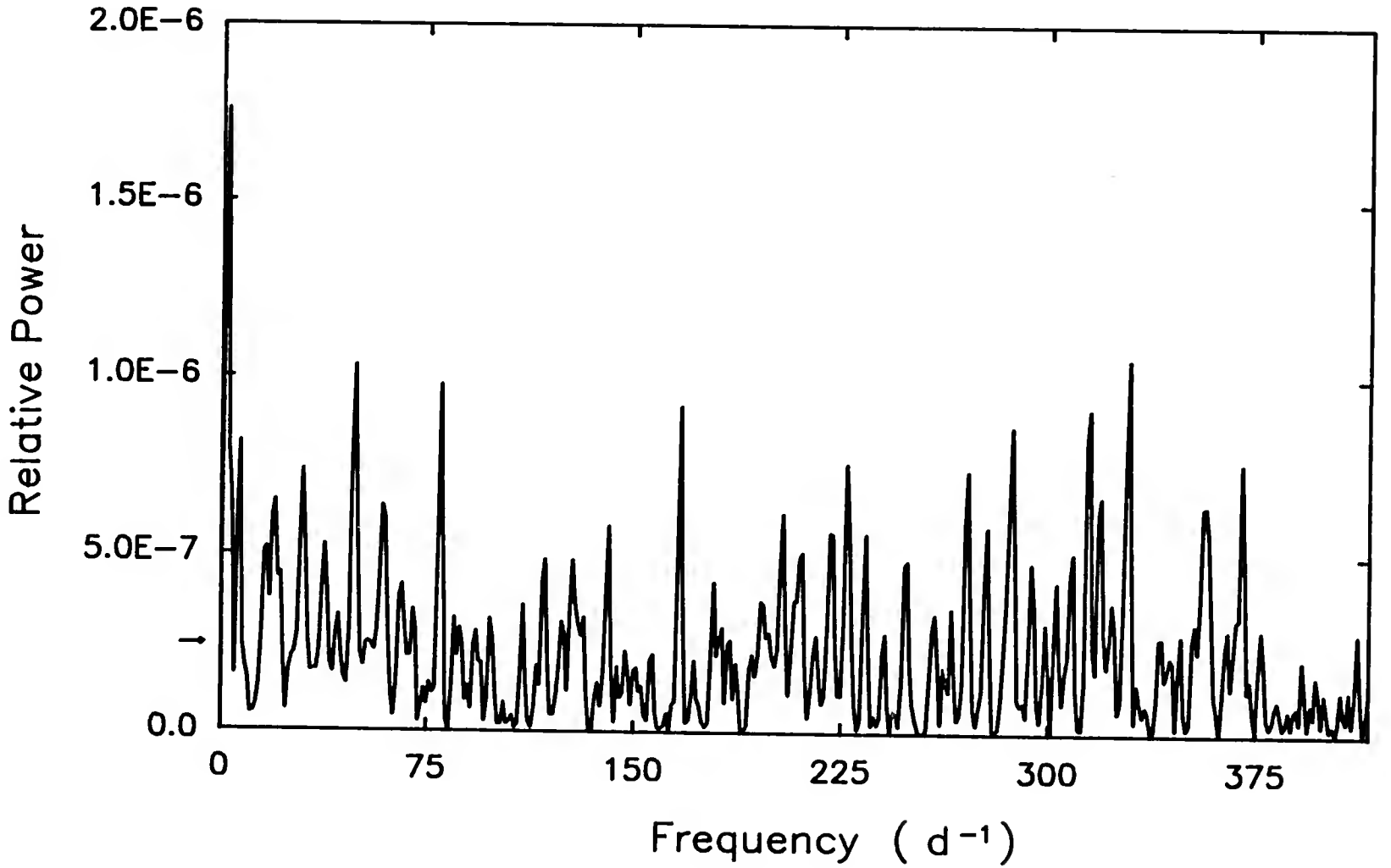

Figure 4-65 Power spectrum for the carbon observations of subset II of data set VI after execution of the clean algorithm.

$$D(t_i) = 0.10728 + 0.00159 * \sin\left(\frac{t_i - 0.81853}{0.01580}\right). \qquad (4\text{-}18)$$

Although the model (Figure 4-66) appears to follow the small changes in the observations, such low amplitude models must be regarded with skepticism.

In summary, the fluctuations present in the helium emission line in particular, are better understood when the data are divided into smaller subsets. In each case, good agreement is achieved with the independent period search techniques used in this study. The beginning of the data set is best described with a period on the order of 1.26 hours. The latter portion of the data are described with either of two periods, P = 8 hours or P = 2.64 hours. Although the variations of the carbon emission data are not conclusive within the limits of this analysis, a model with a period of 1.71 hours is presented.

Data Set VII.

This data set is the last of the data obtained with the SPOT during the 1986 observing season which is included in this dissertation. These data include 243 reduced intensity measurements of the helium emission line and 251 observations of the carbon emission feature. In each case, $0^d.0025$ elapses between consecutive readings for a specific filter. The observing program used in the acquisition of these data is presented in Table 4-2. The instrument

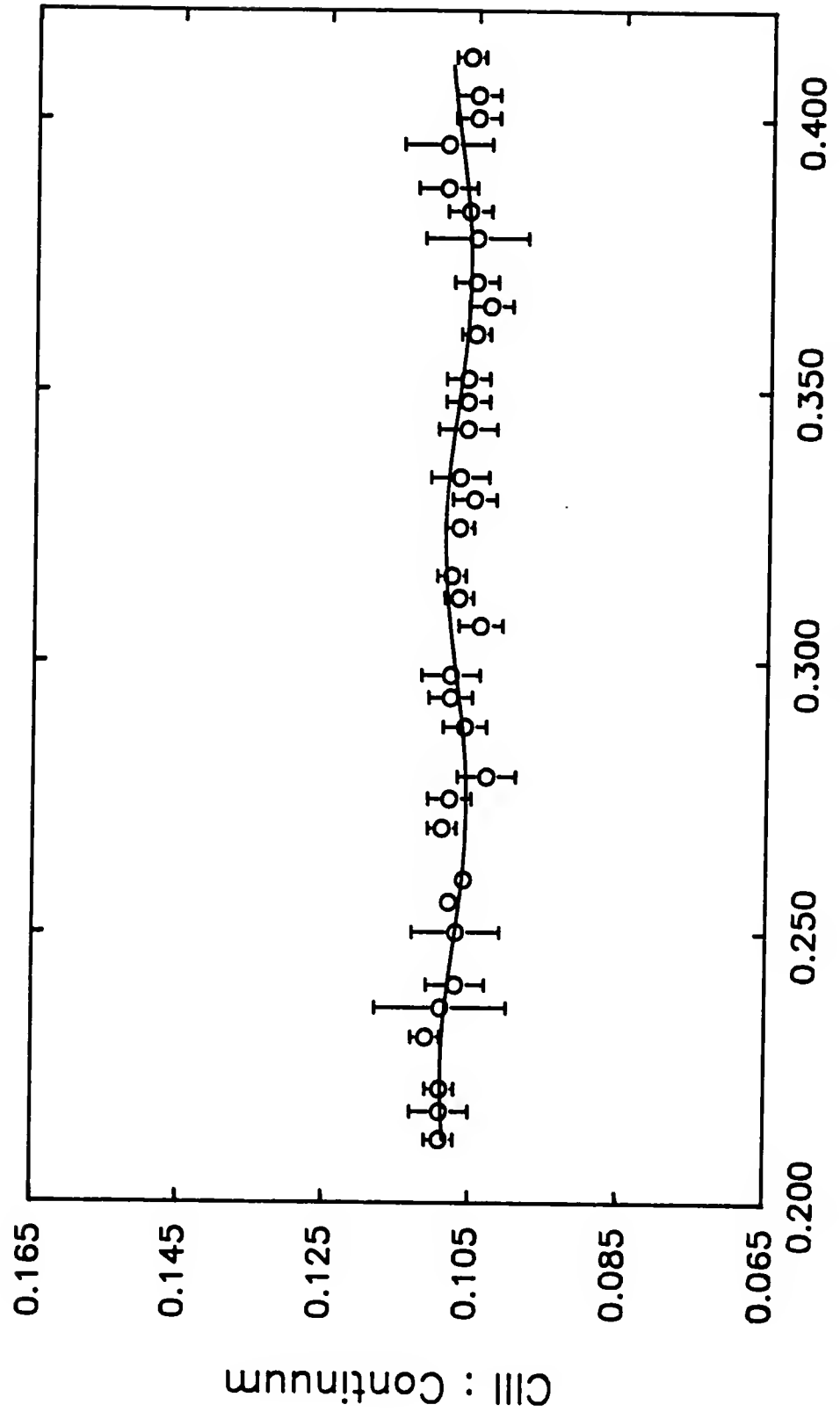

Figure 4-66 Model for the variations of the carbon data for data set VI with P = 2.38 hours. Each plotted point represents the average intensity within a 0.0040 interval.

observed for 14.3 hours, from JD2446662.8415 through JD2446663.4373, before being interrupted by bad weather. The sampling function for this data set is represented by the power spectrum presented in Figure 4-67. Here, the three obvious peaks are the first, second, and third harmonics at $\nu_1 = 20d^{-1}$, $\nu_2 = 40d^{-1}$, and $\nu_3 = 60d^{-1}$. Even though a few additional observations of the carbon emission line were used, the spectral window does not differ from Figure 4-67 for either the helium or the carbon data.

Relative power computed from the real and imaginary components of the Fourier transform of the helium intensity measurements is plotted in Figure 4-68. Features which rise above the statistically significant level of $4\sigma_N$, include peaks at $\nu = 6$, 14, 18, 26, 48, 96, and $140d^{-1}$. Indeed, many of these features rise only minimally above the $4\sigma_N$ level and some are at least part aliases with stronger peaks. The CLEANing function (Figure 4-69) has reduced the strength of each feature quite substantially. However, peaks at $\nu = 6$, 14, 48, and $140d^{-1}$ still need to be considered as possible periodicities within these data. The peak at $\nu = 6d^{-1}$ (P = 4.0 hours) is clearly the strongest feature in both Figures 4-68 and 4-69 at $8.7\sigma_N$; $1\sigma_N = 3.224 \times 10^{-6}$. The next largest peak occurs at $\nu = 14d^{-1}$ (1.71 hours) with a signal-to-noise ratio on the order of 7.0. The other two features in Figure 4-69 correspond to periods of 30 minutes

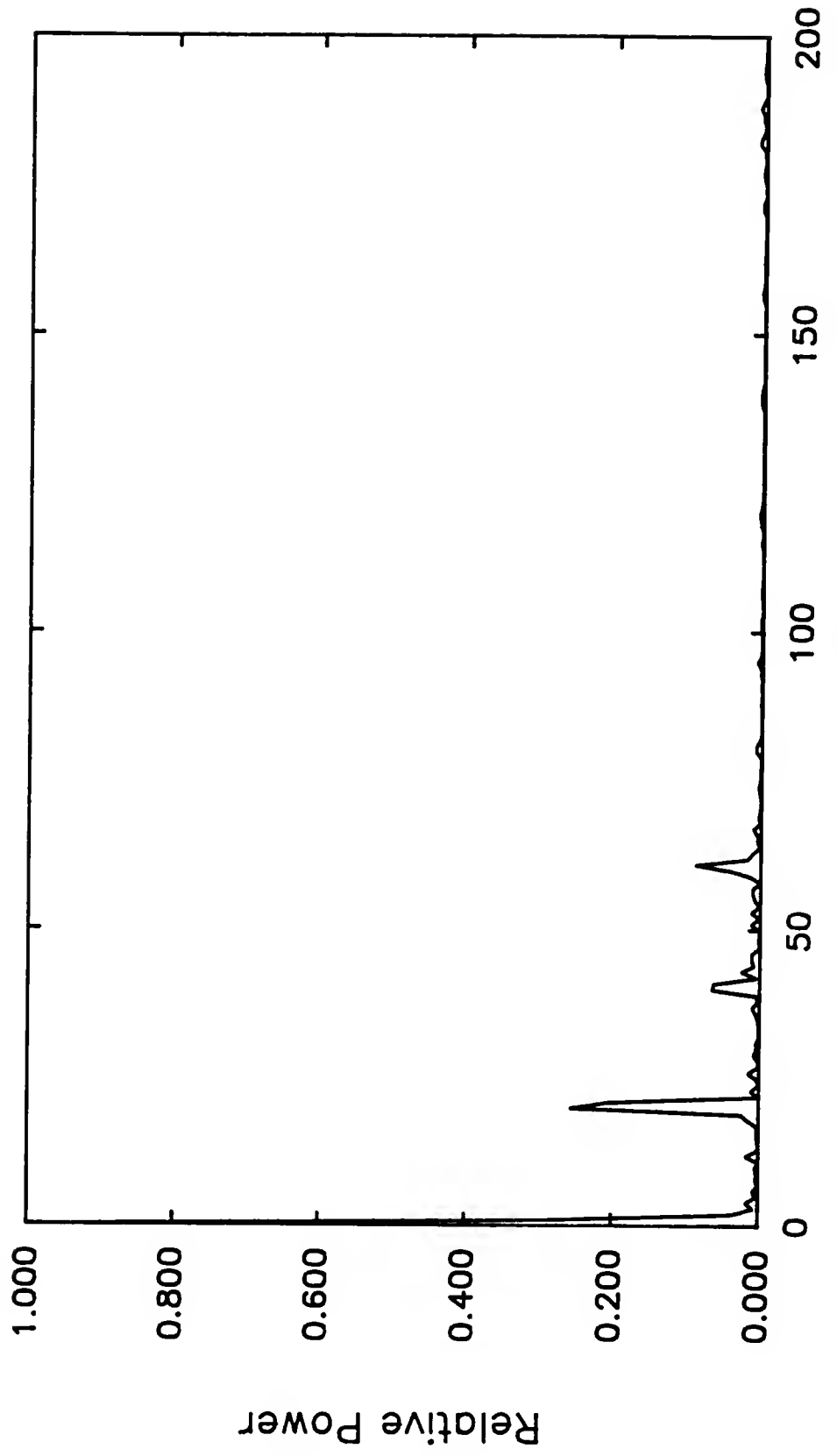

Figure 4-67 Spectral window function for data set VII.

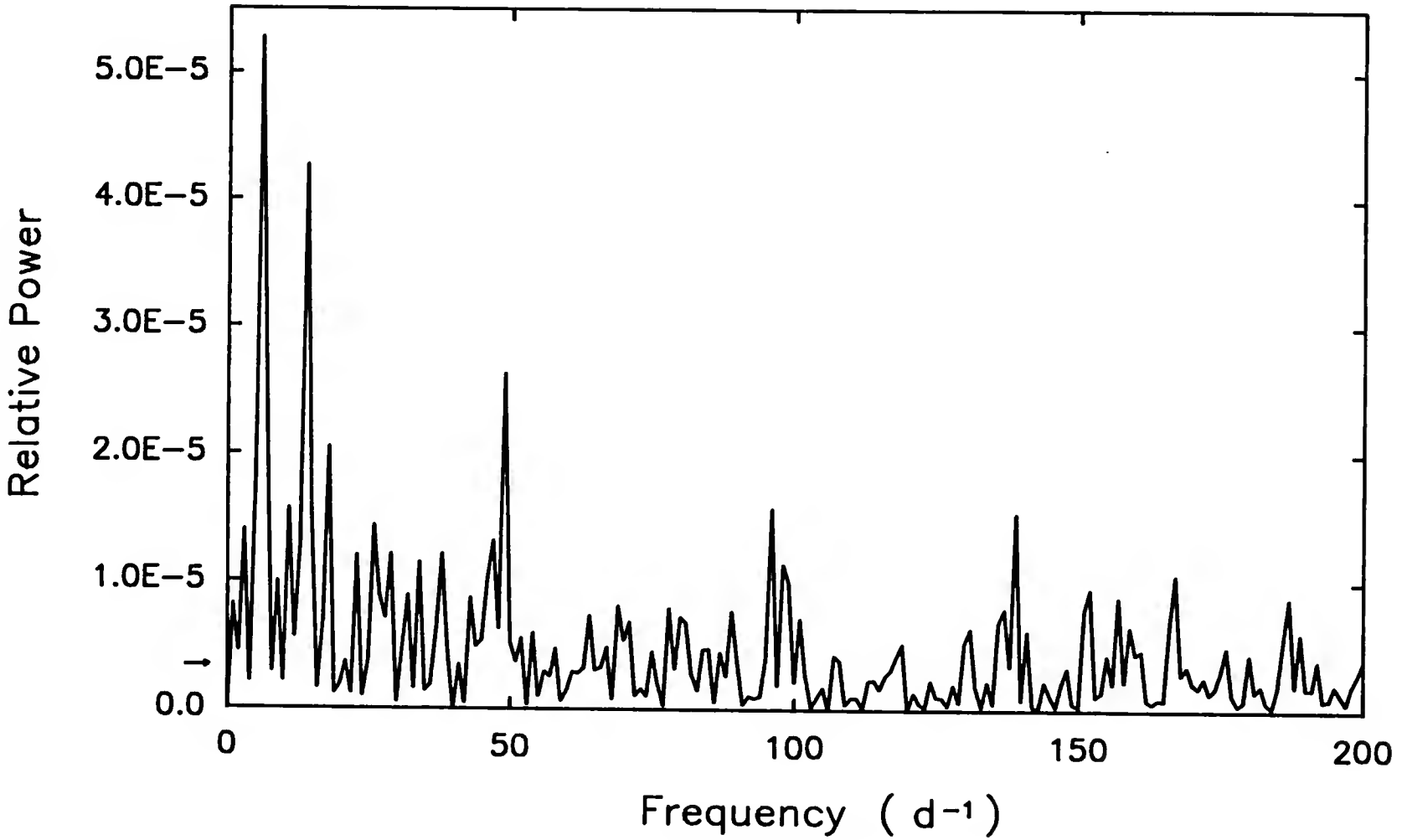

Figure 4-68 Power spectrum for the helium observations of data set VII before execution of the clean algorithm.

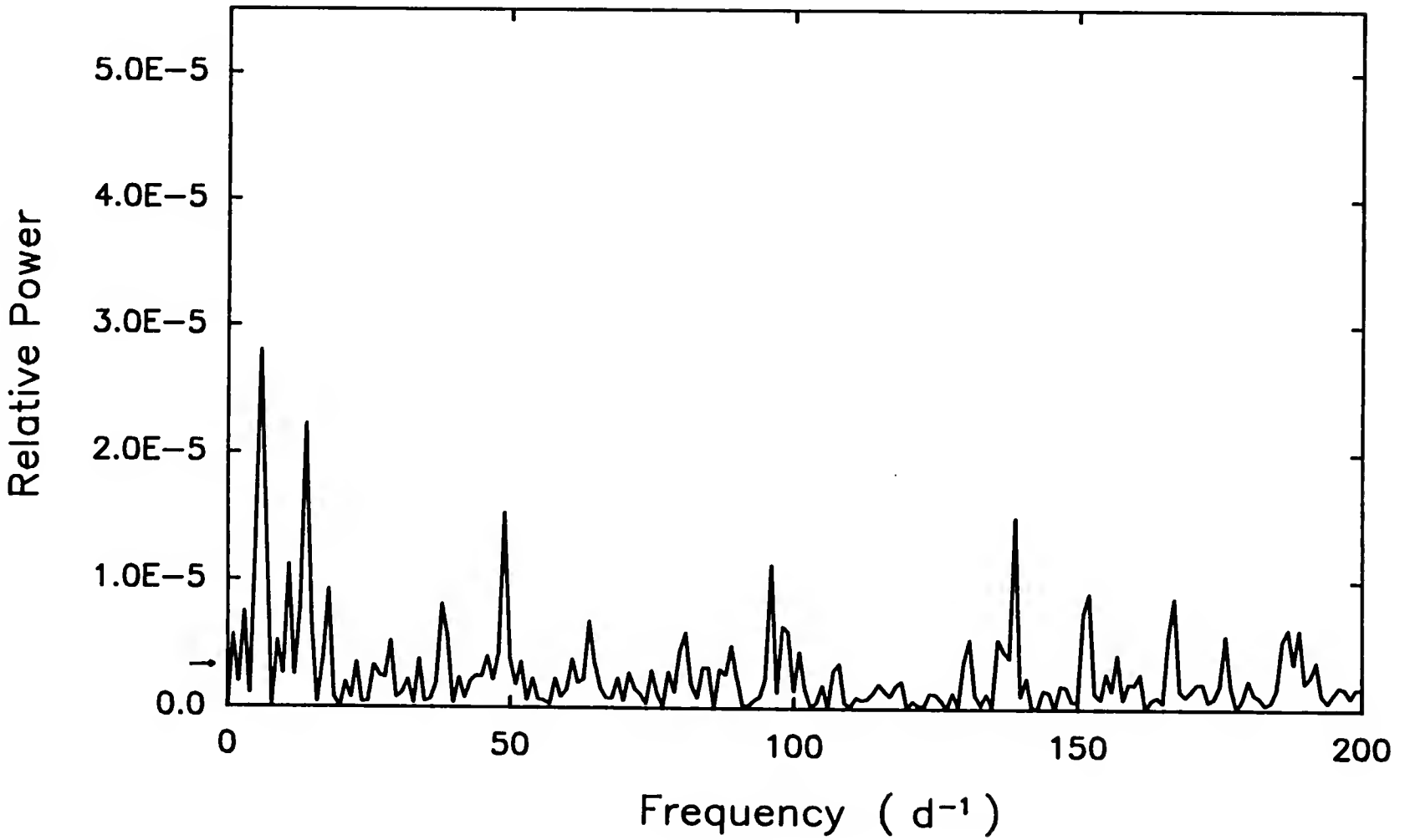

Figure 4-69 Power spectrum for the helium observations of data set VII after execution of the clean algorithm.

and 10.3 minutes, each with relative powers equal to $4.7\sigma_N$.

Execution of the least-squares routine to determine the best-fit sine wave to the data, gives a period of P = 3.72 hours, or, in terms of cycles per day, $\nu = 6.4d^{-1}$. Because of the agreement between these two methods, a model is computed according to the least-squares parameters which are expressed by the relation

$$D(t_i) = 0.35098 + 0.00548 * \sin\left(\frac{t_i - 0.44141}{0.02428}\right). \qquad (4\text{-}19)$$

The model itself is shown in Figure 4-70 together with the standard deviations associated with $0^d.0040$ averages. A variation with a slightly smaller amplitude is also found by the least-squares method of analysis. The second convergence corresponds well with the peak at $\nu = 14d^{-1}$ in the power spectrum of Figure 4-69. The model, shown in Figure 4-71, is computed from equation (4-20):

$$D(t_i) = 0.35094 + 0.00499 * \sin\left(\frac{t_i - 0.81915}{0.01140}\right). \qquad (4\text{-}20)$$

Based on the O-C residuals computed from equations (4-19) and (4-20), the longer of these two periods seems to be a better representation for the variations. The least-squares routine does not converge for periods corresponding

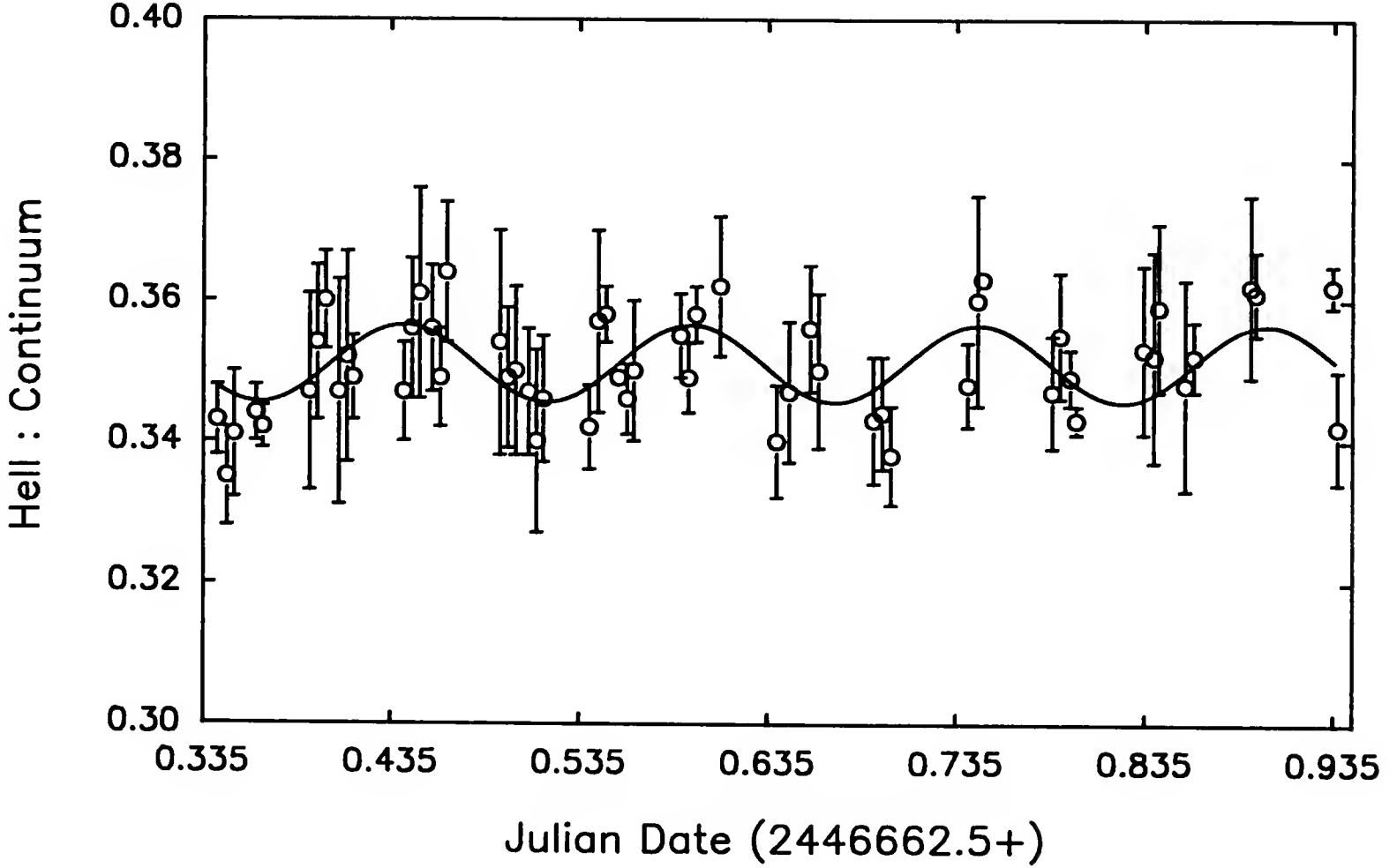

Figure 4-70 Model for the variations of the helium data for data set VII with P = 3.66 hours. Each plotted point represents the average intensity within a $0^{d}.0040$ interval.

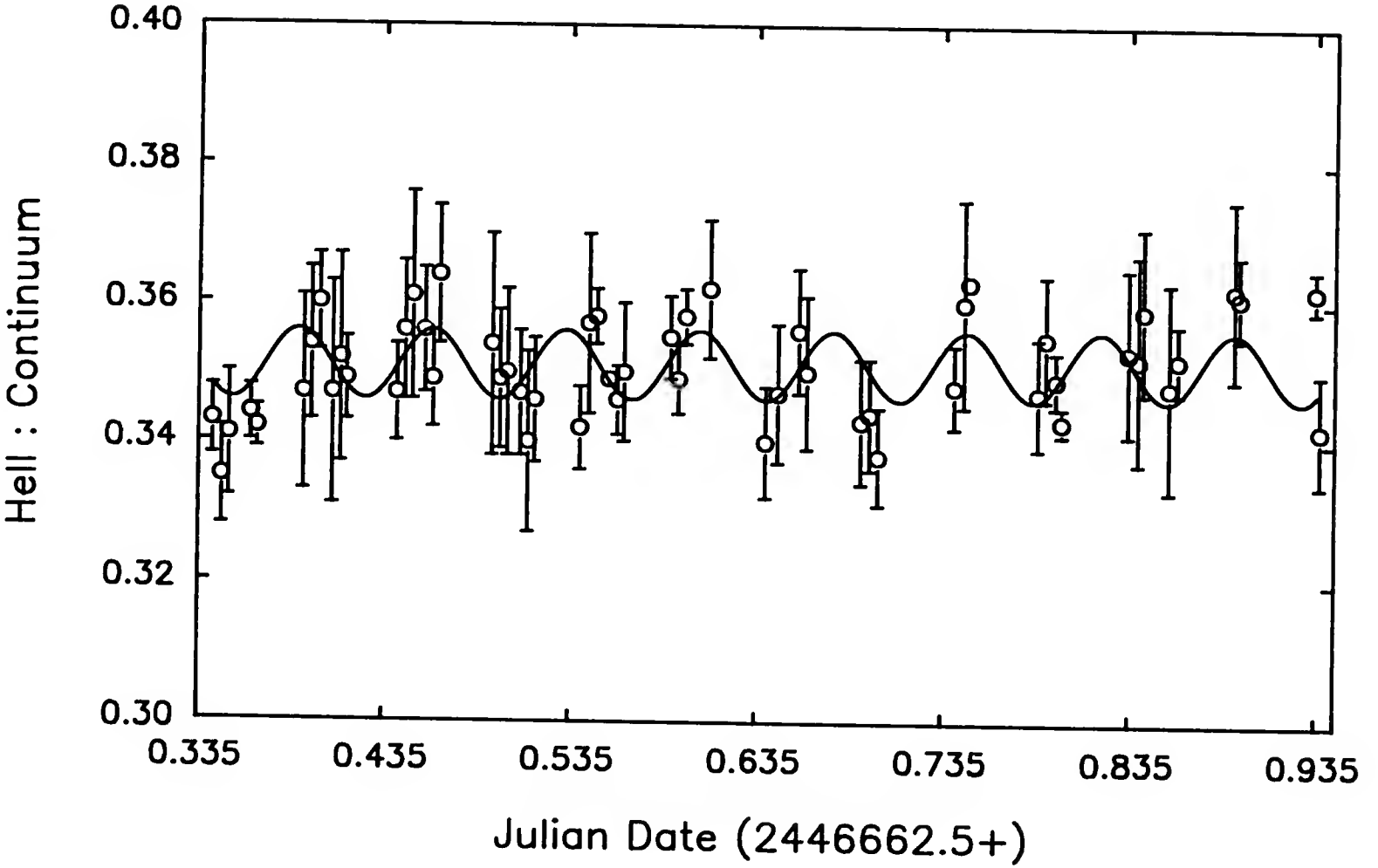

Figure 4-71 Model for the variations of the helium data for data set VII with P = 1.72 hours. Each plotted point represents the average intensity within a $0^d.0040$ interval.

to $\nu = 48d^{-1}$ or $\nu = 140d^{-1}$, and so, no model for these periods is considered successful.

The power spectrum resulting from a convolution of the carbon emission data with the spectral window (Figure 4-67) is given in Figure 4-72. The $1\sigma_N$ level in this plot is at 3.141×10^{-6}, and none of the features rise above the $1.5\sigma_N$ level. Hence, the power spectrum analysis finds no significant periodic variations in these data. Likewise, any convergence in the least-squares algorithm has a very low amplitude and cannot be accepted with confidence.

Briefly, according to either the power spectrum method of analysis or the least-squares analysis procedure, the carbon data exhibit no periodic variations with substantial amplitude above the noise. The power spectrum and the least-squares solutions agree quite well in describing intensity variations of the HeII emission line. The fits proposed here are for P = 3.66 hours and P = 1.72 hours. The intensity changes seem to be better modeled with the longer period of 3.66 hours.

B and V Photometry

The Wolf-Rayet star, γ^2 Vel, is a spectroscopic binary with an orbital period of $78\overset{d}{.}5002$ (Moffat et al. 1986). Although Gaposchkin (1959) reported a period of $16\overset{d}{.}2334$ based on a set of visual and photographic measurements, no other investigator has detected an optical eclipse of this system.

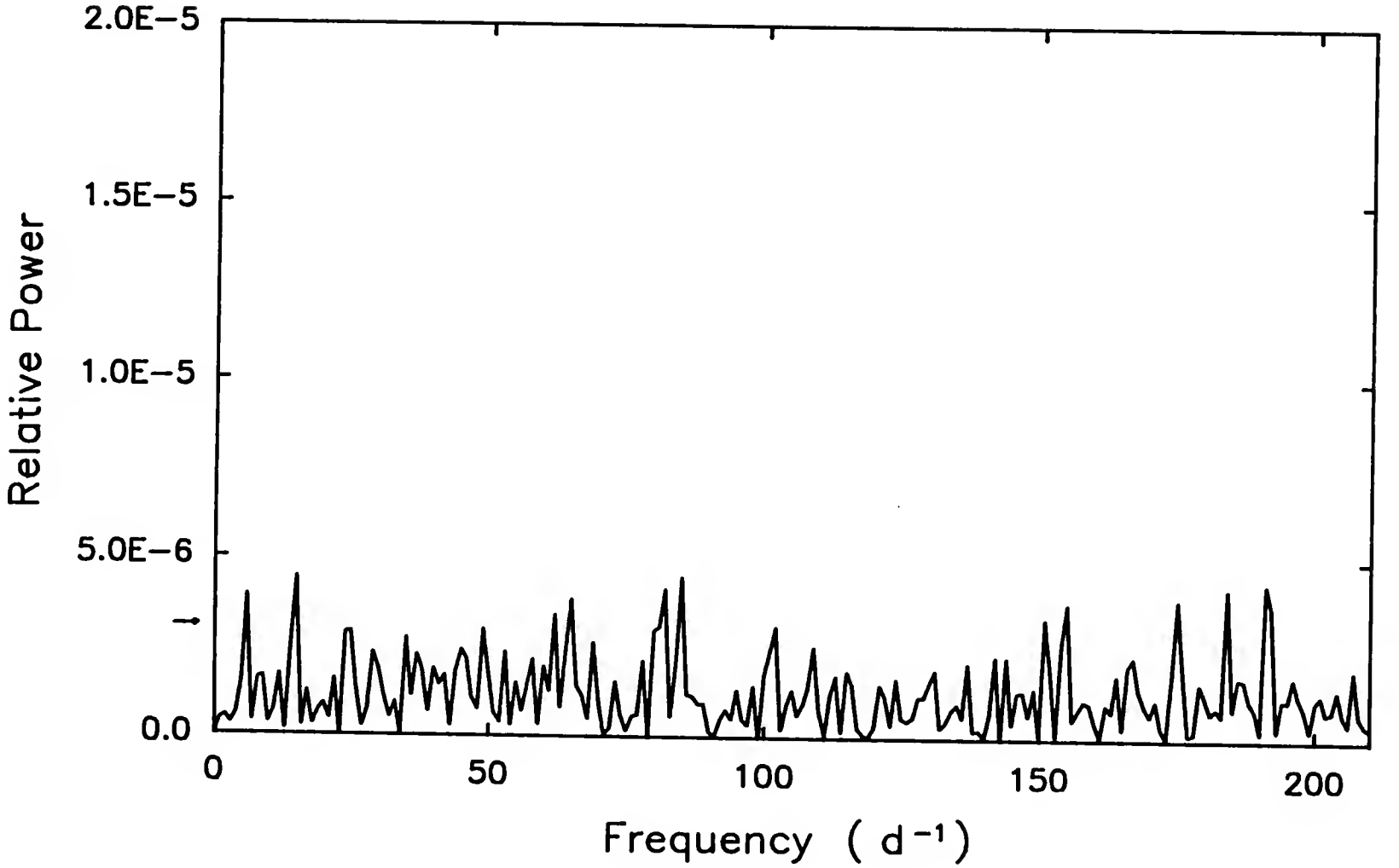

Figure 4-72 Power spectrum for the carbon observations of data set VII before execution of the clean algorithm.

Willis and Wilson (1976) have compared ultraviolet spectroscopic observations of γ^2 Vel at phases 0.30 and 0.65. They detect considerable differences in some of the spectral features at these two phases which they explain as an eclipse effect. These authors conclude that at phase 0.65, the geometry of the system is such that the outermost layers of the extended envelope of material surrounding the WC8 star, eclipse the O9I companion. According to this model, the radius of the circumstellar wind must be on the order of $250R_{\odot}$; substantially different from the result obtained by Brown et al. (1970).

One aspect of this dissertation involves the acquisition of B and V photometry of γ^2 Vel with the SPOT in an attempt to confirm or deny the existence of an optical eclipse. During the 1986 and 1988 observing seasons at the South Pole, several different observing programs were used to obtain B and V photometry of this system. A total of 2,538 observations (JD2446553.6 through JD2447312.6) with the visual filter, and 2,315 observations (JD2446553.6 through 2447309.0) with the blue filter, were recorded. These data were reduced to photometric magnitudes using the techniques described in Chapter 3, with HR3452 as the comparison source. The time of each observation is converted to phase using the ephemeris given by equation (1-1), and average magnitudes are computed at 0.005 phase intervals. Table 4-4 lists the average ΔV magnitudes, the

Table 4-4
Average ΔV Magnitudes for γ^2 Vel

Phase	Magnitude (ΔV)	RMS Deviation	N
0.004	-3.100	0.073	38
0.005	-3.100	0.049	71
0.013	-3.086	0.036	91
0.017	-3.114	0.027	161
0.038	-3.093	0.072	66
0.040	-3.090	0.021	22
0.046	-3.139	0.083	80
0.050	-3.228	0.047	6
0.079	-3.092	0.027	22
0.303	-3.060	0.021	24
0.377	-3.114	0.036	48
0.407	-3.113	0.039	94
0.412	-3.116	0.039	126
0.417	-3.116	0.038	96
0.422	-3.102	0.045	99
0.433	-3.107	0.061	85
0.436	-3.086	0.060	39
0.444	-3.203	0.024	9
0.603	-3.111	0.018	3
0.606	-3.122	0.062	5
0.618	-3.168	0.060	3
0.643	-3.099	0.057	6
0.648	-3.121	0.061	3
0.652	-3.089	0.044	6
0.657	-3.112	0.054	9
0.662	-3.075	0.048	8
0.673	-3.091	0.028	101
0.675	-3.092	0.012	9
0.689	-3.117	0.019	23
0.690	-3.032	0.036	23
0.699	-3.120	0.028	34
0.702	-3.123	0.037	118
0.706	-3.117	0.033	89
0.714	-3.092	0.062	39
0.715	-3.101	0.077	50
0.731	-3.107	0.051	72
0.783	-3.082	0.067	60
0.787	-3.126	0.066	126
0.864	-3.122	0.069	45
0.867	-3.094	0.036	180
0.870	-3.110	0.037	60
0.881	-3.122	0.062	66
0.887	-3.087	0.075	108
0.998	-3.126	0.057	98

average phase within each interval, the standard deviation associated with each average, and the number of points used to determine each average. Table 4-5 contains similar data for observations obtained with the blue filter.

Figures 4-73 and 4-74 are phase-magnitude diagrams for the visual and the blue photometry, respectively. The error-bars in each of these figures are quite large, and therefore, small changes in the brightness of the system cannot be detected. The large standard deviations of these data can probably be attributed to several different circumstances.

Although γ^2 Vel is a very bright object, variations in the sky background will still affect the quality of the data obtained with the SPOT. Auroral events which occur at such a southerly latitude are probably more rapid and more intense than at most other locations on Earth. The spectrum of this sky brightening phenomenon is contaminated with several strong emission features at wavelengths which coincide with our filter bandpasses. Since the half-power band-width of the B and V filters used in this study is about 900Å, rapid variations in the intensity of the sky background cannot be properly accounted for.

Two ways to minimize the effects of variations in the sky brightness would be to observe the sky more frequently and to use a smaller field stop. However, most of the data used in this investigation were obtained during the 1986

observing season. At this point in the project, the effects of variations in the sky brightness were not well understood and the telescope was not equipped with diaphragms other than the 5′ field stop.

In the acquisition of most of these data, a sky observation was obtained only once every 30 to 45 minutes. This is certainly not adequate to account properly for spatial and/or temporal changes. In addition, since these data were obtained with a 5′ diaphragm, intensity variations in a portion of sky with large angular diameter contaminated each stellar measurement.

One must also realize that the telescope used in the acquisition of these data is operated at a remote site with virtually no human intervention. Therefore, if the telescope can find a given star, data are recorded whether the sky is of photometric quality or not. It is the responsibility of the analyst to attempt to distinguish between variations which are intrinsic to the star which is being observed, and variations which are due to bad weather. This is not always a simple task. Weather data are recorded at the South Pole once every six hours, but for astronomical purposes, this is far from adequate. Further, thin clouds which can severely contaminate photometric data are probably not often detected by a visual observer.

These are a few of the problems which arise in the analysis of the B and V observations obtained with the SPOT.

Table 4-5
Average ΔB Magnitudes for γ^2 Vel

Phase	Magnitude (ΔB)	RMS Deviation	N
0.004	-3.507	0.072	34
0.005	-3.484	0.069	67
0.013	-3.461	0.036	79
0.017	-3.485	0.046	153
0.038	-3.469	0.066	54
0.040	-3.434	0.105	20
0.047	-3.511	0.079	57
0.050	-3.516	0.080	7
0.079	-3.428	0.047	22
0.303	-3.414	0.027	24
0.377	-3.474	0.051	46
0.407	-3.484	0.076	100
0.412	-3.476	0.080	125
0.417	-3.469	0.078	85
0.422	-3.482	0.068	99
0.433	-3.480	0.072	64
0.436	-3.435	0.085	36
0.444	-3.558	0.039	9
0.603	-3.498	0.010	3
0.606	-3.521	0.079	5
0.618	-3.518	0.028	3
0.673	-3.439	0.060	99
0.675	-3.344	0.024	9
0.689	-3.489	0.034	23
0.690	-3.389	0.054	22
0.699	-3.472	0.059	33
0.702	-3.460	0.047	116
0.706	-3.489	0.033	89
0.714	-3.458	0.055	39
0.715	-3.463	0.074	46
0.731	-3.491	0.058	72
0.783	-3.481	0.043	36
0.787	-3.472	0.060	95
0.864	-3.497	0.074	45
0.867	-3.456	0.071	171
0.870	-3.468	0.071	54
0.881	-3.463	0.064	56
0.887	-3.482	0.062	112
0.998	-3.510	0.087	93

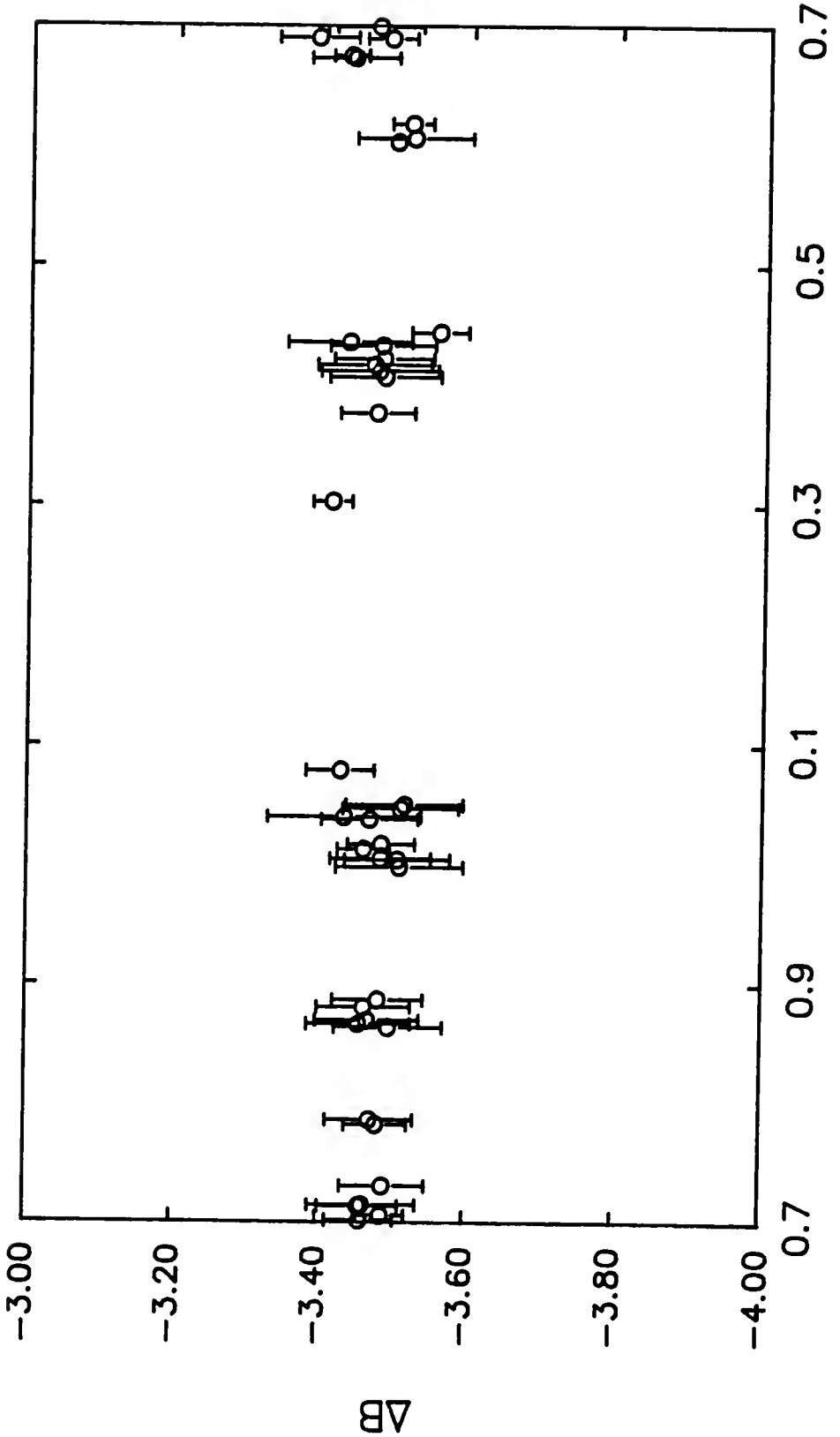

Figure 4-74 Phase-magnitude diagram for the blue photometry of γ^2 Vel. Each point represents the average magnitude within a 0.005 phase interval. The error-bars show the standard deviations associated with each average.

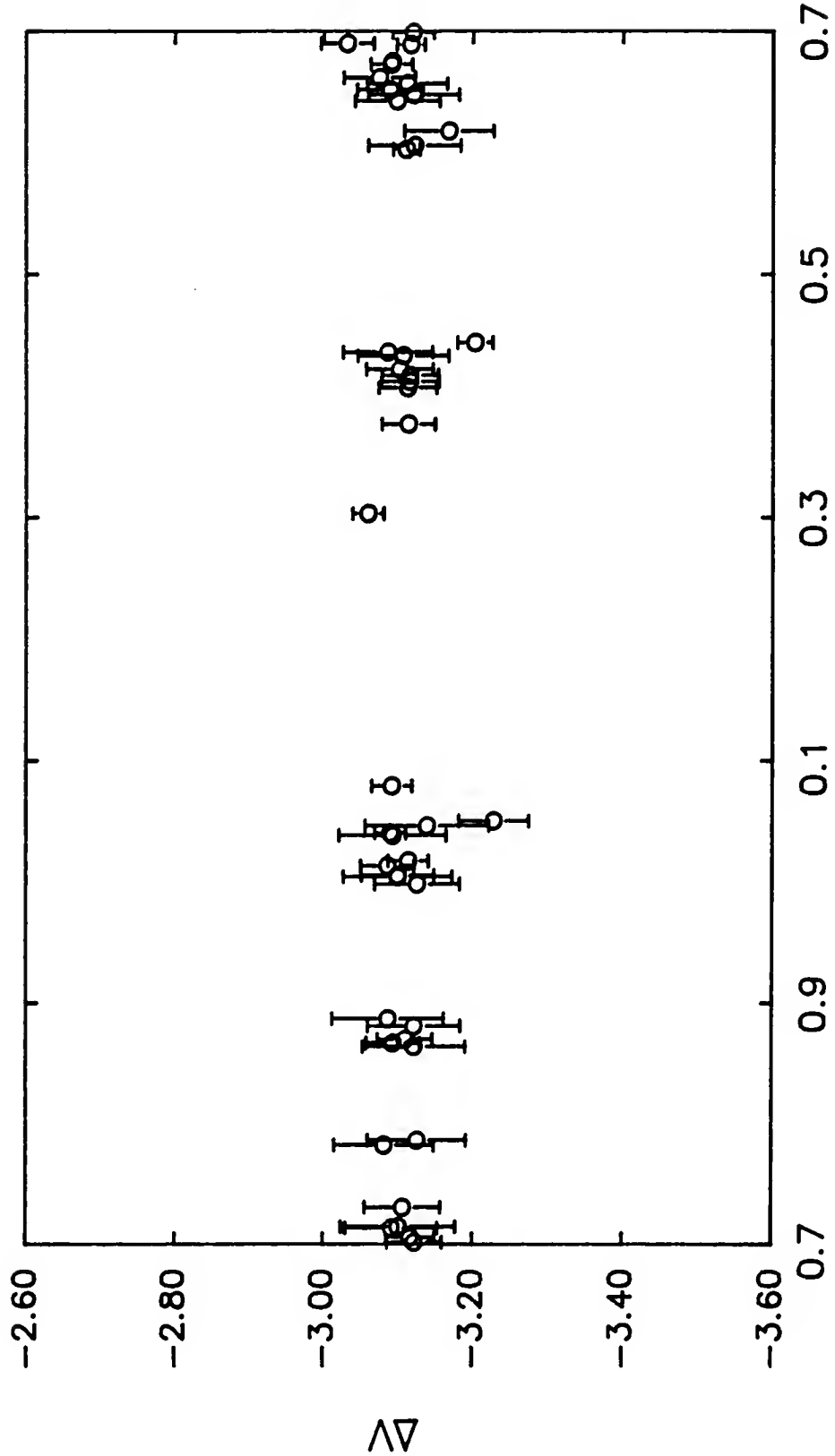

Figure 4-73 Phase-magnitude diagram for the visual photometry of γ^2 Vel. Each point represents the average magnitude within a 0.005 phase interval. The error-bars show the standard deviations associated with each average.

It is probably some combination of these situations that leads to the large rms deviations in the reduced data.

Complete phase coverage in the blue and visual filters has not yet been obtained (Figures 4-73 and 4-74). In fact, observations at certain critical phase positions are missing, particularly those just before phase 0.0. In any case (within the limitations of these data) no eclipse is seen in either the blue or yellow regions of the spectrum. If an eclipse of the extended atmosphere does occur, the change in light would probably be very small.

Additional observations are required before we can fully ascertain whether or not an optical eclipse does in fact occur in the γ^2 Vel system. In addition, and perhaps more importantly, more-accurate observations are necessary. It seems almost certain that any automated optical telescope operating at such a remote site must observe the star and sky simultaneously in order to detect, and subsequently account for, variations in sky conditions.

CHAPTER 5
DISCUSSION AND CONCLUSIONS

One-hundred and fifty-seven of the stars in our Galaxy have been classified as Wolf-Rayet stars. Variations in the spectra of these objects have been detected, but mechanisms which cause such changes in the continuum and emission line features are not well understood. At one time, all Wolf-Rayet stars were assumed to be members of binary star systems. Until recently, it was this binarity which was the most common explanation put forward to describe these spectral variations.

In 1974, Moffat and Haupt stated that the percentage of Wolf-Rayet stars which are members of binary star systems "May be much higher than 73% . . .". As recently as 1982, Bisiacchi et al. reported that up to 100% of the WNE type Wolf-Rayet stars may be members of binary systems. On the other hand, a more recent study by Moffat (1986) shows that the frequency of binarity among this class of stars has probably been largely over-estimated.

Today approximately 40% of the Wolf-Rayet stars in the Milky Way Galaxy are known to be members of binary systems. This new statistic, taken together with the fact that spectral variations have also been observed in Wolf-Rayet

stars which do not have a companion, indicates that another mechanism must exist to explain the changes in the spectra of these stars. Theoretical research now indicates that these changes are probably linked to the high rates of mass loss (i.e., $\approx 2 \times 10^{-5} M_{\odot}$ /yr) associated with this type of object.

Although periodic or quasi-periodic variations resulting from a steady laminar flow of material would simplify the theoretical interpretation of these stars, according to Vreux (1987) it is more likely that random fluctuations in the wind occur. Vreux has suggested that pulsational instabilities may cause changes in the spectral characteristics of Wolf-Rayet stars. In his 1987 paper, Vreux presented a discussion of variations in the spectra of these objects which have been reported in the literature thus far. No ultra-short time variations with periods less than 1 minute have been cited for any Wolf-Rayet star. The only object which has reported periodic variations between 2 minutes and 2 hours is γ^2 Vel. Periodic variations on the order of 150 - 200 seconds have been reported in the literature by only one group. Vreux and others have noted that short period changes have been detected only when high-speed photometry is recorded for a period of about ten minutes. Other investigators, who have recorded longer intervals of observations, report variations of longer duration. Some report periodic behavior, others report

aperiodic behavior. More observations are certainly required before one is able to confirm or deny such rapid variations in intensity. Vreux goes on to mention that no other Wolf-Rayet star, either of the WN or WC type, has been reported to exhibit periodic variations of this order. However, variations on the order of minutes have been detected for some WC type stars, with variability being more common in the later subclasses.

The last period range that Vreux reports concerns periods between $0^d.3$ and $1^d.0$. As one would expect, variations with periods of a day, or a multiple of a day, are difficult to determine from most geographical locations. Still, possible periods on this order have been reported for some stars.

Vreux suggests that spectral changes in Wolf-Rayet stars may be attributed to non-radial pulsations. Until results of a theoretical study carried out by Noels and Scuflaire (1987) were published, theory did not support the existence of non-radial pulsations in helium-burning stars. However, Noels and Scuflaire have considered the evolutionary sequence of a $100M_{\odot}$ star and have shown that non-radial pulsations can produce vibrational instabilities if regions of hydrogen shell-burning persist. This theory pertains most closely to the WN type Wolf-Rayet stars which have higher H/He ratios than do the WC types. These results may lend support to Vreux's suggestion that non-radial

pulsations may contribute to the changes in the spectra of WN type Wolf-Rayet stars. According to the models, periods for these pulsations range from 30 minutes to a few hours, and are in good agreement with observational studies.

In the case of helium-burning stars which no longer have regions of hydrogen shell burning, radial pulsations can actually produce these vibrational instabilities. However, the star must be a helium star, nearly homogeneous in structure, and have a mass larger than the critical mass of $16M_{\odot}$ (Noels and Gabriel 1981, Noels and Gabriel 1984, Maeder 1985). The periods which result from radial pulsations are generally less than an hour in length, considerably smaller than those derived for the WN types.

These theoretical studies suggest that non-radial pulsations contribute to the large rates of mass loss in the case of WN type Wolf-Rayet objects, and that radial pulsations are more appropriate for the WC stars. It is interesting to note that the temperatures which were originally derived for Wolf-Rayet stars were not adequate to provide such intensive winds through radiation pressure. However, it is now suspected that the temperatures are actually much higher than originally believed (Cherepashchuk et al. 1984), and radiation pressure alone can support such a strong and efficient phenomenon.

Cox and Cahn (1988) have carried out an independent study involving the theoretical modeling of these stars as

well. They have computed both radial and non-radial models for the non-adiabatic case, for five different masses of Wolf-Rayet stars. Their results for the linear non-adiabatic radial modes indicate periods from 22 minutes to 2.10 hours. Results for the linear non-adiabatic, non-radial modes, indicate longer periods ranging from 2.9 hours to 20.8 hours.

One of the models considered by these authors was for an originally $120M_{\odot}$ star which had evolved past the hydrogen shell burning stage. This model was found to be unstable only against the radial fundamental mode of pulsation, which agrees well with results of Maeder (1985). Cox and Cahn conclude that if mass loss is to be the result of pulsations, it must be only from the radial fundamental mode which appears in hydrogen-free stars. Their $85M_{\odot}$ model exhibits radial pulsations which are again in agreement with Maeder's study.

One of the few models which has been put forward in an attempt to explain spectral variations in γ^2 Vel includes the presence of a third body. In 1977, Moffat suggested that this star may be one member of a triple-star system. Analysis of narrowband photoelectric-photometry revealed a $5^d.09$ period. In addition, rapid spectrophotometric scans indicated the presence of a longer period of variation between 13 and 19 days. It was not until 1985 that Jeffers et al. pursued Moffat's suggestion, and derived a model for

this system containing a neutron-star companion to the WC8 component. According to their investigation, the Wolf-Rayet component would have a mass of $20M_{\odot}$ and a radius of $13.1 \pm 0.2R_{\odot}$, while the neutron-star would have a mass of $1.4 \pm 0.2M_{\odot}$.

Assuming a circular orbit for the neutron-star, and, because of the lack of optical eclipses, an inclination of 70°, the maximum separation distance between the neutron-star and the WC8 star would be $36R_{\odot}$. Interferometry measurements made by Brown et al. (1970) indicate that the extended wind of the Wolf-Rayet component has a radius of $76R_{\odot}$. Hence, the neutron-star would be contained well within this envelope of material. The orbital period which results from this situation is about $5^{d}.4$.

Since these two stars are reasonably close to one another, one would expect that the accretion of material onto the neutron-star would produce a large flux of hard x-rays. However, observations reveal that very low amounts of hard x-rays are actually detected in the γ^{2} Vel system. Some of the theories which have been proposed to accommodate such a result include the following: Moffat and Seggewiss (1979) state that if the density of material in the wind is sufficiently large, then the hard x-rays may be re-absorbed. Sunyaev (1978) explains that hard x-rays may not be detected if accretion occurs at supercritical rates so that the accretion disk becomes opaque to this radiation.

If a neutron-star is present in the γ^2 Vel system, perturbations in the radial velocity measurements, should, in principle, be detected. Moffat et al. (1986) carried out a spectroscopic study to investigate this possibility and to define the orbital parameters more precisely. These authors tried to fit sine waves with periods between $1^d.675$ and infinity, with arbitrary phases, to the deviations which result from an orbital fit to the data. They did not detect any variations with an amplitude larger than 10km/sec. This low amplitude cannot represent a real physical situation.

According to the model presented by Jeffers et al., the amplitude of variation of the deviations in radial velocity measurements would have to be larger that 21km/sec to accommodate an orbital period of $5^d.4$. The suggested orbital period between 13 and 19 days which was proposed by Moffat (1977) would indicate a lower limit on the amplitude of the radial velocities of 15km/sec. In either case, a 10km/sec variation almost certainly excludes the possibility of a neutron-star companion.

Variations in the strengths and shapes of the emission lines of γ^2 Vel may be explained in the context of the theoretical studies which have been discussed in some detail above. Several mathematical models have been computed that describe the variations in the strength of the HeII emission line. The amplitudes of these fluctuations amount to a few percent of the total intensity, and are in good agreement with variations reported by other authors.

Table 5-1 lists all of the periods and corresponding frequencies found in the analyses of the narrowband photometry used in this study. With the exceptions of the 0.07 hour period (Data Set I) and the 0.57 hour period (Data Set II), the shortest periods in all of these data are P = 1.14 hours (Data Set II), and P = 1.26 hours (Data Set VIa). It is interesting to note that many of the periods listed in column three of the table are near-harmonics or subharmonics of one of these two periods. An average period of 1.20 hours is used to compute the multiplicity of each of the periods in this table. These results are listed in column five. The two periods found to satisfy Data Set III are not simple harmonics of the 1.20 hour fundamental period. However, as stated in the discussion of this data set in Chapter 4, relatively large intervals when γ^2 Vel was not observed, exist, and make it difficult to determine a reliable period. In addition, Data Set VIb has been described with a period of 2.64 hours and a period of 8.03 hours. The longer of these periods is seven times the 1.20 hour period, but, the 2.64 hour period cannot be related to the assumed fundamental period. A look at Figures 4-60 (P = 8.03 hours) and 4-61 (P = 2.64 hours) indicates that the longer period that is found for these data is a better representation of the variations.

At this point, it is interesting to link these results with the results of theoretical modeling of Wolf-Rayet stars

Table 5-1
Summary of Periodicities Found in the
HeII Emission Line

Data Set	Phase Interval	Period (hours)	Frequency (d^{-1})	Multiplicity (P = 1.20)
I	0.302-0.303	0.07	327.3	P/16
		2.40	10.0	2P
II	0.671-0.675	0.57	42.1	P/2
		1.14	21.1	~P
III	0.688-0.691	2.00	12.0	--
		2.75	8.7	--
IVa	0.698-0.703	5.79	4.1	5P
IVb	0.704-0.708	6.31	3.8	11P/2
		2.23	10.8	2P
V	0.782-0.789	----	----	--
VIa	0.863-0.866	1.26	19.0	~P
VIb	0.866-0.872	2.64	9.1	~2P
		8.03	3.0	7P
VII	0.387-0.395	3.66	6.6	3P
		1.72	14.0	3P/2

accomplished by Cox and Cahn (1988). They have computed the evolution of an $85M_{\odot}$ star which has undergone core hydrogen burning and is left with a hydrogen-burning shell. The first-overtone period for the case of non-adiabatic radial mode pulsations is 1.23 hours. This period is in excellent agreement with the results of the observational study presented in this dissertation which indicates a period of 1.20 hours.

In addition, the fundamental period which Cox and Cahn derive for this particular model is 1.98 hours. Perhaps the 2.00 hour period which describes the changes in intensity of the helium emission line in Data Set III, actually represents the fundamental mode of vibration.

An attempt was also made to mathematically model the line intensity fluctuations exhibited by the carbon emission line of γ^2 Vel at 5696Å. This line is considerably weaker than the helium line at 4686Å and variations are much more difficult to model. In almost every case the amplitude of fluctuation amounts to about only 1% of the total intensity. Models have been computed for the two cases when the variation exceeded a 1% fluctuation. Data Set I exhibited the largest percentage of variations in both the carbon and helium emission line strengths. The carbon line was modeled with a period of 1.10 hours and the amplitude of the variation was approximately 2% of the carbon line intensity. Data Set VIb exhibited fluctuations with P = 2.38 hours, and

an amplitude of fluctuation of nearly 1.5% of the intensity. It is interesting to realize that in each of these cases, the period of variation is slightly smaller than that which was derived for the corresponding helium line data. Although the sample is small, this may provide evidence of where the lines are formed in the extended wind. That is, if these variations are a result of pulsational instabilities produced by mass loss, material closer to the surface of the star may exhibit more rapid oscillations than more distant material which may be damped by underlying layers of the wind.

In any case, analyses of narrowband photometry of γ^2 Vel that we have presented in this study may well provide considerable support for recent theoretical developments of Wolf-Rayet stars.

REFERENCES

Austin, R.R., Schneider, W.H., Wood, F.B. 1973, IAU Circ., No. 2552.

Bahng, J.D.R. 1973, Bull. Am. Astron. Soc., 5, 412.

Bahng, J.D.R. 1974, Bull. Am. Astron. Soc., 6, 455.

Bahng, J.D.R. 1975, Astrophys. J., 200, 128.

Banachiewicz, T. 1942, Astron. J., 50, 38.

Bappu, M.K.V. 1973, Wolf-Rayet and High Temperature Stars, IAU Symp. No. 49, eds.: M.K.V. Bappu and J. Sahade, Dordrecht: Reidel.

Barlow, M.J., Hummer, D.G. 1982, Wolf-Rayet Stars: Observations, Physics, and Evolution, IAU Symp. No. 99, eds.: C.W.H. de Loore and A.J. Willis, Dordrecht: Reidel, 387.

Bisiacchi, G., Firmani, C., de Lara, E. 1982, Wolf-Rayet Stars: Observations, Physics and Evolution, IAU Symp. No. 99, eds.: C.W.H. de Loore and A.J. Willis, Dordrecht: Reidel, 583.

Brown, R.H., Davis, F., Herbison-Evans, D., Allen, L.R. 1970, Mon. Not. R. Astron. Soc., 148, 103.

Cherepashchuck, A.M., Eaton, J.A., Khaliullin, K. F. 1984, Astrophys. J., 281, 774.

Conti, P.S., Smith, L.F. 1972, Astrophys. J., 172, 623.
Cox, A.N., Cahn, J.H. 1988, Astrophys. J., 326, 804.

Deeming, T.J. 1975, Astrophys. Space Sci. Rev., 36, 137.

Esper, J. 1986, Master's Thesis, Univ. of Florida.

Ganesh, K.S., Bappu, M.K.V. 1967, Kodaikanal Obs. Bull. Ser. A, No. 183.

Gaposchkin, S. 1959, Astron. J., 64, 127.

Haefner, R., Metz, K., Schoembs, R. 1977, Astron. Astrophys., 55, 5.

Henden, A.A., Kaitchuck, R.H. 1982, Astronomical Photometry, New York, Van Nostrand Reinhold Co.

Högbom, J.A. 1974, Astron. Astrophys., Suppl. Ser., 15, 417.

Jeffers, S., Stiff, T., Weller, W.G. 1985, Astron. J., 90, 1852.

Jeffers, S., Weller, W., Sanyal, A. 1973a, IAU Circ., No. 2495.

Jeffers, S., Weller, W., Sanyal, A. 1973b, IAU Circ., No. 2531.

Kondo, Y., Feibelman, W.A., West, D.K. 1982, Astrophys. J., 252, 208.

Lindgren, H., Lundstrom, I., Stenholm, B. 1975, Astron. Astrophys., 44, 219.

Maeder, A. 1985, Astron. Astrophys., 147, 300.

Moffat, A.F.J. 1977, Astron. Astrophys., 57, 151.

Moffat, A.F.J., Haupt, W. 1974, Astron. Astrophys., 32, 435.

Moffat, A.F.J., Seggewiss, W. 1979, Astron. Astrophys., 77, 128.

Moffat, A.F.J., Shara, M.M. 1986, Astron. J., 92, 952.

Moffat, A.F.J., Vogt, N., Paquin, G., Lamontagne, R., Barrera, L.H. 1986, Astron. J., 91, 6, 1386.

Niemela, V.S., Sahade, J. 1980, Astrophys. J., 238, 244.

Noels, A., Gabriel, M. 1981, Astron. Astrophys., 101, 215.

Noels, A., Gabriel, M. 1984, Proc. 25th Liège Int. Astrophys. Astrophys. Colloq., 59.

Noels, A., Scuflaire, R. 1987, in Instabilities in Luminous Early Type Stars, eds.: H.J.G.L.M. Lamers and C.W.H. de Loore, Dordrecht: Reidel, 213.

Palomar Observatory, 1954. National Geographic - Palomar Observatory Sky Survey, Pasadena: California Institute of Technology.

Perrine, C.D. 1918, Astrophys. J., 47, 52.

Roberts, R.H., Lehàr, J., Dreher, J.W. 1987, Astron. J., 93, 968.

Rublev, S.V. 1972, Izv. Spets. Astrofiz. Obs., 4, 3.

Smith, L.F. 1973, Wolf-Rayet and High Temperature Stars, IAU Symp. No. 49, eds.: M.K.V. Bappu and J. Sahade, Dordrecht: Reidel.

Sunyaev, R.A. 1978, Proc. of the Int. School of Phys., "Enrico Fermi," 697, New York, North-Holland.

Underhill, A.B. 1959, Pub. Dom. Astrophys. Obs., 11, 209.

Underhill, A.B. 1982, Wolf-Rayet Stars: Observations, Physics, and Evolution, IAU Symp. No. 99, eds.: C.W.H. de Loore and A.J. Willis, Dordrecht: Reidel.

Vreux, J.-M. 1987, Instabilities in Luminous Early Type Stars, eds.: H.J.G.L.M. Lamers and C.W.H. de Loore, Dordrecht: Reidel, 81.

West, P.K. 1972, NASA SP - 310, 441.

Willis, A.J. 1980, in Symposium: The 2nd European IUE Conf., eds.: B. Battrick and J. Mort, ESA SP, 157.

Willis, A.J. 1987, Q. J. R. Astron. Soc., 28, 217.

Willis, A.J., Wilson, R. 1976, Astron. Astrophys., 47, 429.

Wood, F.B. 1941, Contrib. Princeton Univ. Obs. No. 21.

BIOGRAPHICAL SKETCH

MaryJane was born in Lake Worth, Florida, on 15 March 1961, to Peter Oates and Constance Ann Taylor. MaryJane's father played a very major role in her life, supplying support and encouragement along the way. At age five she assisted her father in building an 8-inch Newtonian telescope, and then proceeded to assemble her own 6-inch reflector at age six.

In 1968, MaryJane became the youngest member of the American Association of Variable Star Observers (AAVSO) as an active contributor, submitting thousands of sunspot and variable star observations. She continues to use her original 6-inch telescope for solar observations, and is one of about 100 international contributors to the American Sunspot Program.

MaryJane's father offered her an early exposure to mathematics by teaching her first and second year algebra while she was in third-grade. She skipped the fourth-grade, and in 1974, published her first astronomical paper in the Journal of the American Association of Variable Star Observers. Since that time, she has published a number of additional astronomical papers on variable star astronomy.

MaryJane attended Lake Worth High School and was dually and triply enrolled at Palm Beach Junior College and/or Florida Atlantic University during her junior and senior years. During this period, she acquired a background in upper-level mathematics and enrolled in a number of computer classes.

During the summers of 1974 and 1975, MaryJane participated as a research assistant at the Maria Mitchell Observatory, under the direction of Dr. Dorrit Hoffleit, long associated with Yale University. Although designed for college students, she was accepted to the program during the summers following her freshmen and sophomore years in high school. Also, in 1975, MaryJane worked in the Harvard Patrol Plate stacks for the AAVSO to resolve a long-term misidentification of the variable stars, SX and Cl Librae, resulting in the official cataloging of Cl Librae as a newly discovered variable star.

During her high school career, MaryJane was an active participant in science fairs, winning numerous awards on the local and state level. In 1976, MaryJane was awarded first place in the Earth and Space Sciences Division of the 1976 State Science and Engineering Fair and received an award for best overall project in the Physical Sciences Division. In addition, MaryJane won first place in the State Science Talent Search for presentation of a portion of her work at Maria Mitchell Observatory, "Two Variables in Sagittarius."

MaryJane was graduated from high school in June 1978 and became seriously ill in August. The illness pre-empted her college career, and so it was not until August 1980 that she was able to leave South Florida. She was graduated with a Bachelor of Arts degree from Agnes Scott College in 1983 with majors in physics/astronomy and in mathematics.

In August 1983, MaryJane became a graduate student in the Astronomy Department at the University of Florida. During her career as a graduate student, MaryJane has been a teaching assistant in the Mathematics Department where she conducted lectures in Fundamental Mathematics, Survey Calculus I and II, and Science and Engineering Calculus I. In addition, she has had research positions in the Astronomy Department with grants from National Science Foundation and the Division of Sponsored Research from the University of Florida.

In January 1988, MaryJane had the opportunity to travel to the South Pole as a member of the South Pole Optical Telescope research project team. Her duties included installation and testing of software upgrades, training winter-over personnel, and preparing hardware/software/user documentation.

I certify that I have read this study and that in my opinion it conforms to acceptable standards of scholarly presentation and is fully adequate, in scope and quality, as a dissertation for the degree of Doctor of Philosophy.

John Parker Oliver, Chairman
Associate Professor of Astronomy

I certify that I have read this study and that in my opinion it conforms to acceptable standards of scholarly presentation and is fully adequate, in scope and quality, as a dissertation for the degree of Doctor of Philosophy.

Kwan-Yu Chen
Professor of Astronomy

I certify that I have read this study and that in my opinion it conforms to acceptable standards of scholarly presentation and is fully adequate, in scope and quality, as a dissertation for the degree of Doctor of Philosophy.

Jerry L. Weinberg
Research Scientist

I certify that I have read this study and that in my opinion it conforms to acceptable standards of scholarly presentation and is fully adequate, in scope and quality, as a dissertation for the degree of Doctor of Philosophy.

Frank Bradshaw Wood
Professor of Astronomy

I certify that I have read this study and that in my opinion it conforms to acceptable standards of scholarly presentation and is fully adequate, in scope and quality, as a dissertation for the degree of Doctor of Philosophy.

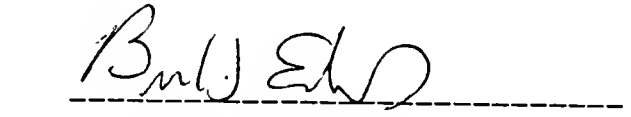

Bruce T. Edwards
Associate Professor of Mathematics

This dissertation was submitted to the Graduate Faculty of the Department of Astronomy in the College of Liberal Arts and Sciences and to the Graduate School and was accepted as partial fulfillment of the requirements for the degree of Doctor of Philosophy.

December, 1988

Dean, Graduate School